JAERI-M
82-114

REACTOR ENGINEERING DIVISION
ANNUAL REPORT
(April 1, 1981-March 31, 1982)

September 1982

Division of Reactor Engineering

日本原子力研究所
Japan Atomic Energy Research Institute

JAERI-Mレポートは，日本原子力研究所が不定期に公刊している研究報告書です。
入手の問合わせは，日本原子力研究所技術情報部情報資料課（〒319-11茨城県那珂郡東海村）あて，お申しこしください。なお，このほかに財団法人原子力弘済会資料センター（〒319-11 茨城県那珂郡東海村日本原子力研究所内）で複写による実費頒布をおこなっております。

JAERI-M reports are issued irregularly.
Inquiries about availability of the reports should be addressed to Information Section, Division of Technical Information, Japan Atomic Energy Research Institute, Tokai-mura, Naka-gun, Ibaraki-ken 319-11, Japan.

編集兼発行　日本原子力研究所
印　　刷　いばらき印刷㈱

JAERI-M 82-114

Reactor Engineering Division Annual Report (April 1, 1981 - March 31, 1982)

Division of Reactor Engineering,
Tokai Research Establishment, JAERI

(Received August 4, 1982)

Research and development activities in the Division of Reactor Engineering in fiscal 1981 are described.

The work of the Division is closely related to development of multipurpose Very High Temperature Gas Cooled Reactor and fusion reactor, and development of Liquid Metal Fast Breeder Reactor carried out by Power Reactor and Nuclear Fuel Development Corporation. Contents of the report are achievements in fields such as nuclear data and group constants, theoretical method and code development, integral experiment and analysis, shielding, reactor and nuclear instrumentation, reactor control and diagnosis, and fusion reactor technology, and activities of the Committee on Reactor Physics.

Keywords : Reactor Engineering, Very High Temperature Gas Cooled Reactor, Thermonuclear Fusion Reactor, Liquid Metal Fast Breeder Reactor, Group Constant, Theoretical Method, Code, Integral Experiment, Analysis, Shielding, Nuclear Instrumentation Reactor Control, Diagnosis

---

JAERI－M 82－114

昭和56年度原子炉工学部年報

日本原子力研究所東海研究所原子炉工学部

（1982年8月4日受理）

昭和56年度における原子炉工学部の研究活動状況をとりまとめた。原子炉工学部の研究は，多目的高温ガス炉の開発，核融合炉の開発，及び動燃事業団による液体金属高速増殖炉の開発に密接に関連するものが多い。核データと群定数，炉理論とコード開発，積分実験と解析，遮蔽，原子炉計装，炉制御と異常診断，核融合炉技術，及び炉物理に関する研究委員会活動の各分野にわたり当該年度に得た多くの成果を述べる。

CONTENTS

Foreword

In the present report is given the annual research activity of Division of Reactor Engineering, Japan Atomic Energy Research Institute, for the period of April 1981 - March 1982. The research activity of the Division extends to a broad area of reactor engineering. The major fields are thermal and fast reactor physics, fusion reactor physics, shielding, reactor instrumentation and control.

The total number of people working in the Division at the end of period was 96 in which regular members totalled to 85. Expenditures during the period amounted to about 0.54 billion yen, without including personnel expenses. In addition, a considerable amount of expenditures was covered under research contracts with outside organizations, among which Power Reactor and Fuel Development Corporation (PNC) offered the largest contribution.

The research activities were conducted in 8 Laboratories and the Committee on Reactor Physics. The Laboratories are

Reactor System Laboratory,
Fast Reactor Physics Laboratory,
Thermal Reactor Physics Laboratory,
Reactor Instrumentation Laboratory,
Reactor Control Laboratory,
Shielding Laboratory,
Fusion Reactor Physics Laboratory and
Reactor Physics Facility Operating Section.

The major research and development projects related closely to research programs in the Division are

(1) Development of very high temperature gas cooled reactor (VHTR) for multi-purpose use,
(2) Engineering research of thermonuclear fusion reactor, and
(3) Development of liquid metal fast breeder reactor (LMFBR).

As concerns research and development of VHTR, Doppler reactivity coefficients were measured for one fuel rod of coated particles heated up to 800°C at a critical assembly SHE. The reconstruction program for the SHE core was started to perform a detailed simulation experiment for the Experimental VHTR by reviewing the safety aspects of the reconstruction. For developed high-temperature neutron detectors, a long-term real-time operation test has been continued in JRR-4 for more than 3

years to prove the high performance at 600°C. In addition, an irradiation test in JMTR was completed for an advanced tungsten-rhenium thermocouple without suffering significant changes in its performance. Furthermore, the development of a computer code system has been proceeded for the computer aided design to have the good control characteristics of VHTR.

Concerning the fusion reactor physics, various reaction rate distributions, including the tritium production rate, were measured in a 20 cm thick lithium oxide sperical system with the graphite reflector by using the FNS (Fusion Neutronics Source) facility. In addition, a large-scale duct streaming experiment was carried out for fast neutrons and gamma-rays by utilizing the access pathway shield structure of the FNS target room.

As for the research and development of LMFBR, integral measurements were completed for 7 FCA standard spectrum cores and the analyses have been proceeded by using the AGLI-2 library. Furthermore, code systems have been developed for analyzing fast reactor neutronics and for producing the group constants. A series of integral experiments using the FCA standard cores has been completed for the cross section evaluation of actinides for burning them in fast reactors.

As concerns researches other than those related closely to the projects, the development of a shield computer code system BERMUDA has been proceeded for dealing with anisotropic transmission problems in 2-dimensional geometries. In addition, improvements have been made on a standard computer code system SRAC for nuclear design calculations of thermal reactors. The development of semiconductor detectors has resulted in various improvements of the characteristics and the theoretical research has been advanced for diagnosis of nuclear reactor systems. Futhermore, studies have been proceeded on various reactor physics problems by the Committee on Reactor Physics.

Takumi ASAOKA, Head
Division of Reactor Engineering

1. Nuclear Data and Group Constants

1.1 Evaluation of Hafnium Neutron Cross Sections

K. Hida*, H. Takano, T. Yoshida*, S. Iijima*, T. Asami

The neutron cross sections of the hafnium isotopes (A=174, 176~180) were evaluated for Japanese Evaluated Nuclear Data Library Version 2, JENDL-2. Although hafnium has good features as a reactivity control material of nuclear reactors, evaluated neutron data are scarce and are included neither in JENDL-1 nor in ENDF/B-IV.

The resonance parameters were adopted from the Drake's evaluation[1] and from BNL 325[2]. Background cross sections were introduced into the resonance region to reproduce the 2200 m/s values and to keep the consistency with measured total cross section data. The unresolved resonance region covers from the top of the resolved region up to 50 keV, the lower-end of the smooth cross section region.

The smooth cross sections were calculated on the basis of the statistical model with neutron penetration coefficient obtained by optical model[3]. The optical model parameters were determined so as to reproduce the total cross section of natural hafnium. The parameters are given in Table 1.1.1. The level density parameters for each isotope were determined from the measured resonance level spacings and the low-lying level scheme information. The value of the gamma strength S_γ was used as an adjustable parameter to obtain consistency with the measured capture cross section. A difficulty encountered in this procedure is that the abundance-weighted sum of the isotope-wise capture cross sections measured by Kapchigashev[4] does not agree with the measured cross section of natural hafnium[5]. The first priority was given to the consistency with natural hafnium cross sections. The adopted cross section curves are shown in Fig. 1.1.1 along with the Drake's evaluation for ENDF/B-V.

The cross sections for processes (n,2n), (n,3n), (n,p) and (n,α) were calculated with GNASH code[6] based upon the multi-step Hauser-Feshbach theory.

---

*) NAIG Nuclear Research Laboratory, Nippon Atomic Industry Group Co., Ltd.

The 2200 m/s capture values and the resonance integrals of the present evaluation are listed in Table 1.1.2 with other evaluation values.

References

1) Drake M.K., Sargis D.A., Maung T. : EPRI NP-250 (1976).
2) Mughabghab S.F., Garber D.I. : BNL 325, Third Edition (1972).
3) Igarasi S. : CASTHY code, private communication.
4) Kapchigashev S.P. : Atomizdat, Moscow (1970), numerical values taken from the NESTOR data base.
5) for example, Kompe D. : Nucl. Phys., A133, 513 (1969); Moxon M.C., et al., AERE-PR/NP21 p.41 (1974) UKAEA.
6) Young P.G., Arthur E.D. : "GNASH: A Preequilibrium, Statistical Nuclear-Model Code for Calculation of Cross Sections and Emission Spectra," LA 6947 (1977).

Table 1.1.1 Optical Model Parameters and Strength Functions

$V_0 = 38.0$, $W_s = 8.0 + 0.5\ E$, $V_{so} = 7.0$ (all in MeV)

$R_0 = R_s = R_{so} = 1.32$ fm

$a_0 = a_{so} = 0.47$ fm, $a_s = 0.52$ fm

$S_0 = 2.0$,* $S_1 = 1.1$, $S_2 = 1.9$, $R' = 6.9$ fm

*) $\times 10^{-4}$ for S_0, S_1 and S_2

Table 1.1.2 Capture cross section at 2200 m and resonance integral

A	Abund. %	σ_{2200}, barn		Res. Integral, barn		
		present	BNL-325	present	BNL-325	SAI
174	0.16	390	390 ± 50	476	465 ± 50	446
176	5.2	38	38 ± 6	357	700 ± 50	337
177	18.6	360	365 ± 20	7230	7260 ±200	7220
178	27.1	86	86 ± 10	1918	1950 ±100	1747
179	13.7	45	45 ± 5	517	600 ± 60	451
180	35.2	12.6	12.6 ± .7	36	43 ± 8	29
nat		103	102 ± 2	1972	2000 ±100	1900

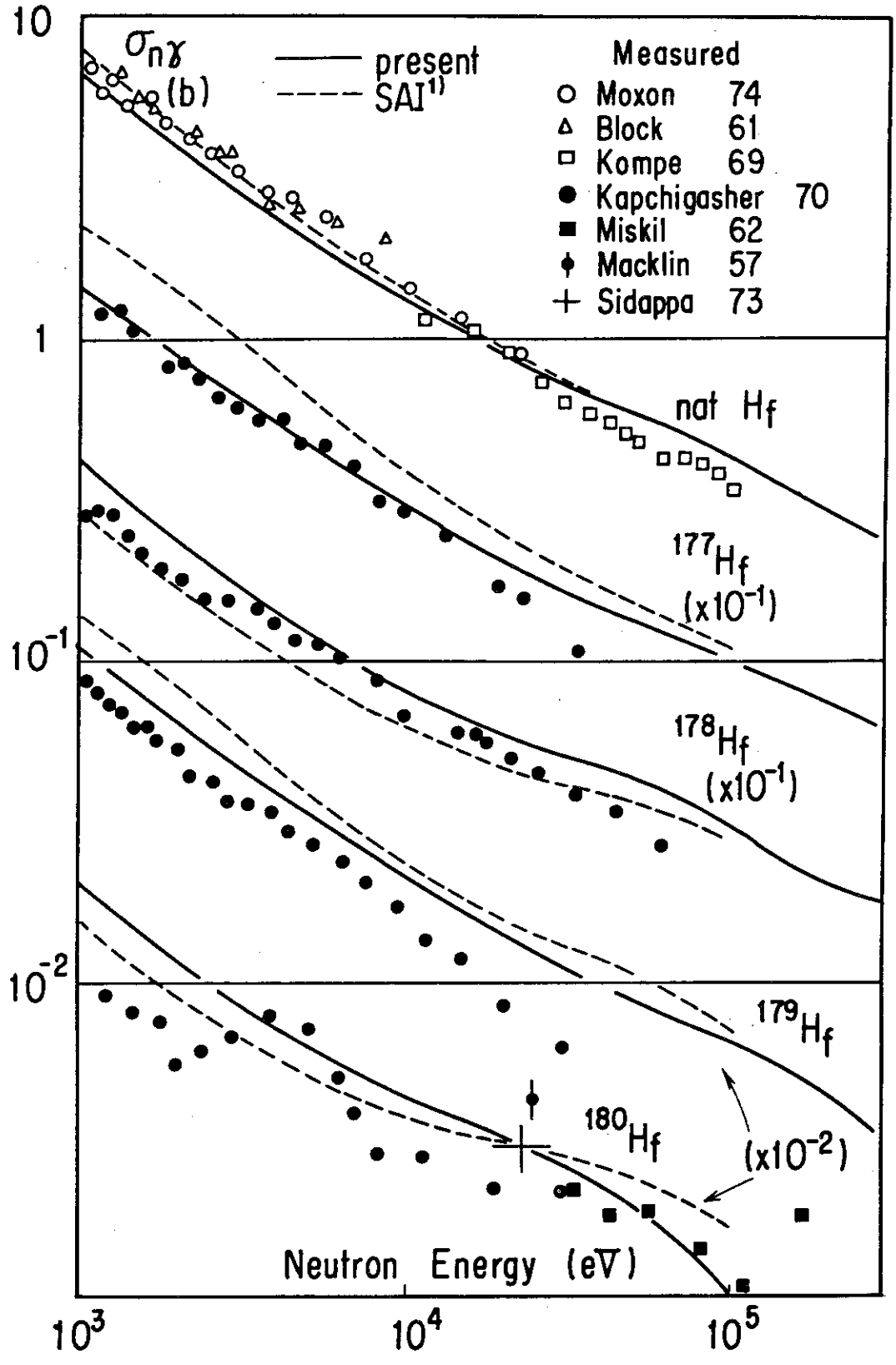

Fig. 1.1.1 Adopted capture cross sections of Hf isotopes

1.2 Two-Dimensional Benchmark Tests of the JFS-3-J2 Set

H. Takano, Y. Ishiguro and H. Inoue*

Benchmark calculations of fast critical assemblies have been performed by using the JFS-3-J2[1] group constant set generated from the evaluated nuclear data compilations JENDL-1[2] and -2.[3] The assemblies selected in this study are the clean physics mockup cores FCA-V-1, FCA-V-2, FCA-VI-1, FCA-VI-2, ZPR-6-7, ZPR-6-6A, ZPPR-2 and ZPPR-9. The FCA assembly V-1 is the first physics mockup for the core composition of the JOYO (Japan Experimental Fast Reactor). The FCA-V-2 is the second physics mockup, and the core composition is the same as the assembly V-3, the engineering mockup experiment for the JOYO control rods. The assembly VI-1 is the outer-core mockup of the prototype fast breeder reactor MONJU and the assembly VI-2 is the second physics mockup for the MONJU inner-core composition. The assemblies ZPPR-2 and ZPR-6-7 (Ref.) are similar in composition to a large LMFBR, and especially ZPPR-2 is convenient to study effect of two-core zones with a more realistic LMFBR height and oxide blanket. The ZPR-6 assembly 7 (H240) has the high 240 plutonium zone at the center of assembly 7 (Ref.) to asses the effect of fuel burnup on the integral parameters. The ZPPR assembly 9 is a clean physics benchmark with a core volume of 4600 litres and is the first assembly of the JUPITER (Japanese United States Program of Integral Tests and Experimental Researches) program.

The physics parameters studied are criticality, central reaction rate ratios, Doppler reactivity coefficients, sodium-void reactivities and reaction rate distributions. All calculations were made using the JFS-3-J2 set and the code system for two-dimensional benchmark calculations. The calculated results are discussed by comparing with the experimental values as follows.

(1) Effective Multiplication Factors : Table 1.2.1

The effective multiplication factors calculated for the FCA assemblies which consist of the uranium and plutonium fuels are overestimated by 0.2 ∿ 0.5%, and they are underestimated by 0.7 ∿ 0.9% for the assemblies ZPPR-9, -2 and ZPR-6-7 with the plutonium fuel.

---

* Japan Information Service Co. Ltd. Tokyo

(2) Central Reaction Rate Ratios : Table 1.2.2

U-238(F)/U-235(F) : The calculated values overestimate the experiments, though an exception is the result for ZPR-6-6A.

Pu-239(F)/U-235(F) : All calculations underestimate the experiments by 3∿6%.

U-238(C)/Pu-239(F) : The result calculated for ZPR-6-7 is overestimated by ∿6%.

(3) Doppler Reactivity coefficients for ^{238}U : Table 1.2.3

The calculated values underestimate the experiments by 10∿25%.

(4) Sodium-void Reactivities : Table 1.2.4

The calculations overestimate considerably the experiments depending on the increase of sodium voided zone.

(5) Reaction Rate Distributions : Figs. 1.2.1∿1.2.4

The ^{239}Pu fission reaction rates calculated for FCA-VI-2 are overestimated in the vicinity of the boundary between the driver and blanket regions, though the calculations for ZPPR-9 are in very good agreement with the experiments.

The ^{238}U capture reaction rates calculated for ZPPR-9 are in very good agreement with the experiments, and they for ZPPR-2 are underestimated for the outer core and blanket regions.

From the results of benchmark calculations described above, the reevaluations for ^{238}U capture and ^{239}Pu fission cross sections will be requested, for instance, such as smaller capture cross section of ^{238}U and larger fission cross section of ^{239}Pu than the presently evaluated data of JENDL-2.

The present work was performed under the contracts between Power Reactor and Nuclear Fuel Development Corporation and Japan Atomic Energy Research Institute.

References

1) Takano H., "Production and Benchmark Tests of Fast Reactor Group Constant Set JFS-3-J2," to be published in JAERI-M report.
2) Igarasi S., et al. : "Japanese Evaluated Nuclear Data Library Version-1, JENDL-1," JAERI-1261 (1979).
3) Igarasi S., et al. : private communication.

Table 1.2.1 Effective multiplication factor (k-eff)

ASSEMBLY	EXPERIMENTS	CALCULATION	CORRECTION FACTOR (% ΔK)		CORRECTED	C / E
			HETEROGENEITY	TRANSPORT		
FCA-V-1	1.00000	0.99505	0.136	0.747	1.00388	1.00388
FCA-V-2	1.00000	0.99260	0.240	0.981	1.00481	1.00481
FCA-VI-1	1.00000	0.99222	0.432	0.595	1.00249	1.00249
FCA-VI-2	1.00000	0.99578	0.421	0.333	1.00332	1.00332
ZPPR-9	1.00000	0.98017	1.175	0.093	0.99285	0.99285
ZPPR-2	1.00000	0.97786	1.140	0.260	0.99186	0.99186
ZPR-6-7 (REF.)	1.00000	0.97704	1.214	0.150	0.99068	0.99068
ZPR-6-7 (H240)	1.00000	0.97732	1.256	0.116	0.99104	0.99104
ZPR-6-6A	1.00000	0.99414	0.470	0.093	0.99977	0.99977

Table 1.2.2 Central reaction rate ratios

ASSEMBLY	SPECTRAL INDIX	EXPERIMENTS (ERROR)	CALCULATION	CORRECTION FACTOR HETERO/HOMO	CORRECTED	C / E
FCA-V-1	U-238(F)/U-235(F)	0.0423 (0.02)	0.0447	1.005	0.045	1.062
	PU-239(F)/U-235(F)	1.161 (0.02)	1.078	1.010	1.088	0.938
FCA-V-2	U-238(F)/U-235(F)	0.0396 (0.03)	0.0428	1.007	0.043	1.088
	PU-239(F)/U-235(F)	1.104 (0.03)	1.064	1.009	1.073	0.972
FCA-VI-1	U-238(F)/U-235(F)	0.0323 (0.041)	0.0335	0.976	0.033	1.012
	PU-239(F)/U-235(F)	1.033 (0.041)	0.990	1.000	0.990	0.959
FCA-VI-2	U-238(F)/U-235(F)	0.0219 (0.03)	0.0232	0.976	0.023	1.034
	PU-239(F)/U-235(F)	0.956 (0.03)	0.913	0.997	0.911	0.952
ZPPR-9	U-238(F)/U-235(F)	0.0185 (0.0004)	0.0207	0.976	0.020	1.092
	PU-239(F)/U-235(F)	0.917 (0.013)	0.903	0.985	0.890	0.970
ZPR-6-7 (REF.)	U-238(C)/PU-239(F)	0.1400	0.1526	0.974	0.149	1.062
	U-238(F)/PU-239(F)	0.023	0.025	1.010	0.025	1.069
	U-235(F)/PU-239(F)	1.061	1.099	1.010	1.109	1.046
ZPR-6-7 (H240)	U-238(F)/PU-239(F)	0.0235	0.0259	1.010	0.026	1.113
	U-235(F)/PU-239(F)	1.031	1.087	1.010	1.098	1.065
ZPR-6-6A	U-238(C)/U-235(F)	0.0241 (0.0007)	0.0234	0.985	0.023	0.956
	U-238(F)/U-235(F)	0.138 (0.0041)	0.140	0.979	0.137	0.995

Table 1.2.3 Doppler reactivity

SAMPLE NAME (NUO2)

ASSEMBLY	TEMPERATURE	REACTIVITY (-DK/K*10E-6) EXPERIMENTS (ERROR)	CALCULATION	CORRECTION FACTOR HETERO/HOMO	CORRECTED	C / E
FCA-V-1	300K - 573K	4.6600	4.0830	1.020	4.165	0.894
	300K - 823K	7.1200	6.3150	1.022	6.454	0.906
	300K - 1073K	9.1800	7.8810	1.022	8.054	0.877
FCA-V-2	300K - 1073K	10.6500	7.7972	1.032	8.047	0.756
FCA-VI-1	300K - 623K	5.1900	4.3300	1.068	4.624	0.891
	300K - 823K	7.5100	6.0230	1.069	6.439	0.857
	300K - 1073K	9.3800	7.6410	1.071	8.184	0.872
FCA-VI-2	300K - 623K	6.8300	5.5470	1.069	5.930	0.868
	300K - 823K	8.7800	7.0840	1.071	7.587	0.864
ZPPR-9	298K - 487.5K	1.0338 (0.0299)	0.8066	1.120	0.903	0.874
	298K - 644.4K	1.6421 (0.0299)	1.2896	1.122	1.447	0.881
	298K - 794.0K	2.1870 (0.0299)	1.6590	1.125	1.866	0.853
	298K - 935.4K	2.4706 (0.0336)	1.9535	1.127	2.202	0.891
	298K - 1087.0K	2.8475 (0.0299)	2.2266	1.129	2.514	0.883

Table 1.2.4 Sodium-void reactivity

ASSEMBLY	VOIDED REGION	REACTIVITY (DK/K*10E-4) EXPERIMENTS (ERROR)	CALCULATION	CORRECTION FACTOR HET.	EP.	TRA.	CORRECTED	C / E
FCA-V-1	1 X 1 DRAWER	-2.3900 (0.11)	-1.0060	1.347	1.000	1.000	-1.355	0.567
	3 X 3 DRAWERS	-20.0100 (0.10)	-10.1700	1.316	1.000	1.000	-13.384	0.669
FCA-VI-2	3 X 3 X 4 PACKS	2.1300 (0.05)	3.2772	0.821	1.000	1.000	2.691	1.263
	5 X 5 X 4 PACKS	5.5100 (0.08)	8.5940	0.813	1.000	1.000	6.987	1.268
	5 X 5 X 6 PACKS	7.6500 (0.08)	12.1830	0.804	1.000	1.000	9.795	1.280
	7 X 7 X 6 PACKS	12.5300 (0.11)	21.6540	0.788	1.000	1.000	17.063	1.362
	7 X 7 X 8 PACKS	14.6500 (0.11)	26.5540	0.774	1.000	1.000	20.553	1.403
ZPPR-9	9 DRAWERS	1.0410 (0.017)	1.2790	0.845	1.026	1.018	1.129	1.084
	37 DRAWERS	3.9720 (0.014)	5.2330	0.844	1.037	1.000	4.580	1.153
	97 DRAWERS	10.0980 (0.007)	13.5900	0.839	1.052	0.968	11.611	1.150
	97 DRAWERS	12.8030 (0.003)	19.4340	0.781	1.091	0.984	16.294	1.273
	97 DRAWERS	10.8850 (0.007)	18.8930	0.720	1.121	0.990	15.096	1.387
	97 DRAWERS	8.3980 (0.010)	17.8760	0.654	1.136	1.002	13.307	1.585

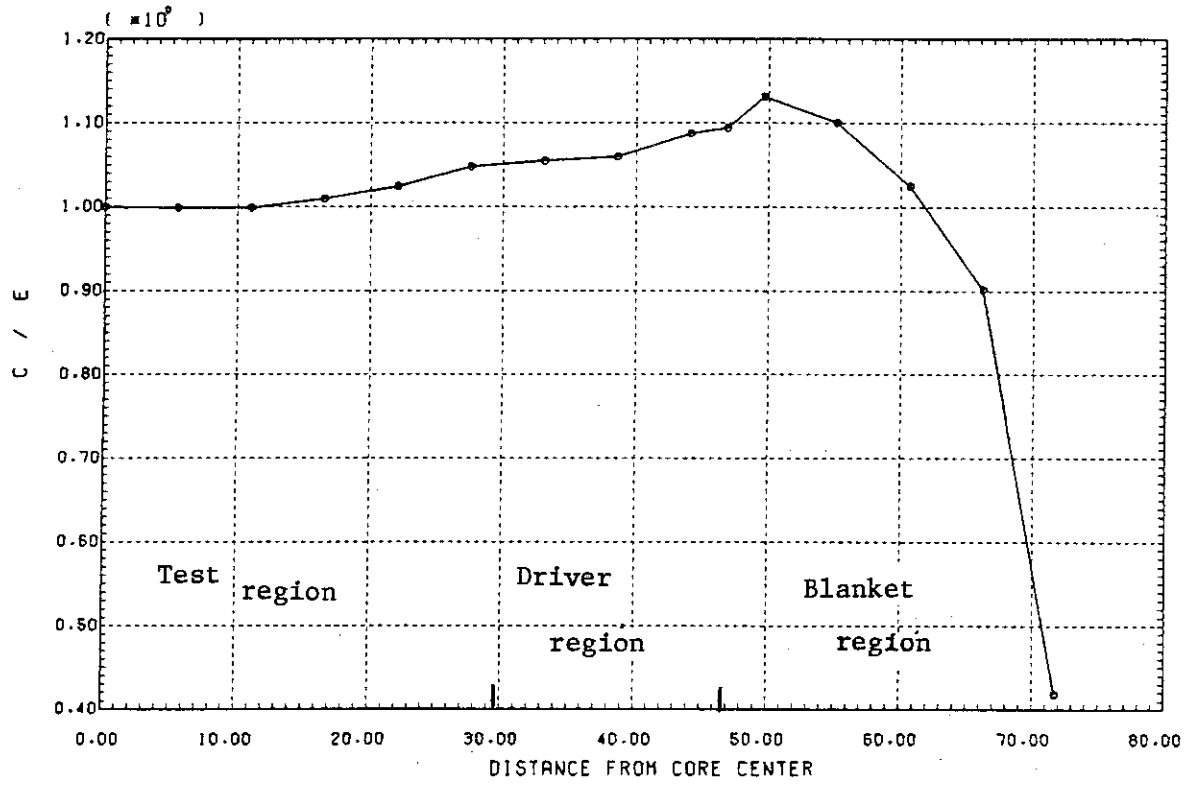

Fig. 1.2.1 FCA-VI-2 Pu-239 fission rate distribution (R-direction)

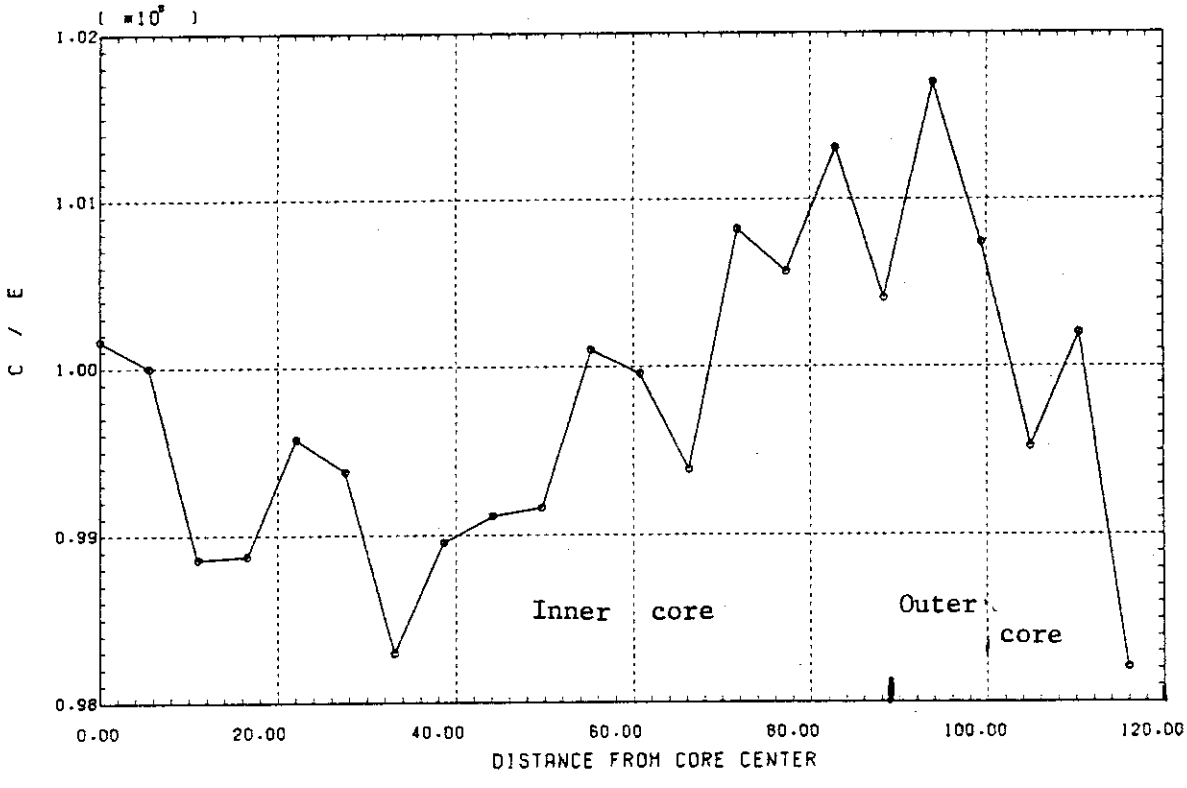

Fig. 1.2.2 ZPPR-9 Pu-239 fission rate distribution (R-direction)

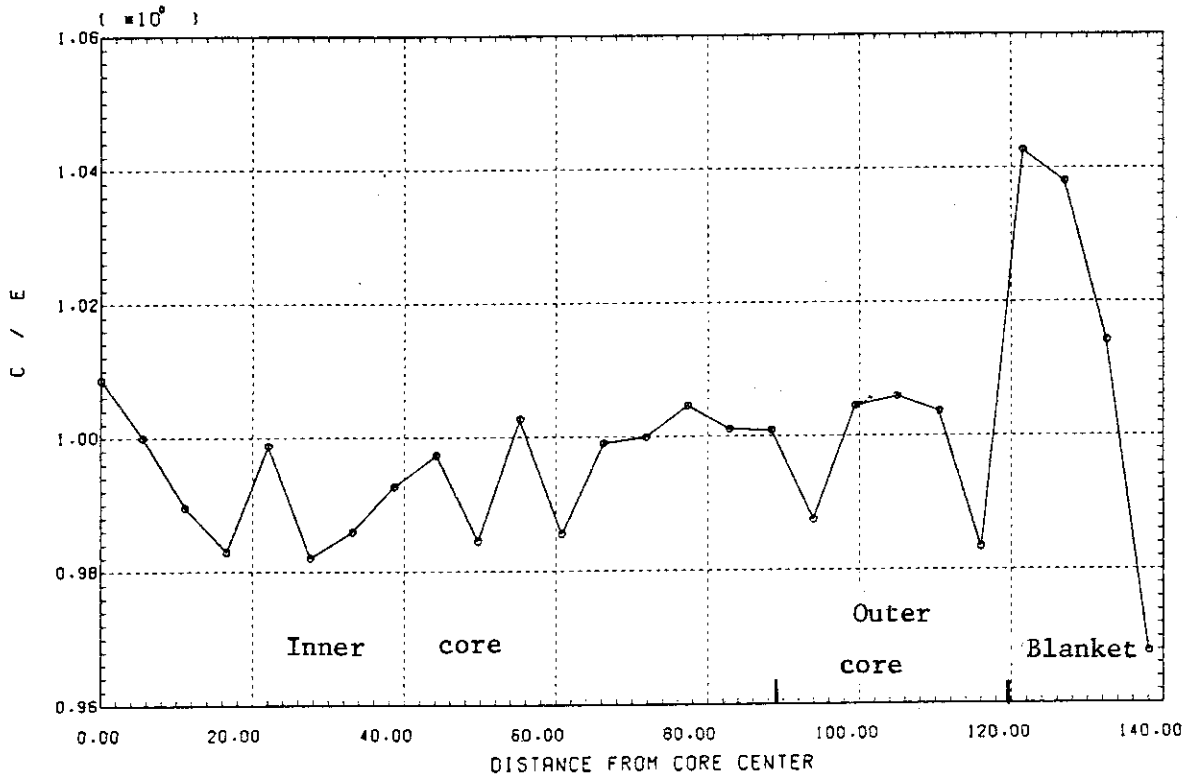

Fig. 1.2.3 ZPPR-9 U-238 capture rate distribution (R-direction)

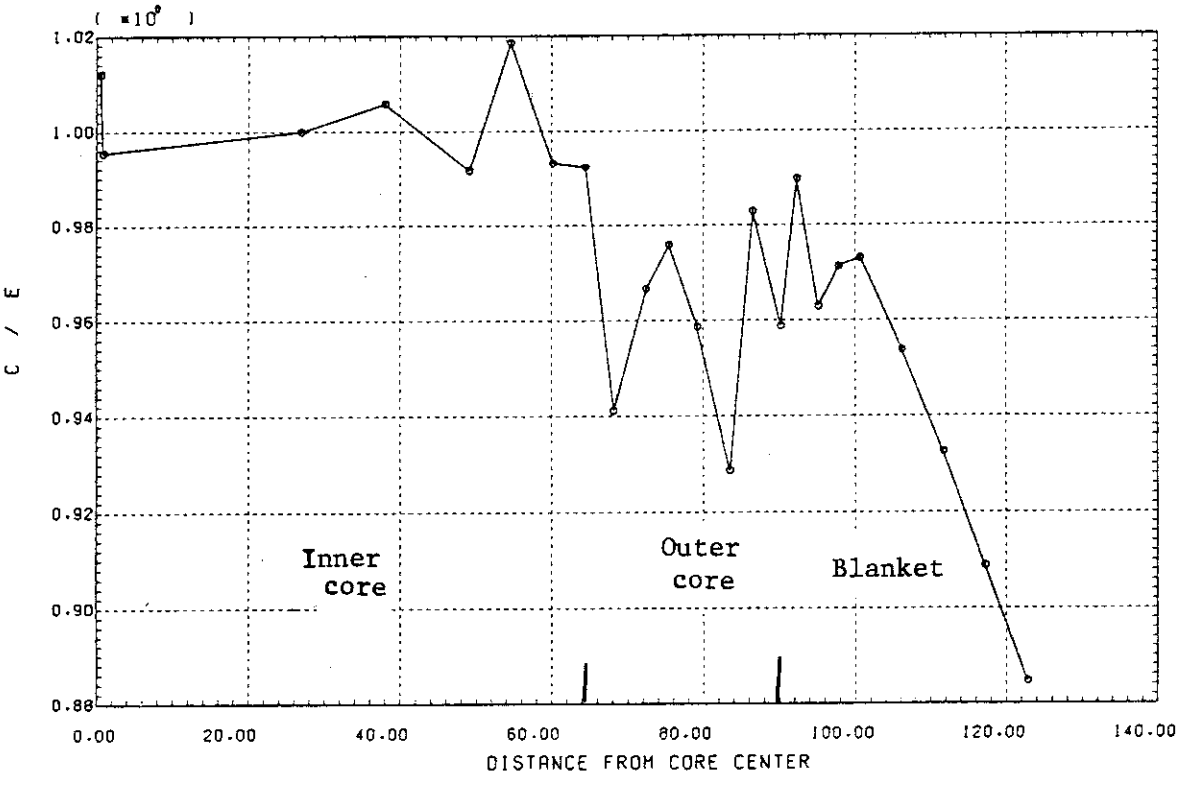

Fig. 1.2.4 ZPPR-2 U-238 capture rate distribution (R-direction)

1.3 TIMS-PGG: A Code System for Producting Group Constants in Fast Neutron Energy Region

H. Takano, A. Hasegawa and K. Kaneko*

The code system TIMS-PGG has been developed to generate group constant library by processing the evaluated nuclear data such as the JENDL-1 and/or ENDF-B-IV compilations. This code system is constructed by connecting functionaly the TIMS-1[1], PROF.GROUCH.G.II R[2], RESENDD[3] and several utility codes, and the flow chart is shown in Fig. 1.3.1. The TIMS-1 and PROF.GROUCH.G.II R were developed for the generation of the JAERI Fast Set version II[4] (JFS-2).

The TIMS-1 calculates the infinitely dilute cross sections and effective cross sections by solving exactly neutron slowing down equation. With this approach, the mutual interference effects between resonances of different nuclides and self-overlapping effects are accurately treated and furthermore the elastic removal cross sections are acculately calculated. The temperature and composition dependent resonance shielding factors for heavy resonant nuclides are generated by using this TIMS-1 code.

The infinitely dilute cross sections, effective cross sections and scattering matrices for light and medium weight nuclides and for smooth cross sections of heavy nuclides are calculated with the PROF.GROUCH.G II R code. In this code, two kinds of neutron spectra for the broad energy behavior, "1/E + fission" and "collision density" spectra are prepared as weighting spectrum. In fast reactor, neutron spectra are steeply reduced in the low energy groups below 10 KeV. Hence, the assumption of "1/E - spectrum" overestimates the elastic removal cross sections. To avoid the overestimate, a collision density spectrum calculated for the core composition in a typical fast reactor is used, and this treatment is called the REMO-correction[5] method. The self-shielding factors for elastic removal cross section are calculated by using the collision density spectrum shown in Fig. 1.3.2.

The results calculated with the TIMS-1 and PROF-GROUCH.G II R are stored on the master file in the PDS format by XTABPDS. The SPEC code

---

* Japan Information Service Co. Ltd., Tokyo.

calculates the group fission spectra from using the distribution given in the ENDF/B-IV format. Finally, the group constants library for the JFS or SRAC type[6] is produced by using the LIBMAKE code.

References

1) Takano H., Matsui Y. and Ishiguro Y. : "TIMS-1 : A Processing Code for Production of Group Constants of Heavy Resonant Nuclei," JAERI-1267 (1980).
2) This code is a modified version of PROF.GROUCH.G II for Producing the group constants of JFS-3 type.
3) Nakagawa T. : Private communication.
4) Takano H., Hasegawa A., Nakagawa M., et al. : JAERI Fast Reactor Group Constants Set, Version II., JAERI-1255 (1978).
5) Takano H. : "The effect of REMO-Correction on Integral Quantities," Reactor Engineering Division Annual Report, JAERI-M 9672 (1981).
6) Tsuchihashi K., et al. : Private communication.

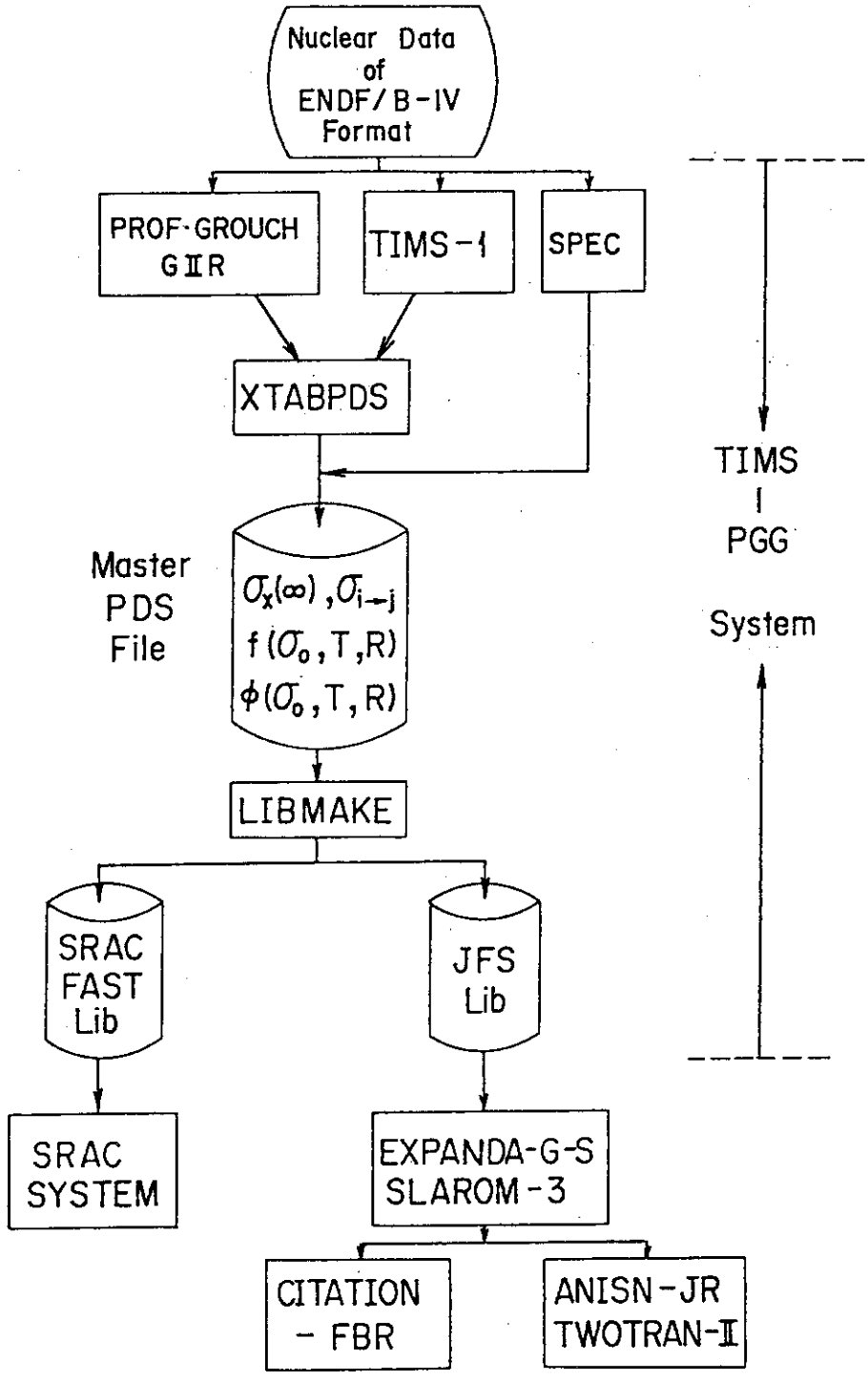

Fig. 1.3.1 Main flow diagram of TIMS-PGG system

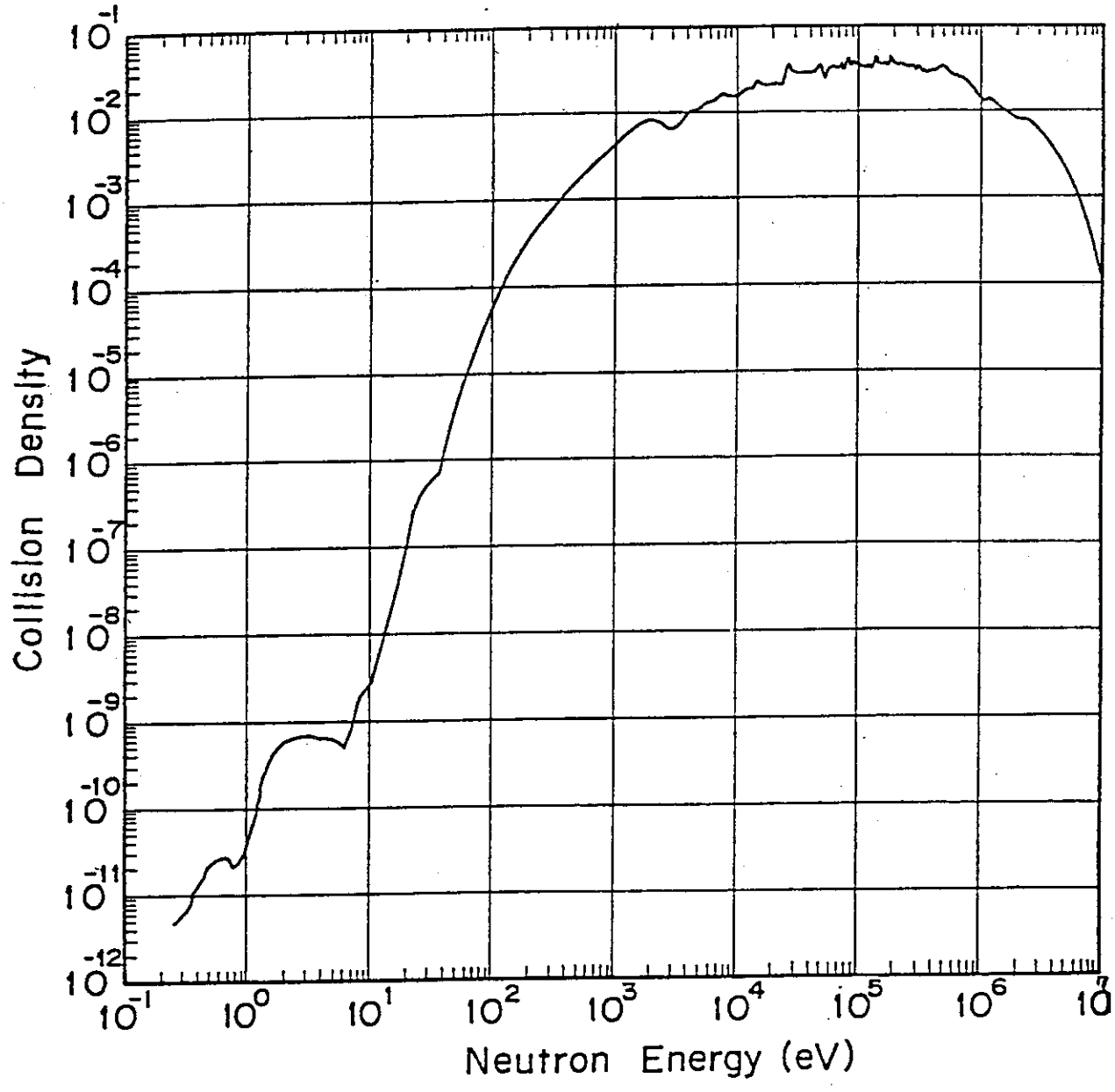

Fig. 1.3.2 Collision density spectrum calculated for the inner core composition of a prototype fast reactor MONJU using the fine neutron spectrum calculation code ESELEM-4.

2. Theoretical Methods and Code Development

2.1 Development of Code System for Analysis of Fast Reactor Neutronics

M. Nakagawa, H. Inoue*, W. Sato* and Y. Ishiguro

A code system for analysis of fast reactor neutronics has been being developed since 1979[1]. This code system consists of three steps. The first step is the production of the cross section library, which generates the JAERI Fast Set type multi-group cross section library or the ultrafine-group library, the second one calculates configuration, composition and temperature dependent effective cross sections, and the third is the calculation step of neutronics parameters and the various edits. In fiscal 1981, the following programs have been incorpolated or modified.

1) Two dimensional burn-up calculation code PHENIX[2] has been incorpolated into the system. This code treats x-y, r-z and r-θ geometries. The JFS type library and cross sections stored in the PDS file are available.
2) Three dimensional burn-up calculation code 3DB[3] has been incorpolated into the system. This code treats x-y-z, r-θ-z and triangular -z geometries. It has been modified to reduce the computation time.
3) The JOINT code has been modified so as to be able to produce a microscopic cross section library for the use in the multi-dimensional diffusion code CITATION.[4] As a result, CITATION can be run basing on both the macroscopic and the microscopic cross sections.
4) The SLAROM[5] code has been extended so as to treat cluster geometries such as square rods cluster and circular rods cluster.
5) Plotter routine PLOT-FBR[6] has been modified to read the data from the PDS file. This routine can plot neutron spectrum, cross section of various types, reaction rate distribution and some other integral quantities.

At the present stage, the following cross section sets are available ; JFS-V2[7], ENDF/B4, JFS-3-J2[8], JENDL-2B-70[9] with seventy group

---

* Visiting researcher from Japan Information Service Co. Ltd.

structure and JFS-V2 library, JENDL-2B[10] library for ultrafine group structure. The anisotropic elastic scattering can be taken into account up to the P_3 order of Legendre expansion. Users can obtain cell averaged values of the P_ℓ components of elastic scattering matrix by the cell calculation code SLAROM. The microscopic and macroscopic cross sections, fission spectrum and buckling are stored in the PDS file with the unified format. The interface program JOINT reads the cross sections from the PDS file and the input data required in the neutronics calculations, and prepares the input data files. Many subroutines have been developed for the utility of the data in the PDS file.

The present work was performed under the contract between Power Reactor and Nuclear Fuel Development Corporation and Japan Atomic Energy Research Institute.

References

1) Nakagawa M. and Abe J. : "Development of Interface program JOINT for Fast Reacter Neutronics Calculation Code System," Reactor Engineering Division Annual Report, 28, JAERI-M 9672 (1980).
2) Douglas R. O'Dell and Hirons T.J., : "PHENIX, a two-dimensional Diffusion Burn-up Refueling Code," LA-4311 (1970) and Ihara H., private communication (1980).
3) Hardie R.W. and Little R.W. Jr., : "3DB, A Three-dimensional Diffusion Theory Burn-up Code," BNWL-1264 (1970).
4) Fowler, T.B., et al. : "Nuclear Reactor Core Analysis Code : CITATION," ORNL-TM-2496 Rev.2 (1969).
5) Nakagawa M., and Tsuchihashi K. : "SLAROM : A Code for Calculation of a Heterogeneous Core in Fast Reactors," JAERI-M 5916 (1974) (in Japanese).
6) Iijima S., Private communication.
7) Takano H., Hasegawa A., Nakagawa M., et al. : "JAERI-Fast Reactor Group Constant Set, Version-II ," JAERI 1255 (1978).
8) Takano H. : to be published in JAERI-M report.
9) Kikuchi Y., et al. : J. Nucl. Sci. Technol., 17[7], 567 (1980).
10) Kikuchi Y., et al. : Private communication.

2.2 Development of EXPANDA-GENERAL: A One Dimensional Diffusion Code for Fast Reactors

A. Hasegawa

Generalized EXPANDA[1] : EXPANDA-General ; A one-dimensional diffusion criticality and perturbation code has been developed based on the code EXPANDA-70DRA[2]. The present code has the following characteristics:

(1) Variable dimensioned coding is adopted. Hence this code is completely free from dimensional restrictions encountering the fixed dimensioned code. There are no limitations for number of energy groups, regions, mesh points, etc.

(2) Acceptable libraries ; JAERI-Fast set[3], JENDL-1[4] and 2[5] set, ENDF/B IV set.

(3) Possibility of the exact perturbation calculation as well as first order perturbation.

(4) Semi-automatic preparation of input data for two or three dimensional criticality calculation codes ; CITATION[6] or EXTERMINATOR-2[7].

(5) Semi-automatic preparation of input data for two- or three-dimensional perturbation calculation codes ; CIPER[8] or PERKY[9].

(6) More accurate treatment of elastic removal effective cross sections of light and medium weight nuclides in the resonance region using the exact weighting fluxes obtained by the recurrence formulae numerically[2].

(7) Proper treatment for gross region heterogeneity due to the large material-change at the interface of regions. In the EXPANDA series developed up to now, effective cross sections used in the code are defined as region dependent cross sections without taking into account the adjacent regions. There were some problems in using flat cross section in one region when analyzing the reaction rate distributions near the region boundary whose materials are largely different. In such regions actual cross sections near the boundary region should contain the influence from adjacent region, that is, the cross sections of this region are expressed as a combination of the cross sections of the adjacent regions. The method predicting the actual cross section in the sub-region near the interface due to the gross region heterogeneity was developed by ISHIGURO[10].

We adopted his method.

(8) More efficient and easy treatment for comparison of C/E (calculated to experimental) values of typical integral data obtained by the benchmark test in order to assess the applicability of the group cross section libraries.

(9) Adoption of self-explanation systems in the group cross section library : General-Library, i.e. all of the informations defining the library are contained in that library itself. Therefore, a structure library containing any group number and any independent parameters of self-shielding factor table and so on is accessible by the present code.

References

1) Hasegawa A. : "EXPANDA-GENERAL USER'S GUIDE," JAERI-M 9791 (1981).

2) Hasegawa A., Tsuruta S. and Ishiguro Y. : "Treatment of the Elastic Removal Cross Sections in Na-Fe Resonance Region and One-Dimensional Code EXPANDA-70DRA," JAERI-M 6081 (1975) (in Japanese).

3) Takano H., Hasegawa A., Nakagawa M., Ishiguro Y. and Katsuragi S. : "JAERI Fast Reactor Group Constants Set, Version II," JAERI-1255 (1977).

4) Igarashi S., Nakagawa T., Kikuchi Y., Asami T. and Narita T. : "Japanese Evaluated Nuclear Data Library, Version 1," JAERI-1261 (1978).

5) Igarashi S. : private communication.

6) Fowler T.B. and Vondy D.R. : "Nuclear Reactor Core Analysis Code : CITATION," ORNL-TM-2496 (1969).

7) Fowler T.B., Tobias M.L. and Vondy D.R. : "EXTERMINATOR-2 A FORTRAN IV Code for Solving Multigroup Neutron Diffusion Equation in Two Dimension," ORNL-4078 (1967).

8) Nakagawa M. and Tokuno Y. : "CIPER A Two- and Three-Dimensional Perturbation Code Based on Diffusion Theory," JAERI-M 6722 (1976) (in Japanese).

9) Iijima S., Yoshida H. and Sakuragi H. : "Calculation Program for Fast Reactor Design, 2 (Multi-Dimensional Perturbation Theory Code based on Diffusion Approximation : PERKY)," JAERI-M 6993 (1977).

10) Ishiguro Y. and Hasegawa A. : Nucl. Sci. Eng., 64, 786-791 (1977).

2.3 SRAC: A Standard Computer Code System for Lattice Cell and Core Calculations on Reator Design and Analysis

—— Cell Burn-up Routine and Its Benchmark Calculations ——

K. Tsuchihashi, Y. Ishiguro, H. Takano, K. Horikami

In the course of our continuous effort to develop the SRAC, a cell burn-up routine with its data library has been installed in the system. This routine is called several times in a cell calculation to calculate the changes of nuclide densities due to burn-up during an exposure step under a given power level and fixed material temperatures.

The input requirements for cell burn-up are minimized to save the elaborate work to organize the chain scheme, to prepare the fission yields, the neutron cross sections, and the decay constants etc. for each fission produced nuclide. All necessary information is stored in a burn-up library so that the user can choose one of four F.P. chain models which will be described below.

Analytical solution of the differential equations

We use explicit form for the solution of the equations as used in the CITATION code[1] to avoid accumulation of numerical error which happens by improper selection of time mesh used in the numerical method such as the Runge-Kutta-Gill method. The solution is based on the assumption that the neutron flux is not time dependent. Throughout the exposure calculations, reaction rates are based on the neutron flux available at the start of an exposure time step.

On the other hand, the given condition 'fixed power' conflicts with the above assumption on the flux level. To escape from the contradiction, we subdivide an exposure step into several sub-steps so as to be able to assume the neutron fluxes are time-independent. In each sub-step the flux renormalization is done.

The nuclides under consideration are classified into 1) Heavy nuclides which may induce fission, 2) Absorber nuclides, 3) Fission produced nuclides. The first approach is to solve the heavy nuclide chains. After finding the average flux and power level in a sub-step, the remaining chains are solved under the fixed flux or reaction rates.

When more than one spatial region contain any burnable nuclides, the above process is repeated by region so that the renormalization

covers all regions. The effective microscopic cross sections are provided for each region.

Now we shall describe about the chain schemes installed in the burn-up library

Heavy nuclide chains

The routine is organized to process (n,2n) reaction. However it is not so important in thermal reactors we neglect it in the present preparation.

Th232 → U233 → U234 → U235 → U236

U238 → Pu239 → Pu240 → Pu241 → Pu242

Absorber chains

We can consider the decrease of concentration of absorbing nuclides contained in burnable poison or control rod.

B10

Gd155 → Gd156 → Gd157

Ag107

Ag109

In113

In115

Cd113

Hf176 → Hf177 → Hf178 → Hf179 → Hf180

F.P. chains

We have four possible options for F.P. chains

Garrison model

The model of Garrison and Roos[2] consists of rapidly saturating, slowly saturating, and non-saturating groups plus two explicit nuclides, Xe-135 and Sm-149. Their neutron cross sections are taken from ENDF/B-II. Each is separately prepared for U-233, U235, and Pu-239 thermal fission.

Iijima model

Iijima et al.[3] has proposed a model containing 45 explicit nuclides and one pseudo nuclide as shown in Fig. 2.3.1 for BWR lattice calculation. We take their chain model and fission yields, but neutron cross sections from ENDF/B-IV except for the pseudo nuclide. We have another option to use fission yields taken from ENDF/B-IV which might be

considered more systematic.

V.S.O.P. models

The code system V.S.O.P.[4] has been employed in extensive calculations of fuel cycle and life history of pebble bed HTR in KFA Jeulich. It keeps four chain schemes. We have taken two of them; Chain 25 most simple, and Chain 40 most precise which are shown in Fig. 2.3.2. Due to the delay of transmission of the copy tape from NEA Data Bank (more than 9 months), we have not yet compiled the cross sections of their pseudo nuclides.

Numerical test

Some numerical tests are achieved to verify the performance of the routine and to compare the results of different models.

The first example shown in Table 2.3.1 is the Kinf values for the pin rod cell which was proposed for the LWR benchmark problem with adjacent poison fuel rods by NEACRP in 1981.

The second example shown in Table 2.3.2 is for the Kinf values of the cell of a MTR type fuel plate of 20% enrichment proposed in the safety related benchmark calculations at the IAEA meeting for RERTR program.

As shown in above examples the difference due to the model is quite small and the user who does not trace burn-up process over so long fuel life may not worry about the model, but use the simple Garrison model.

References

1) Fowler T.B. et al. : "Nuclear Reactor Core Analysis Code : CITATION," ORNL-TM-2496 (1969).
2) Garrison J.D. and Roos B.W., Nucl. Sci. Eng. 12 (1962).
3) Iijima S. et al. : J. Nucl. Sci. Technol 19, (1982).
4) Teuchert E. et al. : "V.S.O.P. - Computer Code System for Reactor Physics and Fuel Cycle Simulation," Jeul-1649 (1980).

Table 2.3.1 Change of Kinf during burn-up in LWR lattice

Days	0.	17.0	421.7	827.2	1232.	1638.
GWD/t metal	0.	.340	8.31	16.2	24.2	32.2
U235 burnt*	0.	.00881	.219	.422	.610	.786
Garrison	1.3518	1.2969	1.1502	1.0410	0.9507	0.8596
Iijima	1.3518	1.2968	1.1395	1.0253	0.9316	0.8389
VSOP25**	1.3518	1.2966	1.1459	1.0369	0.9480	0.8587
VSOP40**	1.3518	1.2957	1.1381	1.0235	0.9297	0.8368

Note * U235 burnt; ratio to the initial value of unity.
** The cross sections for pseudo FP in VSOP models are temporary.

Table 2.3.2 Change of Kinf during burn-up in a 10 MW MTR fuel

Days	0.0	36.6	73.4	187.2	226.0	305.4	387.5
MWD**	0.	363.5	730.9	1860.7	2247.4	3037.	3850
U235 burnt	0.	.05	.10	.25	.30	.40	.50
Garrison	1.5594	1.4728	1.4549	1.3972	1.3764	1.3287	1.2737
Iijima	1.5594	1.4748	1.4559	1.3933	1.3712	1.3204	1.2625
VSOP25*	1.5594	1.4753	1.4571	1.3971	1.3760	1.3273	1.2715
VSOP40*	1.5594	1.4743	1.4550	1.3914	1.3691	1.3179	1.2595

Note * The cross sections for pseudo FP's in VSOP models are temporary.

** The discrepacy appearing between MWD and Days multiplied by the fixed power of 10 MW is attributed to the deviation of flux level during the sub-step where constant flux is assumed.

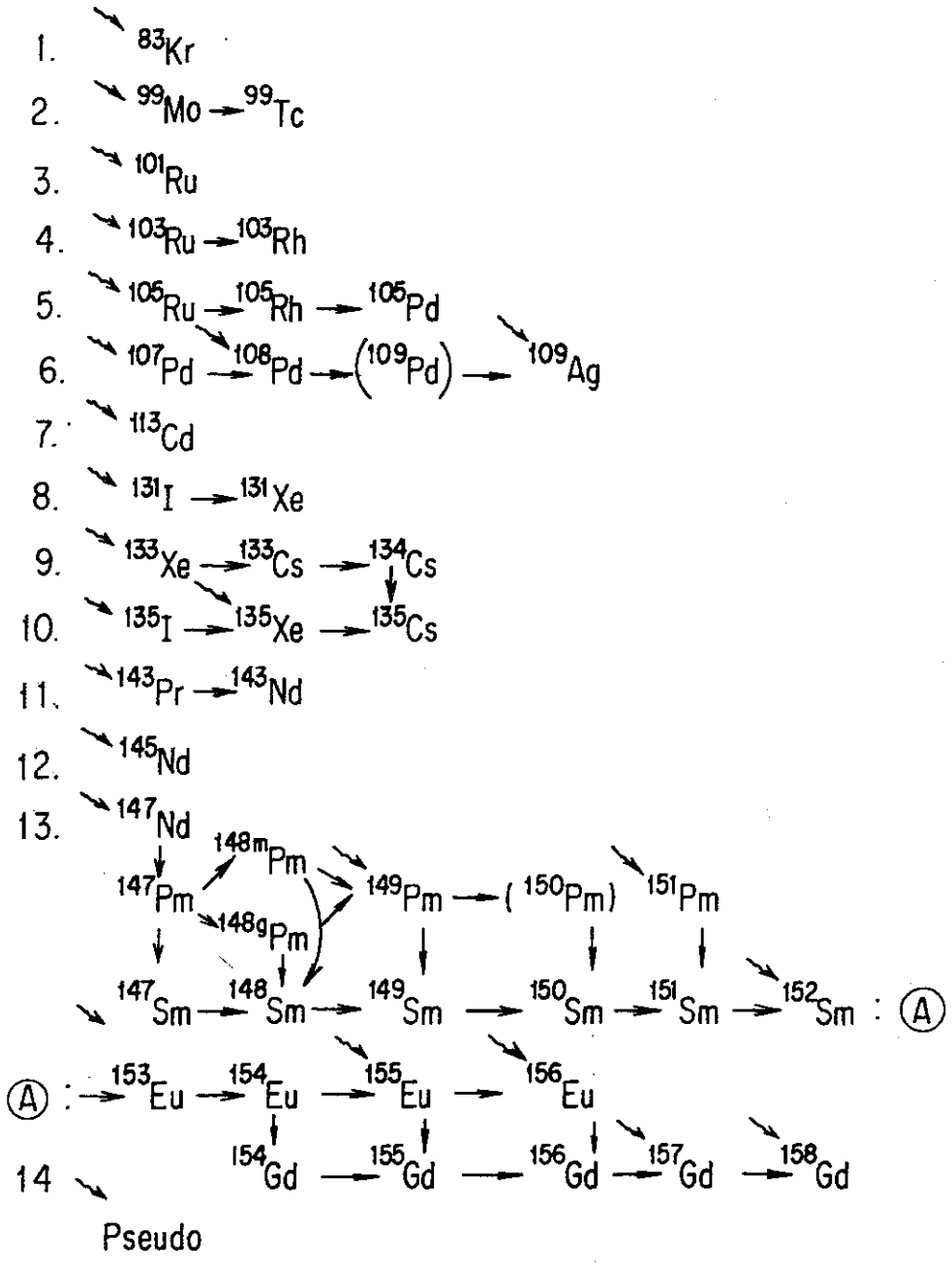

Fig. 2.3.1 Chain scheme of Iijima model

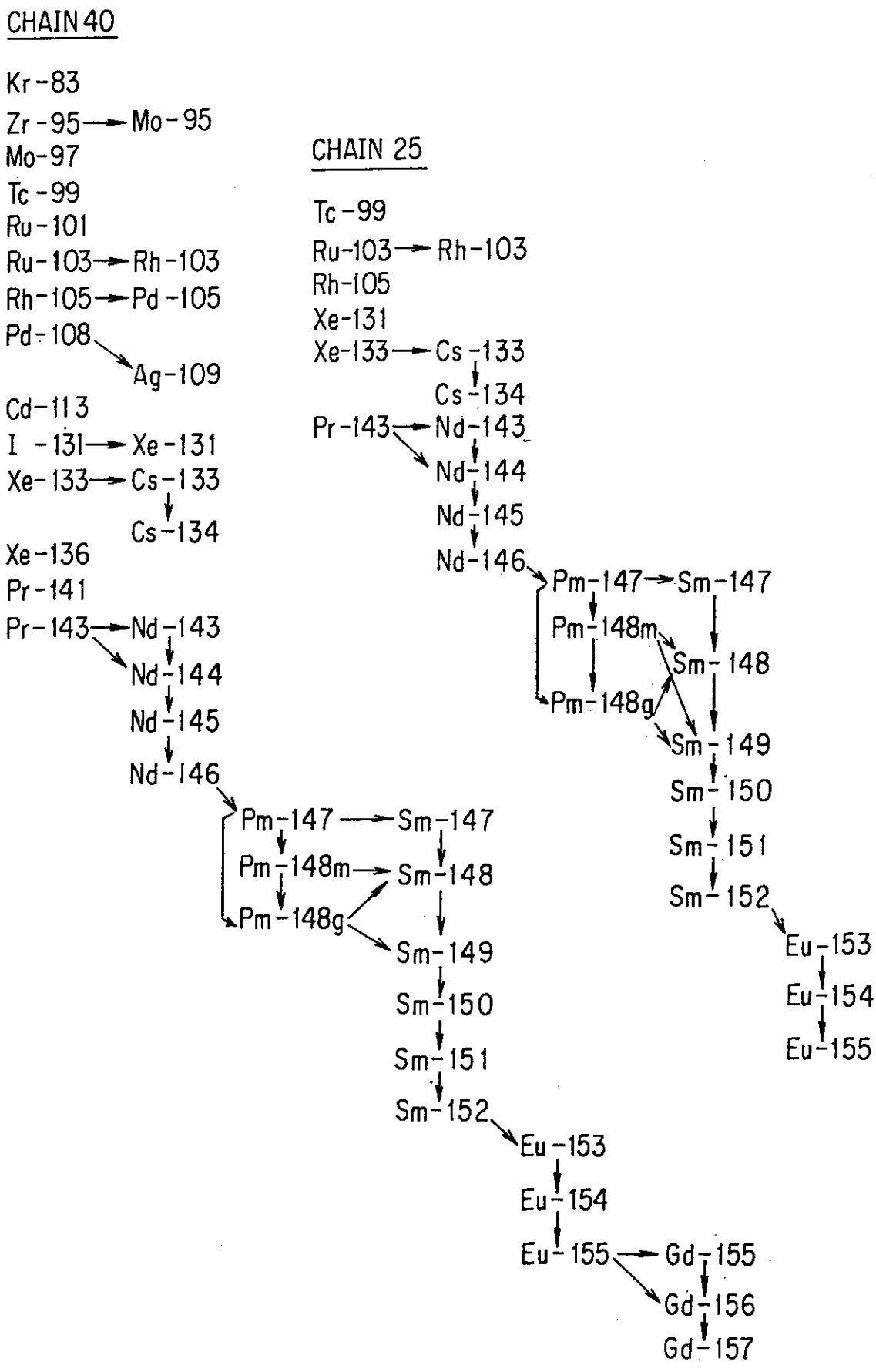

Fig. 2.3.2 Chain schemes of VSOP models

2.4 Estimations of Non-linear Response of Neutron Flux to Reactivity Noise, and of Reactivity Change by Displacement of Absober Plate

Y. Gotoh and H. Yasuda

The space-time dependent integral equation for neutron is developed to study the reactor Kinetic problems which include the vibration of absorber plate and the non-linear response effect to reactivity noise, for example[1].

By using the diagrammatic technique of field theory, a modified Green function of infinite system which has reactivity noise, has been defined. The Green function of finite reactor can be obtained by the image method. To analyze the covariance function of neutron flux, the following assumptions are made[1]. The Green function should be dressed with noise cloud. The ladder type diagrams only contribute to the covariance function. The covariance function satisfies an integral equation which leads to an integral equation for cross power spectral density. This equation is an extension of the one for point reactor which was obtained previously[2].

Applications of this integral equation to the variable strength absorber problem and to the neutron noise field in BWR are made. To take into accounts the local and global concept, the present method is extended to two group theory as developed in linearized theory by Kosaly, Behringer and others, to parametric excitation. Since the major contribution to noise comes from the fluctuation of the removal cross section, the simple integral equations for CPSD of fast and thermal fluxes, are obtained.

The contribution to neutron fluctuation by non-linear response is evaluated numerically by using the point reactor model. A simple exponential cosine correlation function of reactivity noise was used in the evaluation. The calculated results are shown in Table 2.4.1, where Δ is the amplitude of noise, ω_0 is the frequency of oscillation, τ is the correlation time of noise, $|ka|$ and $||ks||$ are the norms of integral kernel, and Ra is the ratio of the doubly integrated term of fourth power of Δ to the integrated term of the square power. It can be seen that for the noise whose correlation time is short, the correction to the variance to mean squared ratio of linear response is small, but for the oscillatory noise of long correlation time, the correction is rather

large, and that the power which is inversely proportional to (kc^*-kc), increases the correction grows.

To analyze the absorber plate vibration problem, the reactivity change due to the displacement of absorber plate is evaluated[3]. The plate is assumed very thin, and Galanin's constant is adopted as the absorber cross section multiplied by the width of plate. The integral equations for CPSD to rod vibration problem are formulated, which are complete provided that the reactivity change due to rod vibration is precisely known.

It is found that the two group theory is required to improve the description of flux depression around the plate. To extend the analysis of vibrating absorber plate problem, a space-time dependent treatment is now in progress.

References

1) Gotoh Y. : Progr. Nucl. Energy, 9, 303 (1981).
2) Gotoh Y. : Ann. Nucl. Energy, 2, 119 (1975).
3) Gotoh Y., Yasuda H. : Annual Meeting of the Atomic Energy Society of Japan (1982).

Table 2.4.1 Calculated results by integral equation of PSD

Δ ($)	ω_0 (Hz)	τ (sec)	k_c ($)	k_c^* ($)	variance / mean squared	$\|Ka\|$	Ra	$\|\|Ks\|\|$
0.02	0	1	-0.001	-0.0004	0.07	0.07	0.07	0.07
0.03	0	0.5	-0.002	-0.0009	0.04	0.04	0.04	0.04
0.02	3	5	-0.0005	-0.00038	0.006	0.86	0.29	0.02
0.02	3	5	-0.0004	-0.00038	0.02	0.86	0.68	0.05

Foot note

Integral equation for PSD is

$$\Phi(\omega) = |\bar{G}_m(i\omega)|^2\bar{D}(\omega) + \int_{-\infty}^{\infty} K_a(\omega,\omega')\Phi(\omega')d\omega' \quad ,$$

where Ka is an asymmetric kernel

$$K_a(\omega,\omega') = |\bar{G}_m(i\omega)|^2\ \bar{D}(\omega-\omega')/2\pi \quad .$$

Fourier transform of reactivity correlation function is given by

$$\bar{D}(\omega) = \Delta^2[1/\{1+\tau^2(\omega+\omega_0)^2\} + 1/\{1+\tau^2(\omega-\omega_0)^2\}] \quad .$$

Variance to mean-squared ratio of power P is defined by

$$\langle(P-\langle P\rangle)^2\rangle/\langle P\rangle^2 = \frac{1}{2\pi}\int d\omega\ |\bar{G}_m(i\omega)|^2\bar{D}(\omega) \quad .$$

Ratio of contribution of Δ^4 to that of Δ^2 is

$$R_a = \int d\omega \int d\omega'\ K_a(\omega,\omega')|\bar{G}_m(i\omega')|^2\ \bar{D}(\omega') \,/\, \int d\omega\ |\bar{G}_m(i\omega)|^2\ \bar{D}(\omega) \quad .$$

Δ = Amplitude of noise,
ω_0 = Frequency of oscillation noise,
τ = Correlation time of noise,
kc = Excess reactivity in $,
kc^* = Excess reactivity of critical state in $,
$|ka|$ = Norm of asymmetric integral kernel,
$||ks||$ = Norm of symmetric integral kernel.

2.5 Improvements of a Double Finite Element Method Program for Solving Three-Dimensional Multi-Group Neutron Transport Equation

T. FUJIMURA, Y. NAKAHARA and M. MATSUMURA*

From the necessity of safety assesments of irregular-shaped nuclear fuel facilities, we have developed a three-dimensional multi-group neutron transport code by means of the DFEM (Double Finite Element Method), in which both the space and angle finite elements are employed[1)2)]. In the algorithm, the g-th group flux ψ^g is approximated by

$$\psi^g(r,\Omega) = \sum_{i=1}^{I} \sum_{j=1}^{6} c_{ij}^g \, \phi_i(r) \, \chi_j(\Omega)$$

where $\phi_i(r)$ and $\chi_j(\Omega)$ are spatial and angular base functions, respectively. We can obtain the $I \times 6$ algebraic equations for c_{ij}^g by the Galerkin method as

$$A_{iji'j'}^g \, c_{i'j'}^g = b_{ij} \qquad (1)$$

which is solved applying the boundary conditions.

For simplicity, let us cosider the case where the front boundary is vacuum. The condition is given by $c_{i3}^g = 0$, where the c_{i3}^g is the nodal value for inward direction at the i-th point as shown in Fig. 2.5.1. If the condition is reflective, it is given by $c_{i3}^g = c_{i5}^g$. The $((i-1) \times I+3)$-th equation in Eq. (1) is then replaced by either of these equations.

Spatial nodes on a boundary edge and vertex, however, have two and three normal directions, respectively. In the original scheme, priority is given to one of the directions. On the other hand, all the normal directions at the node on the edge or vertex are taken into consideration in the second scheme. The effects of these schemes on the flux distribution are examined in sample calculation given later.

Acceleration method of outer iteration is similar to the extrapolation method used in the GAUGE code developed by Wagner[3)], but some improvements have been made. Let f be the fission operator defined as

* I.S.L. Co. Ltd., Tokyo

$$f(\psi) = \sum_{g=1}^{G} \nu\sigma_f^g \phi^g(r) \quad ,$$

where ϕ^g is the g-th group scalar flux. In the usual FDM calculation, element-averaged flux $\overline{\phi^g}$ is used in place of ϕ^g. But the FEM performs exact calculation by

$$f(\psi) = \sum_{g=1}^{G} \frac{\nu\sigma_f^g}{4\pi} \sum_{i=1}^{I} \sum_{j=1}^{b} c_{ij}^g \int_{\Omega} \chi_j(\Omega) d\Omega \, \phi_i(r) \quad .$$

Sample Calculation

In order to illustrate the above discussions, a cubic homogeneous reactor is taken up and shown in Fig. 2.5.2. We have proposed two different treatments on the boundary conditions. As seen in Fig. 2.5.3, the first group flux obtained by the original scheme is lower at the center than in its neighborhood, but the modified scheme gives the reasonable flux distribution near the boundary.

This model problem is used for source extrapolation. The iterations was performed to attain the accuracy

$$\varepsilon_o = |\lambda_\ell - \lambda_{\ell-1}| / \lambda_\ell \qquad (2)$$

less than 10^{-5}, where the λ_ℓ is the eigenvalue in the ℓ-th outer iteration. As shown in Fig. 2.5.4, about one-third iteration was saved by the proposed method against no extrapolation.

References

1) Kaper, H.G., Leaf, G.K., Lindeman, A.M. : "Application of Finite Element Methods in Reactor Mathematics. Numerical Solution of the Neutron Transport Equation," ANL-8126 (1974).
2) Ise, T., Yamazaki, T., Nakahara, Y. : "FEM-BABEL, A Computer Program for Solving Three-Dimensional Neutron Diffusion Equation by the Finite Element Method," JAERI-1256 (1978).
3) Wagner, M.R. : "GAUGE A Two-Dimensional Few Group Neutron Diffusion-Depletion Program for a Uniform Triangular Mesh," GA-8307 (1968).

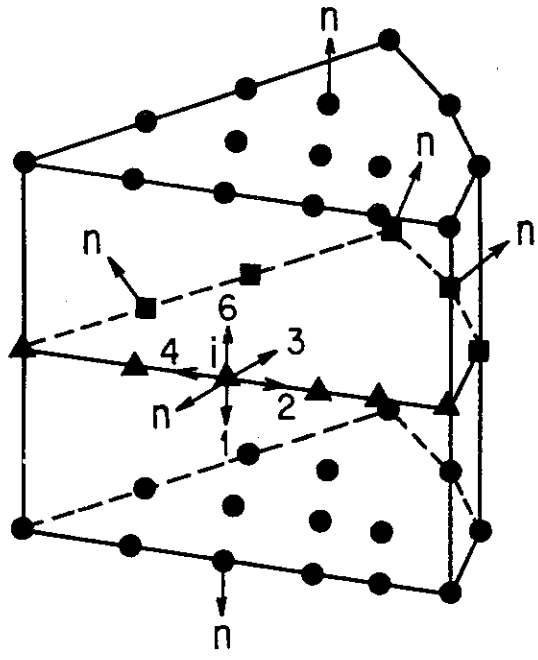

Fig. 2.5.1 Normal directions based on the original scheme for a node arrangement. Dots show the nodes on the top and bottom boundaries. Triangles and squares show the nodes on the front and back boundaries, respectively.

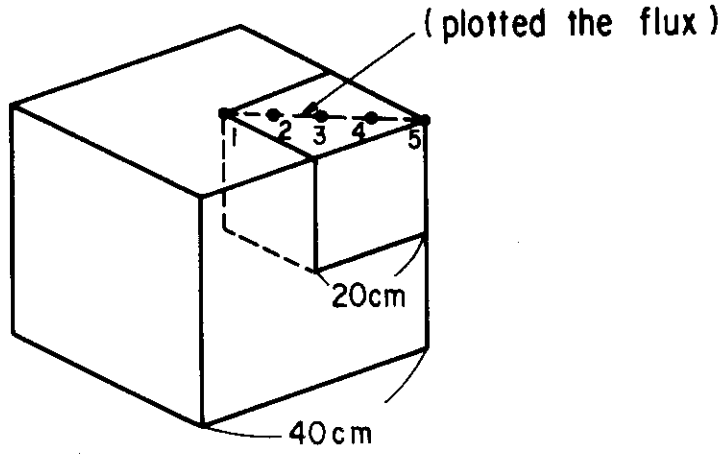

Fig. 2.5.2 A cubic homogeneous reactor which is used in sample calculation.

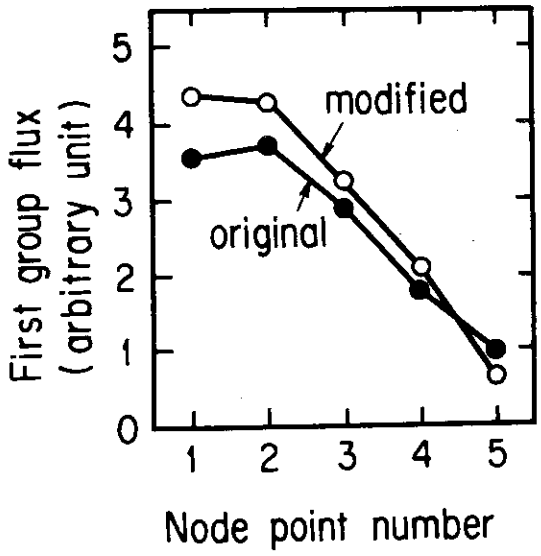

Fig. 2.5.3 Comparison of two schemes on the boundary conditions in the first group flux along a line as shown in Fig. 2.5.2

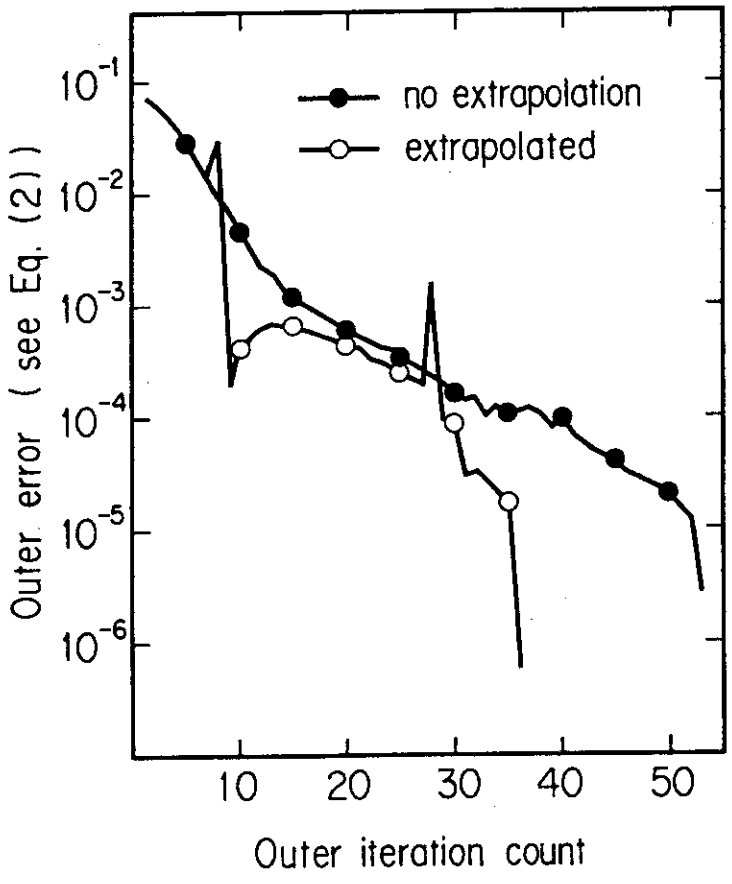

Fig. 2.5.4 Acceleration of the outer iteration convergence by exact source extrapolation.

2.6 Evaluation of Computational Models for Spallation and Fission Reactions

Y. Nakahara and T. Tsutsui

In order to prepare computational tools for the feasibility studies of accelerator driven nuclear fuel producers and radiactive waste transmuters, a code system ACCEL[1] has been developed. The reliability of the code system as a whole has been shown in reasonable agreements between computed and measured neutron yields for various types of target/blanket systems[2]. But this does not necessarily guarantee the accuracy of each of the various computational models employed in ACCEL. The most important and foundamental physical processes in the target/blanket are spallation and fission reactions. The spallation reaction, as progammed in the NMTC code[3], is computed usually as a two step process of intra-nuclear cascade and subsequent particle evaporation. The fission is considered to occur in competition with the evaporation after the high energy nucleon cascade through a nucleus. A computational model based on the statistical model of fission has been incorporated by us in NMTC/JAERI[4].

The computational models for the spallation and fission reactions have been evaluated by performing computations with NMTC/JAERI for thin targets where multiple inter-nuclear collisions can be neglected. Non-elastic and fission cross sections have been derived from counts of real collisions and fission events recorded as the final results of the NMTC/JAERI computations.

Dependence of the non-elastic cross sections on the masses of target nuclei are shown in Fig. 2.6.1 for neutrons with incident energy of 960 MeV in comparison with experimental values due to Shimmerling et al.[5]. Flags attached to computed values show examples of variances in the Monte Carlo countings. Agreement is reasonable over a wide range of nuclear masses. The discrepancy seen for light nucleus such as carbon may be due to a failure of the models, especially of the statistical model. As for the somewhat scattered values for heavy nuclei, intensive computations with as many histories as possible are necessary to give definite explanations. Energy dependence of the non-elastic cross section for U-238 is shown in Fig. 2.6.2, together with the fission cross section. The minimum seen for $\sigma_{\text{non-elastic}}$ around 200 MeV

corresponds to that of the p-p total cross sections used in the cascade calculation.

It has been shown in the parametric studies that the most crucial parameters in computing the fission cross section are the level density parameters in the statistical theory, i.e., a_f and a_n appropriate to the saddle point of fission and equilibrium deformation, respectively. The best fit, as shown in Fig. 2.6.2, has been obtained with the expressions :

$$a_n = A/10$$

$$a_f/a_n = aE^2 + bE + c \quad ,$$

where $a = 1.10107 \times 10^{-7}(\mathrm{MeV})^{-2}$, $b = -2.12189 \times 10^{-4}(\mathrm{MeV})^{-1}$ and $c = 1.11208$, which were derived by fitting the parameters to the data due to Il'inov et al.[6].

References

1) Nakahara Y., Tsutsui T. and Taji Y. : "Reactor Engineering Division Annual Report (April 1, 1980 - March 31, 1981)," p.48, JAERI-M 9672 (1981).
2) Nakahara Y. : Proc. ICANS-IV, Tsukuba, p.289, KENS Report II (1981).
3) Coleman W.A. and Armstrong T.W. : "NMTC Monte Carlo Nucleon Meson Transport Code System," RSIC CCC-161.
4) Nakahara Y. and Tsutsui T. : to be published as JAERI-M in the near future.
5) Schimmerling W., et al. : Phys. Rev.C, 7, 248 (1973).
6) Il'inov A.S., et al. : Sov. J. Nucl. Phys., 32, 166 (1980).

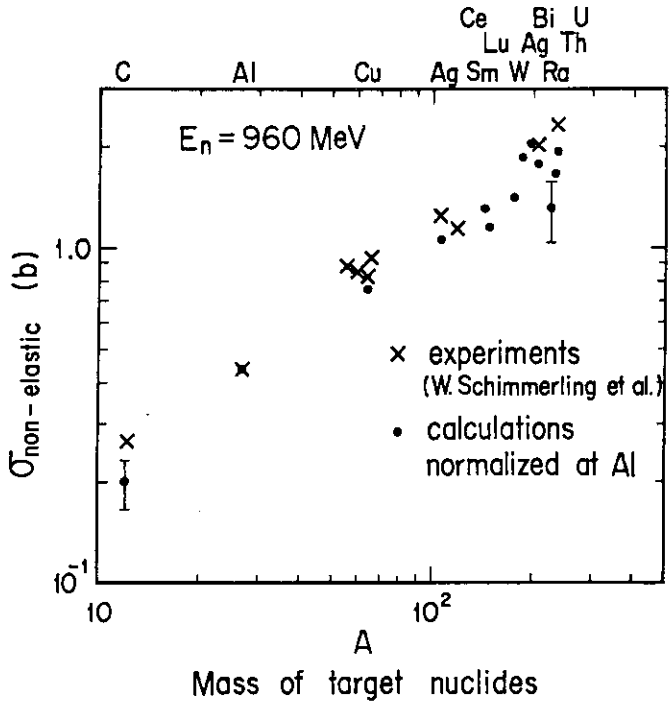

Fig. 2.6.1 Dependence of neutron non-elastic cross sections on masses of target nuclei

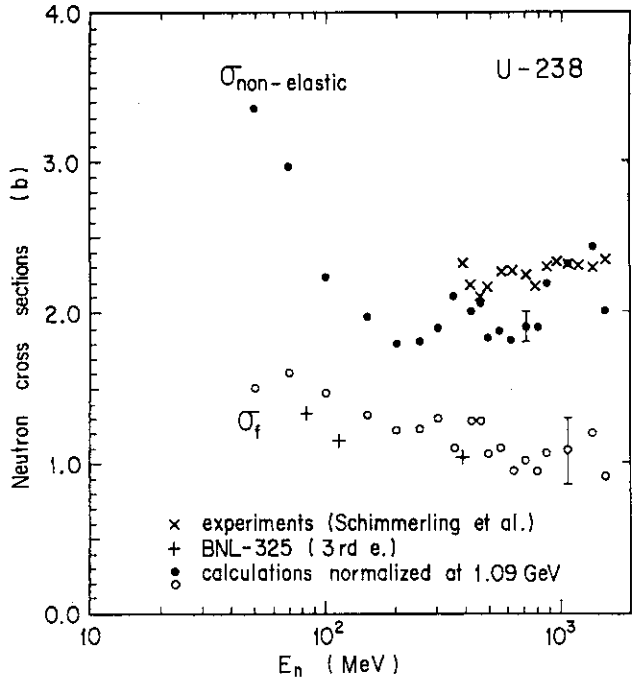

Fig. 2.6.2 Dependence of neutron non-elestic and fission cross sections of U-238 on incident energies

2.7 Extension of the Nucleon Meson Transport Code NMTC/JAERI for Actinide Transmutation Analysis

Y.Nakahara and T.Tsutsui

A code system NMTC/JAERI has been developed for the Monte Carlo simulations of spallation-fission reactions and nucleon-meson transport processes in the energy range higher than the cutoff which is usually taken to be 15 MeV[1]. NMTC/JAERI has been successfully used in the feasibility analyses of accelerator deriven nuclear fuel producers. Its applicability, as well as NMTC[2], however, is limited to the mass range of target nuclei up to 239. For the purpose of transmutation analyses of actinide nuclei such as Am-241 and Cm-242, NMTC/JAERI has been revised anew and the mass range of target nuclei has been extended up to 250.

Foundamental nuclear parameters required in the simulation calculations of nuclear reactions are nuclear structure data such as nuclear radius, nucleon density distribution and potential energy distribution for each nucleus. Because nucleons in the nucleus are assumed to be degenerate Fermions, potential energy is taken to be the Fermi energy plus the binding energy of the most loosely bound nucleon. The internal region of a nucleus is divided by three concentric spheres. The nucleon density in each region is set equal to average value of the continuous distribution in that region. The region boundaries are taken to be the same for neutrons and protons. The Fermi energy in each region is the zero-temperature Fermi energy of nucleons in that region. The binding energy of the most loosely bound nucleon is taken to be 7 MeV for all regions and for all nuclei.

Additional numerical values of the nuclear structure data are summarized in Table 2.7.1, where three numerical values for each parameter correspond to the central, middle and outermost regions in a nucleus. The nucleon density and the Fermi energy in each region are obtained in the code from the values in the Table with the use of the following

relation :

the neutron density , $\rho_i^n = \rho_i(A-Z)$,

the proton density , $\rho_i^p = \rho_i Z$,

the neutron Fermi energy , $E_i^n = U_i(A-Z)^{2/3}$,

the proton Fermi energy , $E_i^p = U_i Z^{2/3}$,

where $i = 1,2,3$, ρ_i and U_i being density and potential parameters given in the Table, respectively. A-Z and Z are the number of neutrons and protons in a nucleus, respectively.

References :

1) Nakahara Y. and Tsutsui T. : to be published as JAERI-M in the near future.
2) Coleman W.A. and Armstrong T.W. :"NMTC Monte Carlo Meson Transport Code System," RSIC CCC-161.

Table 2.7.1 Supplemented nuclear structure data

A	Nuclear radii (10^{-13}cm)	Nucleon density parameters (10^{30}/cm)	Nucleon potential parameters (MeV)
240	5.456 7.413 9.166	7.434 4.137 4.611	1.631 1.103 .2553
241	5.463 7.424 9.179	7.403 4.121 4.592	1.626 1.100 .2545
242	5.471 7.434 9.192	7.378 4.104 4.574	1.621 1.096 .2537
243	5.478 7.442 9.204	7.348 4.088 4.556	1.617 1.094 .2531
244	5.486 7.455 9.217	7.319 4.072 4.538	1.613 1.091 .2525
245	5.493 7.464 9.229	7.289 4.055 4.319	1.608 1.087 .2517
246	5.501 7.475 9.242	7.260 4.039 4.501	1.604 1.085 .2511
247	5.509 7.485 9.255	7.230 4.022 4.483	1.600 1.082 .2504
248	5.516 7.495 9.267	7.202 4.006 4.465	1.595 1.079 .2497
249	5.523 7.506 9.280	7.173 3.990 4.447	1.591 1.076 .2490
250	5.531 7.515 9.292	7.144 3.974 4.429	1.587 1.073 .2484

2.8 Effects of Chromatic Aberration of Objective Lens and Misorientation of a Crystal on High Resolution Images of Simple Defects in Silicon

T. Nishida and K. Izui

We have already reported some results[1),2)] of our studies in high resolution electron microscope images of a point defect cluster by means of computer simulations based on the multi slice method used for images of non-periodic objects, including a simple defect.[3)] For the existing instruments of an electron microscope, it is impossible to remove completely distortions of lattice images due to chromatic aberration of objective lens and slight misorientation of a specimen.[4)] Then, their effects on images of a defect in a silicon crystal oriented in (110) are examined in the present paper. On the other hand, perfect lattice images of silicon misoriented slightly are computed by the matrix method[5)] and multi slice method, respectively, and compared with each other to confirm the collimation of electron beams diversing along the crystal axis.

a) Effect of chromatic aberration

The distortion of images due to chromatic aberration may be estimated with a function of the defocus fluctuation arising from fluctuations in both electron energy and magetic lens current. On the assumption of Gaussian distribution for the defocus fluctuation, the image intensity of a crystal defect is also given as the incoherent average over the defocus region around the imaging defocus, that is, Scherzer focus of 510 Å in the present work. Figure 2.8.1 shows images of a divacancy cluster [3P4V_2^R 3P] (*) with relaxation of atoms simulated for half-width increments of 40 Å for the defocus distribution. As seen in the achromatic image (h.w. = 0) of Fig. 2.8.1 (a), the intensity for pairs of atomic rows including a divacancy cluster 4V_2^R at the center position of the cell is obviously weaker than that for other atom pairs. For values of half width less than about 100 Å, a clear representation of the form of

---

(*) This symbol denotes four slices containing a divacancy with relaxation, sandwiched between three upper slices and three lower slices of perfect lattice layer.

divacancy is observed, whereas, for the larger values, all atom pairs become one bright oval spots. Then, we find that Scherzer focus images of a divacancy cluster are relatively stable to the disturbance due to chromatic aberration.

b) Effect of slight misorientation of a crystal

When the axis of a crystal is slightly tilted from the direction of incident beams, the wave function should be modified in the procedure of the convolution integral which calculates the behavior of an electron transmitting through a crystal before scattered electron waves form an image through objective lens. The images of a defect cluster tilted to the $<2\bar{2}0>$ direction with an angle $\sim 3 \times 10^{-3}$ rad are computed for two clusters with four and ten slices of a divacancy in crystal thicknesses of ten and thirty slices, respectively, as shown in Fig.2.8.2 (a)$\sim$(d). In the formation of images of the thin cluster under ideal lens condition ($\Delta f = 0$Å, $C_s = 0$mm), they give good representations of divacancy and perturbed lattice atoms around it with about 40 percent contrast. For the thicker cluster, however, their contrasts reduce to about 10 percent as a result of crystal misorientation. From the Scherzer focus image of the thin cluster in Fig.2.8.2 (c), we can recognize the presence of divacancy but obtain no informations about relaxation of atoms around it. As seen in Fig.2.8.2 (d), however, ghost peaks appear in the interatomic space of the image formed under aberration free defocus condition ($\Delta f = -68$Å, $C_s = 0.7$mm), preventing the identification of tne original defect structure model. It becomes evident that the adjustment of orientation of a crystal with much higher accuracy is necessary for the case of a relative thick defect cluster to obtain its clear structural image.

c) Estimation of behavior of scattered electrons by the matrix and multi slice methods

Comparisons among the images calculated by both methods were carried out for a silicon perfect crystal with thickness $\sim$130Å, in which the axis tilts slightly to the $<00\bar{4}>$ direction (right direction on the figure) from the beam direction. Figures 2.8.3 and 2.8.4 show the computed images with tilt angles 1.7×10^{-3}, 2.3×10^{-3} and 3.4×10^{-3} rad under conditions of ideal lens ($\Delta f = 0$, $C_s = 0$) and aberration free defocus ($\Delta f = -68$Å, $C_s = 0.7$mm), respectively. The differences between contrasts of each atom in

pairs and the distances between pair atoms represent good agreements among the corresponding images of both calculations. It can be concluded that the behavior of scattered electrons seen in these images has no appreciable difference, regardless of our expectation that we can calculate more exactly the fine derail of electron scattering by the matrix method than by the multi slice method.

References

1) Nishida T., Izui K., Furuno S., Otsu H.:"High Resolution Structure Images of a Simple Defect in a Silicon Crystal Oriented in (110)," JAERI-M 9032, 39 (1980).
2) Nishida T., Izui K.:"High Resolution Electron Microscopy of Simple Defects in a (110) Silicon Crystal," JAERI-M 9672, 59 (1981).
3) Field P.M., Cowley J.M.: Acta Cryst., A34, 103 (1978).
4) Nishida T.:"Electron Optical Conditions for the Formation of Structure images of Silicon Oriented in (110)," Jpn. J. Appl. Phys., 19, 799 (1980).
5) Nishida T., Izui K.:"MSCOPE-I : A Program System for Analyzing the Electron Microscope Images of Crystal Lattice Defects," JAERI-M 5441 (1973) (in Japanese).

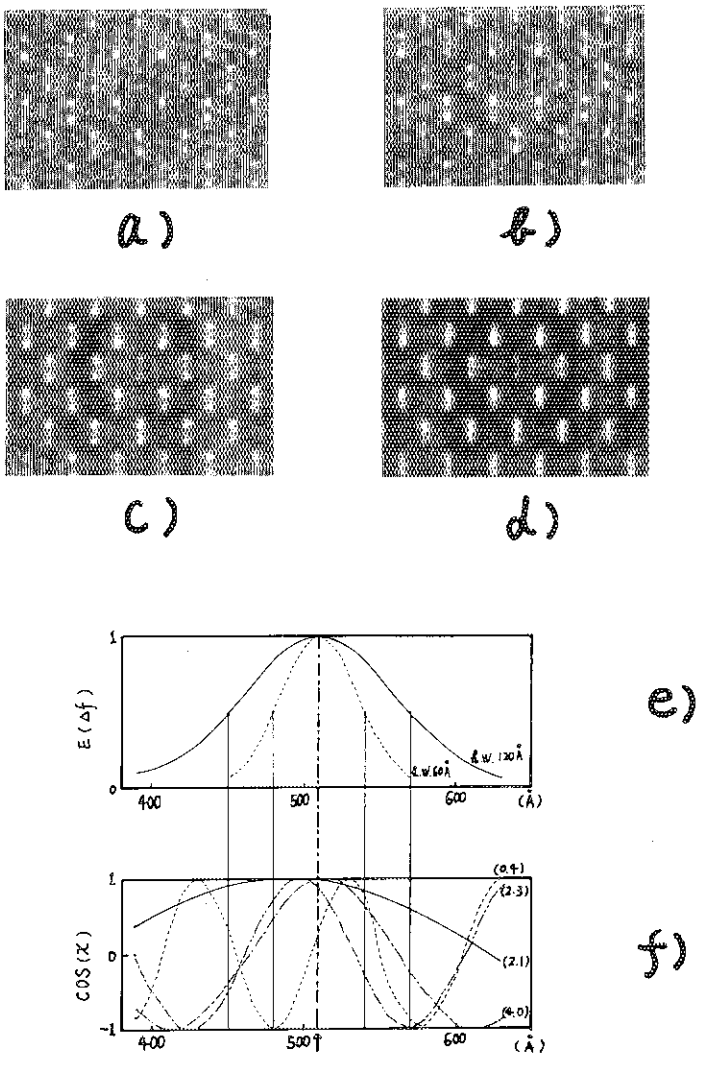

Fig. 2.8.1 a)～d) are divacancy cluster images influenced by the defocus fluctuation due to chromatic aberration with crystal thickness ～ 35Å under Scherzer focus condition (Δf = 510Å, C_s = 0.7mm) at 100 KV. Half-widths of Gaussian distribution, h.w. are given to be a) 0Å, b) 40Å, c) 80Å and d) 120Å. Profiles in e) and f) represent the corelation between the distributions and real parts of lens transfer function for main scattered waves around Scherzer focus.

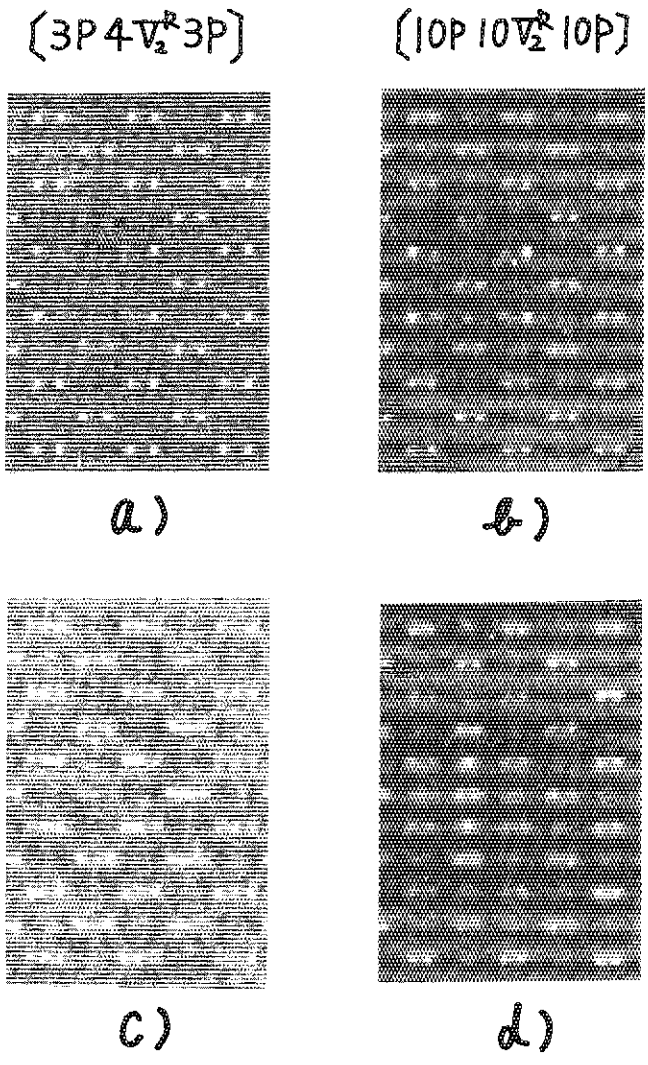

Fig. 2.8.2 Simulated images of divacancy clusters of [3P4V$_2^R$ 3P] and [10P10V$_2^R$ 10P] misoriented with the angle $\sim 3 \times 10^{-3}$ rad under optical conditions, a), b) $\Delta f = 0$, $C_s = 0$, c) $\Delta f = 510$Å $C_s = 0.7$mm and d) $\Delta f = -68$Å, $C_s = 0.7$mm.

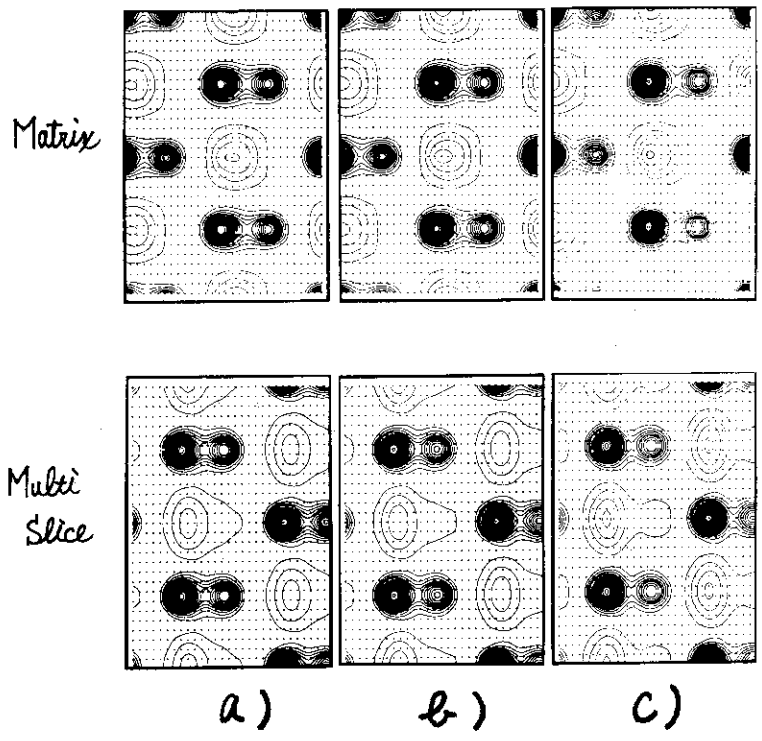

Fig. 2.8.3 Images of perfect lattice of silicon tilting to <00$\bar{4}$> axis with slight angles a) 1.7 x 10^{-3} rad, b) 2.3 x 10^{-3} rad and c) 3.4 x 10^{-3} rad under the ideal lens condition ($\Delta f = 0$, $C_s = 0$).

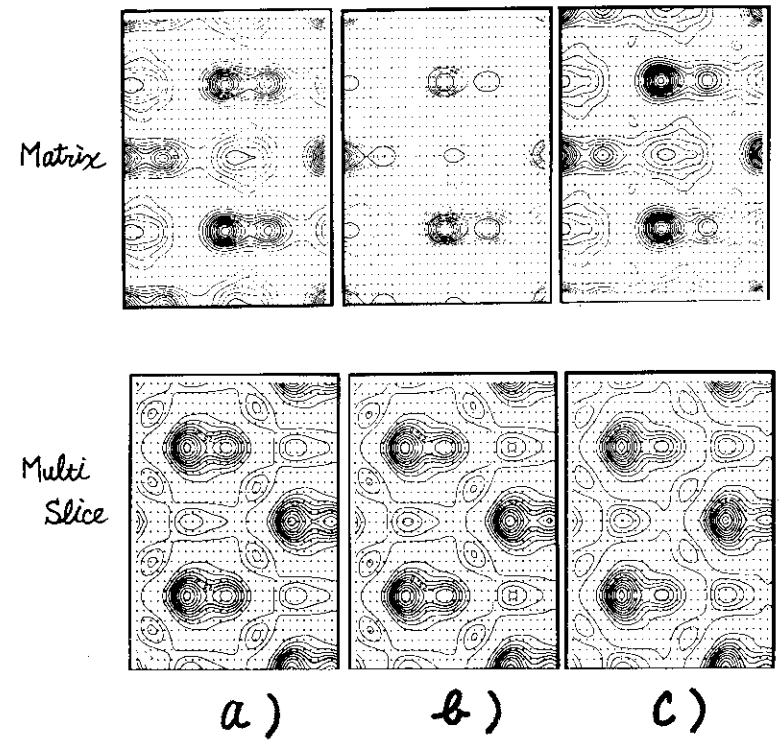

Fig. 2.8.4 Images of perfect lattice of silicon tilting to <00$\bar{4}$> axis with slight angles a) 1.7 x 10^{-3} rad, b) 2.3 x 10^{-3} rad and c) 3.4 x 10^{-3} rad under an aberration free defocus condition ($\Delta f = -68$Å, $C_s = 0.7$mm).

2.9 Analyses of Radiation Damages by Computer Simulation

Y. Taji

Charged atomic projectiles (ions) emerge in the structural materials due to the knock-on reaction by fast neutrons or due to the direct entrance of hot plasma ions. To estimate formation or growth of defects induced by the energetic ions it is very important to attack the transport problem of ions in materials. In order to decrease the radiation damages as low as possible it is desirable to disperse the energy of ions spatially as extensively as possible in the form of inelastic loss.

Then we have simulated the spatial distributions of defects in depth direction which are yielded by ions of carbon injected perpendicularly to the surface of target. As the test material of target iron containing carbon by 1% in atom number has been chosen to compare with the case of pure iron (f.c.c. crystal). The impurity carbon have been located at the lattice sites. Two methods are known to analyze the displacement cascade of atoms, i.e., the method based on the LSS theory and the method of computer simulation based on the mechanics of binary collision. However, the former one is difficult to give meanigful differences between the two cases since the atomic masses are averaged uniformly.

Simulations have been performed by reorganizing the code system CASCMARL[1], which consists of MARLOWE[2] for analysis of cascade, CLUSTER[3] for spontaneous recombination and DAIQUIRI[3] for annealing calculation. The Thomas-Fermi potential is used in the Moriere approximation. As the electronic stopping power the Lindhard model is adopted. The ion of carbon is injected with energy 1 MeV perpendicularly to the surface (3,4,7). The total number 243 of ions are injected into both targets. The displacement threshold energy E_d is 40 eV for ion and 3 eV for carbon and the binding energy are set half of E_d's. The cut-off energy is 40 eV.

The results of cascade calculation for the pure iron and the iron containing 1% carbon are surmarized briefly in Table 2.9.1, in which the first column is the average rate of damage energy, the second one the average number of vacancy produced by an ion injection and the third one the average depth of spatial distribution of vacancies. The spatial distributions of vacancies in depth direction for the pure iron and the iron containing carbon are shown in Fig. 2.9.1 and Fig. 2.9.2, respectively. The spatial distributions of rest position of ions which are

injected from the surface are shown in Fig. 2.9.3 and Fig. 2.9.4. The calculation of spontaneous recombination and, furthermore, the annealing calculation by 10 time steps are performed, which are summarized in Table 2.9.2. We can conclude from these results that the mixture of light atoms play the role of decreasing the formation of defects by dispersing the energy of incident ions in a wider region. The remaining problems are follows : The impurity carbons must be set at the interstitial position though they have located at the lattice site in the present calculation and the effect of heavy irradiation must be taken into account.

References

1) Asaoka T., et al. : "Computer Codes for Simulating Atomic-Displacement Cascades in Solids Subject to Irradiation," JAERI-M 8179 (1979).
2) Robinson M.T., et al. : Phy. Rev. B9 (5008) 1974.
3) Besco D.G., et al. : "CASCADE and CLUSTER-Computer Programs to Simulate Radiation Damage Processes in Metals and Analyze the Distribution of Defects," GEMP-356 (1965); "Computer Simulation of Point Defect Annealing in Metals," GEMP-644 (1967).

Table 2.9.1 Calculation results of cascade in the pure iron and the iron containing carbon

	No. of vac.	Depth (Å)	Damage Ene.
Pure iron	663	7028	7.61%
C^{12}-iron	619	7550	6.96%

Table 2.9.2 Number of vacancies and interstitials per an ion injection at each calculation steps of cascade, spontaneous recombination and annealing of 10 time steps

	Pure iron		C^{12}- iron	
	No.of vac.	No.of int.	No.of vac.	No.of int
Cascade	663	664	619	620
Spont.Recomb.	271	272	253	254
Anneal	161	162	150	151

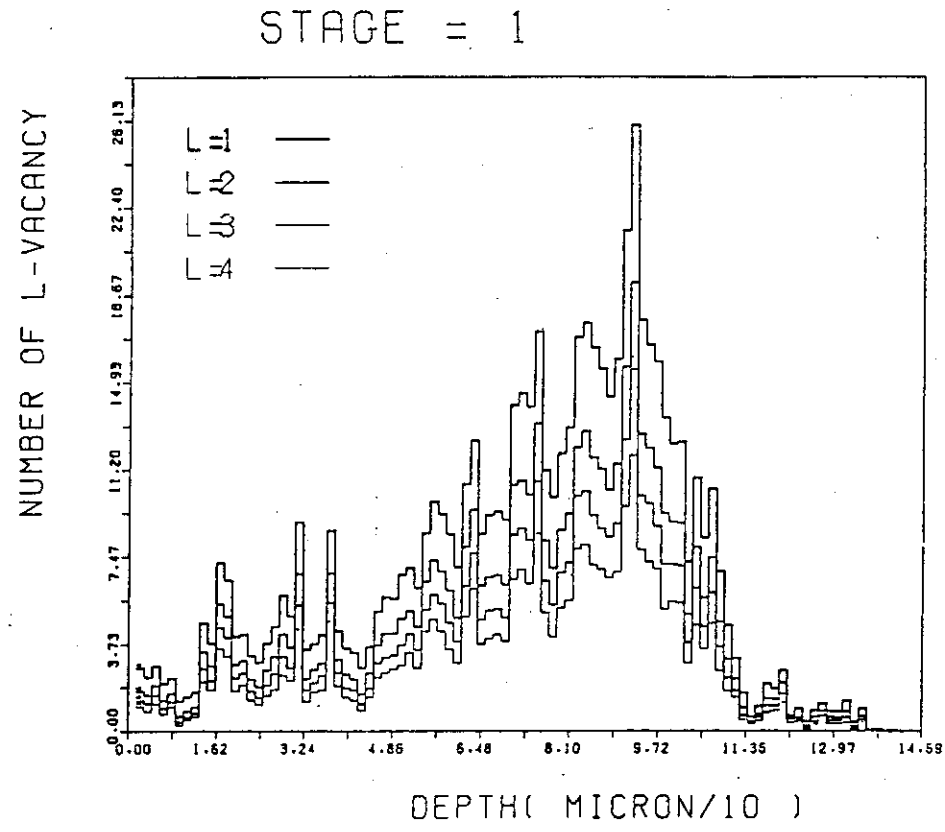

Fig. 2.9.1 Spatial distribution of vacancies in depth direction in the pure iron per an ion injection.

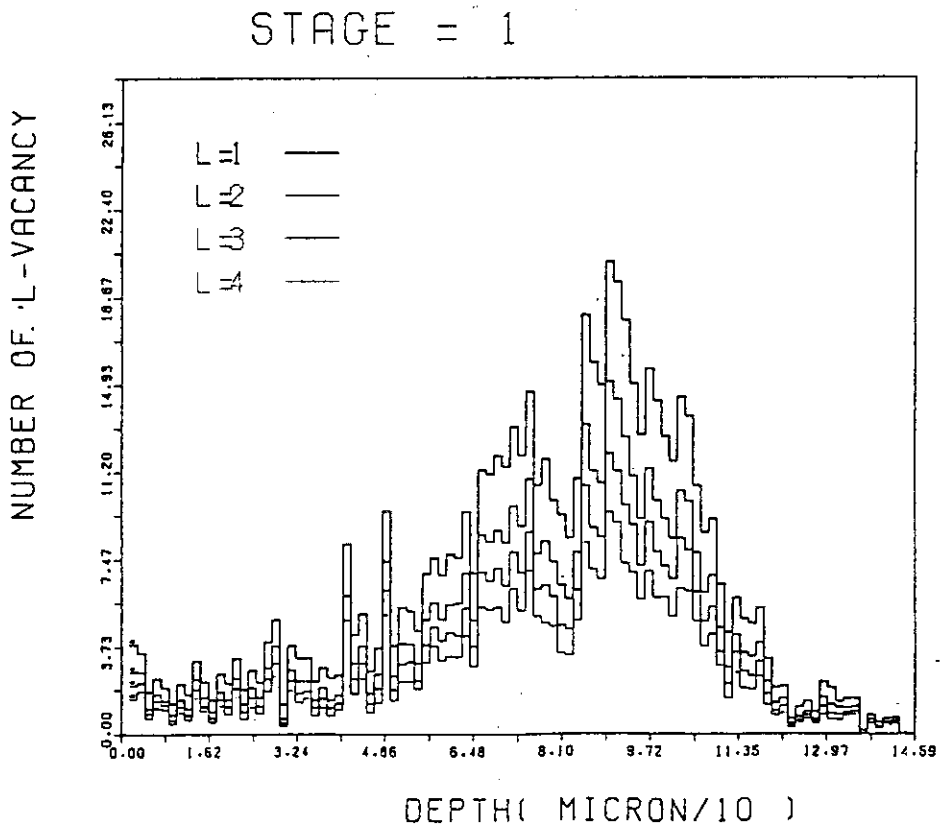

Fig. 2.9.2 Spatial distribution of vacancies in the depth direction in the iron containg carbon per an ion injection.

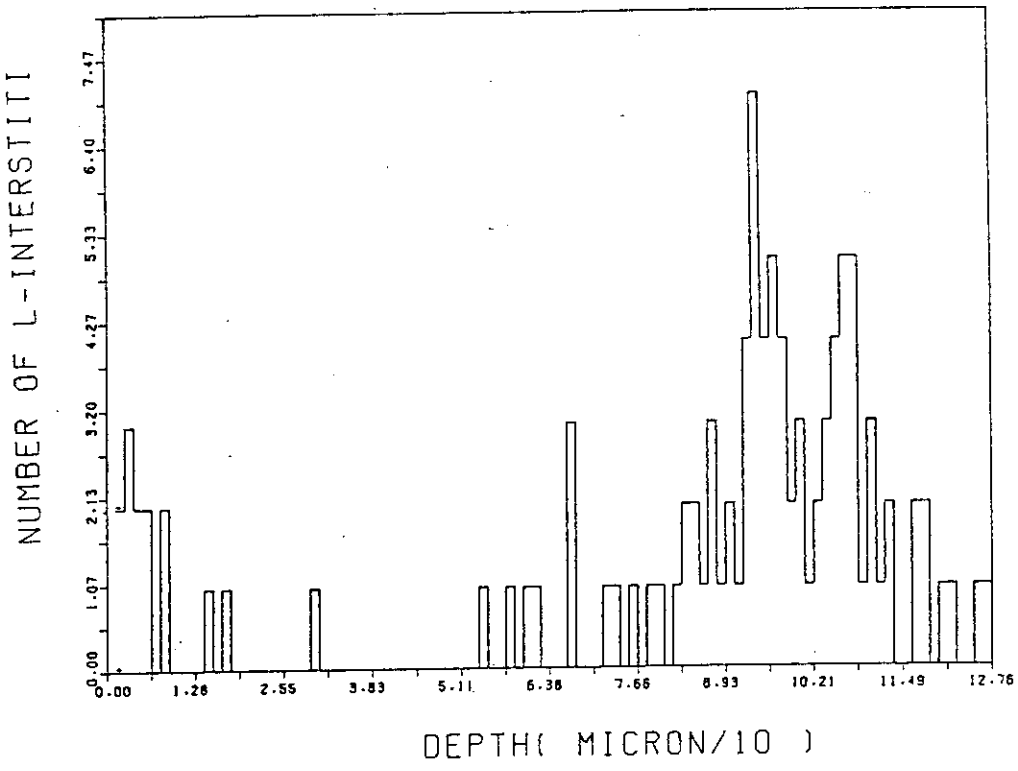

Fig. 2.9.3 Spatial distribution of rest ions in the depth direction in the pure iron (243 ions in total).

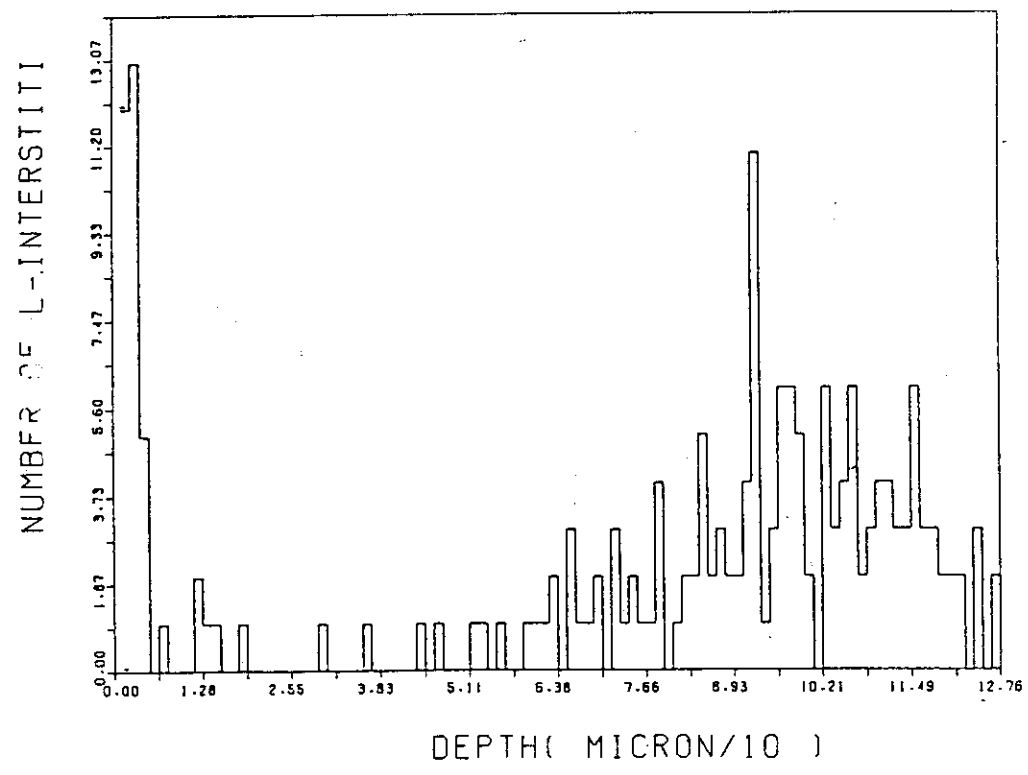

Fig. 2.9.4 Spatial distribution of rest ions in the depth direction in the iron containing carbon (243 ions in total).

2.10 Limitation of the Boltzmann Equation

Y. Taji

A new method for deriving the Boltzmann equation for dilute gases from the basic Liouville equation has been proposed[1], in which binary collisions are assumed to occur in isotropic form and the technique of time average is used. The most essential point in deriving the Boltzmann equation is how to derive the macroscopic chaotic relation $f^{(2)} = f^{(1)}\ f^{(1)}$ ($f^{(n)}$ denotes the n-particle distribution function) from the microscopic relation of the classical mechanics, which determines completely the behaviors of particles through the conservation law of energy, momentum and angular momentum. That is, it is not expected at all that the chaotic state $f^{(2)} = f^{(1)}\ f^{(1)}$ happens to grow in the course of time. However, $f^{(2)} = f^{(1)}\ f^{(1)}$ holds for mass-points having not any spatial extensions. We now consider particles having spatial extension so that they encounter with each other. When binary collisions occur in isotropic form, angular momenta of two particles are canceled and vanish as the ensemble average. The particles which have not angular momentum in collision can be regarded as mass-points having not extension. Thus, we can arrive at $f^{(2)} = f^{(1)}\ f^{(1)}$.

The gases have been assumed to be dilute, in which binary collision occurs isolated from other particles. However, in a system of dense gas or a system of binary mixture (e.g. the system of neutrons and medium nuclei in reactors) binary collisions occur sequentially, that is, the first particle encounters with the second particle and furthermore the first one, which has correlation with the second one, encounters with the third particle. Such an effect of triple collision can be also taken into account in the similar manner as the above. As far as the assumption of isotropic collisions is satisfied, it will be shown that also the Boltzmann equation holds for the dense gases or the mixtures. As the practical problem we are concerned to deal with the case of anisotropic collisions occurred in such dense systems. When anisotropy exists in dilute gases, there are no motive forces for anisotropy to approach to isotropy so that macroscopic equation cannot be expected. In the case of dense gases where triple collisions are not negligible, we can define an average force field for anisotropy to tend to isotropy as reported already in Ref.(2) though in intuitive form. Theoretical derivation of a new kinetic equation with the average force field will

be reported in future.

References

1) Taji Y. : Proc. Spring Meeting of Phy. Soc. Jpn., 31aR10 (1982).
2) Taji Y. : Phy. Soc. Jpn., 41, 2020 (1976).

3. Integral Experiment and Analysis

3.1 Critical Experiments on Enriched Uranium Graphite Moderated Cores Related to VHTR

F. Akino, K. Kitadate, M. Takeuchi, H. Yoshifuji,

T. Ono and Y. Kaneko

As core design for the Experimental High-Temperature Gas Cooled Reactor (VHTR) progresses, evaluation of design precision has become increasingly important. For a high precision design, adequate group constants based on nuclear data and calculation method accurately describing transport of neutrons are required.

We, therefore, assembled many cores using a graphite-moderated 20% enriched uranium Semi-Homogeneous Critical Facility (SHE), and obtained experimental data useful in evaluating design precision. Assembled cores are as follows :

1) Homogeneous cores : SHE-5$\sim$SHE-8,

2) Heterogeneous cores : SHE-12 and SHE-13,

3) Simulation cores for VHTR : SHE-14, SHE-B1 and SHE-B2.

The features of the simulation cores for VHTR are simular to those of VHTR with respect to the following aspects,

1) The configuration of the fuel rods in the column is simular to that in VHTR,

2) $C/^{235}U$ atomic ratio in the column is about 7200 in the whole simulation cores, which is close to that of VHTR

3) SHE-B1 and SHE-B2 core are loaded with one and two burnable poison rods in the column, respectively, like in VHTR.

In Fig. 3.1.1, the measured critical masses of the 9 cores with the range of $C/^{235}U$ atomic ratio being from 2320 to 15700 are plotted for comparsion with the calculated values.

Calculations of the group constants are made by the heterogeneous model in which the lattice structure of the column is taken into account, using SRAC code system.

Young- Koppel neutron scattering law was used for thermal neutron scattering of graphite.

Effective multiplication factors are calculated by one-dimensional 61 group diffusion theory. Here, thermal groups are divided into 39 groups from 0.0 to 1.1254 ev, and fast groups are divided into 22 groups from 1.1254 ev to 10 Mev.

From Fig. 3.1.1, agreement between experiment and calculation is within 0.75% for K_{eff} and 3% for ^{235}U critical mass.

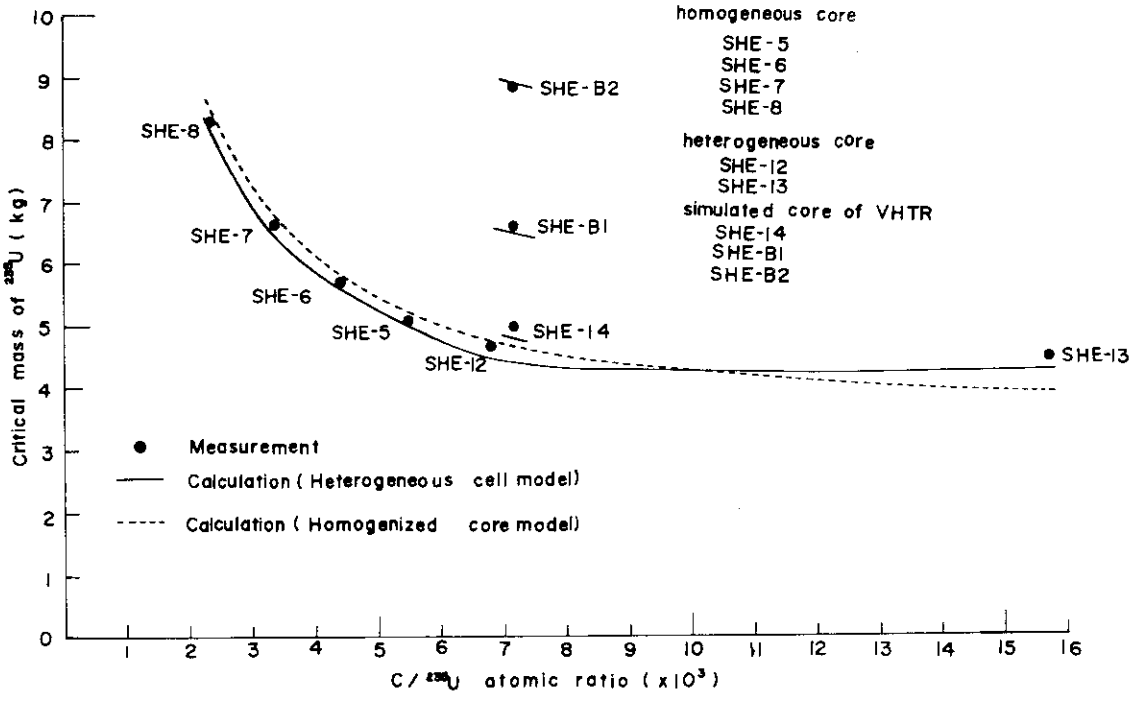

Fig. 3.1.1 Critical mass of 20% enriched uranium graphite moderated and reflected cores of SHE

3.2 Reconstruction Program of SHE for Experimental VHTR

Y. Kaneko, F. Yoshihara, H. Yasuda, F. Akino, K. Tsuchihashi,
T. Ikushima and M. Hishida

Present status

Reconstruction program of SHE, Semi-Homogeneous Experimental Critical Facility, was approved by Japanese government early in 1981. The object of the program is to obtain Experimental verification for the design accuracy of Experimental VHTR fueled with low enriched uranium. Basic design of the reconstructed SHE facility was completed as illustrated in Fig. 3.2.1. Safety analysis was performed with respect to the following major aspects;

(1) Design basis accident
(2) Aseismic design
(3) Core heating by use of electric heaters

Specification of reconstruction

Core geometry : horizontal half machine type hexagonal prism in shape height and length, 2.4 m each
Core lattice : pin in block type same as Experimental VHTR
Core temperature : room temperature to 200°C throughout the whole core including reflector. Single fuel rod will be heated up to 800°C
Fuel : 2, 4 and 6 w/o enriched uranium, 260 kgU in total coated particle fuel compacts of the same size of Experimental VHTR BISO or TRISO

Schedule

After safety examination by government, the reconstructed core will be assembled in 1984.

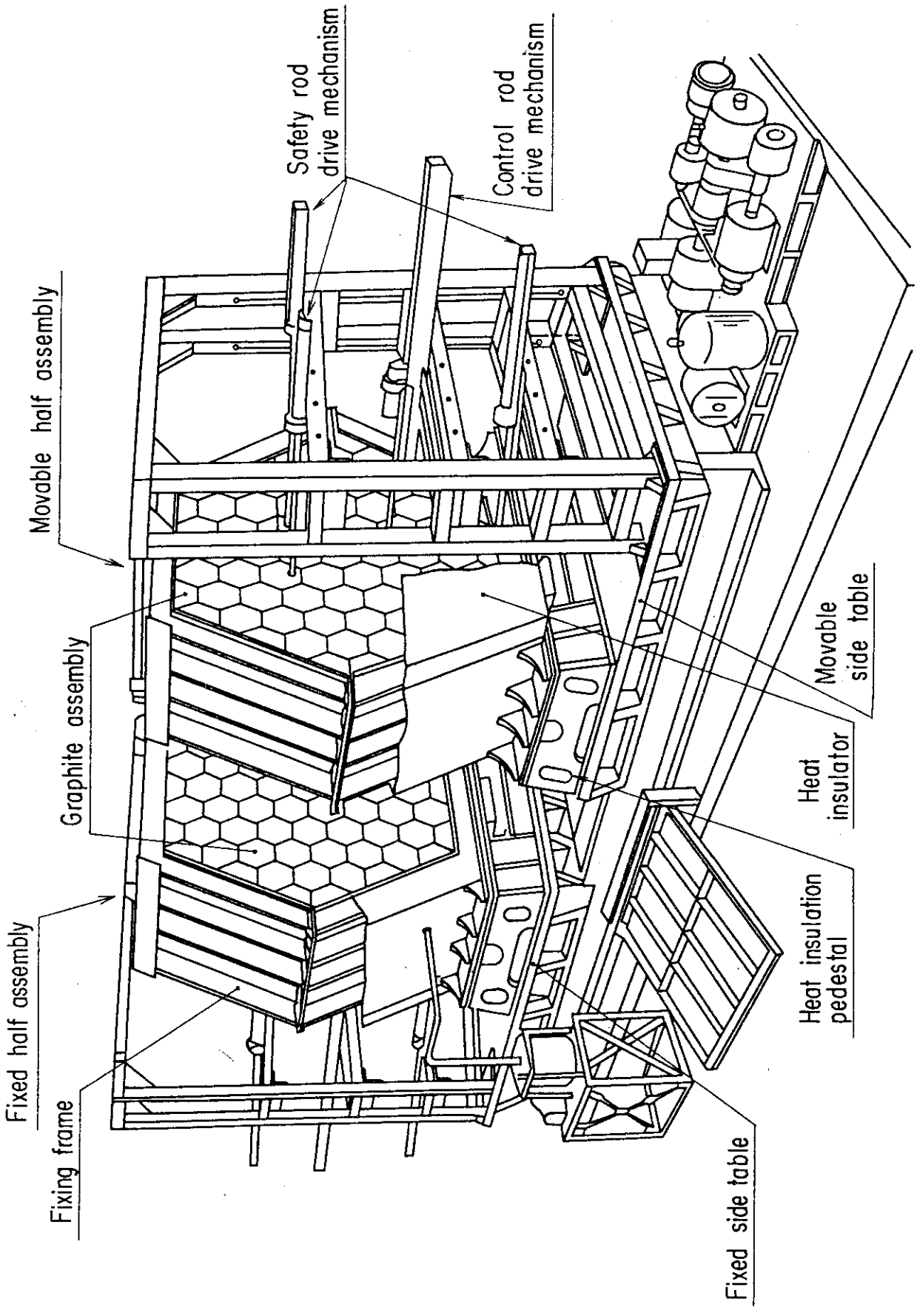

Fig. 3.2.1 Concept of reconstruction of SHE

3.3 Actinide Integral Experiments at FCA

— Selection of Standard Cores and Their Characteristics —

M.Nakano, K.Koyama, T.Koakutsu, S.Okajima and H.Kuroi

Actinide integral experiments have been made on FCA IX assemblies, which were selected to provide FCA spectrum standard cores with appropriate variety of neutron spectra. FCA Assembly IX consists of seven different versions of cores (Assembly IX-1 ∿ IX-7) to cover a wide range of neutron spectra. The core composition of these cores are given in Table 3.3.1.

In Assembly IX-1 to IX-6, only 93% enriched uranium was used as core fuel and each one of graphite or stainless steel was used as a diluent material. Neutron spectrum at the core center becomes soft from Assembly IX-6 to IX-1, systematically. The mean energies of the ^{10}B (n,α) reaction rate were calculated to be about 2keV, 40keV and 150keV for Assembly IX-1, IX-3 and IX-6, respectively. The core of Assembly IX-7 is composed of only 20% enriched uranium and structural material of the FCA matrix and drawer. All the core were constructed to be cylindrical geometry of L/D≒1, which were surrounded by the depleted uranium blanket about 35cm thick.

Criticality and basic parameters of the core including fission rate ratios and sample reactivity worths of standard materials have been measured on FCA Assembly IX. The measured value of k_{eff} for the cylindricalized model with no gap between the FCA half machines was determined within ±0.08% for each assembly.

Fission rates of ^{238}U, ^{235}U, ^{239}Pu and ^{237}Np at the core center have been measured by using the absolute micro-fission chambers of natural U, enriched U, Pu and Np. These chambers are of a cylindrical geometry, 6mm diameter and 32mm effective length. Measurements were carried out in the experimental hole 20mm in diameter made vertically to the cell plates. Sample worths of standard materials were measured in the central cell of each core. Plate samples used include Pu, enriched and natural uranium, B_4C and graphite. The sample plate was substituted for the appropriate spacer loaded in the core cell. Reactivity change was determined from the calibrated control-rod positions. Fission rate ratios of $^{238}U/^{235}U$ and $^{239}Pu/^{235}U$ and sample worth ratio of natural B_4C/93% enriched uranium measured at the center of each core are shown in Fig.3.3.1, which well demonstrates the spectrum shift between the selected cores.

The analysis was made by using the DOYC computer code system and the adjusted data with 1950 group structure AGLI-2[1]. The code SP-2000[2] was utilized to generate 20 group effective cross sections with diagonal P_1 components from the fundamental mode cell calculation for each cell. Using these group constants, RZ calculation was made by the transport theory with S_4 or S_8 approximation. The calculated values of k_{eff} are compared with the measured ones in Table 3.3.2. The calculation with S_4 approximation overestimates the criticality by about 0.2% compared with S_8. The S_8 calculation predicts the measured criticality within ±1% for all the cores except Assembly IX-4 and Assembly IX-5, which are stainless steel diluent cores.

The measured and calculated fission rate ratios of $^{238}U/^{235}U$ and $^{239}Pu/^{235}U$ are compared in Fig. 3.3.2. To calculate the cell averaged fission rate, effective fission cross sections for the uniformly distributed detector in the cell were prepared for each cell. Agreement is fairly well between the measured and calculated fission rate ratios, although a little discrepancy can be seen in the C/E values for Assembly IX-4 (a stainless steel core) and Assembly IX-7. The analysis of the reactivity worth of standard materials is now in progress. Preliminary results indicate that the calculated ratios of the sample worths of 93% EU/Pu and Nat. B_4C/Pu agree fairly well with the experiments for all assemblies.

Refererences

1) Kuroi, H., et al.: Private Communication

2) Kuroi, H., Tone, T.: "SP-2000: Program for Calculating Fine Group Neutron Spectrum in Multi-region Cell and Effective Broad Group Constants," JAERI 1240 (1976).

Table 3.3.1 Core composition of FCA IX assemblies (v/o)

Assembly	IX-1	IX-2	IX-3	IX-4	IX-5	IX-6	IX-7
93%EU	5.3	10.6	15.9	10.6	15.9	15.9	—
20%EU	—	—	—	—	—	—	84.7
C	79.4	74.1	68.8	—	—	—	—
SUS	10.8	10.8	10.8	84.9	79.6	27.9	10.8
Void	4.5	4.5	4.5	4.5	4.5	56.2	4.5

Table 3.3.2 Measured and calculated values of k_{eff} of FCA Assembly IX

Assembly	Experiment	Calculation		C/E
		S_4	S_8	S_8
IX-1	1.0077 ± 0.07%	1.0051	1.0033	0.9956
IX-2	1.0107 ± 0.08%	1.0134	1.0114	1.0006
IX-3	1.0086 ± 0.08%	1.0117	1.0091	1.0005
IX-4	1.0075 ± 0.07%	1.0192	1.0174	1.0098
IX-5	1.0096 ± 0.06%	1.0252	1.0227	1.0130
IX-6	1.0082 ± 0.06%	1.0162	1.0140	1.0058
IX-7	1.0095 ± 0.06%	1.0102	1.0079	0.9984

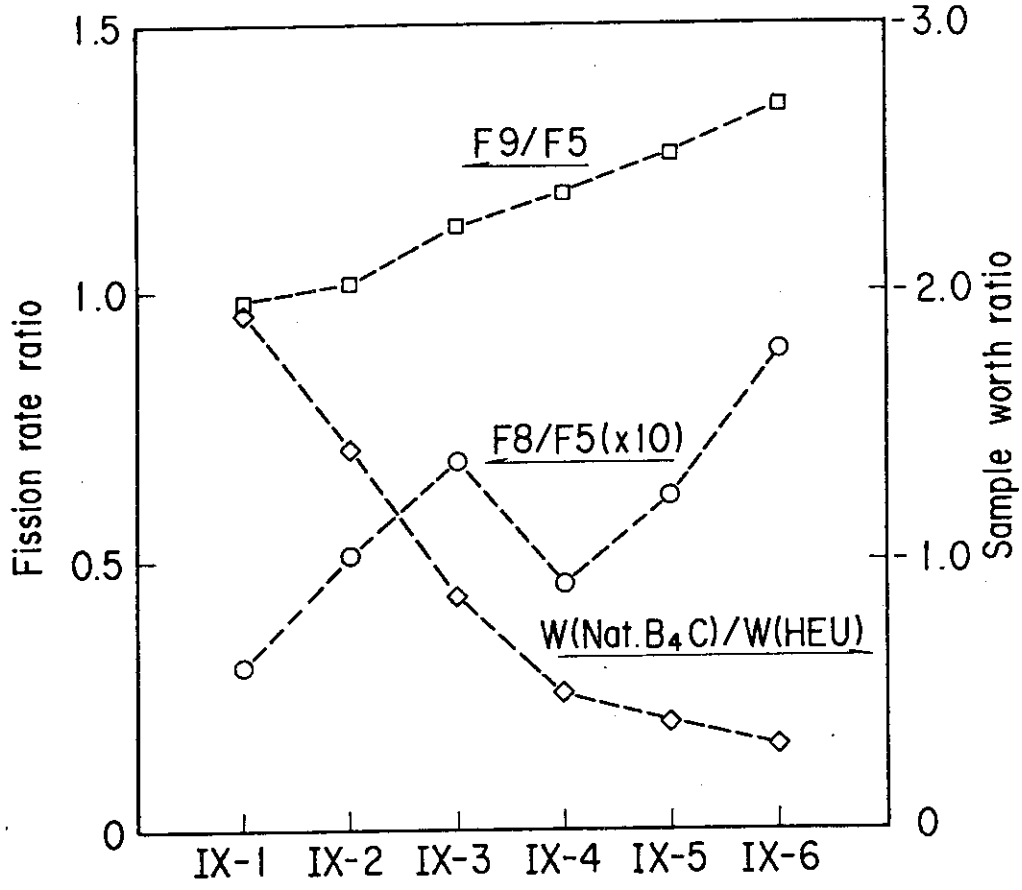

Fig. 3.3.1 Fission rate and sample worth ratios measured at the center of FCA IX assemblies

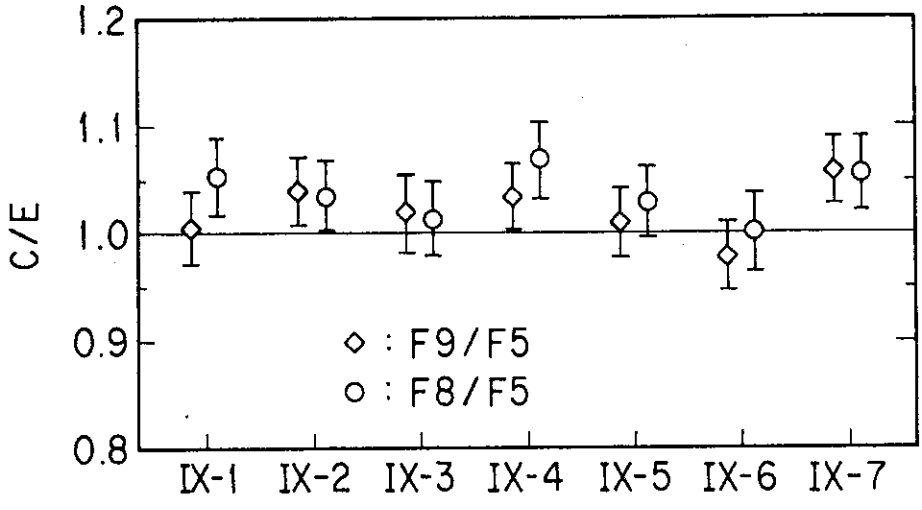

Fig. 3.3.2 C/E values of F9/F5 and F8/F5 at the center of FCA IX assemblies

3.4 Actinide Integral Experiments at FCA

—— Actinide Sample Worth Measurements ——

T. Mukaiyama, S. Okajima, T. Koakutsu and H. Kuroi

Objectives of Integral Experiments

The assessment of the actinide transmutation concepts requires the reliable fission and capture cross sections of actinide elements over the whole neutron energy of potential transmutation system. The status of the cross section data is much less satisfactory. Some of the major actinide cross section data possess the uncertainty up to 50%.[1),2)] For the evaluation and the modification of these data, the integral measurements have been performed at FCA. The realistic integral measurements at fast critical facility like FCA are the measurements of the small sample reactivity worth and the fission rate ratios.[3)]

Sample Worth Measurements

The actinide production and transmutation study of the Actinide Burning Fast Reactor "ABFR" shows that ^{237}Np, ^{238}Pu, ^{240}Pu, ^{241}Am, ^{243}Am, and ^{244}Cm are the ruling nuclides in the transmutation system. The samples of 15 - 20 g of isolated isotopes of above mentioned actinides except ^{244}Cm were prepared at Oak Ridge National Laboratory. Oxide actinide powder is encapsulated into double concentric stainless-steel capsule.[4)] Data of atomic composition of samples were provided by ORNL and these are shown in Table 3.4.1.

Seven cores were set up at FCA to provide the different neutron spectrum fields where sample worth measurements were performed. FCA IX-1 - IX-7 are the FCA standard neutron spectrum series of cores[5)] which caver the as wide variety of neutron spectra as possible which can be established with this kind of a fast critical assembly. A sample is handled with the automatic handling system which picks up a selected sample from the container and places it at a desired position in the critical assembly. Actinide oxide powder worth was measured by the criticality method and the criticality of the system was decided within ±0.02 mm error of a control rod position which is roughly equivalent to less than $\pm 5 \times 10^{-7}$ $\Delta k/k$.

The corrections to the observed value includes worths of impurites, oxygen worth and the spatial distribution of worth along the sample axis.

The final value of an isolated element worth was determined within $\pm 1 \times 10^{-6}$ $\Delta k/k$ accuracy for 15 - 20 g of a sample, however this does not include the impurity uncertainty.

The preliminary result of sample worth measurements is shown in Fig. 3.4.1 as the worth ratio to ^{239}Pu worth. ^{239}Pu sample worth is measured for $2'' \times 2'' \times \frac{1''}{16}$ plate sample. Sample geometry difference effect between actinide samples and the ^{239}Pu sample, and also some of factors are not corrected for the value shown in Fig. 3.4.1 but these corrections are minor ones.

Preliminary results of analysis using ENDL set[2] and ENDF/B-V set show relatively large discrepancy from the measured result. For ^{237}Np, worth ratio to ^{239}Pu calculated using ENDL set agrees well with the measured value for most of cores, whereas the discrepancy of worth ratio between the values calculated using ENDF/B-V and the measured values is more than 30%. For ^{238}Pu, C/E value of worth ratio is 1 - 1.4 for both sets. For ^{240}Pu, C/E value of worth ratio ranges from 0.7 to 0.9 for both sets. For ^{241}Am, C/E value of worth ratio ranges from 0.7 to 1.5 when ENDF/B-V set is used, whereas the discrepancy between calculated values and measured values is more than 30% when ENDL set is used. For ^{243}Am, the discrepancy of worth ratio between the calculated values and the measured values is larger than 30% for both sets. Detailed analysis is under way and the next integral measurement is planned for the different actinides.

References

1) Mitani H., Koyama K., Kuroi H. : "Sensitivity Analysis for Actinide Production and Depletion in Fast Reactors," JAERI-M 8133 (1979).
2) Mukaiyama T., Koyama K., Kuroi H. : "Generation of actinide isotopes cross section set for fast reactor calculations using data from ENDL/B-IV," JAERI-M 8310 (1979).
3) Mukaiyama T., et al. : "Evaluation of Actinide Cross Sections by Integral Experiments," Proceedings of International Conference on Nuclear Cross Sections for Technology (Knoxville, 1979), NBS SP594 (1980).
4) Mukaiyama T., Ōbu M., Kuroi H. : "Integral Experiments for Actinides Cross Section Evaluation (I)," pp.72, JAERI-M 9672 (1981).
5) Nakano M., et al. : "Actinide Integral Experiments at Fast Critical

Facility FCA — Selection of Standard Cores and their Characteristics —," Section 3.3 in this report.

Table 3.4.1 Atomic Composition of Actinide Samples

Sample Name	Principle Element gram	Oxide(w/o)	Impurities (w/o)
Np-237	20.0	99.2	Th-232 Fe,Ni etc. 0.5 total 0.3
Pu-238	13.5	87.6	U-234 Pu-239 Pu-240 Fe,Ni etc. Th-232,NP-237,Pu-241 3.9 7.3 0.6 total 0.2 less than 0.1% each
Pu-240	14.8	98.5	Pu-239 Pu-241 Pu-242 0.6 0.6 0.3
Am-241	19.9	97.5	Fe,Ni etc. Th-232,Np-237,Pu-239 total 2.4 less than 0.1% each
Am-243	20.0	99.4	Pu-240 Cm-244 Fe,Ni etc. 0.2 0.4 total 0.04

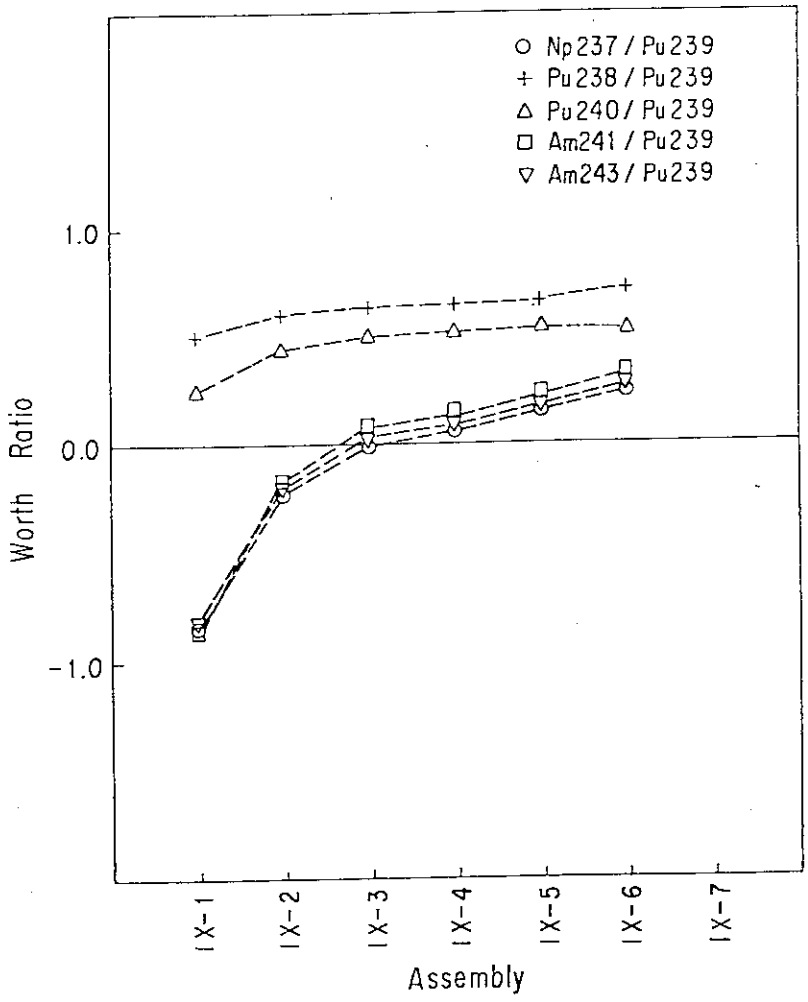

Fig. 3.4.1 Actinide sample worth ratio to Pu-239 worth

3.5 Actinide Integral Experiments at FCA

—— A Measurement of Actinide Fission Rate Ratios ——

M. Ōbu, S. Okajima, T. Koakutsu and H. Kuroi

Integral experiments for evaluating actinide cross section data have been made in the cores of FCA Assembly IX-1 ∿ IX-7[1] whose neutron spectra were changed from soft to hard. These experiments include two measurements for obtaining important physics parameters, one is the measurement of small sample reactivity worths of actinide nuclides,[2] the other is that of actinide fission rate ratios by the fission chamber technique. In this report, the results of the measurement of fission rate ratios for typical seven actinide nuclides, ^{237}Np, ^{238}Pu, ^{239}Pu, ^{242}Pu, ^{241}Am, ^{243}Am and ^{244}Cm to ^{235}U are described.

The fission chambers used in FCA are a parallel-plate type made of thin stainless steel.[3] Dimensions of the chamber head are 37.8 mm outer diameter and 13.4 mm length. The amounts of fissle masses deposited in the chamber are absolutely determined by α-spectrometry. Weights deposited are in the range of 40 ∿ 90 μg, mostly. However, for the nuclides with very high α-specific activity such as ^{244}Cm, ^{238}Pu, and ^{241}Am, the weights are limited to less than 10 μg to improve α-to-fission fragment signal ratio.

The measurements of fission rates are made at the center in each core. The chamber is located at that place by setting 2" × 2" × 1" cavity. The reactor is usually operated in 10 ∿ 40W power in response to the chamber sensitivities, and fission pulses of $1.5 \times 10^4 \sim 1.0 \times 10^5$ counts are accumulated. For ^{244}Cm, however, 200W operation was made in the measurement to reduce back ground from ^{244}Cm spontaneous fission. The cavity effect was estimated from additional experiment by using cylindrical micro fission chamber with aluminum wall. This effect is of the order of 2% for ^{237}Np.

Experimental fission rate ratios of several nuclides are shown in Fig. 3.5.1. The spectrum dependence of the fission rate ratios are clearly observed between different cores. The experimental fission rate ratios are compared with calculated results[4] by transport theory with S_4P_1 approximation. ENDF/B-V data were used. Table 3.5.1 is the lists of experimental fission rate ratios and the C/E.

It is revealed from C/E evaluation that the results of present

calculations are about 4∿17% higher than the experimental fission rate ratios, in most case. However, for the ratio $^{238}Pu/^{235}U$, the calculated results are considerably underestimated, and are about 25% lower than the experimental values. It is pointed out that the fission cross section data for ^{238}Pu include large uncertainties especially which should be adjusted.

References

1) Nakano M., et al. : "Actinide Integral Experiments at Fast Critical Facility FCA (intermediate report), (1) Selection of Standard Cores and their Characteristics," 1982 Annu. Meeting of Atomic Energy Society of Japan, C40, (1982), and Section 3.3 in this report.
2) Mukaiyama T., et al. : "Actinide Integral Experiments at Fast Critical Facility FCA (intermediate report), (2) Actinide Sample Worth Measurements," ibid., C41, (1982), and Section 3.4 in this report.
3) Obu M. : "Preparation and Characteristics of Fission Chambers with Actinide Nuclides," JAERI-M 9757 (1981) (in Japanese).
4) Koyama K., et al. : "Actinide Integral Experiments at Fast Critical Facility (intermediate report), (4) A Preliminary Analysis of Actinide Integral Experiments," 1982 Annu. Meeting of Atomic Energy Society of Japan, C43, (1982).

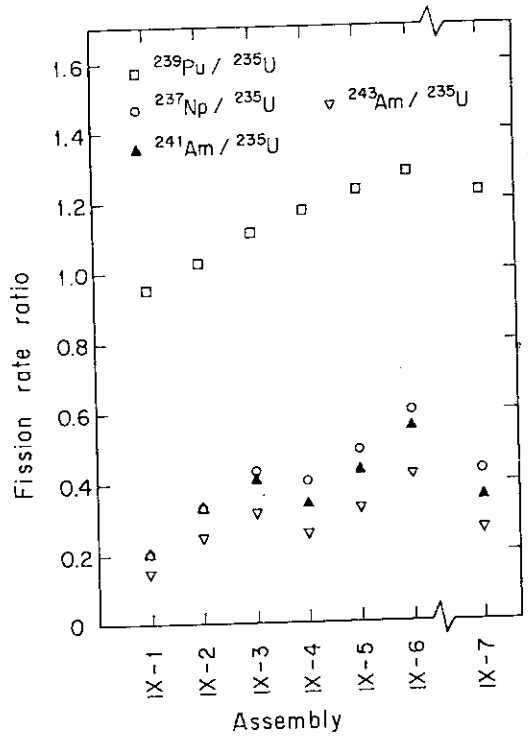

Fig. 3.5.1 Central fission rate ratios in FCA Assembly IX-1 ∿ IX-7

Table 3.5.1 Central Fission rate ratios of actinide nuclides

Assembly	$^{237}Np(n,f)/^{235}U(n,f)$		$^{241}Am(n,f)/^{235}U(n,f)$	
	Exp.	C/E	Exp.	C/E
IX-1	0.2000 ± 1.9%	1.046	0.1915 ± 2.2%	1.072
IX-2	0.3304 ± 2.4%	1.033	0.3229 ± 2.4%	1.023
IX-3	0.4269 ± 2.2%	1.019	0.4092 ± 2.2%	1.027
IX-4	0.4037 ± 1.9%	1.117	0.3443 ± 2.1%	1.106
IX-5	0.491 ± 2.1%	1.081	0.4319 ± 2.2%	1.077
IX-6	0.599 ± 2.1%	1.033	0.554 ± 2.1%	1.036
IX-7	0.4228 ± 2.1%	1.085	0.3603 ± 2.1%	1.075

Assembly	$^{243}Am(n,f)/^{235}U(n,f)$		$^{244}Cm(n,f)/^{235}U(n,f)$	
	Exp.	C/E	Exp.	C/E
IX-1	0.1473 ± 2.1%	1.088	0.2516 ± 3.8%	1.047
IX-2	0.2463 ± 2.3%	1.071	0.393 ± 4.0%	1.062
IX-3	0.3140 ± 2.2%	1.075	0.491 ± 4.1%	1.075
IX-4	0.2591 ± 2.1%	1.174	0.467 ± 4.1%	1.166
IX-5	0.3255 ± 2.1%	1.145	0.558 ± 4.3%	1.144
IX-6	0.4232 ± 2.1%	1.091	0.670 ± 4.6%	1.108
IX-7	0.2662 ± 2.1%	1.166	0.483 ± 4.8%	1.143

Assembly	$^{239}Pu(n,f)/^{235}U(n,f)$		$^{238}Pu(n,f)/^{235}U(n,f)$	
	Exp.	C/E	Exp.	C/E
IX-1	0.957 ± 1.7%	1.034	0.790 ± 2.2%	0.737
IX-2	1.030 ± 2.2%	1.027	0.969 ± 2.9%	0.803
IX-3	1.113 ± 2.1%	1.026	1.238 ± 2.2%	0.732
IX-4	1.174 ± 1.6%	1.048	1.316 ± 2.2%	0.752
IX-5	1.233 ± 2.0%	1.036	1.460 ± 2.2%	0.739
IX-6	1.282 ± 2.1%	1.028	1.606 ± 2.2%	0.727
IX-7	1.215 ± 2.0%	1.037	1.375 ± 2.1%	0.738

3.6 Operation Report of SHE

F. Yoshihara, K. Kitadate, M. Takeuchi, T. Ono and H. Yoshifuji

In the most recent fiscal year, SHE achieved operation of 186 hrs and 57 watt-hours in total power.

During the operation, the following experiments were done on SHE-B2 core, which is a simulation core for Experimental Very High Temperature Reactor ;

i) Change of reactivity worth of a single coated particles fuel rod from room temperature to 800°C,

ii) Reactivity effect of gap between the two half assemblies separated each other,

iii) Reactivity worth of the end caps for the matrix tubes,

iv) Reactivity worths of burnable poison rods.

The critical fuel loading pattern of SHE-B2 core was shown in Fig. 3.6.1. In case of the reactivity change measurement for a single coated particles fuel rod, heating apparatus was reconstructed to get 800°C heating temperature. The reconstruction was licensed by Science and Technology Agency.

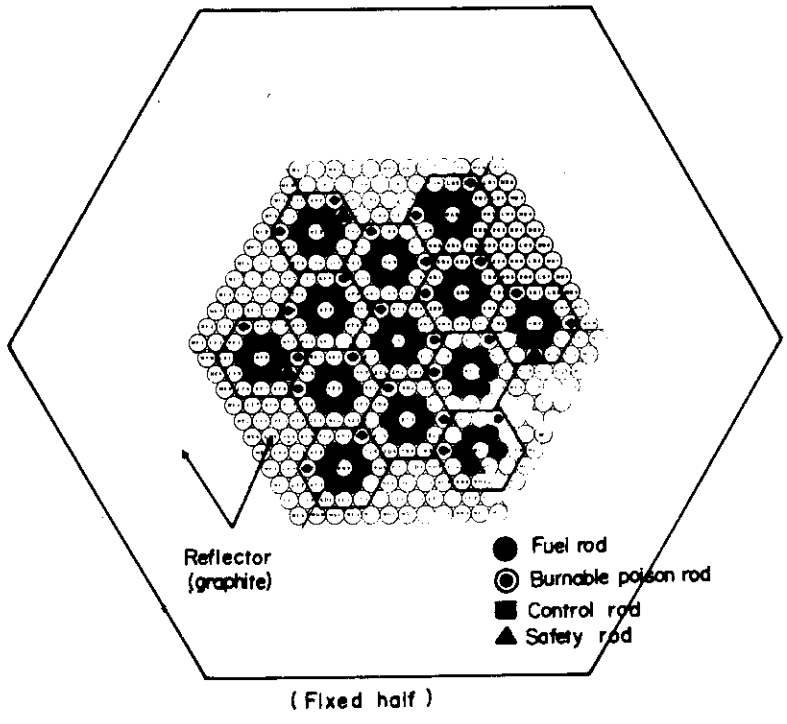

Fig. 3.6.1 Cross section of SHE-B2 core in critical fuel loading pattern

3.7 Operation Report of FCA

H. Watanabe, H. Ogawa, S. Fujisaki, and K. Yamagishi

Operating activities for the Fast Critical Assembly (FCA) including operation and maintenance of the facility, fuel management and technical support for experiments were continued as scheduled and performed without any major trouble which had disturbed the research activities. The facility was operated on the FCA-IX, a set of cores, consisting of the FCA-IX-1 through the FCA-IX-7.

During this fiscal year, 126 days were devoted for operation of the seven cores of the FCA-IX to carry out the characteristic tests and the experiments. The operating time was 725 hours and the integral power for the operations was 5, 159 WH. Among 160 operations, 4 were shut down by scram action. The total numbers of criticality of the FCA reached at 3279 at the end of the fiscal year 1981.

The facility was examined for maintenance monthly (2 days/month) and yearly (3 weeks in October) according to the operational instruction, and received the annual authorization of operation dated 10th of November after the reguratory inspection from 4th to 6th of November. The major maintenance works were the overhaul of the FCA table drive mechanism, the renewal of the thermocouples in the core matrix and of the temperature recorder, the exchange of the filters of core cooling system, and the adjustement of the position sensor indicating contact condition of the half machines.

The IAEA safeguards inspection on the nuclear fuels of the FCA were usually carried out every two weeks. The Physical Inventory Takings (PIT) of the fuels were performed at July 1981 and February 1982 by IAEA and STA under the reguration. No anomaly was indicated. To improve the book keeping works on the fuel management, a computer code was developed. The handling labor for the records on the sealed fuels has been much saved by the code. The defects of thin surface coating on the enriched uranium fuel were repaired for more than 3000 coupons by spraying colloidal solution of fluorocarbon.

As for the safeguards purposes, the following developmental works were made.

A nondestructive passive gamma assay system consisting of a multichannel analyzer and a minicomputer was completed and had been used for the PIT. Development of a core inventory monitor was tried to inspect the loading of a core by measuring gamma activities of indium foils, and a support was devoted to the phase-II field test of the portal monitor.

4. Shielding

4.1 Benchmark Experiment on D-T Neutrons and Secondary Gamma Rays Streaming through a Concrete Bent Duct

S. Tanaka, Y. Oyama, N. Sasamoto and T. Nakamura

In a Tokamak Type fusion reactor, many types of opening in blanket and shield are said to be required. The radiation streaming through the openings may cause undesirable radiation damage and radiation heating in the superconducting magnet and other components surrounding the plasma region. In particular the fast neutrons and the secondary gamma rays induced by the neutrons through such large openings as the Neutral Beam Injector port and as the evacuation duct of cryopump can present some difficulities to the reactor design. Hence it is important to have a reliable data and method by which the streaming radiations could be evaluated accurately. Thus, a streaming benchmark experiment on D-T neutrons and secondary gamma rays induced by the neutrons was carried out at the personnel passageway in FNS of JAERI.

The first leg of the passage way is 254 cm in length and the second one 204 cm. A temporary shield was set up to minimize the effect of parasitic D-D neutrons from the accelerator beam line components to the entrance by stacking polyethylene blocks 30 cm thick. The layout and the neutron source position is shown in Fig. 4.1.1.

Fast neutron and gamma-ray energy spectra were measured by using NE213 scintillator sets 5.08 cm in diam. × 5.08 cm high at the four positions along the center axis of the passageway whose cross section measures 96 cm wide and 200 cm high. In Fig. 4.1.2 the fast neutron spectra measured at the four positions are shown, where the distances are equal to ones from the inlet of the passageway. Neutron and gamma-ray dose distributions along the axis were also measured by a Studsvik Model 2202D rem-counter, by pairs of ^{6}LiF and ^{7}LiF TLDs and by $CaSO_4$(Tm) TLD, respectively. In Fig. 4.1.3 the measured dose distributions are represented as an example.

In the present experiment the detailed informations essential for the analysis of the measured results have been obtained in addition to the measurements of the streaming neutrons and gamma rays. Hence it is expected that this work will be applicable to the verifications of the

nuclear data and methods of the codes used for the shielding design of a D-T fusion reactor.

Reference

1) Tanaka S. et al. : "A Benchmark Experiment on D-T Neutrons and Secondary Gamma Rays Streaming through a Concrete Bent Duct," to be published in JAERI-M.

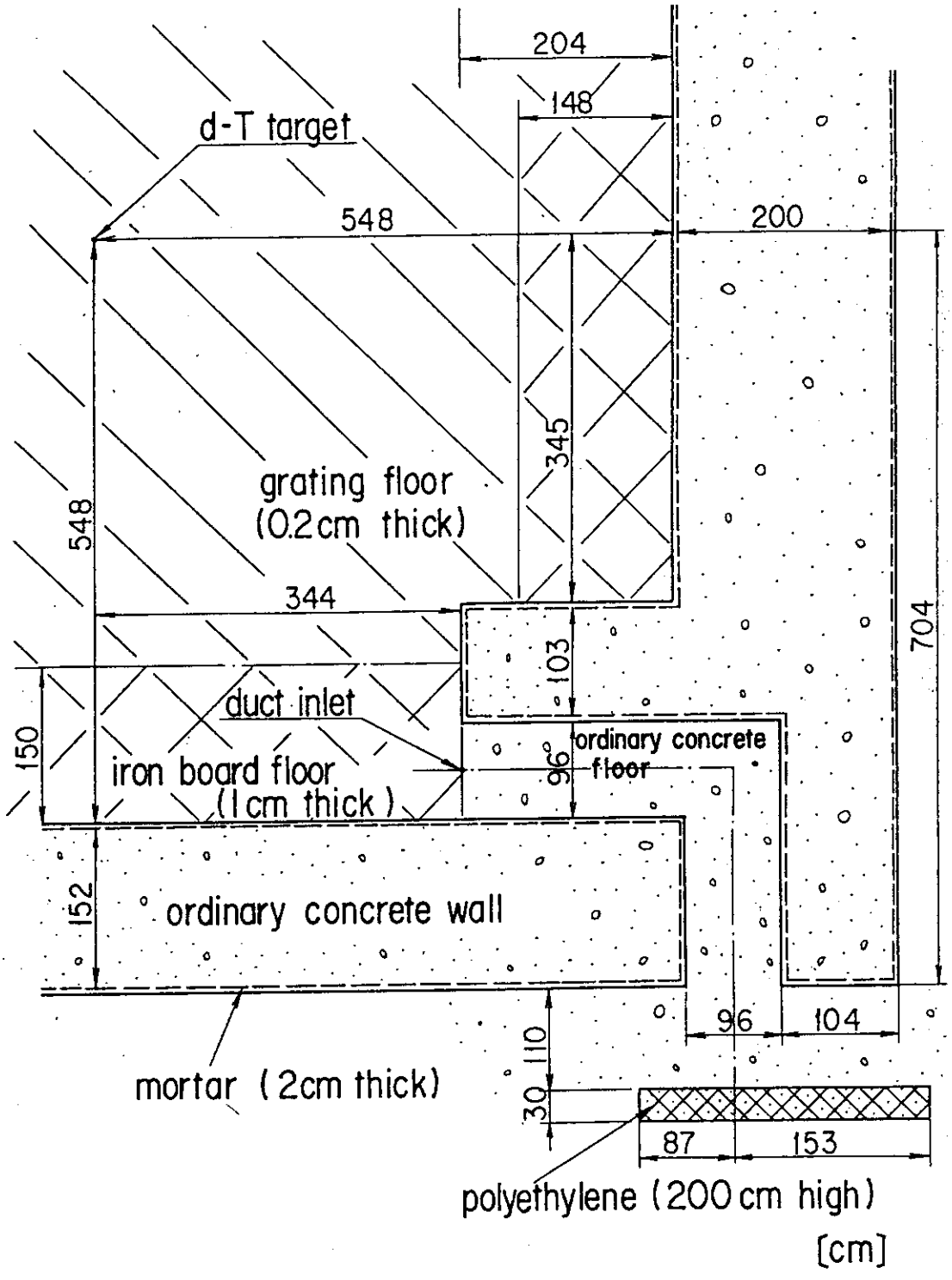

Fig.4.1.1 A floor plan around the personnel passageway

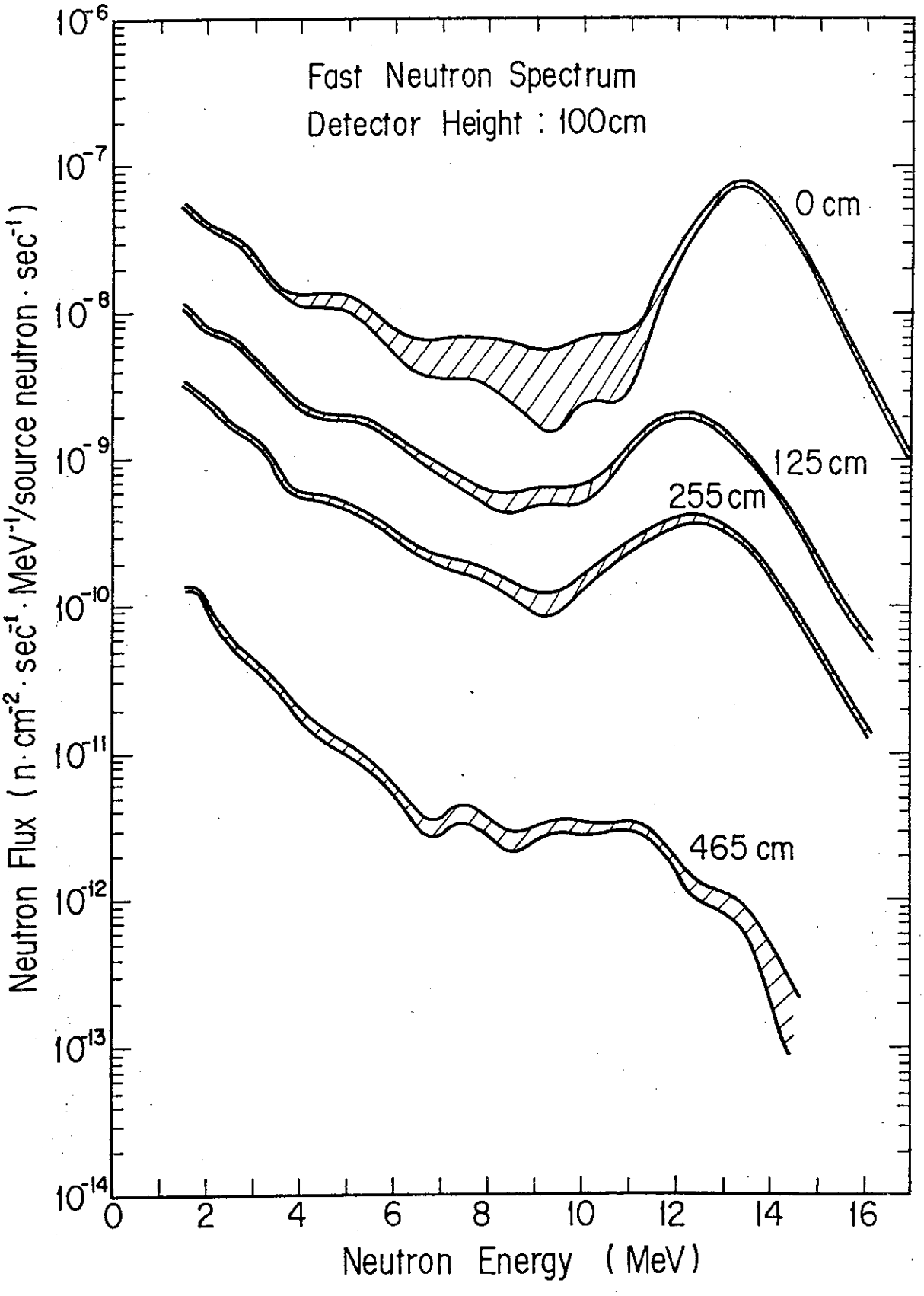

Fig.4.1.2 Fast neutron energy spectra in the duct measured by a NE213 spectrometer

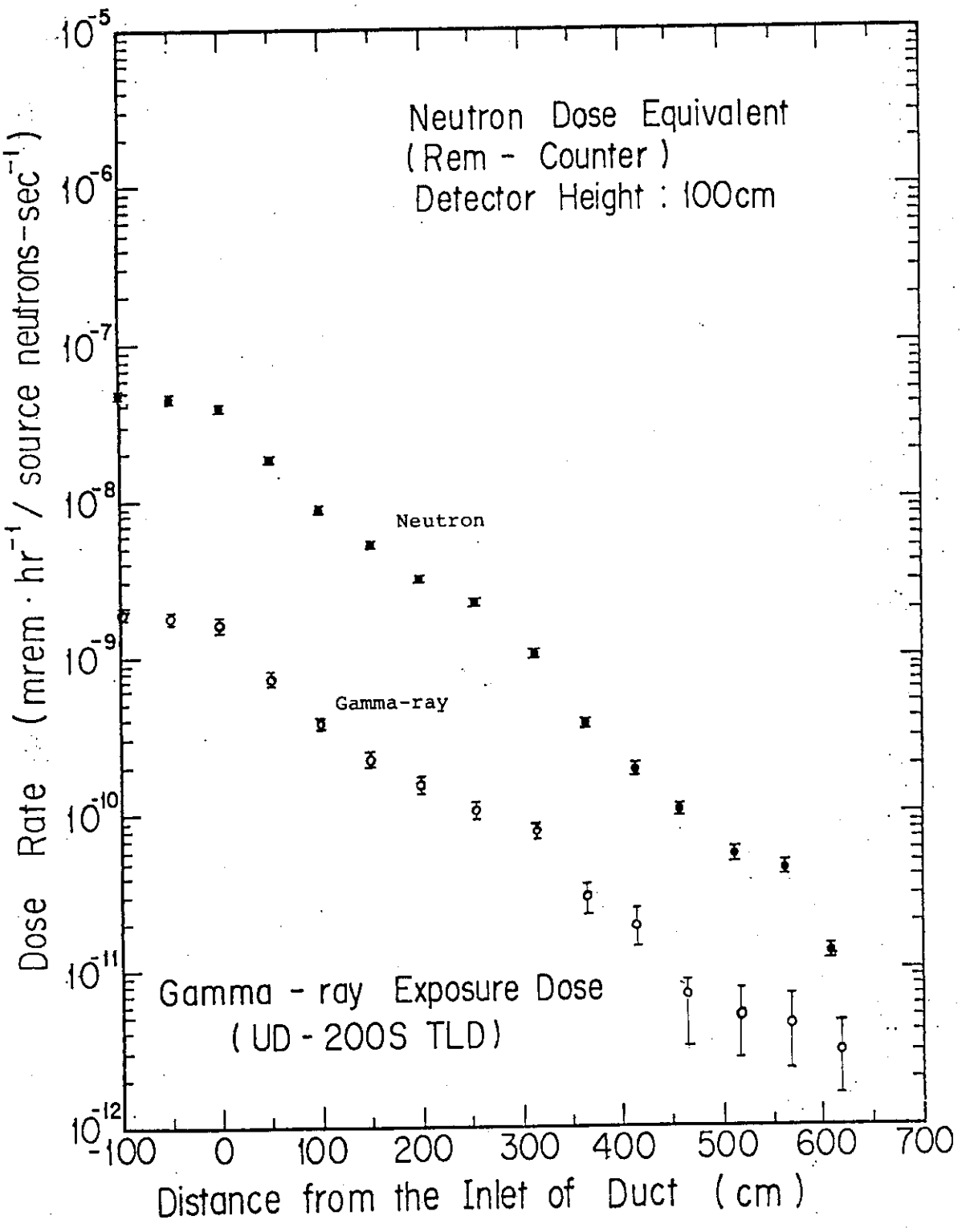

Fig.4.1.3 Distributions of neutron and gamma-ray doses in the duct

4.2 Experiments on Neutron Transport through Annular Duct of Large Radius

T. Miura*, T. Fuse*, N. Yamano** and T. Suzuki

There exist annular ducts of many types in reactor shields and the effective countermeasure is required for the radiation streaming through these ducts. Especially, an annular duct which exists between the pressure vessel and the primary shield is one of the most important object in reactor shielding designs, since a large amount of radiation leaks through this air gap and it affects overall shielding designs. In order to provide experimental data for the assessment of shielding calculations for the problem of this type, measurements were performed in a pool of JRR-4, a swimming pool type research reactor installed at Japan Atomic Energy Research Institute.

The reactor core surrounded with rectangular graphite-reflectors is contained in the aluminum tank. The annular duct surrounds the reactor core simulating the air gap between the pressure vessel and the primary shield. A sketch of the duct is shown in Fig. 4.2.1. As the gap width, 10 and 20 cm were taken. Activation detectors and proton recoil spherical proportional counters were used to measure the reaction rates and the spectra of neutrons. Twentyfive kinds of activation detectors were obtained from the combination of thirteen kinds of activation foils and three kinds of detector covers. The thirteen activation foils consist of five for slow neutrons and eight for fast neutrons. Cadmium cases 1 mm thick and boron covers of two types were used as the detector covers. The reaction rates were obtained within an accuracy of 28%. Neutron spectra in the energy range from thermal to fast were obtained from the measured reaction rates by means of the SAND-II code. Two activation cross section files were prepared for this unfolding by taking cross sections mainly from the ENDF/B-IV dosimetry file and SAND-II library. Neutron attenuation factors in boron covers were calculated with a one-dimensional discrete ordinates code ANISN and a simple absorption calculation. Through the check calculations on SAND-II unfolding, it

* Ship Research Institute

** Div. Reactor Safety Evaluation

was concluded that the spectra obtained by the activation method were reliable except in the energy range of 10 keV∿1 MeV where those obtained by the counter measurement were supplied.

As an assessment of the shielding calculation, the measured values were compared with P_3-S_8 calculations made by a two-dimensional transport code DOT-III in 30-energy groups. Comparisons are shown in Fig. 4.2.2 for the case of 10 cm gap width. Underestimation is found in the calculations. It is larger for the case of the narrower air gap and it increases with distances from the source. For the 10 cm gap, the discrepancy between the measurement and the calculation becomes a factor of 8. As one of the main causes of these discrepancies, the insufficient angular mesh points toward the duct axis is considered.

Reference

1) Miura T., Fuse T., and Yamano N. : J. Nucl. Sci. Technol., 18 [5] 369 (1981).

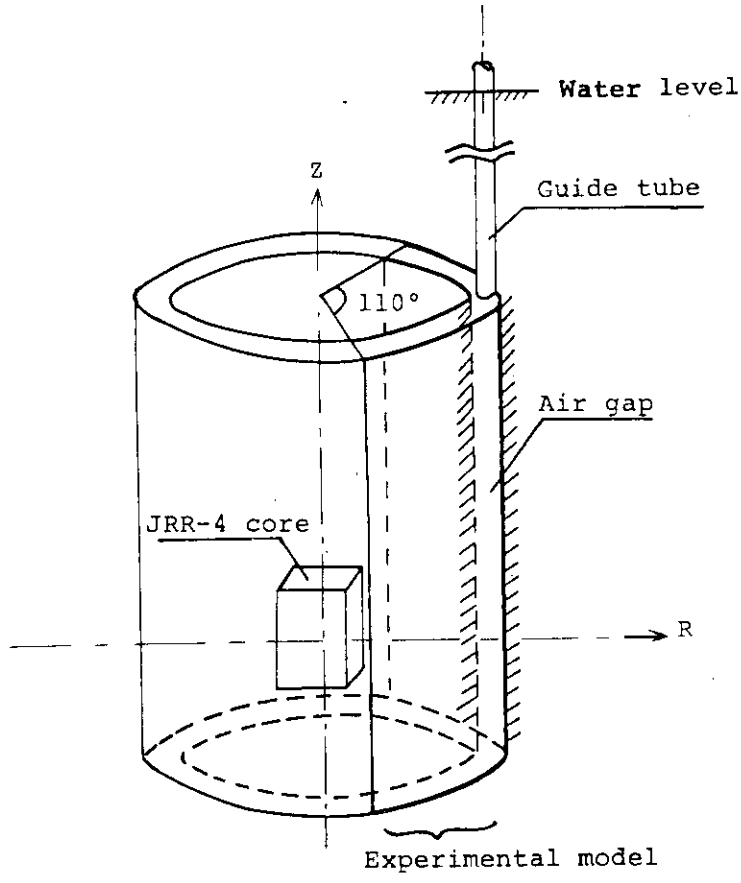

Fig. 4.2.1 Sketch of experimental model of large annular duct used in the experiment

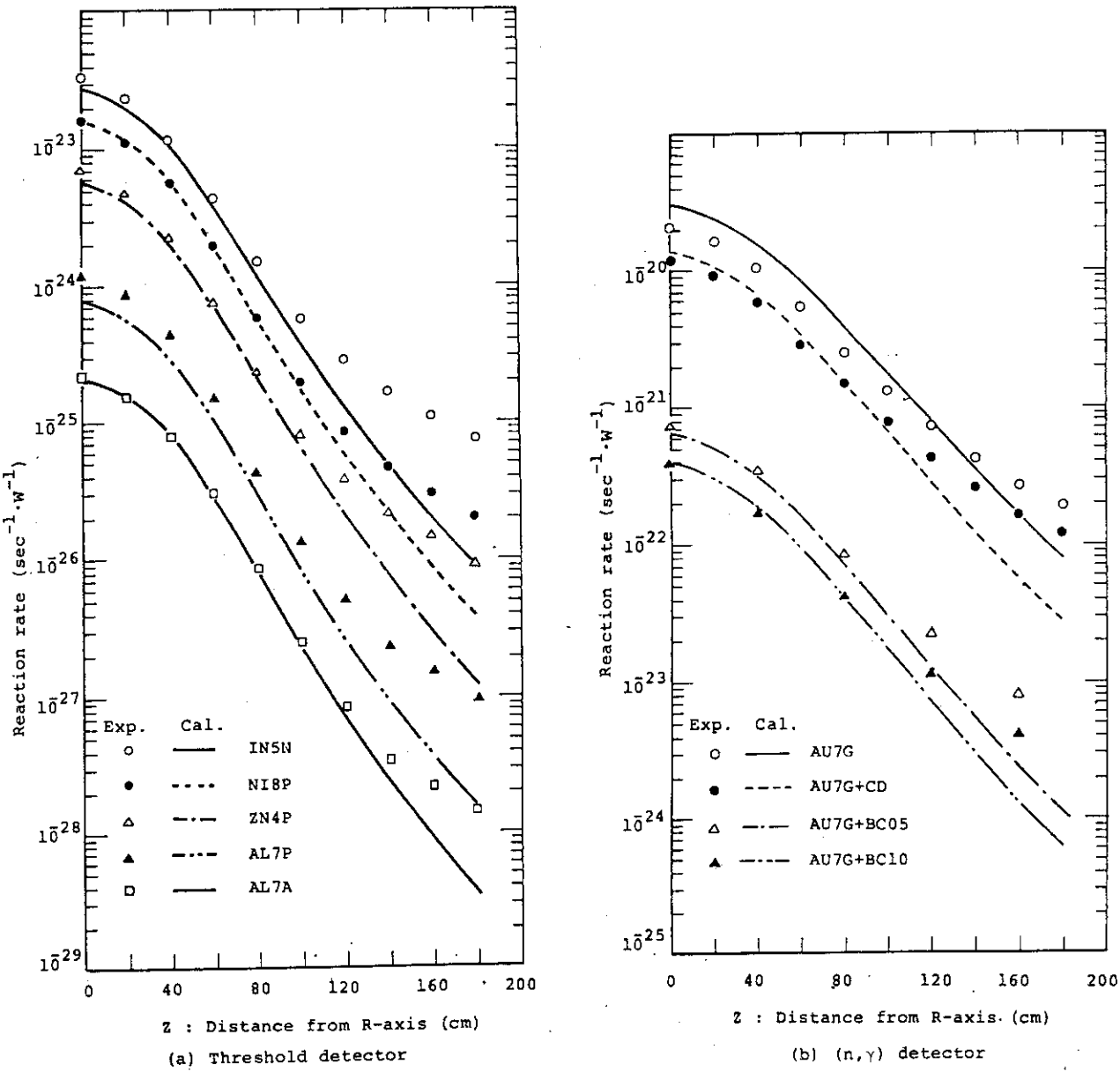

Fig. 4.2.2 (a), (b) Comparisons of the reaction rates measured and calculated along the annular gap of 10 cm width

4.3 Analysis of PCA Benchmark Experiment with Three-Dimensional Transport Code PALLAS-XYZ

N. Sasamoto and K. Takeuchi*

A Pressure Vessel Wall Benchmark Facility was established at the Pool Critical Assembly (PCA) of ORNL to test and validate reactor physics calculations in a simple geometry simulating a commercial power plant. In order to assess state-of-the-art neutronics methodology relative to reactor surveillance, the United States Nuclear Regulatory Commision (USNRC) conducted a computational Blind Test based on the PCA experiment, in which we participated with the PALLAS-XYZ calculation.

The PCA Benchmark Facility consists of the PCA reactor core of $60 \times 38 \times 40$ cm rectangular geometry and the ex-core components that are used to mock up pressure vessel surveillance configurations for light water reactors. The whole configuration immersed in the pool water is shown in Fig. 4.3.1. Dosimetry integral and differential experiments were performed for two different PCA configurations, X/Y=8/7 and X/Y= 12/13, designated as PCA(8/7) and PCA(12/13), respectively. Here, the X/Y refers to the water gaps (in cm) from the core edge to the thermal shield/the thermal shield to the pressure vessel.

The calculational model is given in Fig. 4.3.2. Here, a one-eighth configuration of the actual experimental setup was taken for the calculation because of symmetrical conditions with respect to x-, y- and z-axes. The calculation of the fixed source type was carried out with 21 energy meshes above 78 keV, yielding for the equivalent fission fluxes the reaction rates of fast neutron threshold reactions, the damage exposure parameter dpa, the the integral fluxes in the energy regions greater than 1.0 MeV and greater than 0.1 MeV.

The PALLAS-XYZ calculation was compared with the experiment and with other transport calculations using S_n codes and Monte Carlo codes, in collaboration with the Blind Test. As a result, the PALLAS-XYZ calculation without any geometrical leakage correction was found to provide a good agreement with the experiment within an error of 30% and to be as accurate as or more accurate than the calculations with the

* Ship Research Institute

Monte Carlo and the S_n codes in the two-dimensional (x,y) geometry with three-dimensional leakage corrections. As an example of the comparison, the C/E ratios of the damage exposure parameter dpa within the pressure vessel simulator are presented in Table 4.3.1. The difference between the PALLAS-XYZ calculations for the PCA(8/7) and PCA(12/13) configurations are due to the fact that the PCA(8/7) includes thinner water gaps than the PCA(12/13), resulting in more steeply varying neutron spectrum above 1.0 MeV in the pressure vessel simulator, which cannot be calculated accurately using PALLAS-XYZ relatively coarse energy mesh intervals of 0.2 or 0.4 lethargy.

Reference

1) McElroy W. M., et al. : "LWR Pressure Vessel Surveillance Dosimetry Improvement Program : PCA Experiments and Blind Test," NUREG/CR-1861 (HEDL-TME 80-87, R5) (1981).

Table 4.3.1 C/E ratios of damage exposure parameter based on equivalent fission fluxes

Code[1]	Location[2] in PCA(8/7)			Location[2] in PCA(12/13)		
	A4	A5	A6	A4	A5	A6
PAL3	0.90	0.90	0.89	1.07	1.10	1.13
C1	0.77	0.73	0.69	0.77	0.74	0.73
C2	1.10	1.03	0.97	1.19	1.14	1.10
C3	1.05	1.01	0.99	1.17	1.13	1.10
C4	0.81	0.80	0.78	0.91	0.91	0.92
C5	0.58	0.51	0.41	0.81	0.77	0.73
C6	0.89	0.84	0.81	0.84	0.82	0.81
C7	0.76	0.70	0.67	0.71	0.69	0.68
C8	0.84	0.80	0.75	0.86	0.84	0.80
C9	0.93	0.88	0.83	1.01	0.99	0.95
C10	0.91	0.80	0.83	0.93	0.90	0.88

1) Code PAL3 indicates the PALLAS-XYZ calculation, while Codes C1 through C10 indicate the calculations with S_n codes and Monte Carlo codes.

2) Locations A4, A5 and A6 are at 1/4, 2/4 and 3/4 of thickness of pressure vessel simulators, respectively.

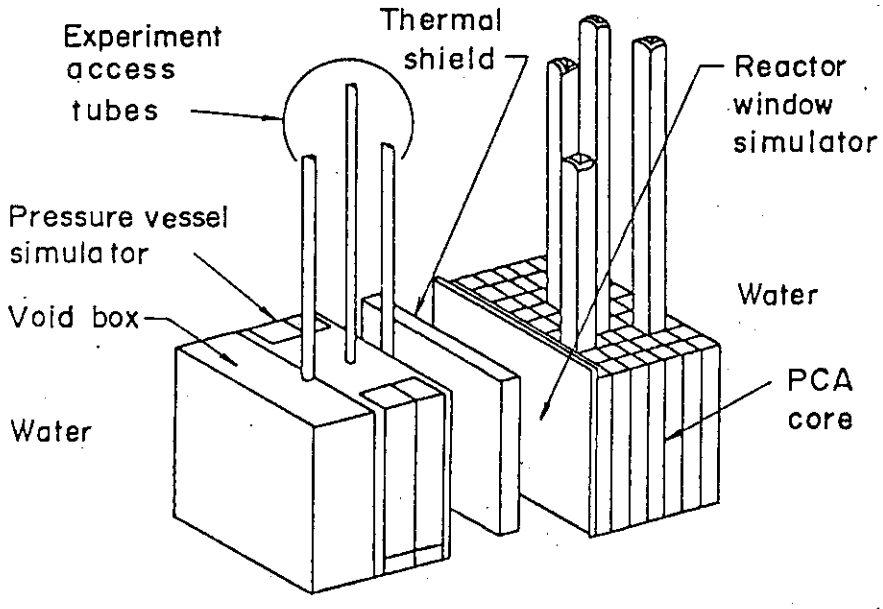

Fig.4.3.1 Experimental setup of the PCA experiment

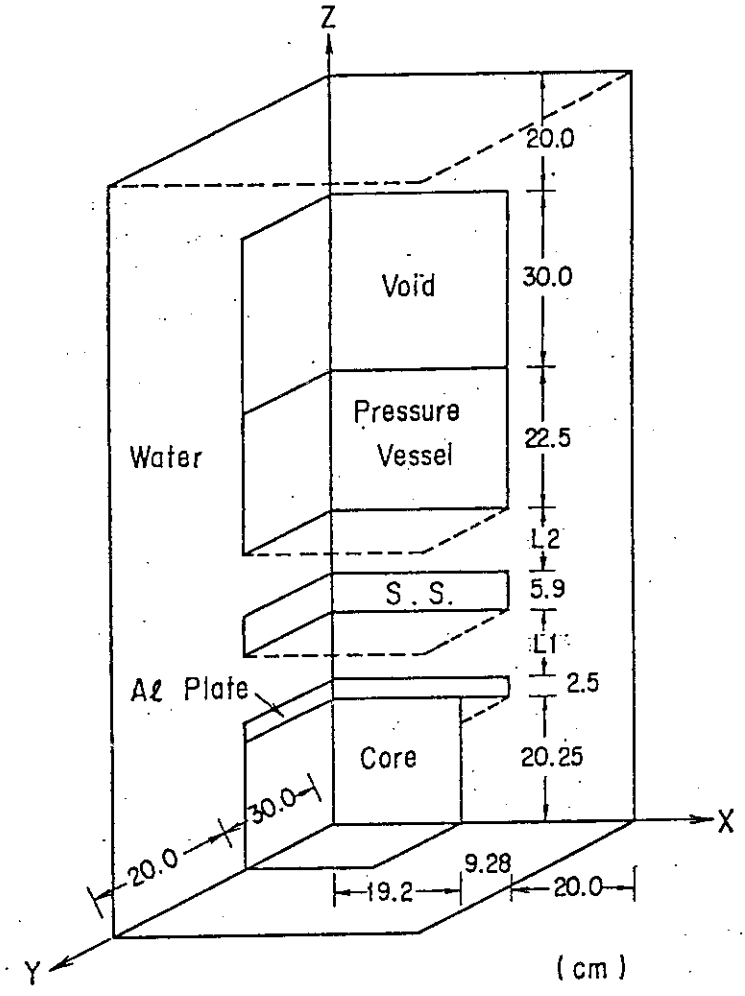

Fig.4.3.2 Calculational model of the PCA experiment for PALLA-XYZ. PCA(8/7) and PCA(12/13) configurations are respectively defined by designating L1/L2 as 8.4/6.7 and 12.3/12.8

4.4 BERMUDA-2DN: A Two-Dimensional Neutron Transport Code for Analyzing Fusion Blanket Neutronics

T. Suzuki and A. Hasegawa

On the basis of PALLAS-TS (BERMUDA-1DN)[1], a two-dimensional neutron transport calculation code, BERMUDA-2DN, has been developed. The main purpose of the new code is to analyze the fusion blanket neutronics experiments for plane or cylindrical assemblies, into which d-T neutrons are injected from the outside along the z-axis.

A 46-group cross-section library has been prepared for this code by collapsing the 120-group library[1] of PALLAS-TS. Furthermore, the both libraries have been equipped with the resonance self-shielding factors for ^{6}Li, ^{7}Li, C, O, Cr, Fe and Ni, and the fission cross section of ^{237}Np as a detector material. The uppermost twenty groups are the same in the two libraries. The succeeding twenty groups in the 120-group library have been collapsed into ten groups in the 46-group library, and the remaining eighty groups into sixteen groups. The weighting spectrum was set to 1/E in the collapsing procedure.

For more consistent scheme of generating group constant library, we are developing a code system, PROF-GROUCH-G/B[2], coupled with the EDFSRS system[3] for a nuclear data file. For the 47th (thermal) group, the necessary constants are to be given as card input for each problem after a preliminary calculation using a thermal spectrum code.

The time-independent transport equation is solved for two-dimensional, cylindrical, multi-regional geometry using the direct-integration method and the usual multigroup model in the same way as in PALLAS-TS.

The special features of the present code may be summarized in the following two points:

(1) For angular discrete ordinates, a set of fourty points are selected over the hemisphere made by unit direction vectors. Not only latitudes but also longitudes are taken into account in calculating the weight ($\Delta\psi$) of azimuthal angle of scattering. The table of $\Delta\psi$ ($\vec{\Omega}' \rightarrow \vec{\Omega}$, ξ) has been obtained, making $\vec{\Omega}$ fixed on its ordinate point over the unit sphere, for eighty values of ξ (the cosine of scattering

angle $(\vec{\Omega}' \cdot \vec{\Omega})$), that is, the ranges over ξ[-1, -0.9], [-0.9, 0], [0, 0.9] and [0.9, 1] are divided into twenty intervals of equal length, respectively. Thus the table of $\Delta\psi$ consists of 40×40×80 data.

(2) For the outer point source which is located on the z-axis of cylinder or on the extension of the z-axis, the direct beam flux is initially obtained at each (r,z) mesh point using the point kernel model, accounting both optical and actual distances between the source point and the mesh point. Next, the first collision source distribution with angular dependence is determined by this direct beam flux. The transport equation,corresponding to this distribution of first collision source plus slowing down source from upper groups, is solved using iteration technique and neutron rebalancing sheme. After convergence of pointwise angular flux due to the first collision plus slowing down sources, the actual flux distribution is obtained as the sum of the direct beam flux and the solution of the transport equation.

The result of test calculation shows fairly good agreement between the BERMUDA-2DN fluxes and the PALLAS-TS fluxes applied to a cylinder and a sphere having similar composition and configuration, respectively. Comparisons of the BERMUDA-2DN calculations with experiments at Fusion Reactor Physics Laboratory are going to be performed.

References

1) Suzuki T., Ishiguro Y., Matsui Y.: "PALLAS-TS: A One-Dimensional Neutron Transport Code for Analyzing Fusion Blanket Neutronics," JAERI-M 9492 (1981) (in Japanese).
2) A. Hasegawa: unpublished.
3) A. Hasegawa: unpublished.

5. Reactor and Nuclear Instrumentation

5.1 Development of High-Temperature Neutron Detectors

N. Wakayama, H. Yamagishi, H. Itoh, T. Tomoda* and S. Fukakusa*

High-performance and high-temperature fission counter-chambers and gamma-compensated ionisation chambers were developed to use as in-vessel neutron sensors for VHTR, HTGR and large scale LMFBR.

Accelerated neutron irradiation life tests at 600°C for the fission counter-chambers were carried out from 1975 to 1977 in the material testing reactor JMTR and research reactor JRR-3.[1] Simulating a reactor accident arisen in the end of mission time of the neutron detector being used, over-heat operating tests at temperature up to 800°C were carried out previously for the same type fission chamber FX-3 in JRR-3 and thermal pile in the Reactor Instrument Laboratory.[2] Long-term real-time in-reactor operating reliability tests were curried out for the same type fission chambers FX-2A and FX-3 in the research reactor JRR-4 from December 1978 to February 1981.[3),4)]

As concerns the high-temperature gamma-compensated ionisation chamber (CIC), the accelerated irradiation life tests for two CICs(#12, #16), (the electrodes of CIC#12 and #16 were made of nickel base super alloy and titanium respectively), were continued in the research reactor JRR-4 since October 1980. The tests were carried out under the condition of the operating temperature between room temperature and 400°C, neutron flux density of 2×10^{11} nv and gamma-ray fluence rate 9×10^{6} R/hr.

At the end of January 1982, the total test period for these chambers in the reactor and the high-temperature operating time at 400°C reached to 472 days and 6,048 hours(252 days), and total irradiation of neutron fluence and gamma-ray fluence reached to 4×10^{17} nvt and 5×10^{9} R. Detailed performance inspections for these chambers were carried out four times in this irradiation period and no change of operating characteristics notable has been observed in these inspections. The fourth inspection was carried

---

*Mitsubishi Electric Corporation

out at the end of January 1982 and the results of the inspection are shown in Figure 5.1.1 to 5.1.3. Figures 5.1.1 and 5.1.2 show results of plateau curve measurements of these CICs as a function of neutron-signal-current at 25 °C and 400 °C. Figure 5.1.3 shows results of the output linearity measurements for the CICs at 25°C and 400°C for the neutron flux density range of 10^2 to $2x10^{11}$ nv.

References

1) Wakayama N., Yamagishi H., Tomoda T., Kawashima K.: "Development of Fission Chambers for High-Temperature Reactors," Symposium proceedings on Nuclear Power Plant Control and Instrumentation, Vol.II, IAEA-SN-226/32, 243 (1978) IAEA.

2) Wakayama N., Yamagishi H., Itoh H., Tomoda T., Fukakusa S.: "Reactor Eng. Div. Annual Report (Apr. 1978 - Mar. 1979)," JAERI-M 8393, 77 (1980).

3) Wakayama N., Yamagishi H., Itoh H., Tomoda T., Fukakusa S.: "Reactor Eng. Div. Annual Report (Apr. 1979 - Mar. 1980)," JAERI-M 9302, 98 (1979).

4) Wakayama N., Yamagishi H., Itoh H., Tomoda T., Fukakusa S.: "Reactor Eng. Div. Annual Report (Apr. 1980 - Mar. 1981)," JAERI-M 9672, 90 (1981).

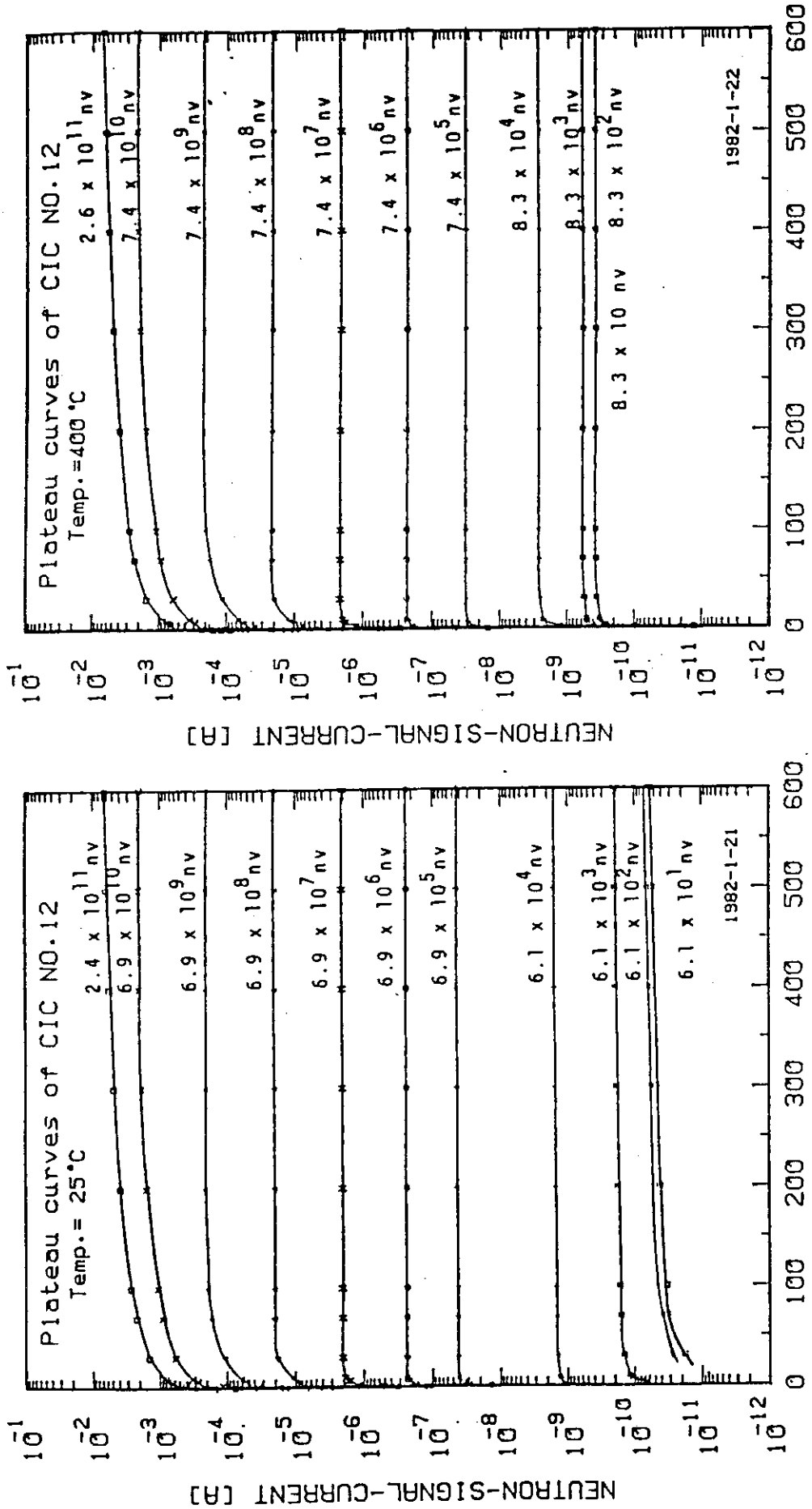

Fig. 5.1.1 Plateau curves of the gamma-compensated ionisation chamber CIC#12 at 25°C and 400°C after the accelerated irradiation life test

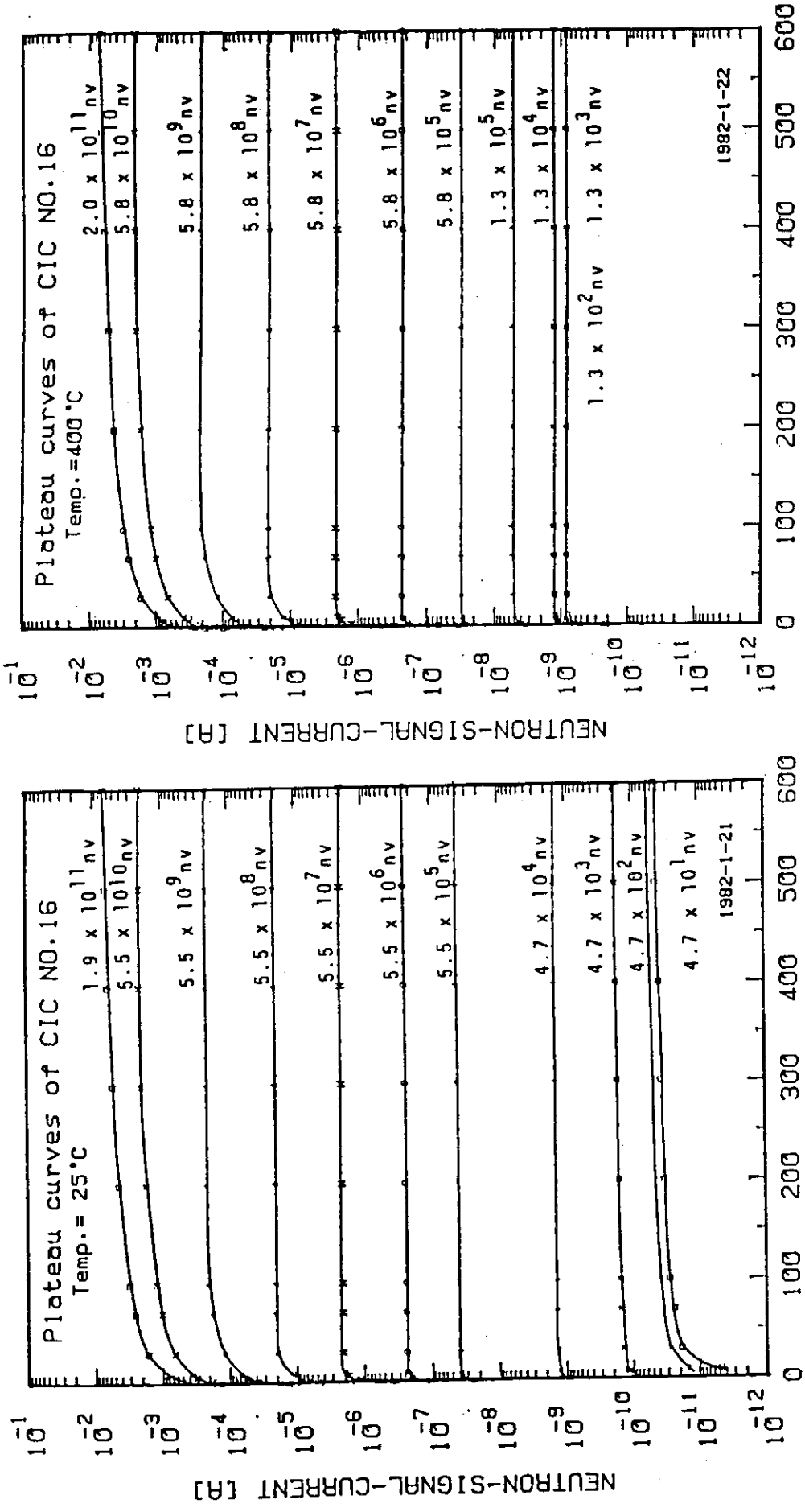

Fig. 5.1.2 Plateau curves of the gamma-compensated ionisation chamber CIC#16 at 25°C and 400°C after the accelerated irradiation life test

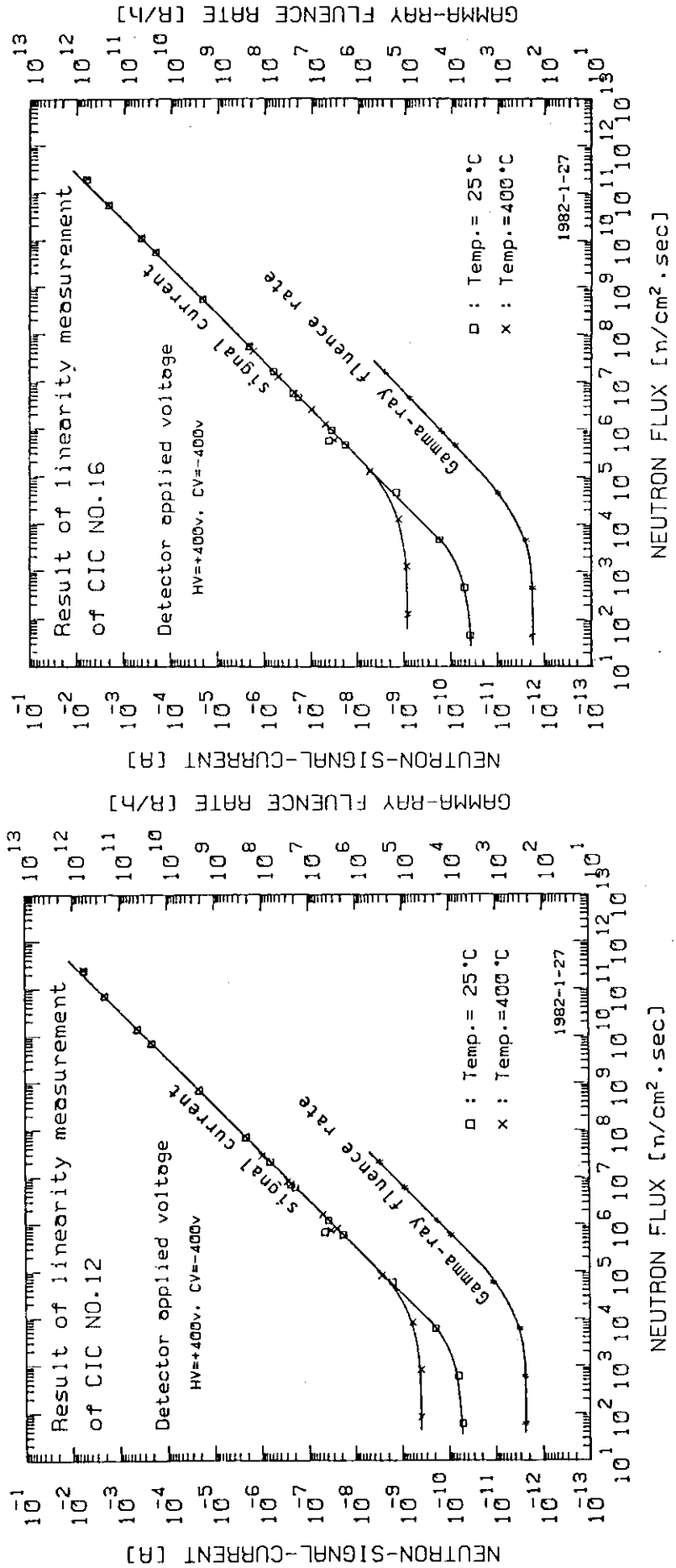

Fig. 5.1.3 Results of linearity measurements of gamma-compensated ionisation chambers(CIC#12 and #16) at 25°C and 400°C after the accelerated irradiation life test

5.2 Development of High-Temperature Thermocouples for VHTR

K. Ara, M. Yamada, K. Shimizu and N. Wakayama

As a part of development of high-temperature thermocouples for measurement of helium-gas temperature at the outlet of fuel region in the multi-purpose VHTR, trial fabrications and tests of W-Re alloy and Pt-Mo alloy thermocouples are progressed.

The W-Re thermocouple consists of stranded W-26Re/W-5Re elements (0.076 mm x 7 - 21), double sheaths and alumina insulators. The elements are connected to the double CA elements at the point of around 600 °C to minimize the necessary length of the W-Re elements. The inner sheath serves not only as a mechanical protector of the elements but also for gettering impurity gases contained in the filled helium gas and liberated from the insulator, and the outer sheath as a mechanical and chemical protector of the inner sheath against the in-core atmosphere containing somewhat reducing impurities under normal reactor conditions and oxidising impurities under accident conditions.

After trial fabrications of about fifteen thermocouples, out-pile high-temperature tests [1] and in-pile high-temperature irradiation tests were carried out. The in-pile tests were made at about 1400 °C for TZM/Nb-1%Zr sheath 21 stranded thermocouples. The results of this test are shown in Fig. 5.2.1. The EMF drifts due to irradiation were about 2% for the thermal neutron fluence of about 5×10^{20} n cm^{-2}. Further, the post irradiation examinations showed no existences of reactions, the insulators and the elements; but small cracks were found in the thermocouple elements as shown in Photo. 5.2.1.

As for the Pt-Mo alloy thermocouples, the bare element wires of Pt-5Mo and Pt-0.1Mo were tested previously in the atmospheres of commercial-grade pure argon, argon containing about 100 ppm O_2 or 100 ppm H_2, and of the vacuum, at 1000 - 1400 °C [2], [3]. Severe corrosions due to selective oxidisation of Mo were observed on Pt-5%Mo element in every cases except in the case of vacuum atmosphere. This means that a perfectly clean atmosphere is needed for the elements. Enclosing the elements with a getter for impurity gases seems to be the best method to keep clean the atmosphere around them. In order to confirm this effectiveness Ta-sheathed

Pt-5Mo/Pt-0.1Mo thermocouples with alumina insulator were tested at 1200°C. The diameter and the thickness of the sheath is 6.4 mm and 1.0 mm respectively, and the diameter of the element is 0.5 mm. The thermocouples were heated for 3000 hours, while the changes of EMF, mechanical strengths and metallographical structures were measured. Some of these results are shown in Fig. 5.2.2 and Photo. 5.2.2. It is seen that the EMFs showed positive drift of less than 0.6%. Although the magnitude of the EMF drifts is about three times larger than those recorded for the bare elements in high temperature vacuum, there is no problem in practical applications. Most EMF drifts were caused within 800 hours, and subsequently the EMFs became somewhat stable. The main reason is probably that it might take a time for the Ta-sheath to absorb completely impurities, contained in the filled helium-gas and released from the alumina insulator. Photograph 5.2.2 shows the metallographical structures of the elements after heating at 1200 °C for 3000 hours; any corrosion cannot be seen. From these results, the effectiveness of the adopting getter sheath was confirmed.

References

(1) Ara K., Yamada M., Wakayama N.: JAERI-M 9672, pp. 95-97(1981).
(2) Ara K., Wakayama N., Yamada M.: JAERI-M 8393, pp. 88-91(1979).
(3) Ara K., Wakayama N., Yamada M.: JAERI-M 9032, pp. 100-102(1980).

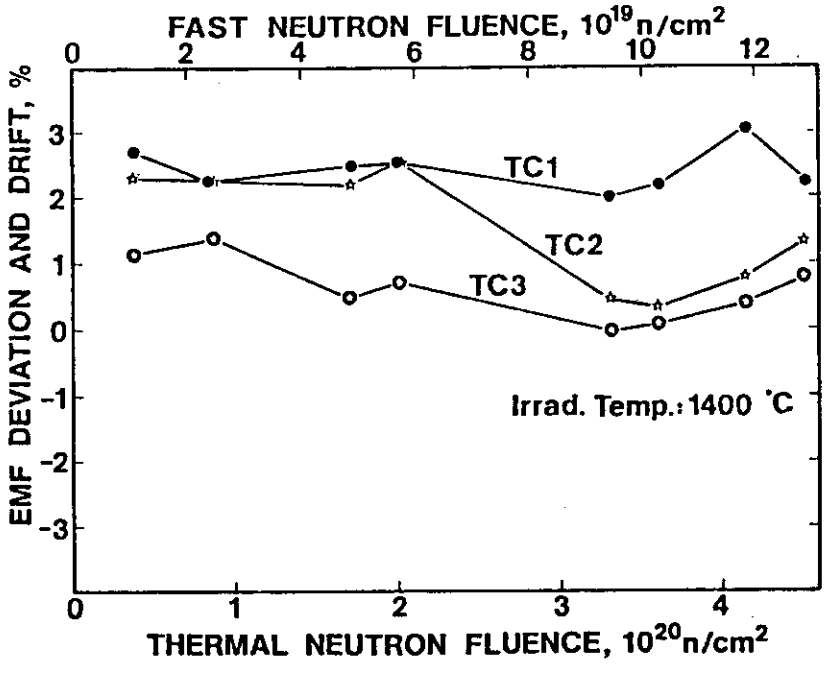

Fig. 5.2.1 EMF drifts of TZM/Nb-1%Zr sheathed W-26Re/W-5Re thermocouples in vacuum at 1200°C.

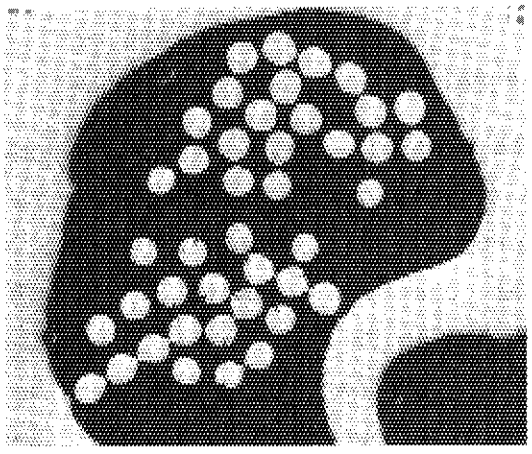

Photo. 5.2.1 Microphotography of hot-junction of irradiated W-26Re/ W-5Re thermocouple.

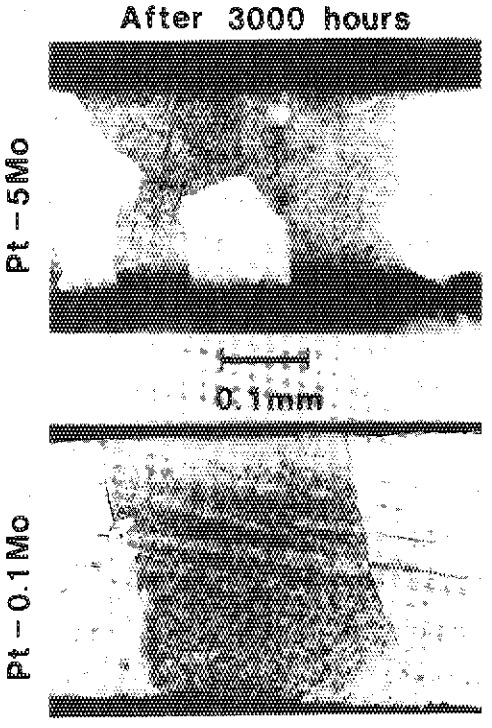

Photo. 5.2.2 Metallographical change of Ta-sheathed Pt-Mo alloy TC elements.

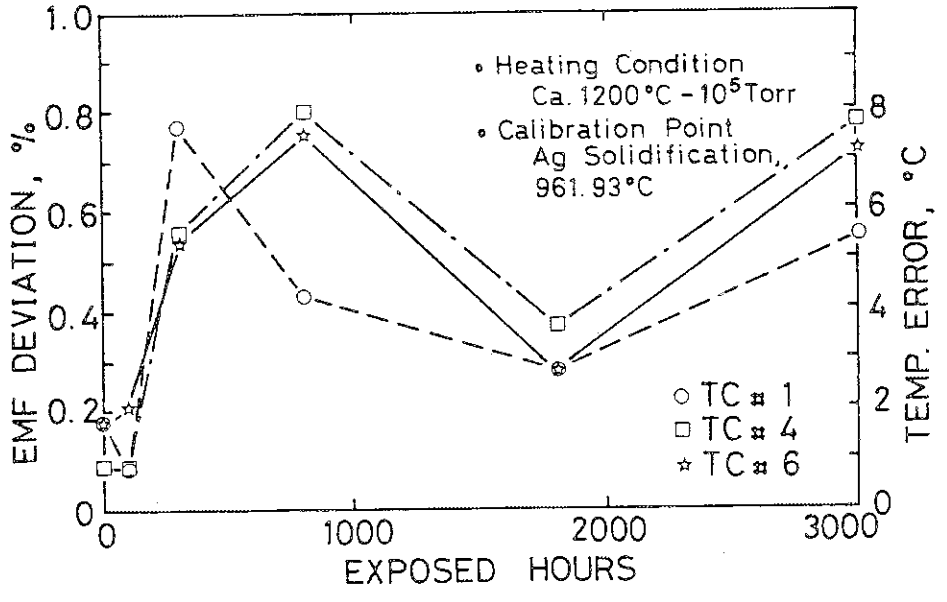

Fig. 5.2.2 EMF drifts of Ta-sheathed Pt-Mo alloy TC.

5.3 Development of Fuel Failure Detection System for the Coated Particle Fuel for VHTR

H. Terada, M. Katagiri and N. Wakayama

Fuel failure detection for the coated particle fuel (CPF) is extremely difficult as compared with that for the conventional metal cladding fuel. In general, the CPF releases fission products little by little to the primary coolant even during the normal operation condition of HTGR. Therefore, the radiation background level due to FP nuclides in the primary coolant is rather higher than those in conventional type reactors using metal cladding fuels. Moreover, as widely known, the background level changes considerably depending on the fuel temperature, reactor power, burn-up rate, and others. These facts make it difficult very much to detect the small increase of FP level due to fuel failure of the CPF.

Supposing that the ordinary fuel failure detection system for the conventional GCRs would be applied to the EVHTR and the total activities in the primary coolant would be monitored including piled-up long-life nuclides, it is estimated that the system can only distinguish the abnormality in a short time when the CPFs of 8 to 11 % exsisting in the monitoring region would have failed even under the rated power and constant temperature operating condition. Such scale of the fuel failure is not so small from the reactor operation and core management point of view.

In order to solve this problem, development of high sensitive fuel failure detection system for the CPF has been started on the basis of following considerations:

1) In order to reduce the effect of long-life FP-nuclides accumulated in the primary coolant and to make the measurement of newly born FP-nuclides easy, short-life FP-nuclides are monitored selectively.

2) A state equation is established on the concentration of the short-life FP-nuclides in the primary coolant. This is introduced into the FFD in order to distinguish the small change of concentrations of the short-life FP-nuclides, caused by CPF failures, from the variation of the concentration of the same sort of nuclides, caused by the change of the reactor operating state parameters such as fuel temperature and local power density.

The state equation in the normal operation can be represented as follows;

$$G = F(T,P,B,F,Q, - - -),$$

where G: concentration of short-life nuclides
or its measured value,
T: fuel temperature,
P: reactor power,
B: burn-up ratio of the CPF,
F: flow rate of the primary coolant helium,
Q: a measure of fuel quality obtained at
sampling batch test of the fuel production.

Then the failure of the CPF can be detected by means of judging whether the behaviour of the short-life background measured in a certain reactor operating conditioin is deviating from a certain range given by the state equation or not.

As the first step of the development, a selective detection system for short-life FP-nuclides was made up combining a multi-interval counting system and a wire precipitator. This detection system was connected to the primary circuit of an CPF-irradiation rig under sweeping gas, named FGS, in the JMTR as shown in Fig. 5.3.1. The irradiation rig supplies sample gas containing FP-nuclides released from CPFs to the precipitator. This irradiation rig was originally prepared for the CPF research and has an ability to irradiate several fuel samples and to control the irradiation condition, such as irradiation temperature and gas flow, individually for each fuel, and has FP-gas analysing system including a gamma-ray spectrometer. Consequentry, it is relatively easy to investigate the quantitative relationship between the irradiation condition of CPF and the counting rate of the precipitator to obtain the state equations for the FP monitoring.

The FFD experimental device system has been installed at the site of the JMTR and the experiment has been started at the end of 1981. Figure 5.3.2 shows a typical measured data by this system during a start-up period of the JMTR. In this experiment, it is expected to detect short-life FP-nuclides, for example Kr-89(3.18m), Kr-90(32.3s) and Xe-139(39.7s). Up to now, however, as the irradiated CPF samples have had only low failure rates, detected FP-nuclides are mainly of moderate-life; e.g., Xe-138(14.1m) and Kr-88(2.84h).

This experiment using FGS will be proceeded until the end of 1985 and it is expected to obtain the precise state equation for the high sensitive fuel failure detection system.

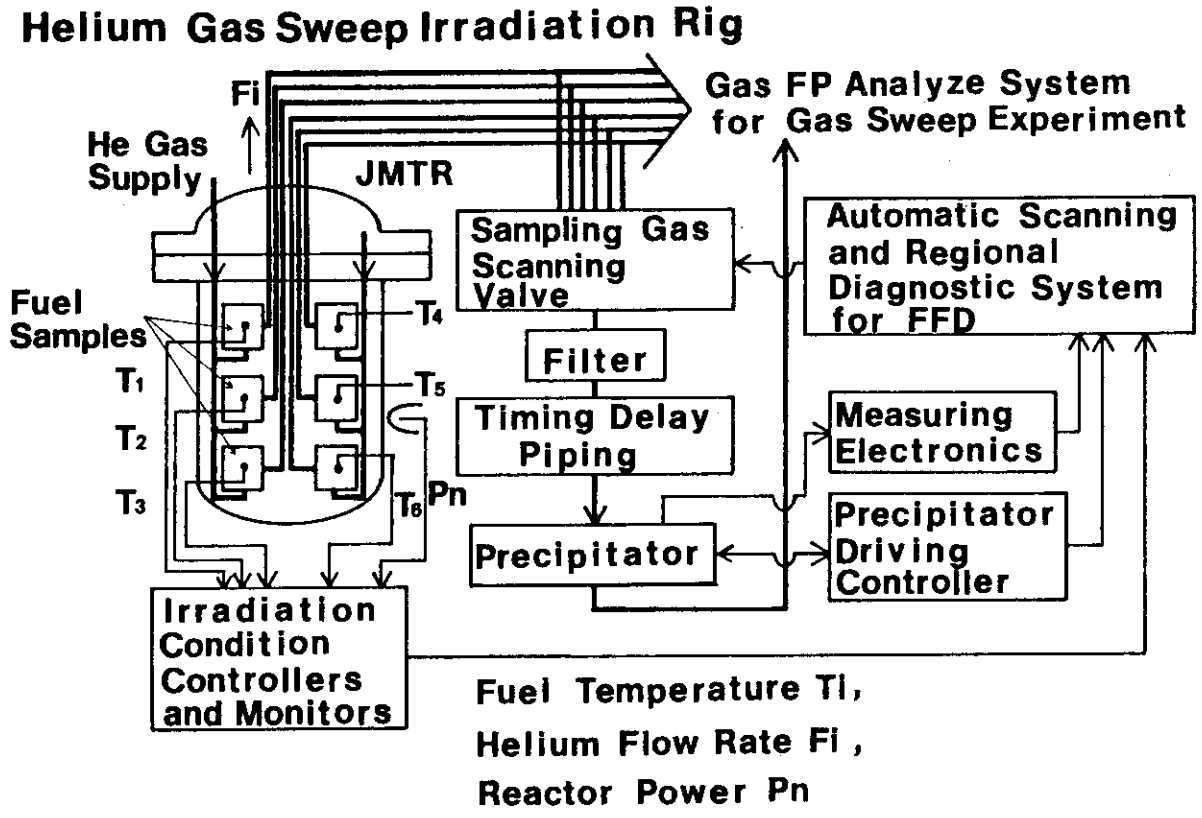

Fig. 5.3.1 Schematic diagram of the FFD experimental devices

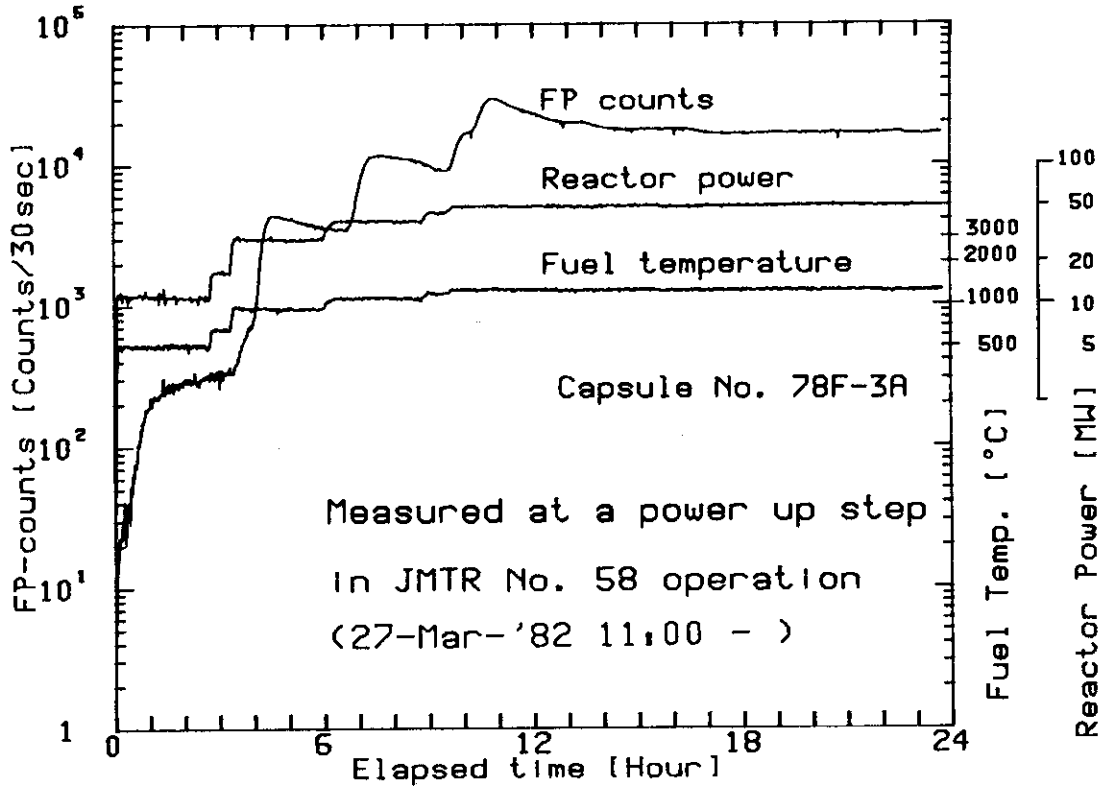

Fig. 5.3.2 A measured result of the FFD experiment in the JMTR no. 58 operation

5.4 JRR-3 Cover Gas Experiment on Various Types of Fuel Failure Detection Systems for LMFBR's

E. Sakai and H. Yoshida

In order to obtain basic data on the use of fuel failure detection systems to be used in the experimental LMFBR "JOYO" and for designing those systems for the prototype LMFBR "MONJU", experiments have been continued using the Cover Gas Monitor Test Facility located in JRR-3 nuclear reactor.[1)-3)] The main results obtained are as follows:

(1) The temperature dependence of the breakthrough curves, breakthrough times and static adsorption coefficients of charcoal (5g TSURUMICOAL 2GM in 10 cm^3 chamber) for 5000 ppm and 100 ppm Kr or Xe in He or Ar carrier gas at 1 liter/min flow was measured at 50°C, 30°C, 0°C, -40°C and -70°C. The effects of the charcoal temperature and the concentration of Kr or Xe became clear.

(2) The gamma-ray spectroscopy of the charcoal chamber at various temperatures and the charcoal outlet chamber was made using JRR-3 He cover gas which included radioactive Kr and Xe as well as Ar-41.

(3) The long-term performance of a fixed-wire type precipitator system was tested using JRR-3 cover gas.

(4) The gamma-ray spectra of JRR-3 cover gas were measured using a room temperature semiconductor detector made of HgI_2.

(5) A survey of fuel failure detection systems for LMFBR's was made including the attendance at IAEA/IWGFR Specialists' Meeting on Fuel Failure Detection and Localization at Karlsruhe on 11 - 14 May 1981.[4)]

The cooperation of Messrs. K. Kubo and Y. Kobayashi, Toshiba Corporation, is deeply acknowledged.

References

1) Sakai E., Kubo K. : "Development and test of cover gas on-line gamma-ray monitor (I)," SJ-250 79-06 (April 1979) (in Japanese).

2) Sakai E., Kubo K., Yoshida H. : ibid. (II), SJ-250 80-27 (June 1980) (in Japanese).

3) Sakai E., Kubo K., Yoshida H. : ibid. (III), SJ-250 81-07 (March 1981) (in Japanese).

4) Sakai E., Miyazawa T., Sekiguchi N. : "Summary of in-pile loop

experiments related to the development of the fuel failure detection systems for LMFBR's in Japan," IAEA/IWGFBR Specialists' Meeting on Fuel Failure Detection and Localization, Karlsruhe, 11 - 14 May 1981.

5.5 Temperature Dependence of Thermal Neutron Detection Performance of BF_3 Proportional Counters

E. Sakai, Shuzo Usui*, Hideo Ohkado*, Yoshimitsu Hayashi* and Hideo Nakatani*

No paper was found which described temperature dependence of thermal neutron pulse height distributions obtained from BF_3 proportional counters. We have tested several BF_3 counters of 1" diameter of Japanese made, i.e., (1) Mistubishi Electric ND-8537-90 (Al cathode, 90 cmHg, 17 cps/nv), (2) Mitsubishi Electric ND-8537-55W (Al cathode, 55 cmHg, 13 cps/nv) and (3) Hitachi Ltd. EB-125-7 (Cu cathode, 70 cmHg) at temperatures up to 200°C.

All the detectors tested showed a decrease in the pulse height and a broadening of the peak width for thermal neutrons. Figure 5.5.1 shows the pulse height distributions, thermal neutron counts, peak pulse heights and peak widths observed in the counter (1) at various temperatures. The counts stayed constant up to 150°C and decreased above 150°C. The counter (2) showed almost the same performance as the counter (1) although the counts increased above 150°C. The counter (3) showed an increase in the counts above 100°C.

The decrease in the pulse heights at higher temperatures is in contrast with the increase in the pulse heights observed in He-3 proportional counters[1] and seems to be caused by some impurities desorbed from the counter walls at higher temperatures.

Reference

1) Sakai E., et al. : IEEE Trans. Nucl. Sci., NS-27, No.1, 776 (1980).

* Faculty of Engineering, Toyama University, 1-1, Nakagawasonomachi, Takaoka, 933, Japan.

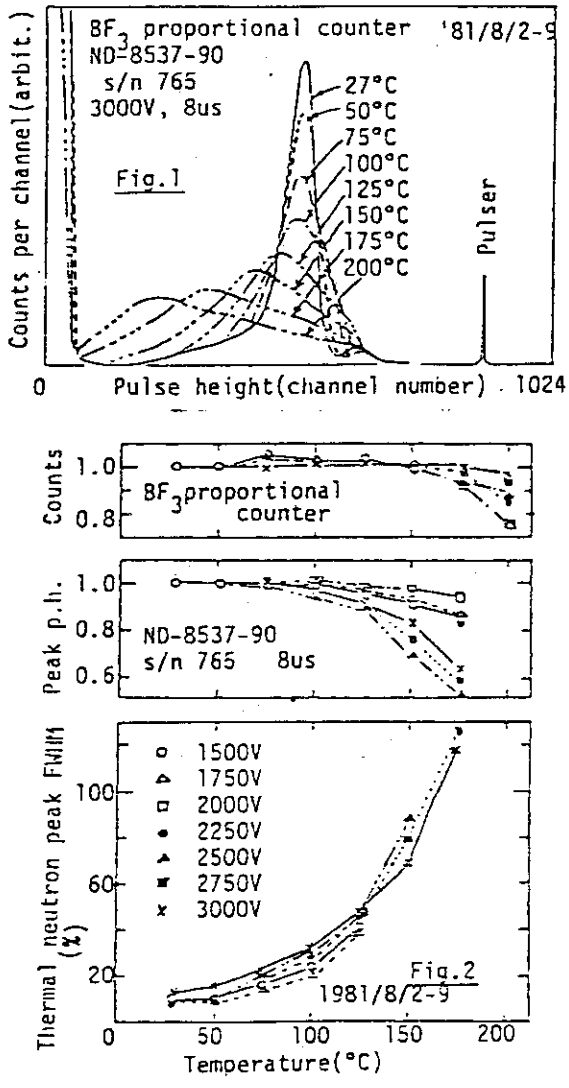

Fig. 5.5.1 Thermal neutron pulse height distributions, counts, peak pulse heights and peak widths observed in BF_3 proportional counter Mitsubishi ND-8537-90 at various temperatures

5.6 Development of Cable Insulators and Cables for LMFBR Instrumentation

T. Kakuta, K. Ara and N. Wakayama

Several mineral-insulated cables were developed in order to be used in high-temperature and high-radiation environments around the primary circuits of LMFBR. Their performances were tested under simulated FBR conditions.

The 600-V power cables, type FML-600P and GSB, were designed to have enough flexiblity, as shown in Fig. 5.6.1; and they were gamma-irradiated up to 1 x 10^{10} R. The results are shown in Fig. 5.6.2. Both the cables showed good electrical performances. The organic sheath material was, however, deteriorated by the irradiation near to 10^{10} R, causing a slight corrosion of the conductor and armour material. One needs some care in their use in high-radiation environments.

The structure of control cables, type 78-01 and 78-02, are shown in Fig. 5.6.3. They were tested under simulated accident conditions; namely, the cables were heated up to 360 °C twice and then maitained at 270 °C for 100 hours. In this test, A.C. 100 V and 12 A were applied to the cables for observation of electrical performances. Cables showed excellent electrical performances. Further, their dielectric breakdown strengths were examined after the tests and enough strengths were recorded. It was concluded that the cables could demonstrate the whole of their cable functions even under FBR-conditions. The results are shown in Fig. 5.6.4.

The SiO_2-insulated metal-sheathed tri-axial cables, RR-TRIAX-50, are shown in Fig. 5.6.5. They have been developed for nuclear instrumentation. For the tests, the cables were connected with the N-type connectors which were machined of the end seals sent from DOE,(see Fig. 5.6.6). Their total performances were examined from an applicative point of view. The test results showed their excellent performances, B.P.N. characteristics, and insulation resistances, up to the temperature of 550 °C. The results are shown in Fig. 5.6.7 and Fig. 5.6.8

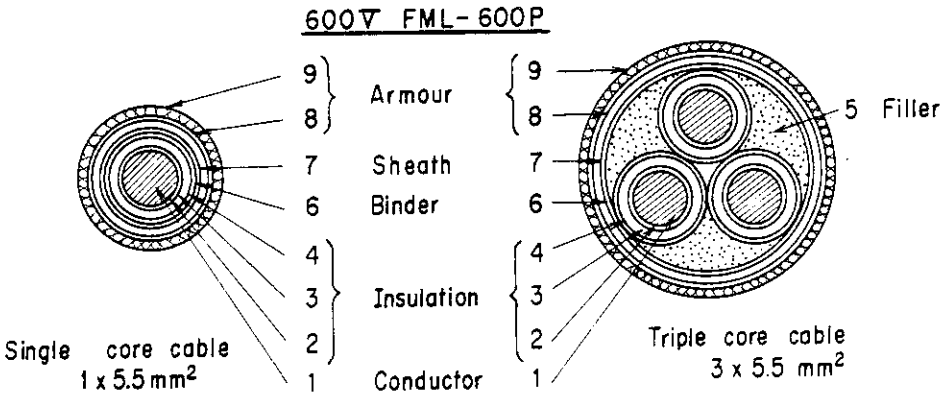

1 Sn-plated Cu wire 7/10 5.5 mm² ----- Conductor
2 Poly imide tape
3 Mica-poly imide tape
4 Glass fiber braid ----- Insulation
5 Asbest (wet type) ----- Filler
6 Glass fiber tape ----- Binder
7 Chlorosulphonated polyethylene ----- Sheath
8 Glass fiber braid
9 SUS wire braid 0.32 dia ----- Armour

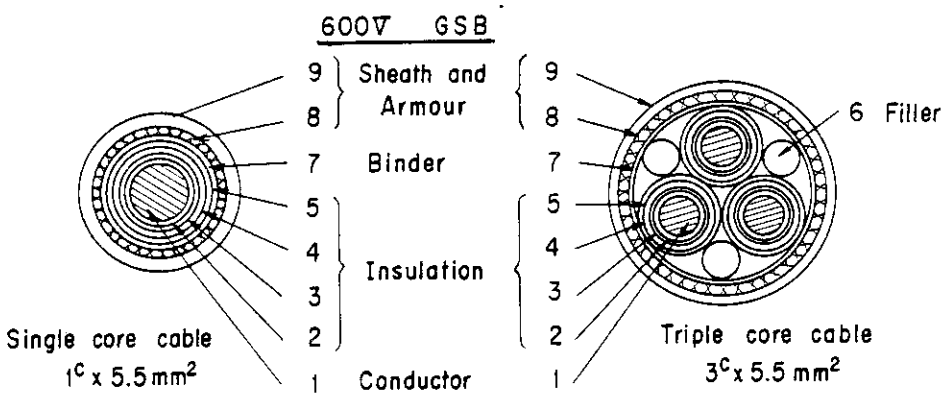

1 Sn-plated Cu wire 7/1.0 5.5mm² ----- Conductor
2 Poly imide tape
3 Mica-(Silicone)-Glass tape
4 Silicone varnished glass tape
5 Glass fiber braid ----- Insulation
6 Silicone rubber ----- Filler
7 Glass fiber tape ----- Binder
8 SUS wire braid 0.32 dia
9 Fire retardant poly ethylene ---- Sheath and Armour

Fig. 5.6.1 Structure of 600-V power cables

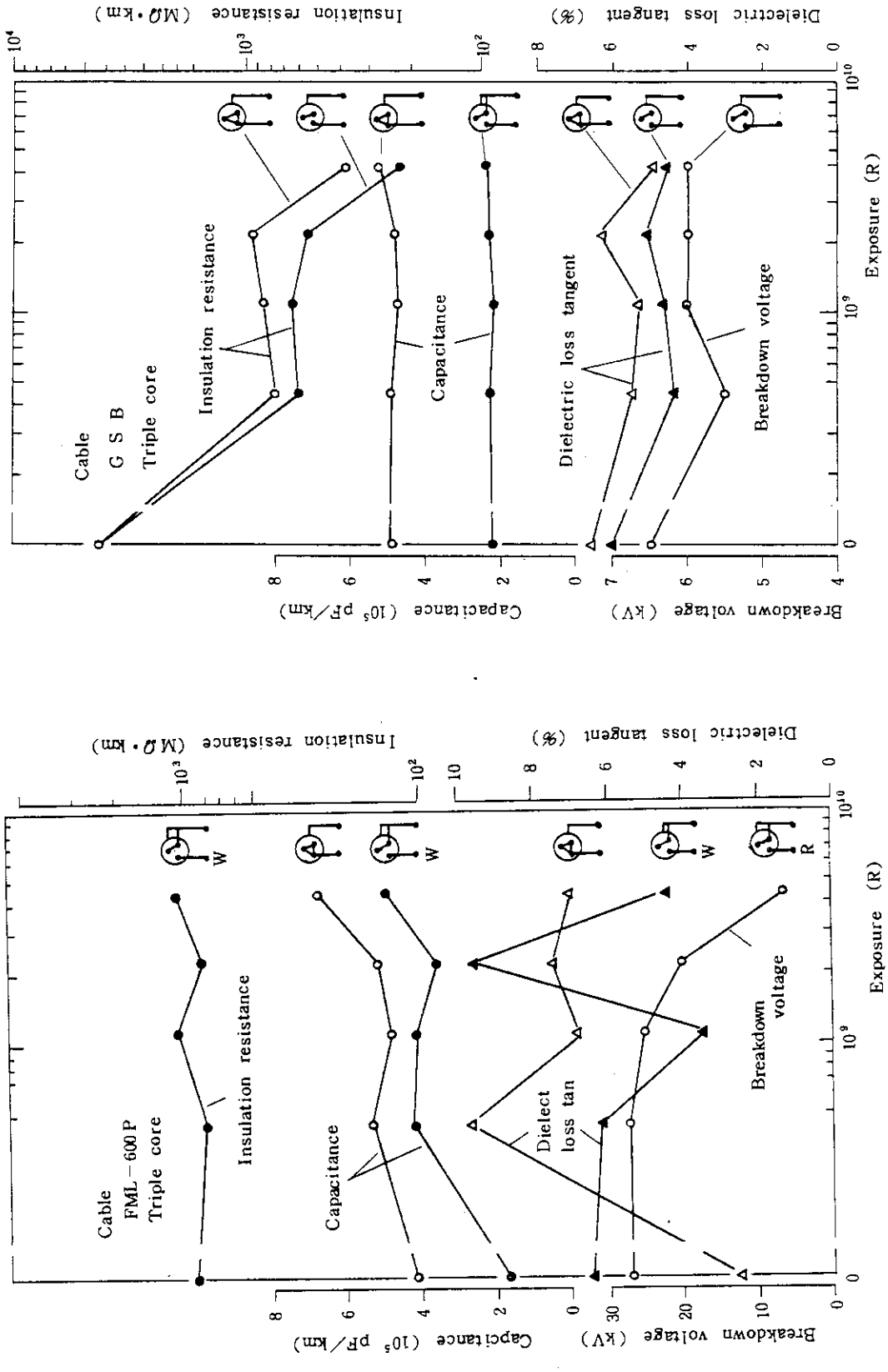

Fig. 5.6.2 Gamma-irradiation test results of 600-V power cables

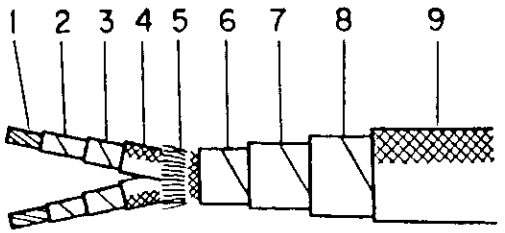

1 Ni-plated Cu wire — $2^C \times 2mm^2$ — Conductor
2 Poly imide film
3 Mica-Imide tape — Insulator (thick. 0.9mm)
4 Braided fiber glass
5 Fiber glass sleeve — Filler
6 Fiber glass tape — Binder
7 Ni-plated Cu tape — Shield
8 Fiber glass tape — Binder
9 Braided SUS wire — Jacket

Cable : 78-01

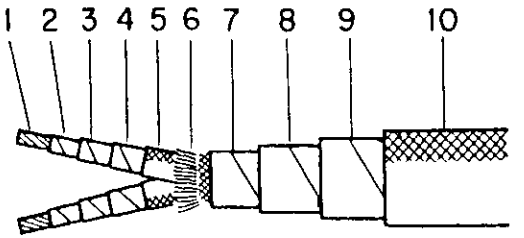

1 Ni-plated Cu wire — $2^C \times 2mm^2$ — Conductor
2 Poly imide film
3 Fiber glass tape — Insulator (thick. 0.9mm)
4 Poly imide film
5 Braided fiber glass
6 Fiber glass sleeve — Filler
7 Fiber glass tape — Binder
8 Ni-plated Cu tape — Shield
9 Fiber glass tape — Binder
10 Braided SUS wire — Jacket

Cable : 78-02

Fig. 5.6.3 Structure of control cables

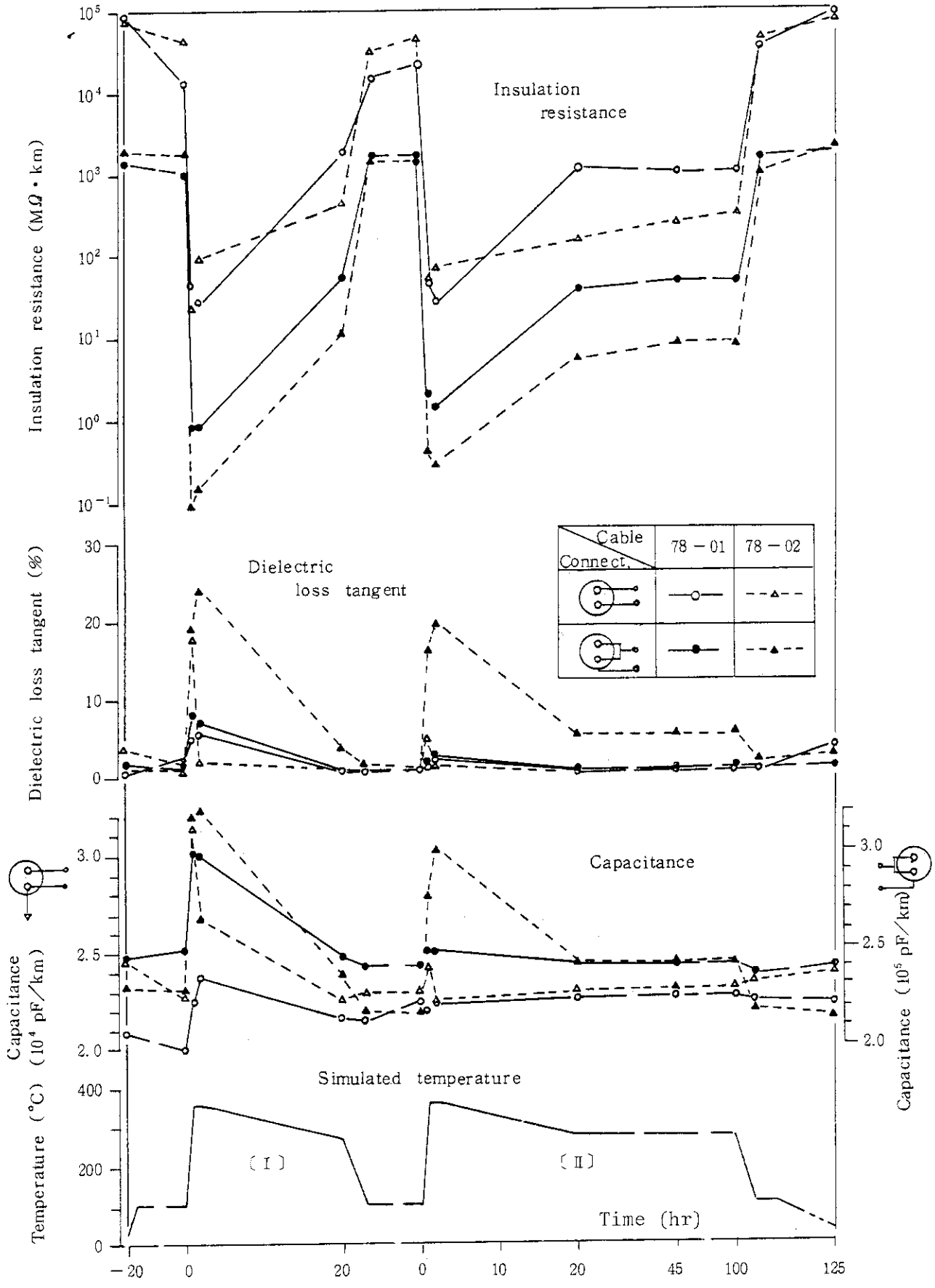

Fig. 5.6.4 Results of simulated accident test for control cables

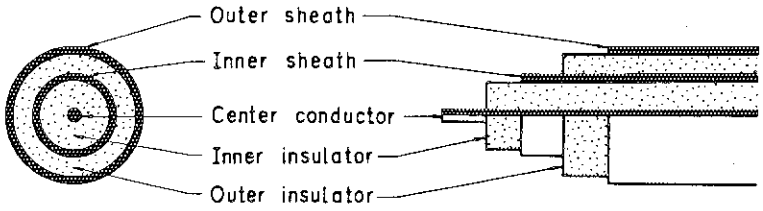

Fig. 5.6.5 S_iO_2 insulated tri-axial cable (RR-TRIAX-50)

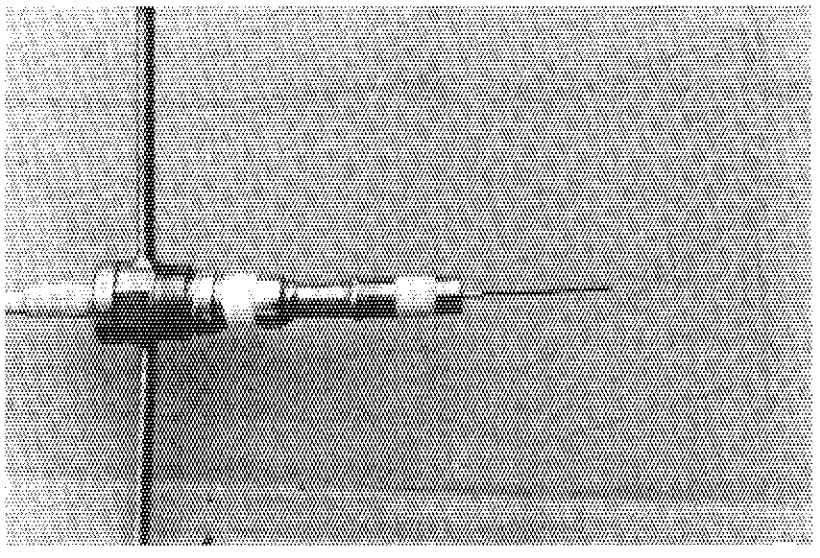

Fig. 5.6.6 Cable end seals for tri-axial cable

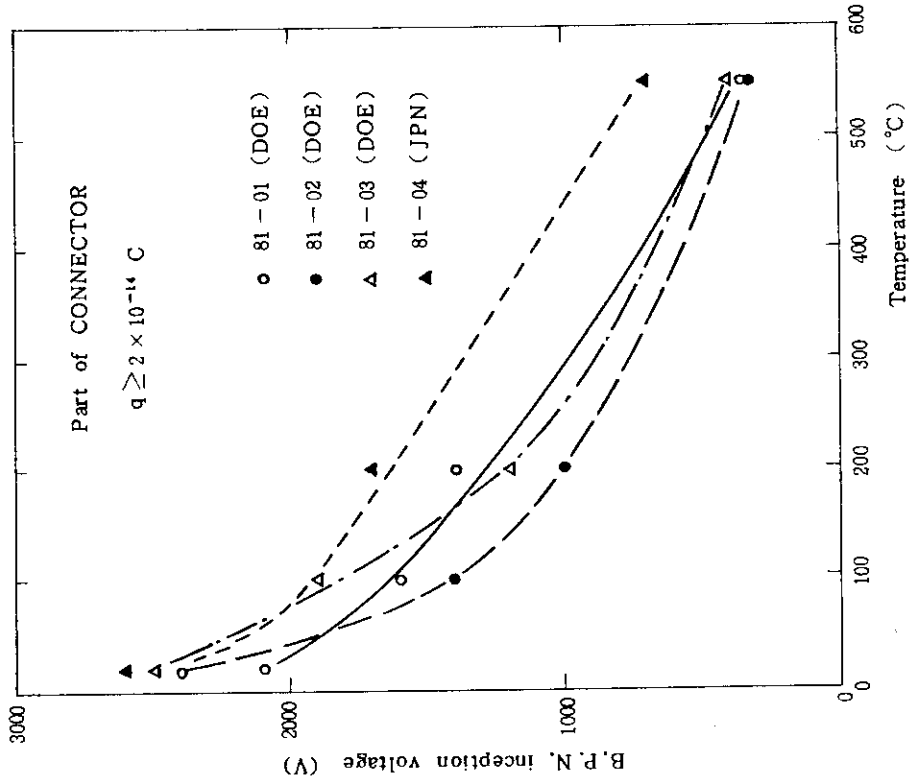

Fig. 5.6.8 Breakdown pulse noise inception voltages of cable end seals

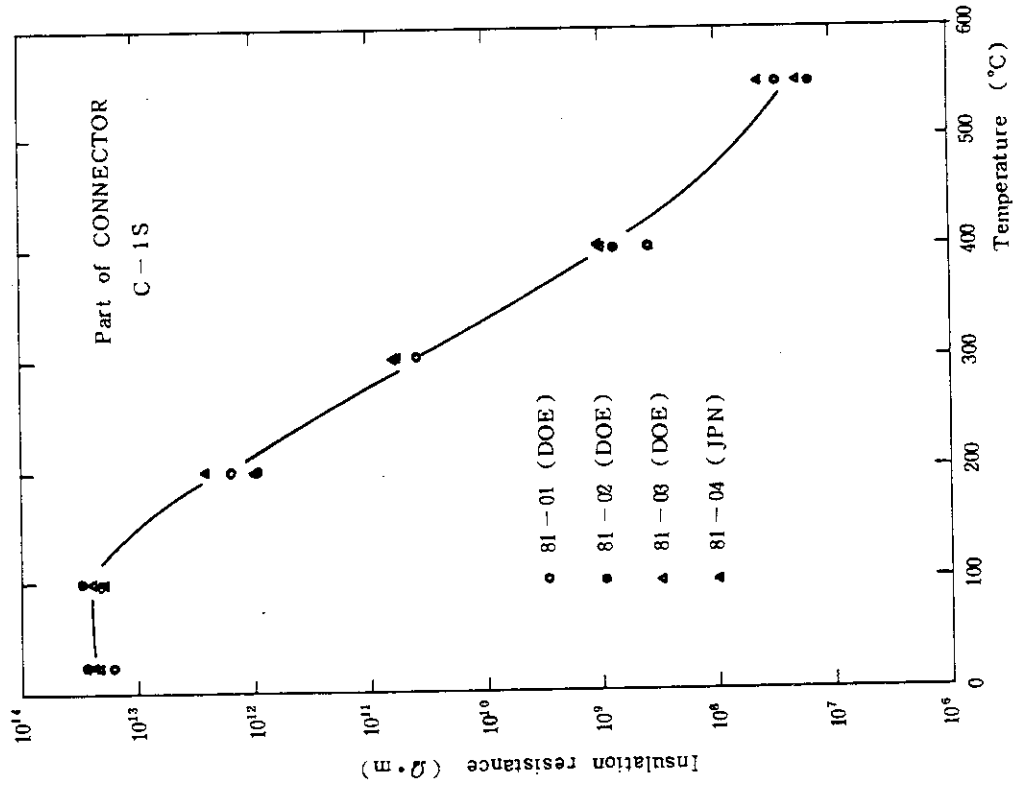

Fig. 5.6.7 Insulation resistances of cable end seals

5.7 Development of Pressure Sensor for Measurement of Fuel-pin Inner Pressure

K. Ara, M. Yamada, K. Shimizu and N. Wakayama

A pressure sensor using a bellows and a differential transformer was developed for the purpose of measuring the internal pressure of reactor fuel rod. It was designed under performance requirements as follows : (1) operating temperature , 300 °C ; (2) measuring range of pressure , 0 - 150 kg/cm^2 ; (3) environment, high-temperature and high-pressure water of 320°C - 170 kg/cm^2 in a reactor core.

Figure 5.7.1 shows the structure of the bellows assembly. The bellows is made of Inconel 718 and has twenty threads. Its spring modulus is about 9 kg/mm and effective area is 0.166 cm^2. The spring is used for keeping balance in order that the bellows may contract 1 mm when the assembly is pressurized to 150 kg/cm^2. The spring, being made of Inconel X750, has the modulus of about 16 kg/mm.

Figure 5.7.2 shows the structure of the differential transformer developed as a secondary sensor. Both the primary coil and the secondary coil are in the cylindrical yoke whose cross section looks like a letter E. The yoke is made of ferromagnetic stainless steel SUS403, and the coils are of ceramic-coated heat-resistant wire with the diameter of 0.15 mm. A cylindrical magnetic core (SUS403, 3 mmOD x 2.15 mmL) which is set up at the edge of the extension bar of bellows assembly, moves inside the coil along the axial direction. The area of a gap of magnetic circuit, therefore, changes as the core moves. Bobin is made of SUS316, and coated with alumina. Its thickness is about 150 μm.

The bellows assembly and the differential transformer were combined by welding to be a pressure sensor. It was tested for calibration under the helium-gas pressure of 0 - 100 kg/cm^2. The test was carried out at R.T.(about 20 °C), 100 °C, 200 °C, and 300 °C. The results of these tests are shown in Fig. 5.7.3. Each shows little hysteresis and good linearity. However both the zero point and the sensitivity change with temperature linearly. The change of the zero point is caused by a thermal expansion of the bellows assembly, and that of the sensitivity by the change of the permiability of the ferromagnetic material used in the differential

transformer. Here, two secondary outputs of differential transformer, E1 and E2, are treated to compensate for the sensitivity change in some degree; namely, the differential output (E1-E2) is normalized by the summed output (E1+E2).

From the results shown in Fig. 5.7.3, it was found that the relationship between the output of the sensor, Eps, and the pressure P is expressed as a linear function, Eps=A+BP; where both A and B are given by linear functions with temperature T as follows; $A=-0.11495(1+0.165\times10^{-3}T)$, $B=0.001039(1+0.565\times10^{-3}T)$. Therefore, if only the temperature T can be known by any method, temperature compensation would be possible by using a microprocessor. Here, the summed output of the differential transforemer was used for this compensation also. Figure 5.7.4 shows the variation of the summed output Es with temperature within the measuring range of pressure. A primary regression straight line for T and Es was obtained as T=-1218.6+769.9Es. A simple calculation using the above equations was tried to estimate the compensation accuracy. The results are shown in Fig. 5.7.5. The compensation can be made within the errors of 1%. In a practical system, two outputs of the differential transformer are amplified and rectified separately, and converted to digital signals and computed on time by the microprocessor.

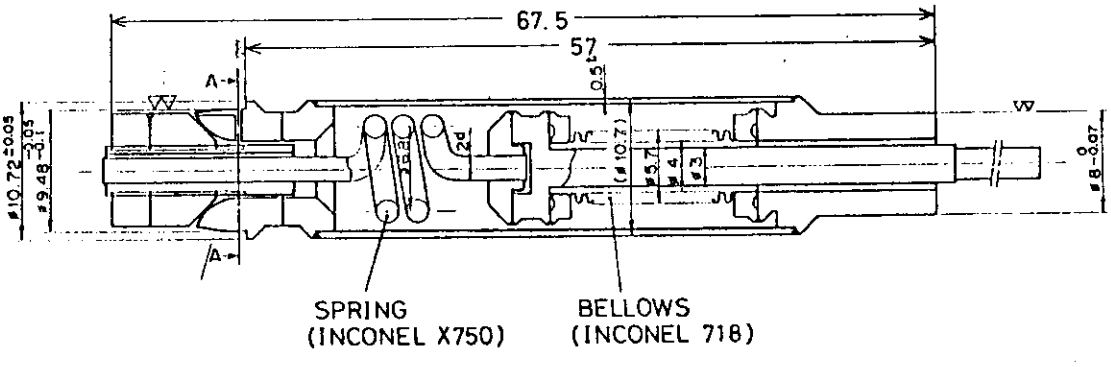

Fig. 5.7.1 Bellows assembly

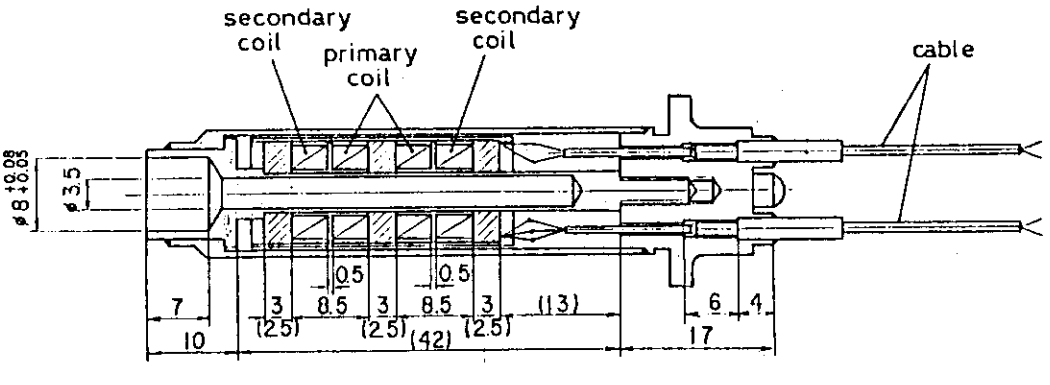

Fig. 5.7.2 Differential transformer

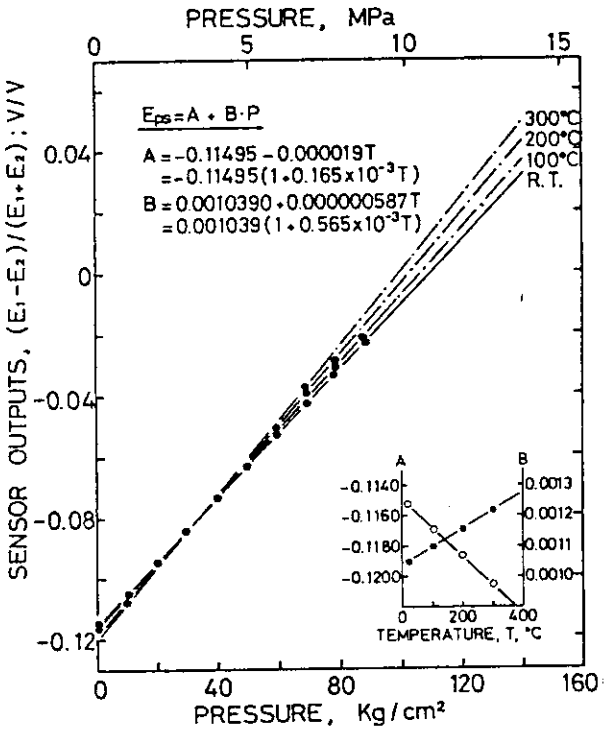

Fig. 5.7.3 Results of pressure sensor calibration

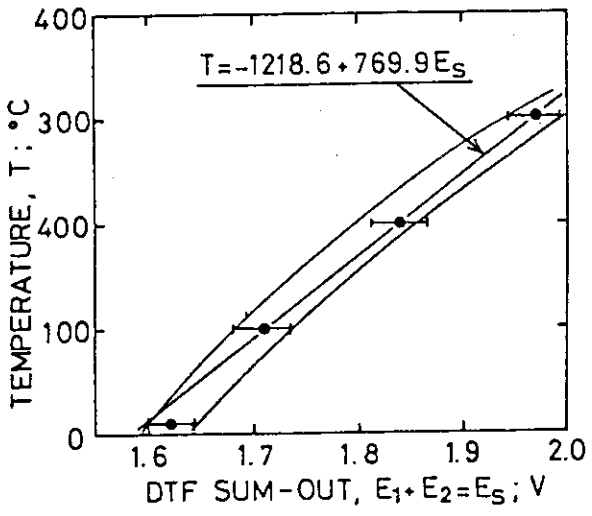

Fig. 5.7.4 Variation of "summed-output" with temperature

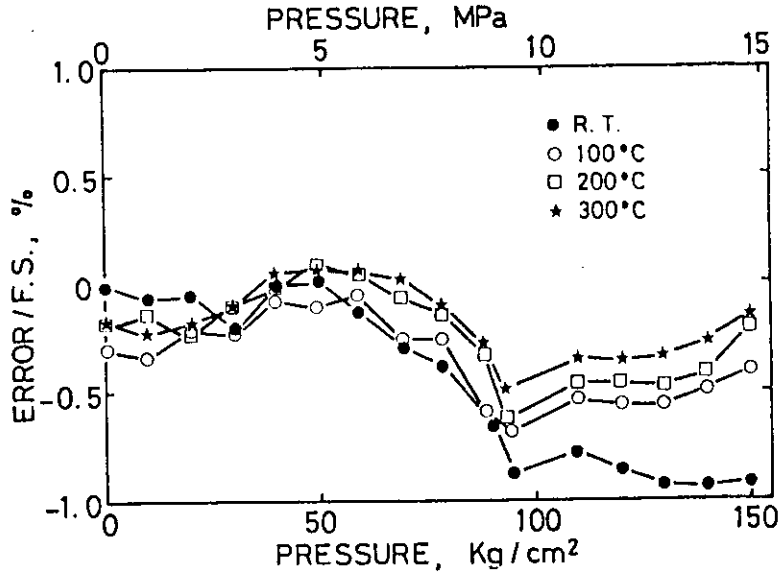

Fig. 5.7.5 Measuring errors, simulated by calculation

5.8 Development of Nitrogen Gas-cooled Ge(I) Gamma-ray Detector System

M. Katagiri, H. Terada, S. Matsunaga, H. Nakatsuka and N. Wakayama

Evaluation of the amount of radio-activities accumulated in pipings and machineries in the nuclear power plant is very important for planning of plant maintenance, safety evaluation of maintenence work and for disassembling and repairment of plant components. For such purposes, the gamma-ray spectroscopy has been applied. The ordinary semi-conductor gamma-ray detectors, however, need liquid-nitrogen cooling. This makes sometimes troubles and causes limitation of their application in the plant. Therefore, the detector system without liquid-nitrogen cooling is required today, and also the small detector size is preferred since shielding of the detector from the background gamma-rays is needed in many cases. This motivated the development of a nitrogen gas-cooled Ge(I) detector system.

The developed nitrogen gas-cooled Ge(I) detector system utilizes a Joule-Thomson refrigerator being driven with nitrogen gas. Figure 5.8.1 shows schematically the structure of the detector system. The planar Ge(I) detector of the volume 5 cm^3 (3.3 $cm^2 \times 1.5$ cm) and molecular sieves are mounted on the cooling part. The size of the detector system including the refrigerator is 50 mm × 170 mm and the weight 900 g. The nitrogen gas is supplied to the gas inlet port from a high pressure gas bottle through a 1/4 inch flexible nylon pipe.

The cooldown time to 90 K is about 20 minutes in conditions of gas pressure, 109 kg/cm^2, and gas flow rate, 20 litters/min. The conditions for keeping the temperature 90 K are: gas pressure, 65 kg/cm^2, and gas flow rate, 12 litters/min. In these conditions, the duration time is about 5 hours when a bottle of 47 litters-150 kg/cm^2 nitrogen gas is used. Figure 5.8.2 shows a pulse height distribution of ^{60}Co gamma-rays measured by the detector with the nitrogen gas flowing. The FWHM energy resolution for 1.33 MeV gamma-rays is 2.8 keV under the condition where there exist considerable microphonic noises due to nitrogen gas flow. The absolute detection efficiency for 1.33 MeV gamma-rays is 3×10^{-6} when the source-to-detector distance is 25 cm.

It has made clear by this experiment that the nitrogen gas-cooled Ge(I) detector has enough performances. Hereafter some effort should be inclinded to increase the duration time and to reduce the microphonic noises for the improvement of energy resolution.

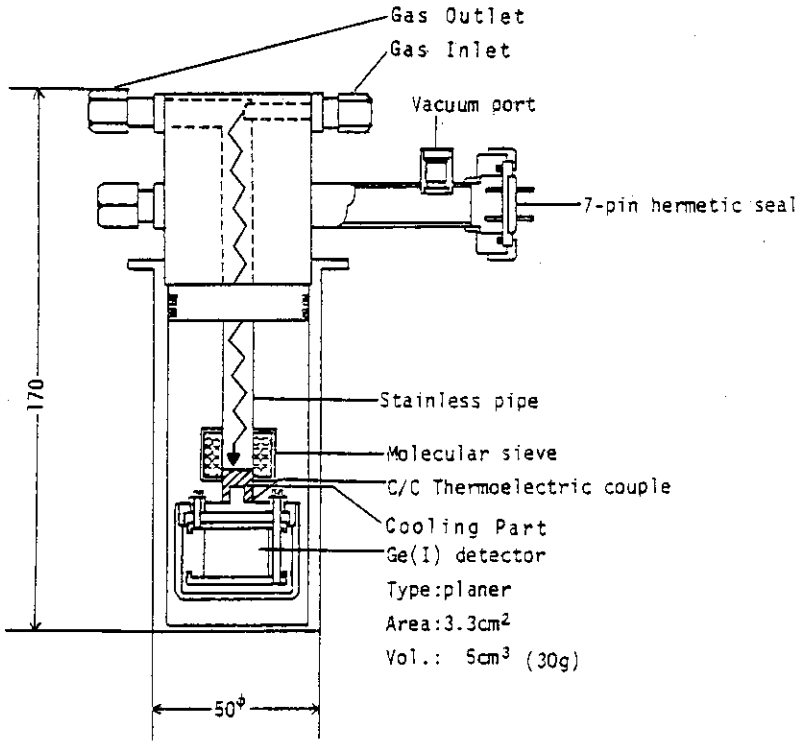

Fig. 5.8.1 The schematic structure of the nitrogen gas-cooled Ge(I) gamma-ray detector

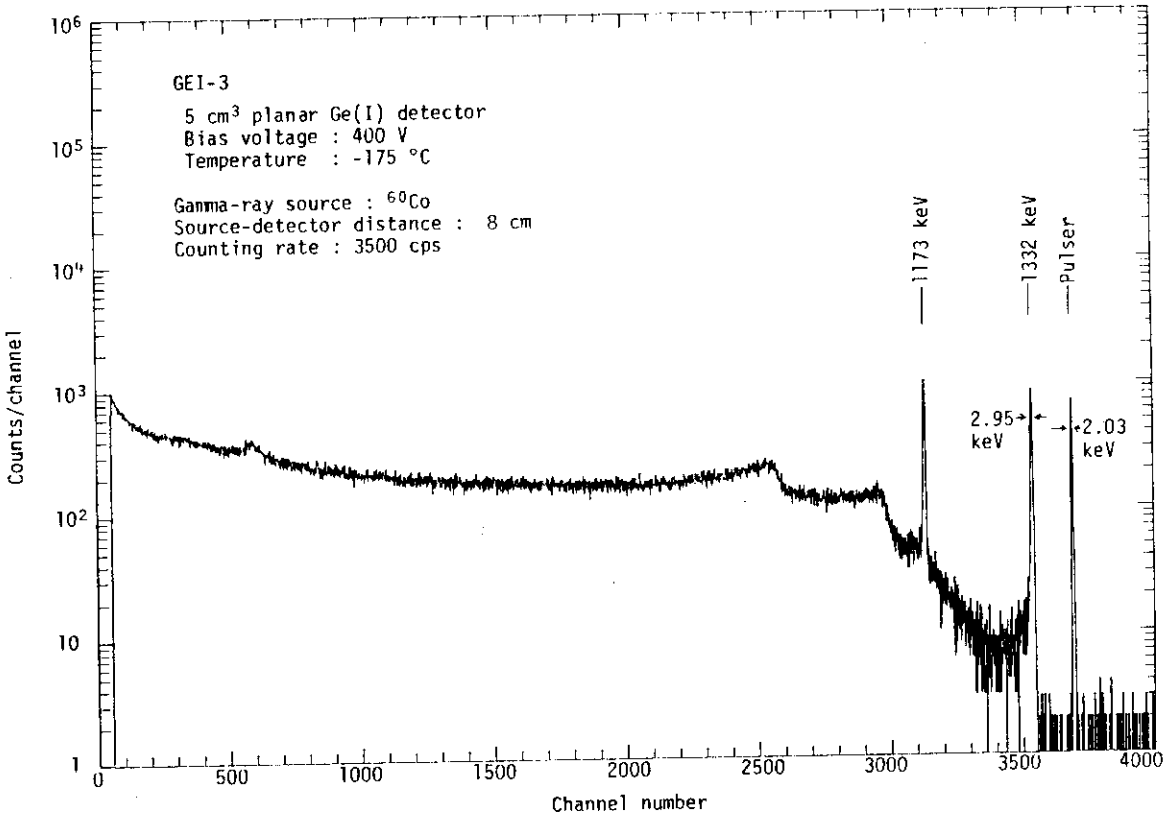

Fig. 5.8.2 The pulse height distribution of ^{60}Co gamma-ray measured by the developed nitrogen gas-cooled Ge(I) detector

5.9 Improvement of a High-purity Germanium Detector System Coupled to a Closed-cycle Cryogenic Refrigerator

E. Sakai, Y. Hayashi*, S. Usui*, H. Ohkado* and H. Nakatani*

Germanium gamma-ray detectors have been usually operated in the cryostats cooled by liquid nitrogen, and produced sometimes maintenance problems related to supplying liquid nitrogen. Recently, the requirement of maintenance-free germanium gamma-ray spectrometers arises, especially in gamma-ray spectrometry application in nuclear industry. We reported our experience on the use of a closed-cycle cryogenic refrigerator (Lake Shore Cryotronics, Inc. Model 21, down to 15K, 2W at 20K, ±0.5K) for cooling a small high-purity germanium detector (APTEC Ltd., Model 05005B, 50 $mm^2 \times 5$ mm planar charged-particle detector, 10^{-10}A at 600V at 77K) in Annual Report last year (JAERI-M 9672, pp.111 - 115 (Sept. 1981)). The present report describes the results of the fourth experiment which used two bellows for reducing the effect of vibration of the cold head of the refrigerator on the detector output. The first stage FET of the preamplifier was cooled in the cryostat.

The vibration noises reduced significantly to an almost negligible amount with this anti-vibration mount while the noise pulse height corresponded to about 1/4 the 1.3 MeV gamma-ray pulses were observed otherwise. Figure 5.9.1 shows gamma-ray pulse height distributions obtained with the bellows for Am-241 X-rays and gamma-rays in the left figure and for background gamma-rays in the second figure which had been taken with 2 μs shaping time of the main amplifier. The symmetric pulser peak distributions mean very little effect of vibration. The counts seen below 300 channel seems to be caused by hum. The 59.5 keV gamma-ray peak FWHM of 0.93 keV is expected to be improved by FET selection and adjustment. Table 5.9.1 summarizes the results of the 1st to the 4th experiments.[1)]

Reference

1) Sakai E., Murakami Y. and Nakatani H. : IEEE Trans. on Nucl. Sci., NS-29, pp. No.1, pp.760-763 (1982).

* Faculty of Engineering, Toyama University, 1-1, Nakagawasonomachi, Takaoka, 933, Japan.

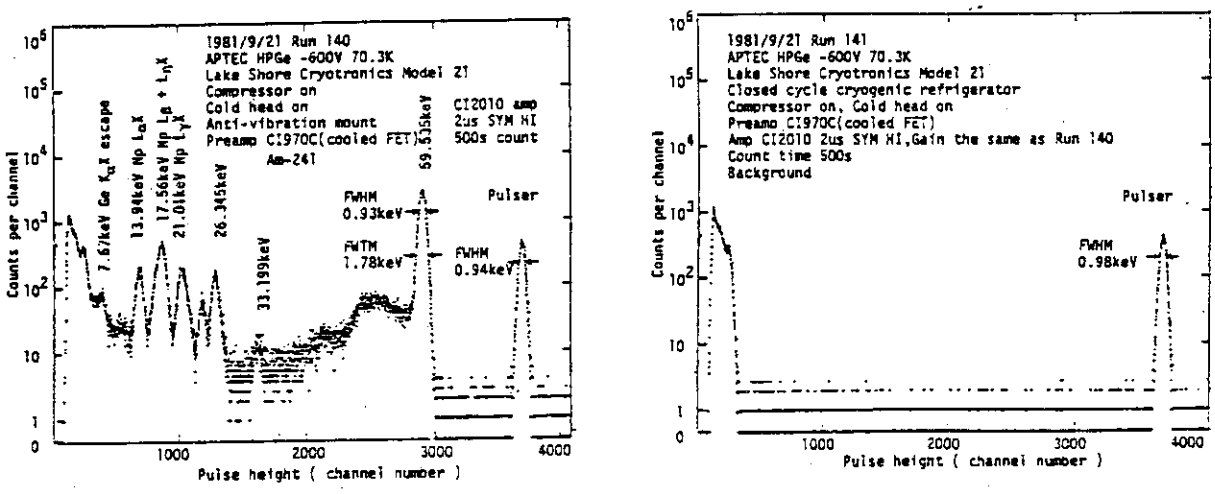

Fig. 5.9.1 Pulse height distributions of Am-241 X-rays and gamma-rays (left figure) and background gamma-rays(right figure) obtained from a small high-purity germanium detector mounted on an anti-vibration mount using two bellows for noise reduction. The shaping time of the main amplifier was 2us.

Table 5.9.1 Comparison of FWHM's of 60keV and 1333keV gamma-ray peaks obtained in various experiments using a closed-cycle cryogenic refrigerator Lake Shore Cryotronics Model 21

Experiment	Cryostat	Preamplifier	CI 2010 Spectr. Amp.SYM III Uni Shaping time(μs)	60keV gamma-rays FWHM (keV)	60keV gamma-rays FWTM (keV)	1333keV gamma-rays FWHM (keV)	1333keV gamma-rays FWTM (keV)
1st	Standard universal sample chamber Photo 1	CI 2001	0.25 1 2 4	1.90	3.62	2.60 4.33 4.13 10.5	5.52 11.5 11.3
2nd	Ordinary end-cap Photo 3	CI 2001	0.25	4.32		3.43	6.96
3rd	Ordinary end-cap Photo 3	CI 970C (cooled FET inside the cryostat	0.25 1 2 4	1.77 3.26 4.36 6.23		2.77 3.72 4.31 3.04	5.06 8.74 7.92 6.59
4th	Anti-vibration mount Photo 5	CI 970C (cooled FET inside the cryostat	0.25 1 2 4	1.47 0.84 0.93 1.06	2.82 1.64 1.78 2.02		

5.10 Application of a Portable High-purity Germanium Detector to In-situ Environmental Gamma-ray Spectrometry

E. Sakai, M. Honda*, M. Yokoyama*, H. Ohkado**, S. Usui**, Y. Hayashi** and H. Nakatani**

Portable high-purity germanium detectors as shown in Fig. 5.10.1 become commercially available recently from several manufacturers and are expected to be used in various fields applying gamma-ray spectrometry. We had an experience on applying our home-made Ge(Li) detectors of upward-looking as well as downward-looking dipstick types to in-situ environmental gamma-ray spectrometry[1),2)] originally developed by H.L. Beck, et al. at HASL[3)]. The present paper will describe the use of a portable high-purity germanium detector (ORTEC, 10%, 1.90 keV, 38.6:1, crystal diameter 45 mm, length 41 mm) in in-situ environmental gamma-ray spectrometry.

The detector weighs 3 kg and 3.5 kg without and with liquid nitrogen, respectively. The detector can be used as a high-resolution spectrometer with +3000V bias 2 hours after liquid nitrogen cooling started. Liquid nitrogen lasts about 8 hours and the detector can be used about 9 to 9.5 hours when the detector was fully filled with liquid nitrogen.

The handle of the detector was removed to fix on a tripod as shown in Fig. 5.10.2. Angular dependence of gamma-ray peak detection efficiency of the detector was measured using an Eu-152 source at a distance of 100 cm and is shown in Fig. 5.10.3. When angle θ was taken as 0° for the source down below the detector and as θ = 180° for the upward direction, the angular dependence is given by $R(\theta) = 1 \pm 0.05$ at θ = 0° - 120° for gamma-rays of energies above 120 keV and $R(\theta)$ is less than 1 at gamma-rays of energies larger than 120 keV. Therefore, the correction of angular dependence is found not necessary for gamma-rays above 120 keV at $0° \leq \theta \leq 90°$. Figure 5.10.4 shows the peak count rate N_0(cps) per unit gamma-ray flux Φ(photons/cm^{2}s) at θ = 0°.

This type of portable high-purity germanium detectors are found to

---

* Japan Nuclear Ship Research and Development Corporation, 1-15-16, Toranomon, Minatoku, Tokyo, 105, Japan.

** Faculty of Engineering, Toyama University, 1-1, Nakagawasonomachi, Takaoka, 933, Japan.

be used very conveniently and will become into popular use for in-situ gamma-ray spectrometry with suitable 4000 channel analyzers. We are using one of NAIG Model E-560 MCA at various locations. One example shows that Cs-137 fallout could not be detected on the sand of the seashore although it was found everywhere else such as on the lawn and in the forest.

References

1) Sakai E., et al. : IEEE Trans. Nucl. Sci., NS-23, No.1, 726 (1976).
2) Sakai E., et al. : ibid., NS-25, No.1, 404 (1978).
3) Beck H.L., et al. : HASL-258 (1972).

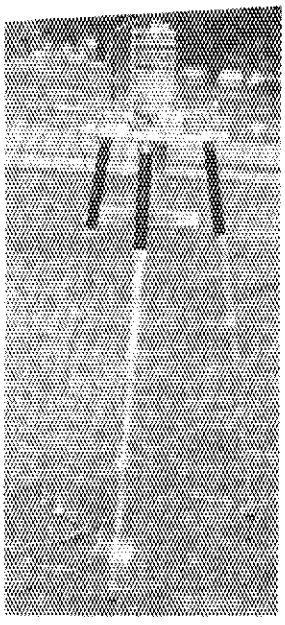

Fig.5.10.1 Portable high-purity germanium detector

Fig.5.10.2 Portable high-purity germanium detector system fixed on a tripod

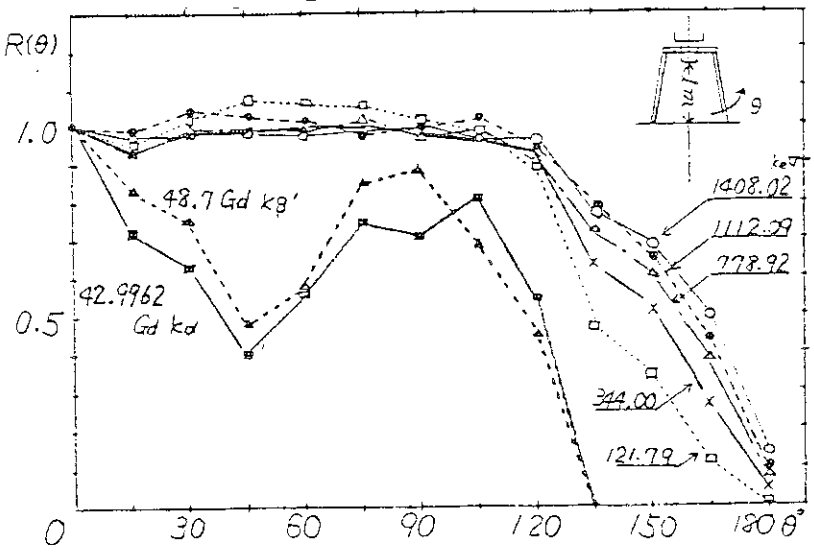

Fig.5.10.3 Angular dependence of gamma-ray peak detection efficiency of a portable high-purity germanium detector

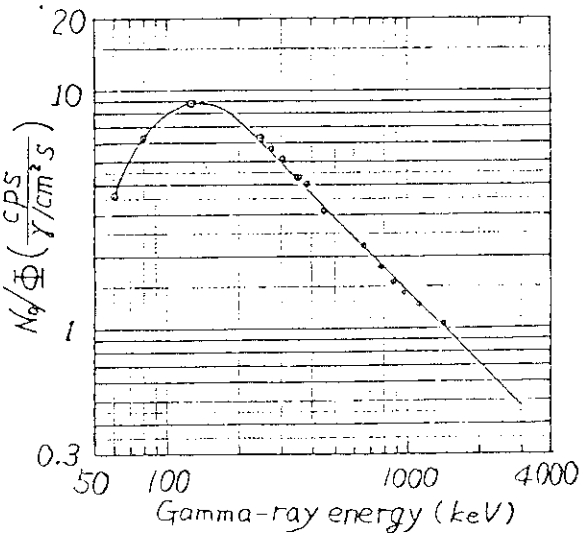

Fig.5.10.4 Peak count rate per unit gamma-ray flux of a high-purity germanium detector

5.11 Program Development for Environmental Gamma-ray Measurement with CANBERRA 8100/QUANTA System

H. Yoshida and E. Sakai

The programs which collect and analyze the data of gamma-ray spectra automatically by Canberra Industries 8100/Quanta System consisting of Canberra 8100 multichannel pulse height analyzer (MCA) and DEC PDP-11/05 minicomputer were prepared and developed by the proper programming language "CLASS" (= Canberra Laboratory Automation Software System).[1),2)] From the source programs described above, those which collect and analyze the data of environmental gamma-ray spectra obtained by semiconductor detectors were developed; the main parts of data process are as follows.

If the counting rate of a photopeak of a specific nuclide and energy obtained by a semiconductor detector supported at a constant height (ordinary 1 meter) above the ground is N_f(dps), then

counting rate per unit radioactivity N_f/S $(\frac{cps}{pCi/g*})$

(* mCi/km^2 unit is used for fallout nuclides as Cs^{137})

counting rate per unit exposure rate N_f/I $(\frac{cps}{\mu R/h})$

are the proper values to this detector under the specific condition;[3),4)] these values are able to be derived from the theory and the experimental values.[5)] In practice, the values of N_f/S and N_f/I, names of nuclides, and values of photopeak energy are stored in the data library on the disk: the data stored in the memory of MCA are analyzed with the same algorithm as GAMMAJ[6)] and GAMMAK[7)] programs to detect photopeaks and their counting rates are calculated; the values of N_f/S and N_f/I with energies equivalent to those of photopeaks are picked out from the library, then dividing the counting rates by these values, the objects are obtained.

The main programs are as follows;

(1) GAMMAE program: it analyzes the data in the memory of MCA directly, performs the procedures described above, and prints the list of resultant data.

(2) GAMMAF program: it analyzes the data of MCA stored in the files on the disk, performs the same procedures as GAMMAE. The resultant

data are printed and stored on the disk.

(3) ENVLST program: it prints the list of resultant data which are stored on the disk by the GAMMAF program.

References

1) Yoshida H., Kubo K. : Programming of Canberra Industries 8100/Quanta System - Program Development with "CLASS," JAERI-M 8694 (March 1980) (in Japanese).

2) Yoshida H., Kubo K., Sakai E. : "Programs for the Automatic Gamma-Ray Measurement with Canberra 8100/Quanta System," JAERI-M 82-056 (June 1982) (in Japanese).

3) Sakai E., Terada H., Katagiri M. : IEEE Trans. Nucl. Sci., NS23(1), pp.726-733, (February 1976).

4) Sakai E., Terada H., Katagiri M. : "In-Situ Measurement of the Environmental Gamma-Rays by Portable Ge(Li) Detectors," JAERI-M 6498 (March 1976) (in Japanese).

5) Reference[4], Chapter 2, pp.4-11.

6) Reference[2], 3.1.

7) Reference[2], 2.7.3.

5.12 Development of Mercuric Iodide Nuclear Radiation Detectors

E.Sakai, H.Ohkado* and H.Nakatani*

We reported last year (Annual Report, JAERI-M 9672, pp.116 - 117(Sept. 1981) that we had grown one HgI_2 crystal of about 30g, 30mm diameter x 25mm height in a rotating vertical ampoule with temperature oscillation method although the crystal consisted of one single crystal region surrounded by poly-crystal regions. This crystal was cut with a wire-saw made by ourselves as shown in Fig.5.12.1, polished on emery papers and etched in KI solution. The crystals were mounted in the detector cases as shown in Fig.5.12.2 after painted with aquadag to make electrodes. Six detectors were made. The largest detector had a dimension of 5mm x 16mm x 0.4mm (J-1).

The gamma-ray detection performance of these detectors was tested with 5.5MeV alpha-particles and 60keV gamma-rays using Am-241 sources. The detectors showed output pulses all right, but with no 60keV gamma-ray peaks even at 1000V bias. This means that the charge collection in the crystal was very poor. We are planning to grow next crystals.

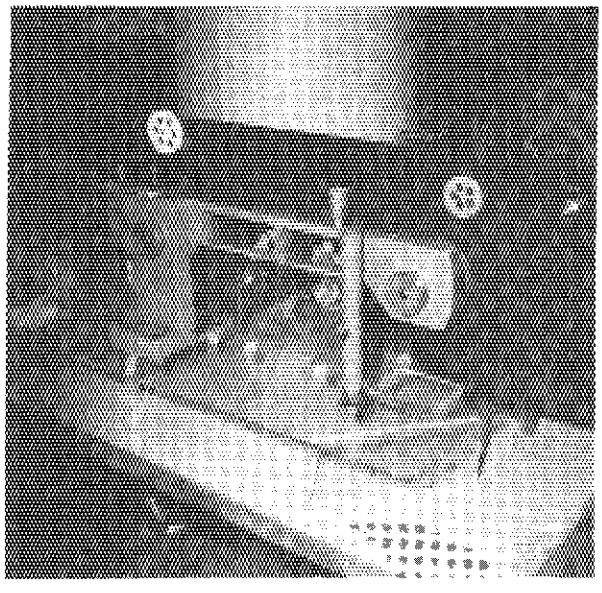

Fig.5.12.1 Wire-saw cutting a HgI_2 crystal

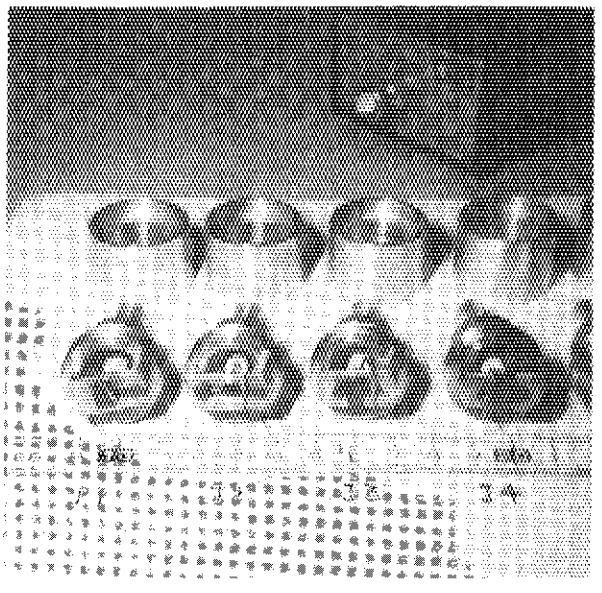

Fig.5.12.2 Four HgI_2 detectors

* Faculty of Engineering, Toyama University, 1-1, Nakagawasonomachi, Takaoka, 933, Japan.

5.13 Induced Radioactivities in Various Materials for Solid-State Physics Research Irradiated by High-Energy Heavy Ions

E.Sakai

Various kinds of experiments using high-energy heavy ions accelerated by 20MeV Tandem Accelerator started in Tokai Research Establishment, JAERI. In order to investigate radiation damage in various materials, single crystals of Si, Al_2O_3, graphite, amorphous $Pd_{80}Si_{20}$, stainless steel had been irradiated with 100MeV Cl^{8+}, 128MeV Cl^{9+}, 112MeV O^{7+} and 80MeV I^{7+} in a liquid nitrogen cooled irradiation chamber. The construction materials of the chamber such as Cu, Ni, Al, SiO_2 had also been irradiated. After the irradiation, gamma-ray spectra from these irradiated materials were measured using a high-purity germanium detector of relative detection efficiency of 10% in a lead shield to obtain residual nuclides, their radioactivities, their numbers of atoms and their production cross sections. Table 5.13.1 shows the results obtained. It was found that Cl and O beams produced radioactivities by nuclear fusion reactions which introduced new nuclides as well as radiation damage although very little radioactivities were made with 80 MeV I^{7+}. For examples, Co-56($T_{1/2}$=78.8d), Co-57(269.8d) and Co-58(70.8 d) were introduced in Si irradiated by 100MeV Cl^{8+} and 128MeV Cl^{9+}, therefore, an increase in background counts is expected in irradiated Si detectors in addition to a degradation of their performance due to radiation damage.

Table 5.13.1 Residual nuclides, their radioactivities, numbers of atoms and production cross sections found in various materials irradiated by high-energy heavy ions

Heavy ions	Numbers of particles	Irradiated material	Residual nuclide	Radioactivity(uCi)	Numbers of atoms	Cross section(mb)
128MeV Cl^{9+}	1.18E15	p-type Si	Co-56(78.8d)	7.3E-3	2.65E9	9.7
			Co-57(269.8d)	8.2E-3	1.02E10	37.3
			Co-58(70.8d)	2.2E-3	2.2E8	2.6
128MeV Cl^{9+}	2.90E14	Al	Mn-54(312.3d)	9.2E-5	1.32E8	1.8
			Co-56(78.8d)	4.4E-3	1.59E9	29.2
			Co-57(269.8d)	1.05E-3	1.30E9	18.1
			Co-58(70.8d)	7.15E-2	2.33E9	32.4
128MeV Cl^{9+}	4.4E13	Al_2O_3	V-48(15.98d)	7.41E-3	5.5E8	
			Co-56(78.8d)	2.4E-4	8.7E7	
			Co-57(269.8d)	4.6E-5	5.7E7	
			Co-58(70.8d)	4.4E-4	1.44E8	

128MeV Cl^{9+}	6.66E14	Ni	Zr-88(83.4d)	2.92E-4	1.12E8	0.78
			Y-88(106.6d)			
100MeV Cl^{8+}	2.51E14	C	Sc-46(83.8d)	2.3E-5	8.9E6	0.65
			V-48(15.98d)	1.0E-4	7.5E6	0.54
100MeV Cl^{8+}	2.28E15	Al	Co-56(78.8d)	1.16E-3	4.2E8	0.59
			Co-57(269.8d)	8.05E-5	1.0E8	0.14
			Co-58(70.8d)	1.19E-3	3.9E8	0.55
100MeV Cl^{8+}	3.74E14	P-Si-1	V-48(15.98d)	3.5E-4	2.55E7	1.39
			Co-56(78.8d)	5.3E-4	1.9E8	10.6
			Co-57(269.8d)	2.14E-3	2.66E9	145
			Co-58(70.8d)	2.26E-4	8.54E7	4.7
100MeV Cl^{8+}	3.00E14	p-Si-2	V-48(15.98d)	3.4E-4	2.5E7	2.1
			Co-56(78.8d)	7.14E-4	2.6E8	21.9
			Co-57(269.8d)	2.5E-3	3.14E9	265
			Co-58(70.8d)	3.6E-4	1.18E8	9.98
100MeV Cl^{8+}	3.92E15	Cu	V-48(15.98d)	2.09E-4	1.54E7	0.002
128MeV Cl^{9+}	3.19E14	$Pd_{80}Si_{20}$	Co-57(269.8d)	2.21E-4	2.75E8	
			Rb-83(86.2d)	5.3E-4	2.1E8	
			Zb-88(83.4d)	4.37E-3	1.68E9	
			Y-88(106.6d)			
100MeV Cl^{8+}	unknown	SiO_2	V-48(15.98d)	2.42E-2	1.78E9	
			Co-56(78.8d)	2.66E-4	9.68E7	
			Co-57(269.8d)	5.0E-4	6.22E8	
			Co-58(70.8d)	7.0E-5	2.3E7	
80MeV I^{7+}	2.93E14	n-Si	None			
80MeV I^{7+}	1.65E14	Cu	None			
112MeV O^{7+}	2.9E16	Cu	Mn-54(312.38d)	5.5E-2	7.86E10	4.8
			Co-56(78.76d)	7.3E-4	2.64E8	0.016
			Co-58(70.8d)			
			Zn-65(243.5d)	6.0E-3	6.77E9	0.41
			Cu-67(61.9h) or Ga-67(78.26h)	2.04E-1 1.66E-1	2.43E9 2.50E9	0.15 0.15
			Ge-69(39.05h)	8.00E-1	6.0E9	0.36
			As-71(61h)	7.65E-1	9.0E9	0.54
			Se-72(8.40d) - As-72(26.0h)	1.93	9.7E9	0.58
			As-74(17.79h)	6.3E-3	5.2E8	0.03
			Se-75(118.45d)	5.5E-2	3.0E10	0.18
			Kr-76(14.82h)	1.84	5.24E9	0.32
			Br-76(16.6h)	4.83	1.5E10	0.9
			Br-77(57.0h)	6.7E-1	7.4E9	0.44

5.14 Effective Aperture Area of Gamma-ray Collimator

H. Gotoh and K. Teranishi*

Gamma-ray collimators are frequently used in passive gamma assay of uranium samples in order to define the field viewed by the gamma-ray detector. Within the authors' knowledge, no one has been aware of the existence of exact analytic expressions to estimate the number of 186 keV gamma-rays passing through a gamma-ray collimator.

As the half-thickness of lead against 186 keV gamma-ray is so thin as 0.5 mm, the number of the gamma-rays passing through a collimator is determined by the geometrical shape and the size of the collimator hole, if the size is ten times as large as the half-thickness. The uncollided gamma-ray flux emitted from an infinitely thick uniform radioactive material is, as well-known, equivalent to that produced by a uniform cosine surface source lying on the surface of the material. Then, if a uranium sample covers the entrance of the hole and if a gamma-ray detector covers the exit of the hole, the number of 186 keV gamma-rays incident on the detector passing through the hole in unit time is represented as

$$n = 7.2 \times 10^{3} \cdot E \cdot \left(1 + \frac{\sum_i \rho_i \mu_i}{\rho_u \mu_u} \right)^{-1} \cdot A_{eff}, \qquad (1)$$

where E = the enrichment of the uranium sample (≤ 1),

ρ_u, ρ_i = the densities of uranium and of the i-th matrix element (in $g \cdot cm^{-3}$),

and μ_u, μ_i = the mass attenuation coefficients of uranium and of the i-th matrix element against 186 keV gamma-rays (in cm^{-1}).

The effective aperture area A_{eff} is generally given by

$$A_{eff} = \frac{1}{\pi} \cdot \int_{\substack{\text{entrance} \\ \text{surface}}} dA \int_{\substack{\text{exit} \\ \text{surface}}} dA' \frac{\cos\theta \cdot \cos\theta'}{r^2}, \qquad (2)$$

where dA and dA' are respectively the surface elements of the entrance surface and the exit surface of the collimator hole, and r is the distance between the elements. Angles θ and θ' are respectively angles between the normals to the surface elements and the line segment connecting dA and dA'.

---

* Hitachi Ibaraki Technical College, Hitachi Ltd.

The equation (2) is the same mathematical expression with the configuration factor or the shape factor used in the field of radiation heat transfer except for the multiplication factor. And we can look for formulas useful to us in the list of shape factors.[1] Three formulas are deeply related to gamma-ray collimators. Here we show them in the style of effective aperture area.

(1) Right circular cylindrical hole

$$A_{eff} = \pi r^2 \cdot \left\{ 1 + \frac{1}{2} \cdot \left(\frac{t}{r}\right)^2 - \left[\left(1 + \frac{1}{2} \cdot \left(\frac{t}{r}\right)^2\right)^2 - 1\right]^{1/2} \right\}, \qquad (3)$$

where r is the radius of the hole and t is the thickness of the collimator.

(2) Rectangular slit

$$A_{eff} = \frac{2t^2}{\pi} \left\{ \frac{1}{2} \ln \frac{(1+X^2)(1+Y^2)}{1+X^2+Y^2} + Y\sqrt{(1+Y^2)} \cdot \mathrm{Tan}^{-1} \frac{Y}{\sqrt{(1+X^2)}} \right.$$

$$\left. + X\sqrt{(1+X^2)} \cdot \mathrm{Tan}^{-1} \frac{X}{\sqrt{(1+Y^2)}} - Y \cdot \mathrm{Tan}^{-1} Y - X \cdot \mathrm{Tan}^{-1} X \right\}, \qquad (4)$$

where X=a/t and Y=b/t; a and b are lengths of the two sides of rectangular hole, and t is the thickness of the collimator.

(3) Collimator with a truncated right circular cone-shaped hole

$$A_{eff} = \frac{\pi}{2} \left\{ r_1^2 + r_2^2 + t^2 - \left[(r_1^2 + r_2^2 + t^2)^2 - 4 \cdot r_1^2 \cdot r_2^2\right]^{1/2} \right\}, \qquad (5)$$

where r_1 and r_2 are radii of the upper and lower faces of the truncated right circular cone, and t is the thickness of the collimator.

Reference

1) R. Siegel and J. R. Howell, Appendix B in Thermal Radiation Heat Transfer, McGraw-Hill Book Company(1972);
E. M. Sparrow and R. D. Cess, Radiation Heat Transfer, McGraw-Hill Book Company(1978)

5.15 An Algorithm for the Determination of Peak Area

H. Gotoh, H. Yagi and K. Teranishi*

The method for peak area determination has a vital importance in passive gamma assay of nuclear materials. The present authors invented a method to calculate the area with high stability for a well-resolved total energy absorption peak in gamma-ray spectra. The method uses a step function for the background curve as shown in Fig. 5.15.1. The function fits the pulse height distribution at the lower- and the upper-plateau regions and has a step at a pulse height named the peak position near the center of the peak. The peak area is defined as the sum of counts which exceed the background function in the peak region.

Mathematical expressions for the peak position $\hat{p}$ and the peak area $\hat{S}$ are represented as

$$\hat{p} = \frac{1}{2}(x_2 + x_3), \tag{1}$$

and

$$\hat{S} = A_2 + A_3 + C_p - \frac{1}{2}(m - l)(a_1 + a_4) + \frac{1}{2}(a_4 - a_1)(x_2 + x_3 - l - m + 1), \tag{2}$$

where k = the starting channel number of the lower plateau region,
l = the starting channel number of the peak region,
m = the starting channel number of the upper plateau region,
n = the final channel number of the upper plateau region,
p = the channel number with the highest count,
C_i = the count of the i-th channel (i = k to n),

$$A_1 = \sum_{i=k}^{l-1} C_i, \quad A_2 = \sum_{i=l}^{p-1} C_i, \quad A_3 = \sum_{i=p+1}^{m-1} C_i, \quad A_4 = \sum_{i=m}^{n} C_i, \tag{3}$$

$$a_1 = \frac{A_1}{l - k}, \qquad a_4 = \frac{A_4}{n-m+1}, \tag{4}$$

$$x_2 = p - 0.5 - \frac{A_2 - a_1(p - l)}{C_p - a_1}, \tag{5}$$

---

* Hitachi Ibaraki Technical College, Hitachi Ltd

$$x_3 = p + 0.5 + \frac{A_3 - a_4(m - p - 1)}{C_p - a_4}. \tag{6}$$

Geometrical meaning of some of parameters are illustrated in Fig. 5.15.1.

Biases induced by the finite width of channels and by the amplifier gain shift were investigated. And statistical variances of $\hat{p}$ and $\hat{S}$, $V(\hat{p})$ and $V(\hat{S})$, were formulated. Results are as follows:

$$V(\hat{p}) = \frac{1}{4}\left\{\left[\frac{p - x_2 - 0.5}{C_p - a_1} - \frac{x_3 - p - 0.5}{C_p - a_4}\right]^2 \cdot C_p \right.$$

$$+ \frac{1}{(C_p - a_1)^2}\left[A_2 + \left(\frac{x_2 - l + 0.5}{l - k}\right)^2 \cdot A_1\right]$$

$$\left. + \frac{1}{(C_p - a_4)^2}\left[A_3 + \left(\frac{m - x_3 - 0.5}{n + 1 - m}\right)^2 \cdot A_4\right]\right\}, \tag{7}$$

$$V(\hat{S}) = \left\{1 - \frac{a_1 - a_4}{2}\left[\frac{p - x_2 - 0.5}{C_p - a_1} - \frac{x_3 - p - 0.5}{C_p - a_4}\right]\right\}^2 \cdot C_p$$

$$+ \left\{ \frac{1}{2(l - k)}\left[l - m - \frac{C_p - a_4}{C_p - a_1}(x_2 - l + 0.5)\right.\right.$$

$$\left.\left. + (m - x_3 - 0.5)\right]\right\}^2 \cdot A_1 + \left\{\frac{1}{2(n + 1 - m)}\left[l - m - \frac{C_p - a_1}{C_p - a_4}\cdot\right.\right.$$

$$\left.\left.\cdot(m - x_3 - 0.5) + (x_2 - l + 0.5)\right]\right\}^2 \cdot A_4$$

$$+ \left[1 + \frac{a_1 - a_4}{2(C_p - a_1)}\right]^2 \cdot A_2 + \left[1 - \frac{a_1 - a_4}{2(C_p - a_4)}\right]^2 \cdot A_3. \tag{8}$$

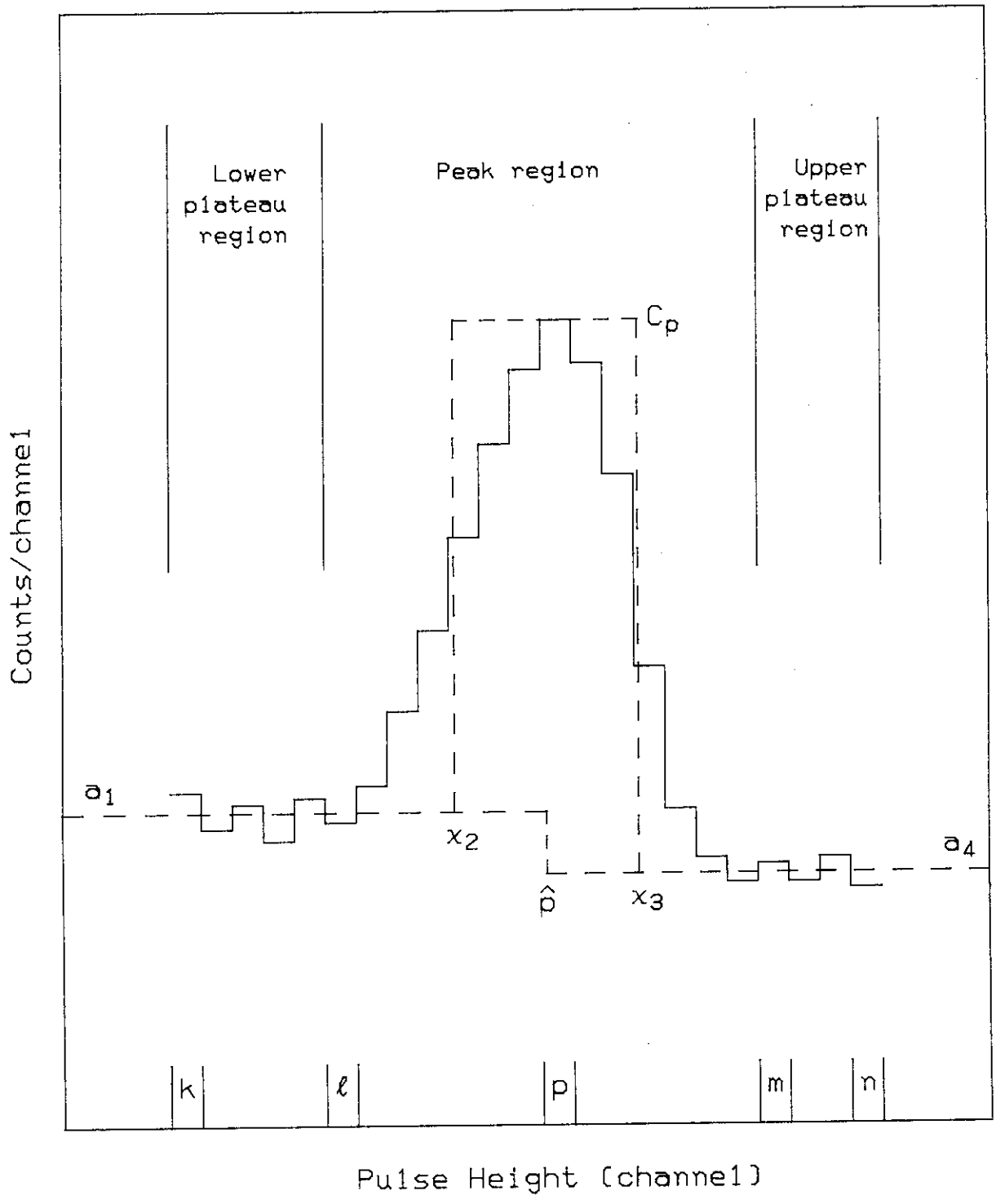

Fig. 5.15.1 A pulse height distribution showing region setup

5.16 Development of Portal Monitor at FCA for IAEA Safeguards

T. Mukaiyama and H. Kuroi

Design Philosophy of Portal Monitor

As an acceptable international safeguards system, a portal monitor must demonstrate the capability of meeting a number of basic functional requirements and conditions including the followings:

(1) High confidence in detecting diversion,
(2) Timely detection of diversion,
(3) Low false alarm rate,
(4) Unattended operation capability for a certain period of time,
(5) Tamper resistance,
(6) Timely report of detection of illicit activities,
(7) High reliability and low maintenance,
(8) Acceptably low level of interference with facility operations, and
(9) Acceptable cost.

A number of these requirements tend to be mutually exclusive. From the facility operator point of view, the requirements No.3, 8 and 9 are a primary matter of concern.

FCA Portal Monitor[1)]

As the IAEA safeguards equipments, the portal monitor must meet the requirements and conditions described in the previous section. After the basic requirements and conditions are satisfied, the acceptability of the portal monitor installation to the facility should be pursued. This feature of portal monitor will be easily achieved when the system is designed by a facility operator.

The design features of the portal monitor system developed at FCA are following :

(1) Walk-through metal detector for detection of diversion,
(2) Visual surveillance to secure the unattended operation using closed circuit TV (CCTV) and VTR,
(3) Tamper indication system to secure the unattended operation and tamper resistance using different kinds of sensors and techniques,
(4) Compatibility with RECOVER[2)] (Remote Continual Verification) system for the timely report of the status of the portal,
(5) Recording system for anormalies or status of the system using VTR and

hard-copy.

The illustration of FCA portal monitor developed is shown in Fig.1.

Field test of FCA portal monitor system

The very comprehensive evaluation of the system is essential so that the system is accepted as the international safeguards equipments.

In accordance with the research agreement between the IAEA and FCA/JAERI, the Phase I field test of the portal monitor installed at FCA was successfully conducted under the collaboration of the IAEA and FCA. The purpose of this test was to evaluate the various features and performance of the system. Several system modifications were agreed prior to start of the Phase II test. The separation of the portal monitor from any facility interface, the door lock up to prevent anomaly situations, the availability of the performance/ state-of-health data of the portal monitor to facility personnel and so forth were discussed.

The purpose of the Phase II test is to evaluate the performance of the portal monitor under the normal facility operating circumstances. Emphasis will be placed on the metal detection capability, tamper indicating performance, false alarm rates, overall system reliability and impact on facility operation. The Phase II test has been commenced on March 1982 for the expected period of 6 - 9 months.

The purpose of the Phase III test is to evaluate the potential applicability of the FCA portal monitor to international safeguards. Independent verification of all system components and interconnections by the IAEA is essential during the Phase III test.

Conclusion

Under the strong collaboration between the IAEA and FCA/JAERI for research and development for the advanced C/S measures, the efforts will be concentrated to make this portal monitor system more reliable and acceptable.
The further modifications will be made after the Phase II field test activities so that this system is accepted as the IAEA equipment not only at FCA but also at other nuclear facilities.

References

1) Mukaiyama T. and Kuroi H.: "The Expected Performance and Benefits of an Advanced Containment and Surveillance System at the Fast Critical Facility of JAERI," Proceedings of 22nd Annual Meeting of Institute of Nuclear Matarial Management (San Francisco, July 1981).

2) U. S. Arms Control and Disarmament Agency: "Initial Implementation and Demonstration of the Remote Continual Verification (RECOVER) System," ACDA REP 78-4 (1978).

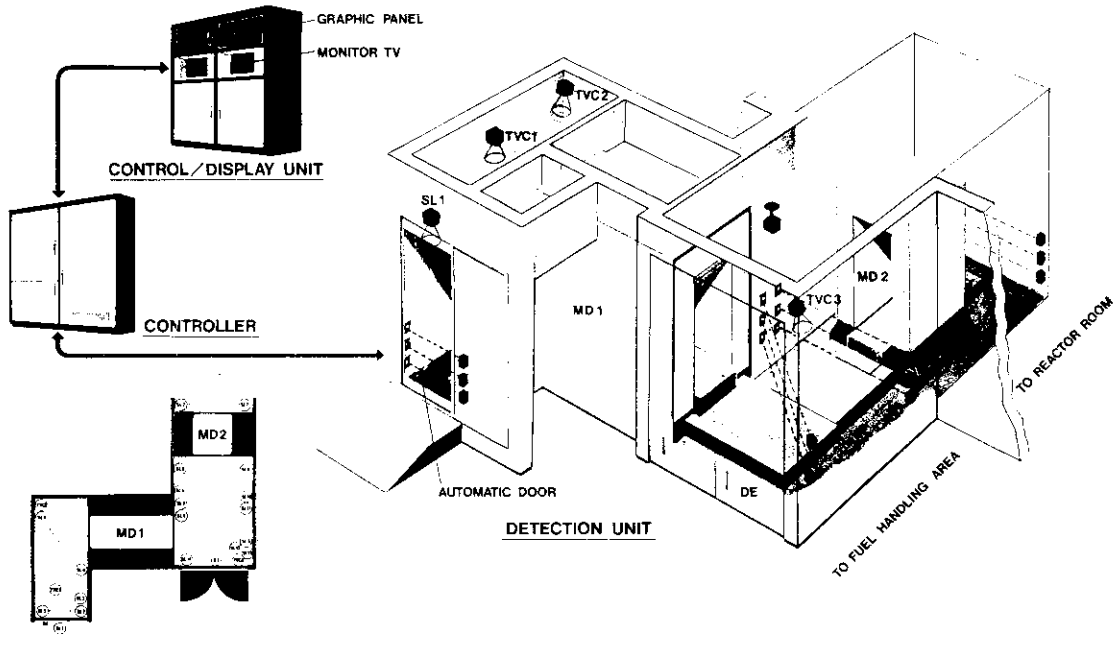

Fig. 5.16.1 FCA Portal Monitor System
MD 1 shows the main Metal Detector
TVC shows CCTV camera

6. Reactor Control and Diagnosis

6.1 A CAD System for Control System Design and Evaluation

J.Shimazaki, H.Usui and Y.Shinohara

A CAD (Computer Aided Design[1]) system has been developed to do control design work effectively. This is an interactive design system utilizing time sharing option on FACOM M200 computer. In the design of control system, there exists a lot of works which consist of description of dynamic model of an objective plant, analysis of inherent charateristics of the model, determination of a goal and objectives of control, construction of a better control system, and simulation analysis for various kinds of disturbance and different plant parameters. A chain of the work is carried out within a short time using the CAD system. And the control designer can concentrate his efforts on the evaluation of simulation results and the construction of a better control system.

The CAD sytem was made in consideration of new techniques which were applied to the generation of a total system from its subsystems including a control system, effective computation of dynamic simulation, graphic display of the simulation results, and iterative computer use. The system consists of seven subprograms [2] shown in Figure 6.1.1. These subprograms are independently executable and described as follows:

(1) Description of a Subsystem and Calculation of Discrete-Time Model (SSD)

The plant is divided into its subsystems from a dynamic point of view. A subsystem is described in the form of state variable representation, and transformed to its dicrete-time model using the Pade and extention methods already developed.[3]

(2) Description of Control System (CSD)

A control system is described by a discrete-time model and transfered so as to have a good characteristics of control by adjusting control parameters and changing control structure.

(3) Description of User Functions (UFD)

Typical functions are used for simulation of input disturbance and nonlinear elements, and sixteen functions are available.

(4) Total System Connection (TSC)

The total system is constructed by conecting the subsystems, the control system, and the user functions defined in plant dynamics.

(5) Dynamic Simulation (SIM)

Dynamic simulation is executed by use of four files prepared for data of the subsystems, the control system and the total system connection. The results of simulation stored in a file are used for data in graphic display to evaluate the response curves to various types of disturbance.

(6) Stability Test of Subsystems (SST)

All eigenvalues of a subsystem are calculated and plotted in Gaussian plane to evaluate its stability. Stability of total system can be estimated not in the same way but through dynamic simulation because of the nonlinearity included.

(7) Edition of Simulation Results and Output Selection (OSEL)

Time series data prepared for control system design are selected from the dynamic simulation results and output to printer, graphic display, or plotter. This subprogram provides a designer to evaluate a control system easily by comparing the response curves in graphic display.

The CAD system was tested for the evaluation of pressure control of a BWR plant and for the dynamics analysis of VHTR primary loop system. As the results of these test cases, it was shown that the system is promising for wide use in for control system design and evaluation of nuclear plant.

References

1) Furuta K., Kajiwara H.: "CAD for Control System," Jounal of the Society of Instrumentation and Control Engineers,Vol.19,No.9,55 (1979) [in Japanese].

2) Shimazaki J., Usui H., Shinohara Y.: "Development of CAD System for Design Analysis of Contol System of Nuclear Plant," Fall Meeting of the Atomic Energy Society of Japan,C32 (1981) [in Japanese].

3) Shimazaki J.: "Computer Programs for Dynamic Analysis and Control of a Large Scale Dynamical System," The 4-th System Symposium, Kyoto,315 (1978) [in Japanese].

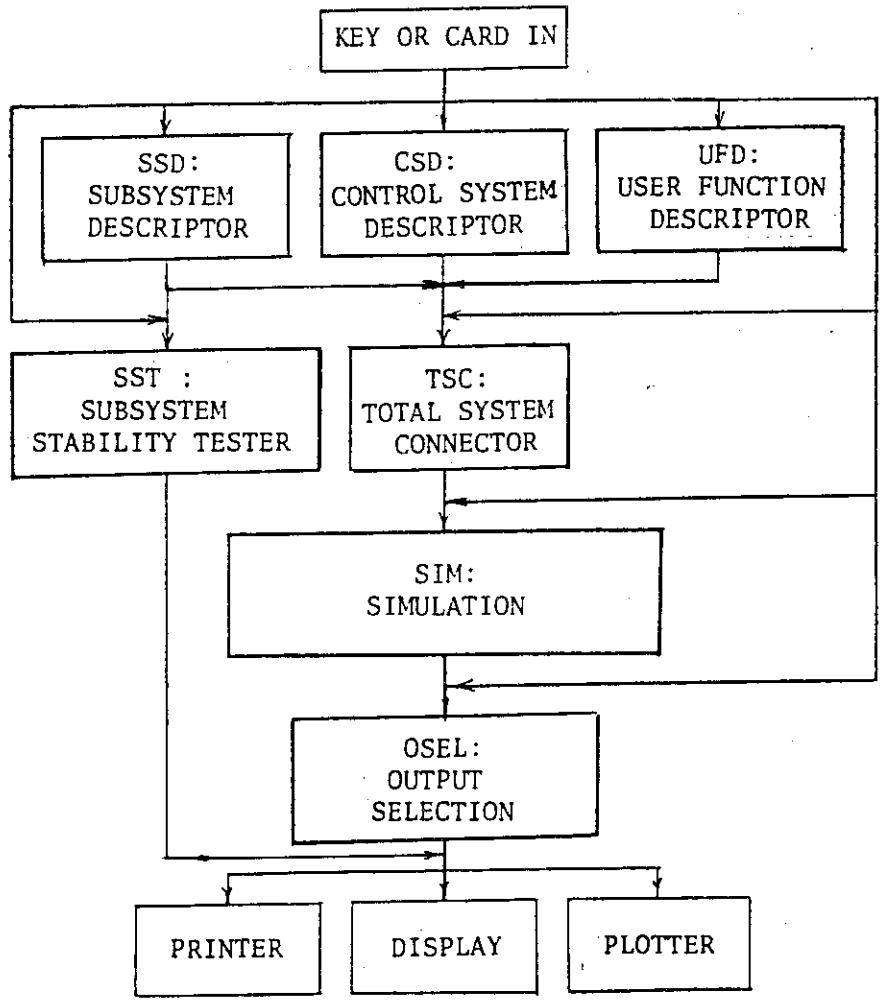

Fig.6.1.1 Structure of CAD system for control system and evaluation

6.2 Simulation Study of Boiling Detection Methods

J. Shimazaki, Y. Fujii and Y. Shinohara

As a part of the work on the development of a diagnostic system for detecting anomalies in the core of an operating reactor, a study is being made on the methods of abnormal reactivity and coolant boiling detection by computer simulation and in-pile experiment. The objective of the study is to obtain basic information useful for developing an effective method of signal processing suitable for boiling detection.

In computer simulation, neutronic and acoustic signals as well as background noises are simulated on a hybrid computer using a magnetic data recorder as a multichannel noise generator. The void patterns used for generating reactivity and acoustic signals are chosen from typical void formation patterns experimentally observed and are generated using a function generator. It has been shown that cross-spectral and coherence analyses between neutronic and acoustic signals are effective methods for detecting boiling when the signal-to-noise ratio is small.

In order to confirm the results of computer simulation by experiment, an in-pile water loop for boiling detection experiment has been constructed and installed at the tank-type thermal crtical assembly TCA. The in-pile boiling test section consists of coaxial aluminum tubes which form the coolant channel and an electrically heated pin which simulates the fuel rod and is inserted in the central part of the core. The coolant enters the test section downward through the gap between the outer and inner tubes and flows upwards through the gap between te inner tube and the heater pin. The heater section which is 50 cm long is located at lower one third part of the core height. The performance test of the loop has been completed. In order to check the boiling condition by visual observation, an out-of-pile test section is also being constructed. The boiling detection experiment will be conducted in later half of 1982.

Reference

Shimazaki, J., Fujii, Y., Shinohara, Y. and Araki, H.: "Simulation Study of Neutronic and Acoustic Methods of Boiling Detection," PNC N941 81-116 (1981)

6.3 A New Method of Coherence Analysis for Systems with Feedback and Its Application to Reactor Noise Investigation

R. Oguma

Coherence analysis has been one of the most fundamental tools in various studies associated with reactor noise. However, the conventional coherence analysis has some difficulties when applied to systems with feedback. In order to enable coherence analysis even for systems with feedback, we introduce a new method that we perform the analysis through comparison of the ordinary coherence(OCH) function and the noise power contribution(NPC) function derived from a two variable autoregressive(AR) model. Through the coherence analysis for noise data from JPDR-II(Japan Power Demonstration Reactor-II), the method presented here is shown to be effective for investigation of power reactor noise.

Coherence Analysis for Two Variable System

Consider a two variable linear dynamic system as shown in Fig. 6.3.1. Using a z transform, the system equation can be described by

$$x_1(z) = G_{12}(z)x_2(z) + n_1(z), \qquad x_2(z) = G_{21}(z)x_1(z) + n_2(z), \qquad (1)$$

where x_1 and x_2 are measurement variables, n_1 and n_2 are noise sources that are mutually independent, and $G_{12}(z)$ and $G_{21}(z)$ are transfer functions from x_2 to x_1 and from x_1 to x_2, respectively. With a minor calculation using Eq. (1), we obtaine power spectral densities for x_1 and x_2, and cross-power spectral density between them as shown in Fig. 6.3.2. Then the OCH between x_1 and x_2, and the NPC ratio for these two variables are derived, as also indicated in Fig. 6.3.2, in terms of the spectral density functions. Through comparison between the OCH and NPC functions, it can be shown that they have the following intimate relations:

(a) if there is no dynamic relation between x_1 and x_2 and hence $G_{12}(f) = G_{21}(f) = 0$, then $\gamma_{12}^2(f) = \Gamma_{12}(f) = \Gamma_{21}(f) = 0$, where γ_{12}^2 denotes the OCH between x_1 and x_2, Γ_{12} the NPC ratio from x_2 to x_1 and Γ_{21} the NPC ratio from x_1 to x_2, respectively.

(b) if the system is of an open loop structure as x_2 being the input and x_1 being the output i. e. $G_{21}(f) = 0$, then $0 < \gamma_{12}^2(f) = \Gamma_{12}(f) < 1$ and $\Gamma_{21}(f) = 0$. Same argument holds for the case where $G_{12}(f) = 0$.

(c) if the system constitutes a closed-loop, then $\gamma_{12}^2(f) \neq \Gamma_{12}(f)$, $\gamma_{12}^2(f) \neq \Gamma_{21}(f)$, and $0 < \gamma_{12}^2(f), \Gamma_{12}(f), \Gamma_{21}(f) < 1$.

Therefore, using these relations between the OCH and NPC functions, we can identify the causal structure of the system as well as detect feedback, if it exists. Furthermore, it can be shown that for a system with low pass characteristic comparison of the OCH and NPC functions by an equation

$$\Psi(f) = \gamma_{12}^2(f) - (\Gamma_{12}(f) + \Gamma_{21}(f)), \quad (2)$$

provides information on the property of the feedback; $\Psi(f) < 0$, if the feedback effect is positive and vice versa. Hence, Eq.(2) may be a useful index to evaluate the property of the feedback effect. We call the coherence analysis carried out through comparison of the OCH and NPC functions as "OCH-NPC comparison approach".

Application to JPDR-II Noise Data

The new coherence analysis method, OCH-NPC comparison approach, was applied to JPDR-II noise data which had been collected in the reactor dynamics experiment using pseudo-random-binary-sequence(PRBS) disturbance signals at power level of 45 MWt. In the experiment, mutually independent PRBS signals were applied at two terminals, i. e., one at the bypass pressure regulator(BPR) valve and the other at the master controller(MC) set point of forced circulation pumps. Shown in Fig. 6.3.3 is a schematic diagram of the JPDR-II plant and signals' measurement points.

Figure 6.3.4 shows results of the OCH and NPC calculations based upon the AR model identified for neutron and pressure signals. The difference between the OCH and the NPC ratio for either direction is clearly observed in frequencies lower than 0.04 Hz. Moreover, the OCH far exceeds the sum of the two NPC ratios in that frequency range. Hence, the present analysis suggests that a positive feedback effect plays an important role in determining dynamic characteristics of the neutron and pressure. The result of the present analysis indicates that the OCH-NPC comparison approach can be a useful tool to investigate feedback effect active in the system under evaluation.

References

(1) Oguma R.: Nucl. Sci. Technol., 18, pp.835-844 (1981).

(2) Oguma R.: "A New Method for Coherence Analysis of Systems with Feedback Effect Based on Autoregressive Modeling," JAERI-M 9756, (1981).

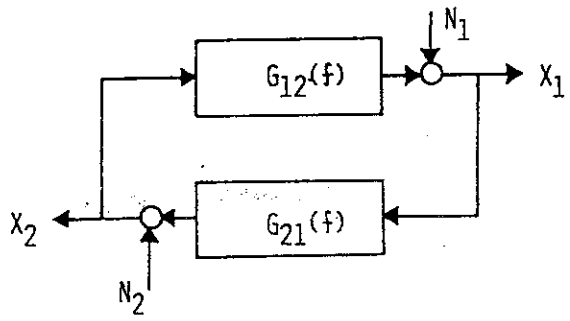

Fig. 6.3.1 Block diagram of a two variable system with feedback

$$P_{11}(f) = \frac{1}{\Delta}\{|G_{12}(f)|^2 Q_{22}(f) + Q_{11}(f)\},$$

$$P_{22}(f) = \frac{1}{\Delta}\{|G_{21}(f)|^2 Q_{11}(f) + Q_{22}(f)\},$$

$$P_{12}(f) = \frac{1}{\Delta}\{ G_{21}^*(f)Q_{11}(f) + G_{12}(f)Q_{22}\},$$

$$\Delta = |1 - G_{12}(f)G_{21}(f)|^2 .$$

$$\gamma_{12}^2(f) = \frac{|G_{21}^*(f)Q_{11}(f)+G_{12}(f)Q_{22}(f)|^2}{\{|G_{12}(f)|^2 Q_{22}(f)+Q_{11}(f)\}\{|G_{21}(f)|^2 Q_{11}(f)+Q_{22}(f)\}}$$

$$\Gamma_{12}(f) = \frac{|G_{12}(f)|^2 Q_{22}(f)}{|G_{12}(f)|^2 Q_{22}(f) + Q_{11}(f)} ,$$

$$\Gamma_{21}(f) = \frac{|G_{21}(f)|^2 Q_{11}(f)}{|G_{21}(f)|^2 Q_{11}(f) + Q_{22}(f)} .$$

$P_{11}(f)$: Power spectral density of x_1
$P_{22}(f)$: Power spectral density of x_2
$P_{12}(f)$: Cross-power spectral density between x_1 and x_2
$\gamma_{12}^2(f)$: Ordinary coherence between x_1 and x_2
$\Gamma_{12}(f)$: Noise power contribution ratio from x_2 to x_1
$\Gamma_{21}(f)$: Noise power contribution ratio from x_1 to x_2

Fig. 6.3.2 Power spectral density, cross-power spectral density, ordinary coherence and noise power contribution ratio for the system shown in Fig. 6.3.1

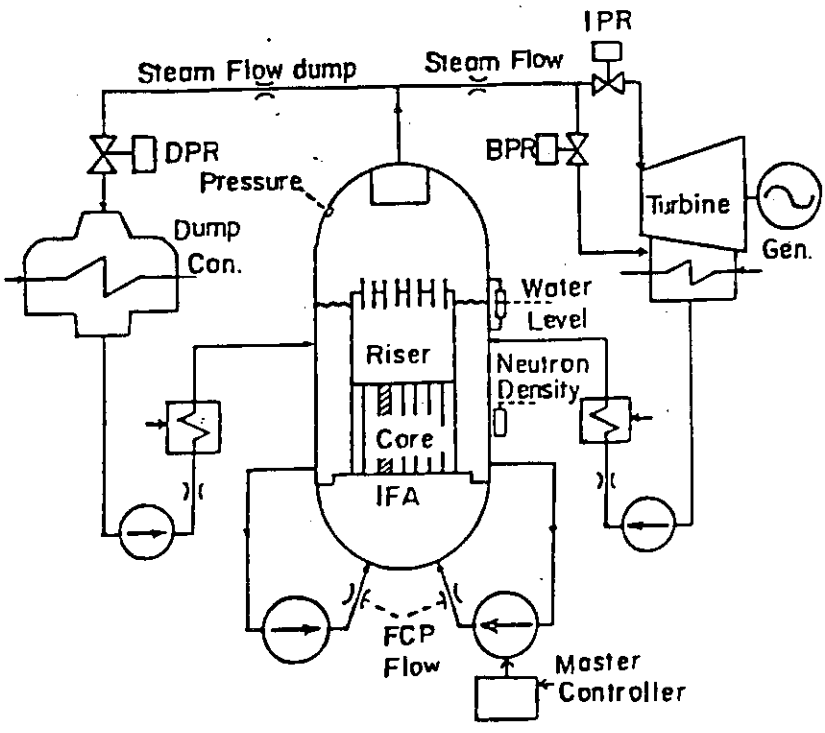

Fig. 6.3.3 Schematic diagram of the JPDR-II plant

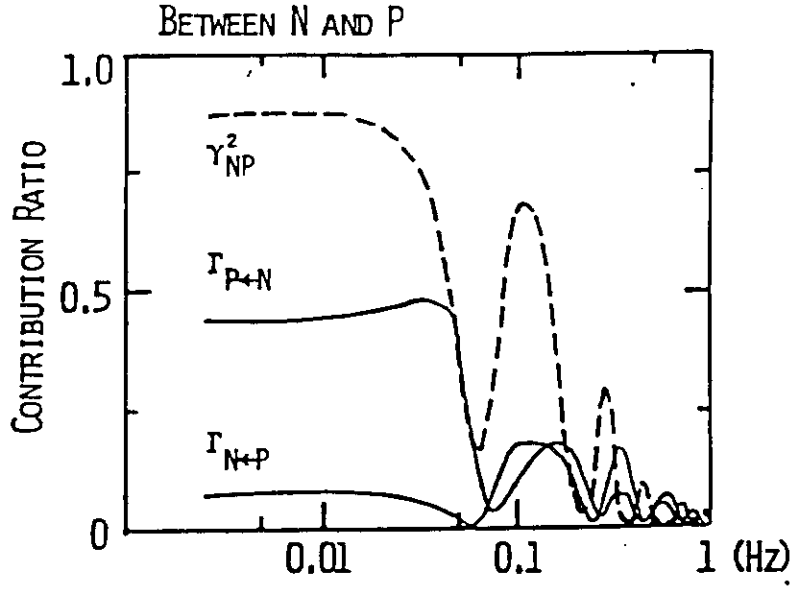

Fig. 6.3.4 Results of the comparison between the ordinary coherence and the noise power contribution functions for neutron(N) and pressure(P) signals collected from JPDR-II

6.4 Development of Computer Code - STAR - for Dynamics Analysis and Diagnosis of Nuclear Reactor systems

K. Hayashi, R. Oguma and K. Watanabe

The computer code "STAR : Statistical Analysis of Random Data" has been developed for a hybrid computer for dynamics analysis and diagnosis of nuclear reactor systems using reactor noise.[1)-3)]

This code performs system dynamics analysis in both time and frequency domain based on time series analysis using autoregressive (AR) modeling.[4)] This code can also perform spectral analysis by Blackman-Tukey method which is mainly used for checking the validity of the identified AR model. The various diagnostic studies are possible by use of this code.

In order to facilitate handling of analog data measured on a system in operation, the hybrid computer system is used. Furthermore, this code includes various routines necessary for the analysis works, i.e. those for data acquisition, preprocessing, data management by use of the magnetic tape and disk system, display of the obtained results on the graphic display and so forth.

The code consists of following seven independent programs.

(1) STAR11 ... Data acquisition, preparation of temporary files, data management, modification and test
(2) STAR22 ... Multivariate correlation and spectral analysis
(3) STAR33 ... Identification of Multivariate AR model, prediction and state estimation
(4) STAR44 ... Analysis in time domain based on MAR model
(5) STAR55 ... Analysis in frequency domain based on MAR model
(6) STAR66 ... Spectral analysis based on MAR model
(7) STAR67 ... Identification of univariate AR model and its applications

These programs have a mutual relation as shown in Figure 6.4.1. The detailed descriptions about the functions of these programs are listed in Table 6.4.1.

The feature of this code are such that it includes the programs for

control of the linkage part which combines analog part with digital part, uses the overlay programming method, and executes the data processing and the analysis through communications between man and machine.

This code has been developed for the hybrid computer EAI PACER-600 system. The most part of the code is programmed in FORTRAN-IV and some part by assembler language on PACER-600 operating system.

References

1) Hayashi K., Oguma R. and Watanabe K.: "Computer Code - STAR : Statistical Analysis of Random Data - for Dynamics Analysis and Diagnosis of Nuclear Reactor Systems," JAERI-M 9761 (1981) (in Japanese).
2) Oguma R., Fujii Y. and Watanabe K.: "Computer Code DYSAC for Identification and Dynamics Analysis of Multivable Systems Based on the Autoregressive Model," JAERI-M 6897 (1977) (in Japanese).
3) Oguma R., Fujii Y., Usui H. and Watanabe K. : "Computer Code MLCOSP for Multiple-Correlation and Spectrum Analysis with a Hybrid Computer," JAERI-M 6252 (1975) (in Japanese).
4) Akaike H., Nakagawa T.: "Statistical Analysis and Control of Dynamics Systems," Saiensu-sha (1971) (in Japanese).

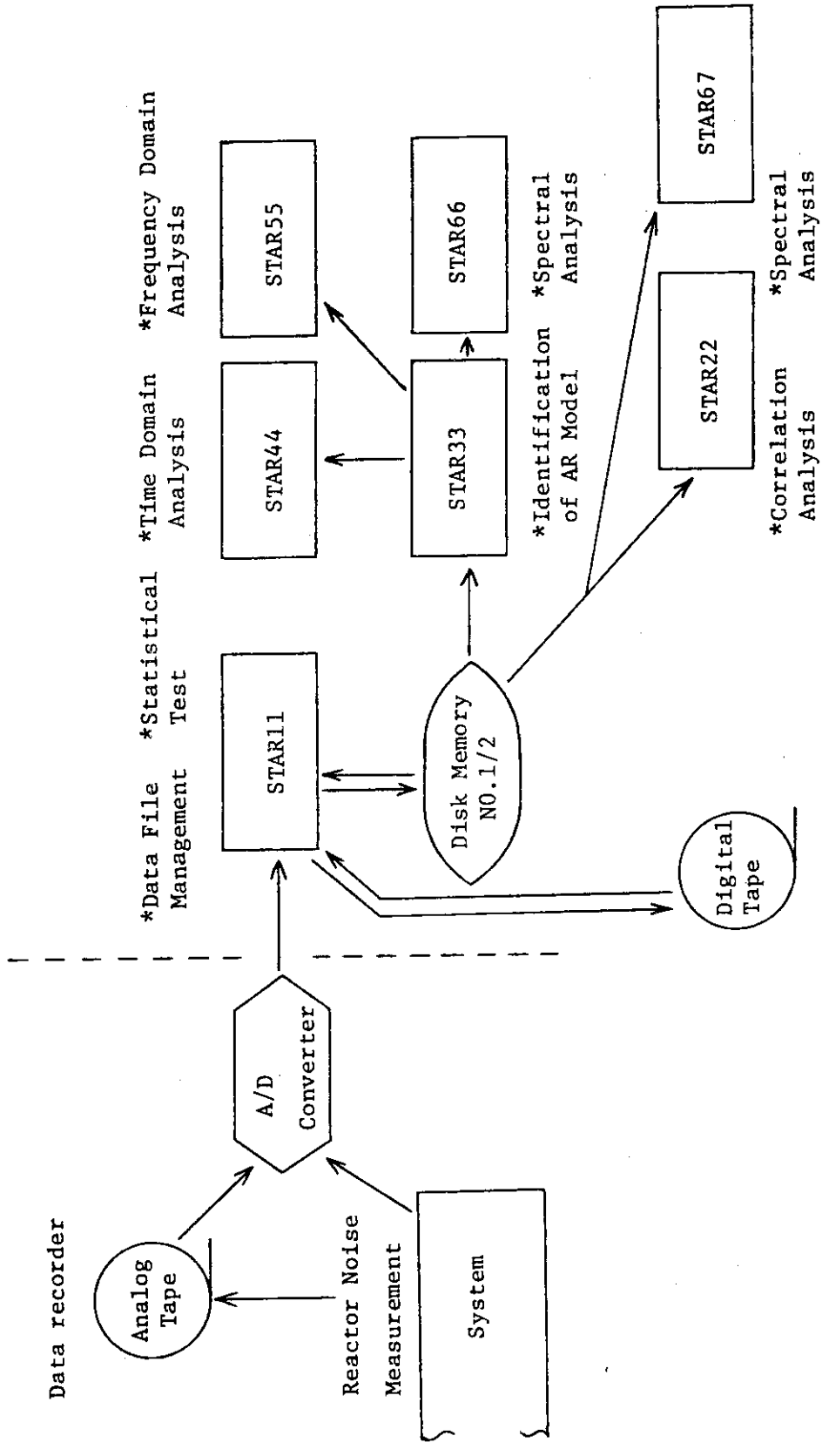

Figure 6.4.1 Flow diagram of STAR code

Table 6.4.1 Functions of STAR code

Program	Functions
STAR11	(1) Initialization of temporary files (2) Making of original data file (i) Acquisition of time series data (a) Cards (b) Analog signals (ii) Preprocessing (a) Spike noise elimination (b) Trend removal (c) Calibration (d) Data selection (3) Statistical Test (i) Normality (ii) Stationarity (4) Management of data file (i) Copy from/to MT (ii) Print out
STAR22	(1) Estimation and display of correlation functions (i) Auto correlation function (ii) Cross correlation function (2) Estimation and display of spectra (i) Auto power spectrum (ii) Cross power spectrum (3) Analysis of single input/ single output system and display (i) Frequency response (ii) Ordinary coherence (4) Analysis of multiple input/ single output system and display (i) Conditional frequency response (ii) Partial coherence (iii) Multiple coherense
STAR33	(1) Identification of multivariate AR model (i) Estimation of correlation matrix (ii) Calculation of AR coefficients and residual covariance (iii) Determination of model order (2) State estimation, prediction and display (i) One step prediction (ii) State estimation

Program	Functions
STAR44	(1) Dynamics analysis of open system and display (i) Step response function (ii) Mode characteristics function (2) Dynamics analysis of feedback system and display (i) Step response function (ii) Mode characteristics function
STAR55	(1) Fourier transformation of AR coefficient matrix (2) Analysis for noise source and display (i) Estimation of noise source APSD (ii) Estimation of noise power contribution ratio (3) Dymamics analysis of open loop system or feedback system and display (i) Frequency response function (ii) Transfer function
STAR66	(1) Fourier transformation of AR coefficient matrix (2) Estimation of spectral density matrix and conversion to vector form and display (i) Auto power spectrum (ii) Cross power spectrum (3) Analysis of single input/ single output system (see STAR22 (3)) (4) Analysis of multiple input/ single output system (see STAR22 (4))
STAR67	(1) Identification of univariate AR model based on Yule-Walker method or Burg's method (i) Calculation of AR coefficients and residual covariance (ii) Calculation of auto correlation function based on AR coefficients (iii) Determination of model order (2) Estimation of auto correlation function and display (i) Extrapolated correlation (3) Estimation of auto power spectrum and display (i) Maximum entropy spectrum

6.5 Application of Burg's MEM to Diagnosis of Nuclear Reactor[1)]

K. Hayashi and R. Oguma

The present study is concerned with experimental evaluations of autoregressive modeling based on Burg algorithm,[2)] the so-called maximum entropy method (MEM), and its application to reactor noise analysis.

Generally speaking, in order to obtain certain results from the analysis using statistical method for random processes, most conventional methods require long enough sampled data. However, such situations often occur that the measurement time of data is insufficient or the stationary part in the measured data is very short. As a way to analyze such short data, autoregressive modeling based on Burg's algorithm is thought to be effective. But,it is known that the spectral sift problem occurs when sampled data are extremely short.[3)]

With a view to analyze short data recordings, the Burg algorithm was evaluated in comparison with that based on Yule-Walker method, through model fitting to simulation data using sinusoidal signal with and without additive white noise. The influence of the model order, the number of sampled data and the initial phase of data are considered in these evaluations.

As a typical example, Figure 6.4.1 shows a case which used only a 5-points data set sampled with a time interval of 0.061 sec from a sinusoid with the frequency 1.5 Hz. The data length of 5-points sampled is equal to about 0.37 times the period of the sinusoid.

In order to evaluate the influence of the initial phase of data, the behaviors of the identified AR parameters and the frequency of peak in the estimated spectra were examined. In this case, the spectral shift problem occurred. It should be noted that the AR coefficients and residual covariance of the identified model seem to depend on the estimated covariance of the data.

Figure 6.4.2 shows a case in which a 12-points data sets sampled from the same sinusoid is used. The data length of 12-points covers about one period of the sinusoid. In this case, the estimate of the covariance of the data was relatively good. The behavior of each AR parameters seem to be constant. And the estimated frequency of the spectrum indicated the correct value of 1.5 Hz. The result stated above suggest that the

spectral shift problem is occurred by the incorrect estimate of the variance of the data.

This method was applied to the neutron noise data sampled from a power reactor. It is known that the neutron noise of this reactor has two remarked spectral peaks at about 0.04 Hz and 0.7 Hz.[4] The spectral analysis was performed for individual short data recordings with an equal length of a 300-points data set obtained by dividing an original long data recordings of a 3300-points data set. The time history of frequency points of the two peaks on the estimated spectra is shown in Figure 6.4.3. The result suggests that the present method is capable of detecting time dependent variation of spectral peaks, if they exist.

References

1) Hayashi K. and Oguma R.: "Identification of Autoregressive Model Based on Burg Algorithm and Its Application to Diagnosis of Nuclear Reactor," JAERI-M 82-009 (1982)(in Japanese).
2) Burg J. P. : "Maximum Entropy Spectral Analysis," (1967) Modern Spectrum Analysis (edited by Childers D. G.) p.34, IEEE Press (1978).
3) Chen W. Y. and Stegen G.R.: J. Geophys. Res., 77, 1396, (1976).
4) Oguma R.: "Applications of the Multivariate Autoregressive Modeling Technique to Study of the Resonant Power Oscillation in the Halden Boiling Water Reactor," JAERI-M 8579 (1979) (in Japanese).

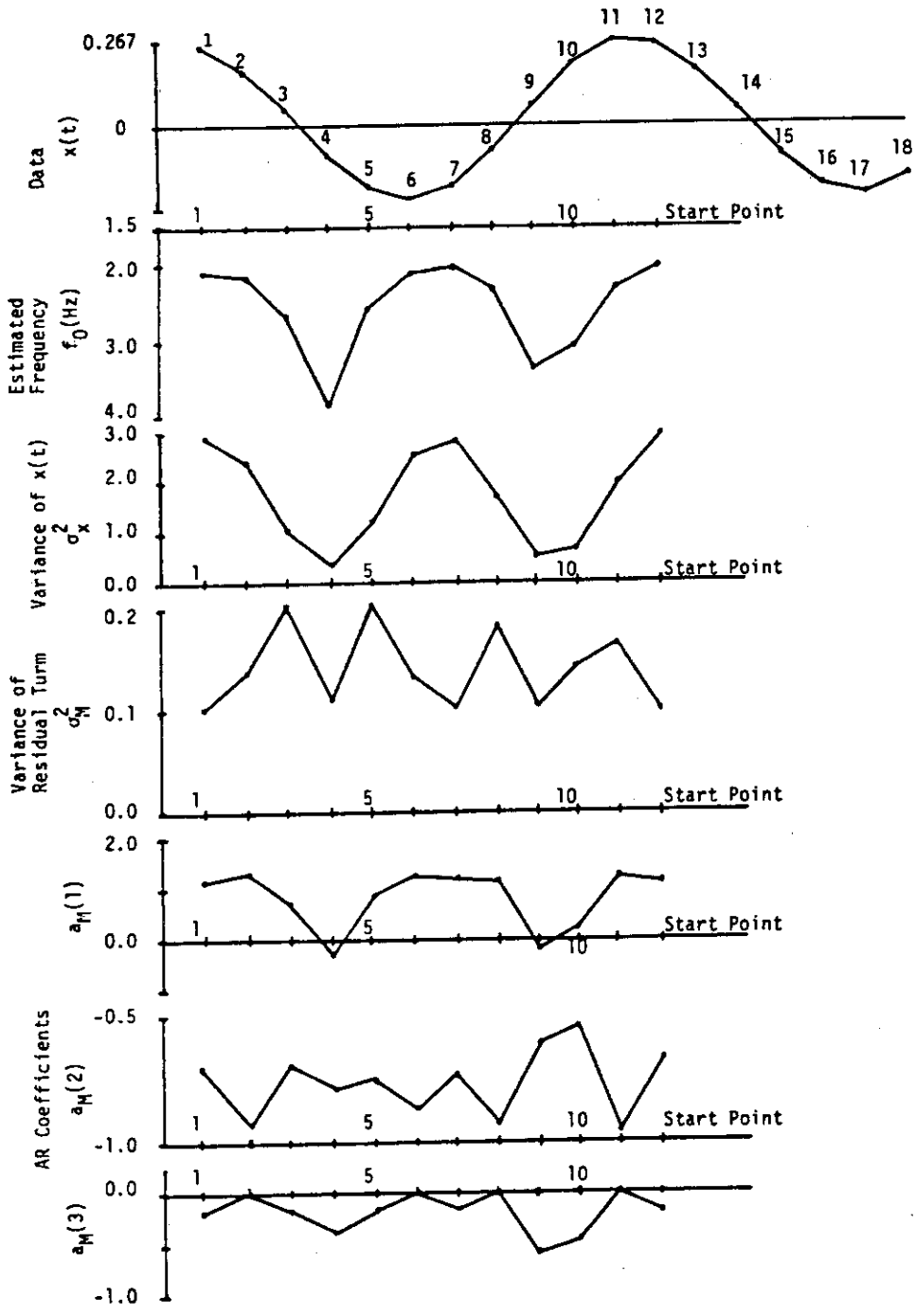

Fig. 6.5.1 The behaviors of the estimated frequency f_0 and the identified AR parameters for various initial phases (start points) of a 5-point data set sampled from a sinusoid. Here AR model order M=3 is used.

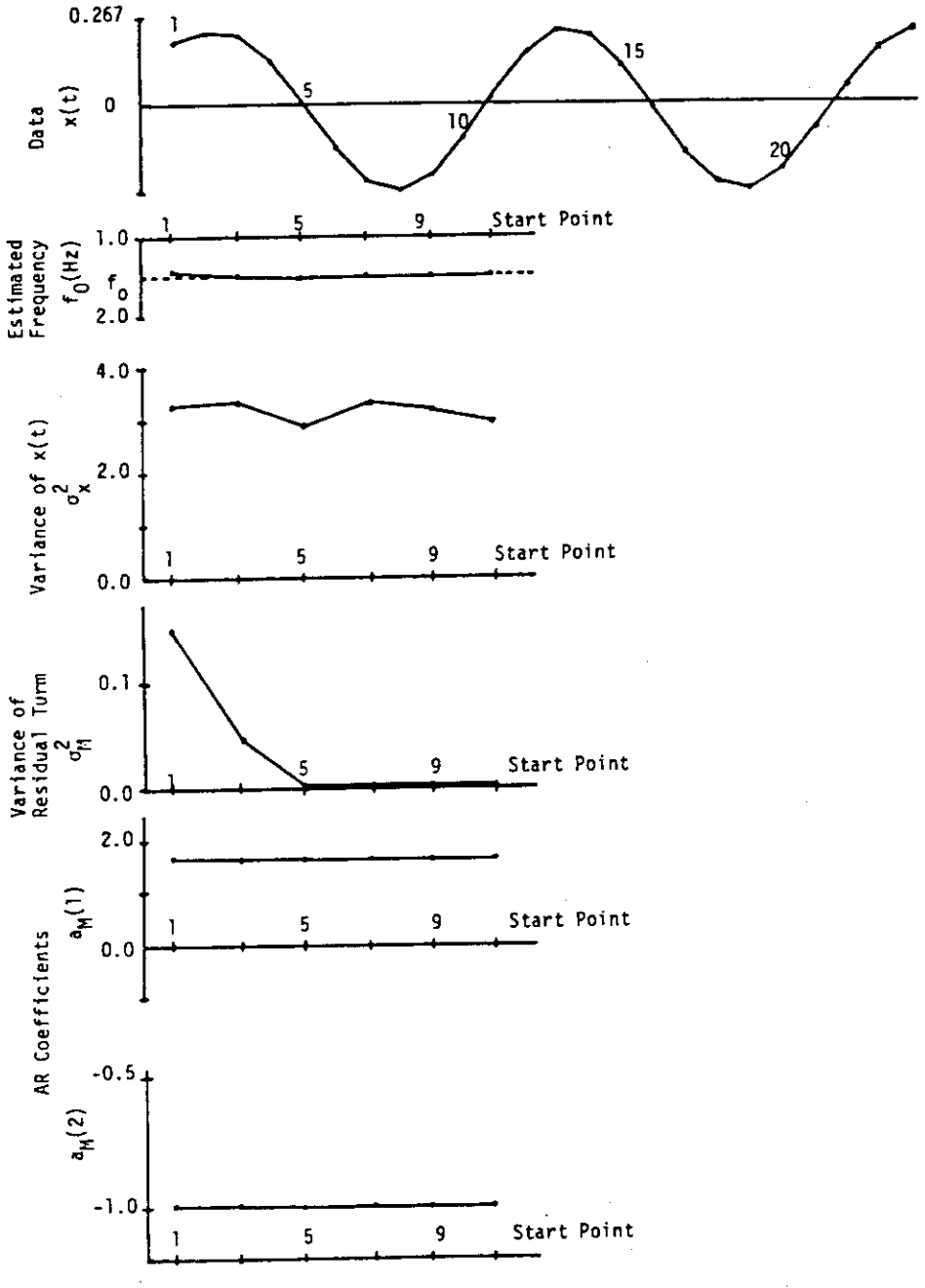

Fig. 6.5.2 The behaviors of the estimated frequency f_0 and the identified AR parameters for six different initial phases (start points) of a 12-point data set sampled from a sinusoid. Here AR model order M=2 is used.

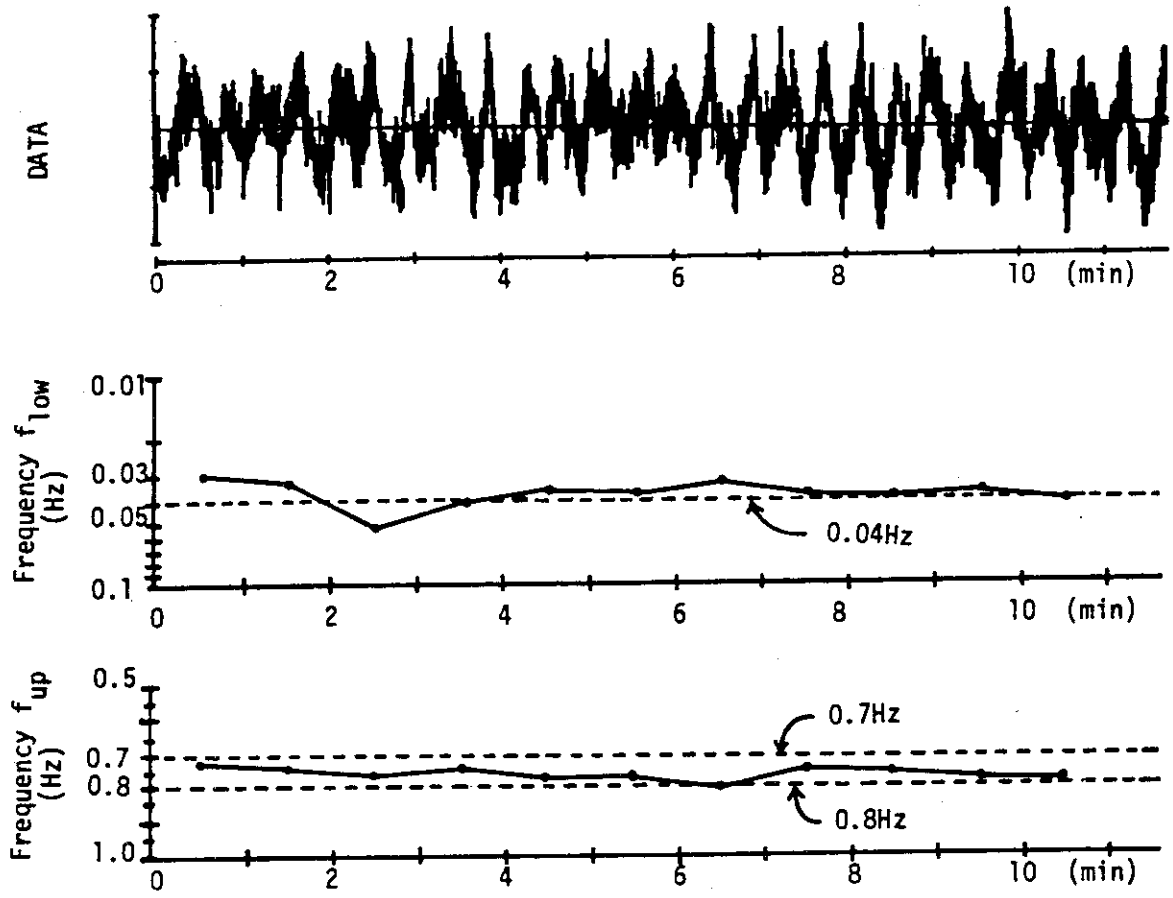

Fig. 6.5.3 Time history of frequency of two peaks in power spectrum of the neutron noise. Each spectra are estimated using a 300-point (1 min) data.

7. Fusion Reactor Technology

7.1 Tritium Production-Rate Distribution in a Li_2O-C Assembly
—— Measured by Li_2CO_3 Pellets ——

T. Iguchi*, H. Maekawa, Y. Seki, Y. Ikeda, Y. Oyama, M. Nakazawa*
and T. Nakamura

As one of the fusion blanket neutronic experiments at FNS, the direct measurement of tritium production-rate in a pseudo-spherical lithium-oxide assembly with graphite reflector has been carried out by Dierckx's method using Li_2CO_3 pellets.[1] In order to provide the good data for benchmark, the present experiment emphasizes not only on obtaining the data as accurate as possible but also on determining the confidence limit of results through the quantitative uncertainty analysis.

The Li_2CO_3 pellets (10 mmϕ × 5 mm, ∿0.7 g) of natural abundance and enriched ^7Li (99.952 atom %) were set in the Li_2O blocks having a hole of 16.6 × 16.6 mm^2, and arranged as shown in Fig. 7.1.1. After the irradiation of 4.5×10^{15} neutrons, the samples were chemically treated and measured by the liquid scintillation technique.

The cross section of $^7Li(n,n'\alpha)T$ reaction at ∿14.9 MeV has been also measured to back up this experiment. Two kinds of Li_2CO_3 pellets put between activation foils (Al,Ni,Au) were set in front of the target and simultaneously irradiated. The cross section was estimated by the ratio of tritium production to activity of foils.

The estimated uncertainty in each parameter used to calculate the absolute value of tritium production-rate is summarized and classified into random and systematic components in Table 7.1.1. Considering that random components can be further reduced by repeating the measurements, it is evident that systematic errors of the source neutron yield and standard HTO have great influence on the total accuracy, particulary in this case of intense irradiation.

Results of tritium production-rate distribution in the assembly separated into $^6Li(n,\alpha)T$ and $^7Li(n,n'\alpha)T$ components are shown in Fig. 7.1.2 with the results of preliminary analyses. Further analysis will

---

* University of Tokyo

be done using a more accurate model, especially for the target region.

The estimated tritium production cross sections of ^{7}Li are summarized in Table 7.1.2. They are within a reasonable range comparing with evaluated data in the past.

Judging from these results of tritium production-rate distribution and activation foils having higher threshold energy, it seems to be advisable to reduce the cross section of $^{7}Li(n,n'\alpha)T$ reaction in current use for the calculations.

Reference

1) Dierckx, R. : Nucl. Inst. Meth., 107, 397 (1973).

Table 7.1.1 Results of uncertainty analysis

EFFECTS	ESTIMATED UNCERTAINTY			
	RANDOM ERROR		SYSTEMATIC ERROR	
	(%)	CONTENTS	(%)	CONTENTS
Li-ATOM NUMBER IN A PELLET	0.18	MEASUREMENTS OF WEIGHT	0.8 >	PURITY OF Li_2CO_3
SOURCE NEUTRON YIELD	NEG-LIGIBLE	COUNTING STATISTICS	0.67	SOLID ANGLE OF ALPHA-MONITOR
			3.6	CORRECTION FACTOR OF NON-ISOTROPY
			4.7 >	EFFICIENCY OF ALPHA-MONITOR
DPM MEASURED BY LIQUID SCINTILLATION SYSTEM	0.7 ~ 4.4	COUNTING STATISTICS		
	1.4	QUENCHING CORRECTION	2.5 <	ACCURACY OF STANDARD HTO
	1.2	SCINTILLATION EFFICIENCY		
DECAY CONSTANT OF TRITIUM	0.11 ~ 1.0	VARIATION OF REFFERENCE DATA	?	
TOTAL	1.98 ~ 4.88		6.51	

Table 7.1.2 Estimated $^{7}Li(n,n'\alpha)T$ cross section at ~14.9 Mev

REACTION TYPE	REACTION RATE AT 19.7 CM	ACTIVATION CROSS SECTION AT 14.9 MEV	T-PRODUCTION RATE DUE TO $^{7}Li(N,N'A)$	RATIO OF REACTION RATE	ESTIMATED T-PRODUCTION CROSS SECTION
	SEC^{-1}	BARN	SEC^{-1}		BARN
$^{27}AL(N,A)^{24}Na$	5.5093 E-18 (2.26 %)	1.061 E-01		2.421 (6.22 %)	2.68 E-01 (11.8 %)
$^{58}Ni(N,P)^{58}Co$	1.3051 E-17 (2.83 %)	3.065 E-01		1.022 (6.45 %)	3.13 E-01 (11.9 %)
$^{58}Ni(N,2N)^{59}Ni$	2.1013 E-18 (2.38 %)	3.852 E-02 (ENDF/B-IV) 4.620 E-02 (LASL)	1.334 E-17 (5.80 %)	6.348 (6.27 %)	2.45 E-01 (11.8 %) 2.93 E-01
$^{197}Au(N,2N)^{196}Au$	6.0507 E-17 (2.54 %)	2.093 E+00		0.1500 (6.33%)	3.14 E-01 (11.8 %)

SOURCE FLUX =5.330 E+07 ($N/CM^2.SEC$)

UNCERTAINTY:±10.0% FROM ENDF/B-IV DOSIMETRY FILE

(CF.) $^{7}Li(N,N'A)T$ CROSS SECTION AT 14.9 MEV

ENDF/B-IV: 320 MB

M.T.SWINHOE ET AL. AERE-PR/NP-26(1978) : 220 MB

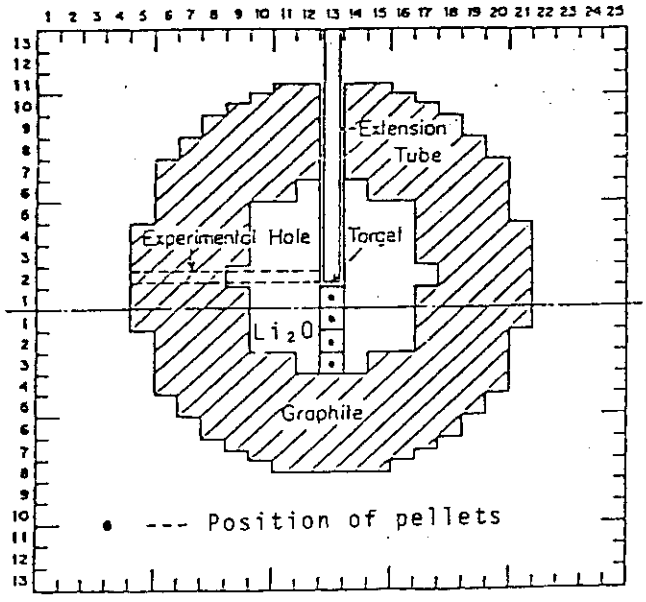

Fig. 7.1.1 Horizontal section across the center of Li_2O-C assembly

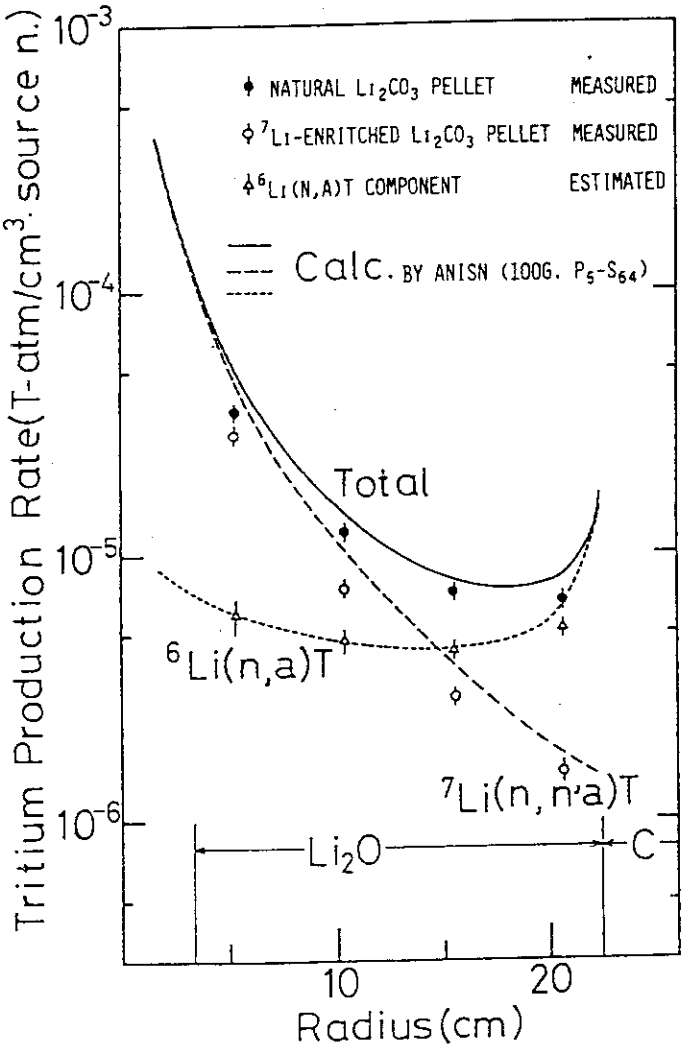

Fig. 7.1.2 Tritium production-rate distribution in Li_2O-C assembly measured by Li_2CO_3 pellets

7.2 Tritium Production-Rate Distribution in a Li_2O-C Assembly

—— Measured by Self-Irradiation Method of LiF TLD's ——

H. Maekawa

Seven years ago, a self-irradiation method using LiF TLD was proposed as a new method to measure the tritium production-rate distribution in a simulated fusion blanket assembly and was shown to be feasible by a experiment using FCA VI-3 core assembly.[1] As a intense neutron source, FNS, was complete in March 1981, it was the first time to apply this method to the fusion blanket experiment.

The system for this experiment was the pseudo-spherical lithium-oxide assembly with graphite reflector (Li_2O-C). It was just the same assembly as that to measure the absolute fission-rate distribution in the previous experiment performed with the PNS-A neutron source.[2] The sizes of central cavity, Li_2O and graphite regions are 3.3, 22.4 and 46.8 cm, respectively, in the effective outer radius. The homogenized nuclide densities of respective regions are given in Table 7.2.1.

The powder of TLD-600 (^6Li : 95.62 atom %) and TLD-700 (^7Li : 99.993 atom %) manufactured by Harshaw Chemical Co. Ltd. was sealed in 2 mmϕ × 12 mm glass ampoules. Two pairs of TLD-600 and -700 were set along both 0° and 90° directions to the incident d^+ beam (See Fig. 7.2.1). Li_2CO_3 pellets discribed in 7.1 of this report were set simultaneously along to the 0° direction. For thirteen days after neutron irradiation to wait the full decay of activated nuclei except for tritium, the TLD's were annealed twice in the condition of 400°C and one hour. After then, they were stored in a special-ordered low background storage for 2215 hours (about three months). The thermoluminescence caused by the self-irradiation of β-rays from tritium during the keeping were measured by a TLD Reader. The data were processed considering the atomic densities of ^6Li and ^7Li in the TLD's. Measured tritium production-rate distributions of total, $^6Li(n,\alpha)^3T$ and $^7Li(n,n'\alpha)^3T$ were shown in Fig. 7.2.2 with the results of preliminary analyses. The experimental values were normalized to the result of Li_2CO_3 pellet at 5.3 cm. The data of TLD and Li_2CO_3 pellet agree well each other.

It can be proved that the self-irradiation method of LiF TLD's is practical and useful for the measurement of tritium production-rate in the fusion blanket benchmark experiments.

References

1) Maekawa, H. : "A Method for Obtaining the Tritium Production Rate Distribution with a LiF Thermoluminescence Dosimeter," JAERI-M 6055 (1975) (in Japanese) ; UCRL-TRANS-11196 (1977).

2) Maekawa, H., et al. : J. Nucl. Sci. Technol. 16 [5] 377 (1979).

Table 7.2.1 Nuclide densities in individual regions

Nuclide	Nuclide density (10^{24} atoms/cm^3)			
	Void	Li_2O	Graphite	Lattice
^6Li		3.355×10^{-3}		
^7Li		4.1855×10^{-2}		
O		2.2605×10^{-2}		
C			6.9298×10^{-2}	
Cr	1.751×10^{-3}	1.935×10^{-3}	1.751×10^{-3}	1.161×10^{-3}
Mn	8.185×10^{-5}	9.632×10^{-5}	8.185×10^{-5}	5.632×10^{-5}
Fe	6.349×10^{-3}	7.030×10^{-3}	6.349×10^{-3}	4.159×10^{-3}
Ni	7.303×10^{-4}	8.106×10^{-4}	7.303×10^{-4}	4.821×10^{-4}

* This table is a revised version of Table 2 in the reference 2). Please don't use the old table from this time on.

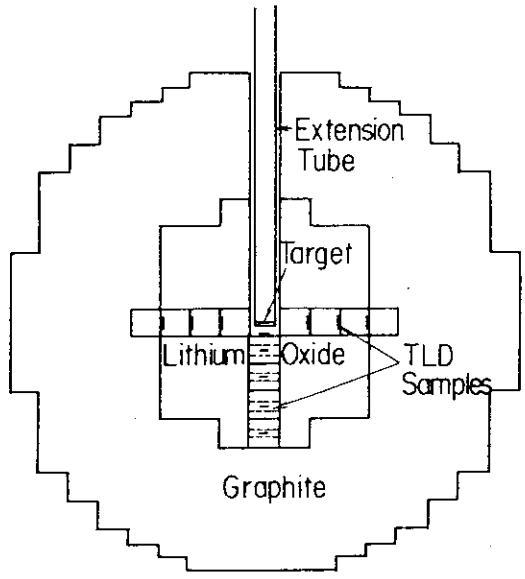

Fig. 7.2.1 Horizontal section across the center of Li_2O-C assembly

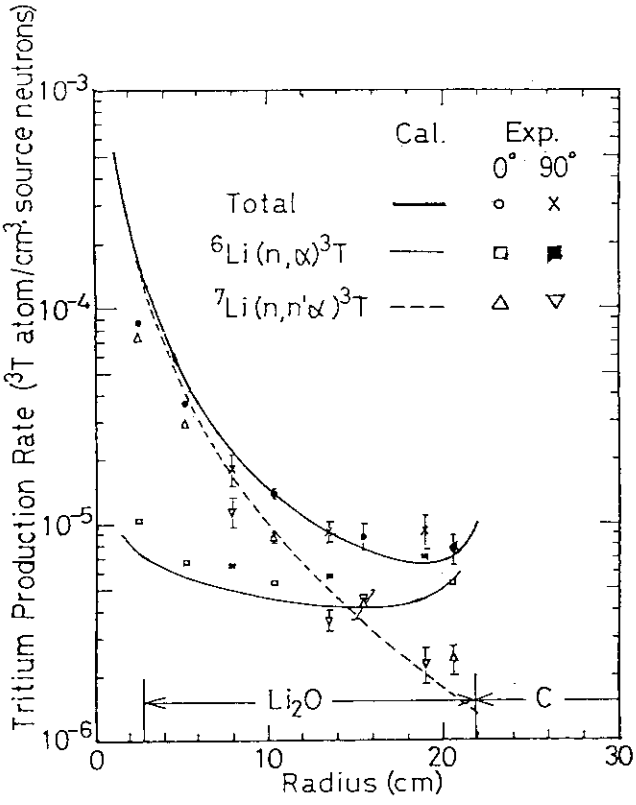

Fig. 7.2.2 Tritium production-rate distribution in Li_2O-C assembly measured by LiF TLD's
The tritium production rates were calculated by ANISN with P_5-S_{10} using the cross section set, GICXFNS, that was obtained from ENDF/B-IV except C and ^7Li data. The data of C and ^7Li were refered from ENDF/B-V and P.G. Young (Tras. Am. Nucl. Soc., 39, 272 (1981)), respectively.

7.3 Fission-Rate Distribution in a Li_2O-C Assembly Measured by Solid State Track Recorder

T. Nakamura, H. Maekawa, F. Fujita*, M. Narita* and Y. Miyazaki*

Distinctive features of solid state track recorder (SSTR) applied in the reactor physics experiments are small detector size and high detection sensitivity. The former ensures good spatial resolution as well as minimum disturbance in the measuring field and the latter facilitates a measurement in a weak neutron flux environment.

Fission-rate distributions for U-238 and Th-232 were measured by the SSTR method in the Li_2O-C spherical assembly described in 7.1 and 7.2. Detectors, each composed of a fission foil radiator and a polycarbonate (Teijin Takiron PC-1600) film, were inserted in the media along the lines at the angles of 0° and 90° to the incident deuteron beam. The effective detection efficiencies were determined seperately in a 14 MeV neutron irradiation where the absolute yield was obtained by the associated particle method.

After the irradiation, the films were etched with 30% KOH aqueous solution for 30 minutes at 60°C. To get the most favorable etched track density for observation, the irradiation time was adjusted to keep the track density within the range between 10^4 to 10^5 /cm^2 for the films at different locations. The etch-pits were counted by using an optical microscope and an automatic counting system (LUZEX-450).

The data on the effective detection efficiency are summarized in Table 7.3.1 and the measured fission distributions are shown in Fig. 7.3.1 with micro fission chamber results and the calculated values by ANISN. The agreement is reasonably good, indicating that the SSTR method is a useful tool in the field of fusion neutronics.

References

1) Narita, M., et al. : J. Nucl. Sci. Technol, 14, [1] 65 (1977).
2) Nakamura, T., et al. : "Integral Experiments on Lithium Oxide Spherical Assembly with Graphite Reflector and on Duct Streaming," Third IAEA Technical Committee Meeting and Workshop on Fusion Reactor Design and Technology, Tokyo, Oct. 5-16, (1981).

* Hokkaido University

Table 7.3.1 Parameters for sensitivity measurement

SSTR	Th + Polycarbonate		D.U. + Polycarbonate	
No.	A-1	A-2	B-1	B-2
Irradiation time T (sec)	3600	1800	3600	1800
Total neutron yield S	8.43×10^{13}	4.00×10^{13}	8.43×10^{13}	4.00×10^{13}
Distance from target r (cm)	20	20	30	30
Total neutron fluence nvt (cm^{-2})	1.66×10^{10}	7.96×10^{9}	7.38×10^{9}	3.54×10^{9}
Etchpit density P (cm^{-1})	$(7.17 \pm 0.19) \times 10^{4}$	$(3.81 \pm 0.11) \times 10^{4}$	$(7.83 \pm 0.23) \times 10^{4}$	$(4.23 \pm 0.13) \times 10^{4}$
Effective sensitivity K	$(4.32 \pm 0.11) \times 10^{-6}$	$(4.79 \pm 0.14) \times 10^{-6}$	$(1.06 \pm 0.031) \times 10^{-5}$	$(1.19 \pm 0.036) \times 10^{-6}$
Prime sensitivity k (cm^{-2})	$(1.04 \pm 0.027) \times 10^{19}$	$(1.15 \pm 0.033) \times 10^{19}$	$(0.835 \pm 0.025) \times 10^{19}$	$(0.937 \pm 0.029) \times 10^{19}$

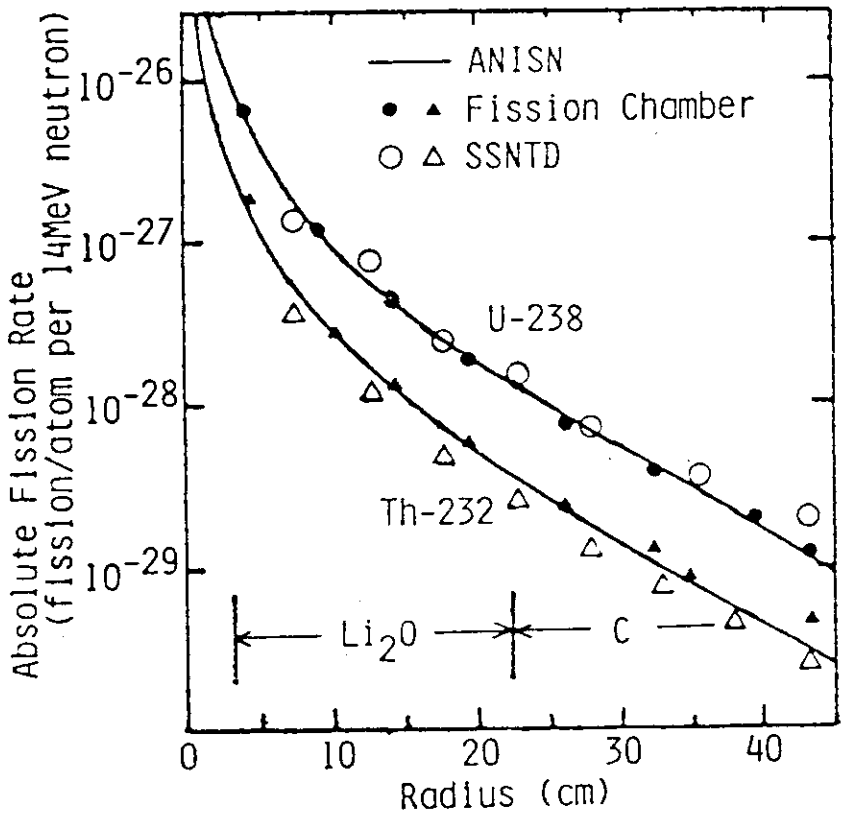

Fig. 7.3.1 Absolute fission-rate distributions in Li2O-C assembly

7.4 Feasibility Test of SUS316 Stainless-Steel as a Neutron Dosimeter for Fusion Reactor Dosimetry

Y. Ikeda, S. Tanaka, Y. Oyama, H. Maekawa and T. Nakamura

The need for experiments to aid fusion reactor dosimetry is recognized as the important part of Controlled Thermo-Nuclear Reactor (CTR) development. In order to make diagnosis on the neutron field in these experiments, the activation method can be used to determine the fast neutron spectra produced by interaction of the 14 MeV D-T fusion source neutrons with the structural materials. Stainless-steel, SUS316, which are comprehensively considered as the structural materials of CTR, consists of several kind of elements, for example, Fe, Ni and Cr and each has some isotopes. They are activated by various types of reactions in the intense fast neutron field. Some of these reaction cross sections are well studied. Then, it is able to deduce the neutron spectra and the reaction rate distribution by selecting an adequate reaction set in the same manner as the method of multi-foils activation. From this point of view, a feasibility test of SUS316 as a neutron dosimeter has been performed using FNS (fusion neutronics source).

SUS316 disks (each $10\phi \times 2$ mm) were irradiated at several positions in the Li_2O-C fusion blanket assembly in which the D-T neutron source was located. The positions are schematically shown in Fig. 7.4.1. After irradiation for eight hours, activities were measured using a 60 cm^3 Ge(Li) detector and each reaction rates were deduced by performing several corrections. Reactions such as $^{56}Fe(n,p)^{56}Mn$, $^{54}Fe(n,p)^{54}Mn$, $^{58}Ni(n,p)^{58}Co$ and $^{58}Ni(n,2n)^{57}Ni$ were selected in order that those threshold values cover the range from 1 MeV to 12 MeV. In Fig. 7.4.2, these neutron energy responses are shown. Spectra in each positions were unfolded by the SAND-II unfolding code[1] with the use of the measured reaction rates and activation cross sections taken from ENDF/B-V dosimetry file.[2] For example, the unfolded neutron spectrum in the case of position 2 is shown in Fig. 7.4.3 and both of the measured reaction rates and calculated ones from unfolded spectrum are given in Table 7.4.1. The deviations of each reaction rates are within the range of 20% and the spectrum could be well unfolded using only the four reactions.

There are two main feature to be considered in this method as the neutron dosimetry. One important object is to get an outline of the

fast neutron spectrum and the other is to obtain absolute flux distributions. From the results of this experiment, this method using SUS316 revealed to be a powerful tool for the fusion reactor dosimetry because of the direct use of the structural material as the dosimeter.

References

1) Berg S. and McElroy W. : "A Computer automated iterative method for neutron flux spectra determination by foil activation," AFWL-TR-67-41, Vols. I-IV, Air Force Weapons Laboratory (1967).
2) Kinsey R. : "ENDF/B Summary Documentation, BNL-NCS-17541 (ENDF-201), 3rd Edition (ENDF/B-V)," available from the National Nuclear Center, Brookhaven Laboratory, Upton, N.Y. (July 1979).

Table 7.4.1 Measured and calculated saturated reaction rates

reaction	measured(/sec)		calculated(/sec)		devuation(%)
$^{56}Fe(n,p)^{56}Mn$	1.498	E-17	1.590	E-17	6.1
$^{54}Fe(n,p)^{54}Fe$	9.110	E-17	8.671	E-17	4.8
$^{58}Ni(n,p)^{58}Co$	4.982	E-17	5.655	E-17	13.5
$^{58}Ni(n,2n)^{57}Ni$	5.813	E-18	5.047	E-18	13.2

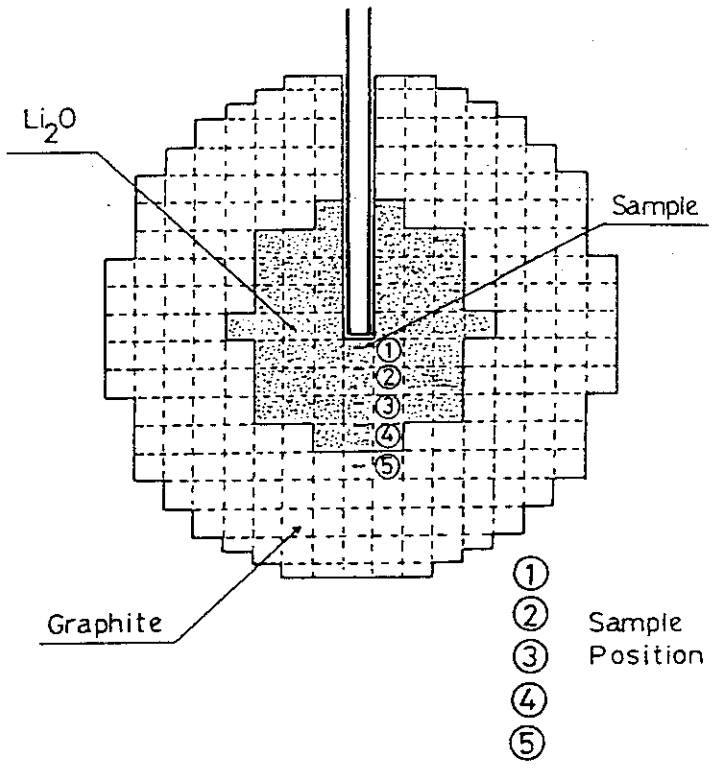

Fig. 7.4.1 Horizontal section across the center of Li_2O-C assembly

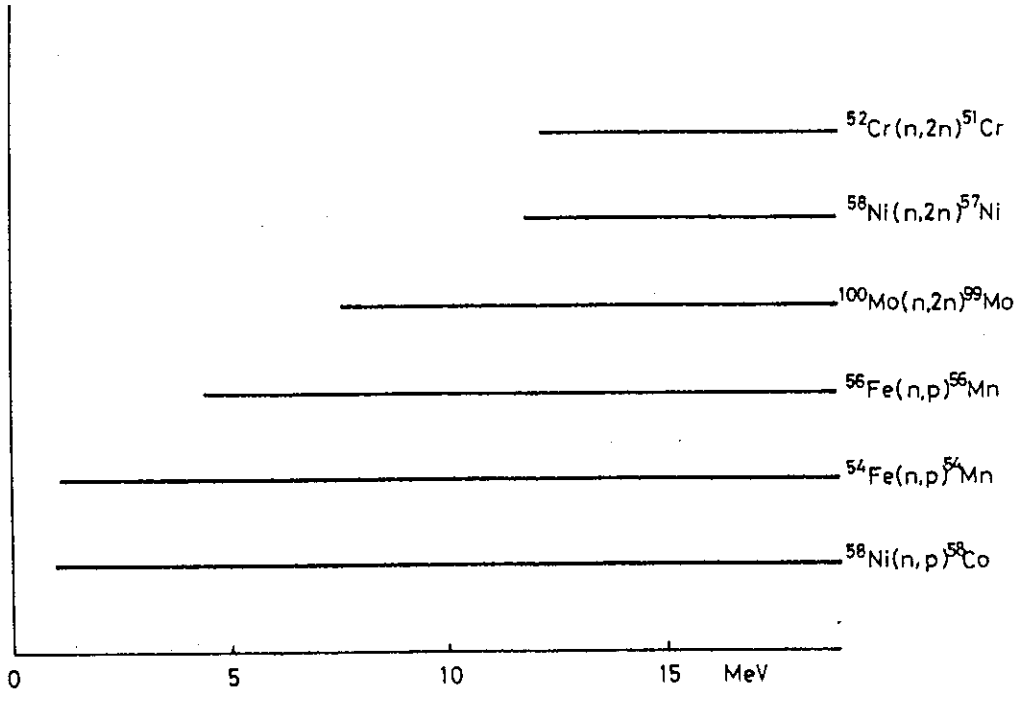

Fig. 7.4.2 Sensitivity ranges of typical reaction in SUS 316

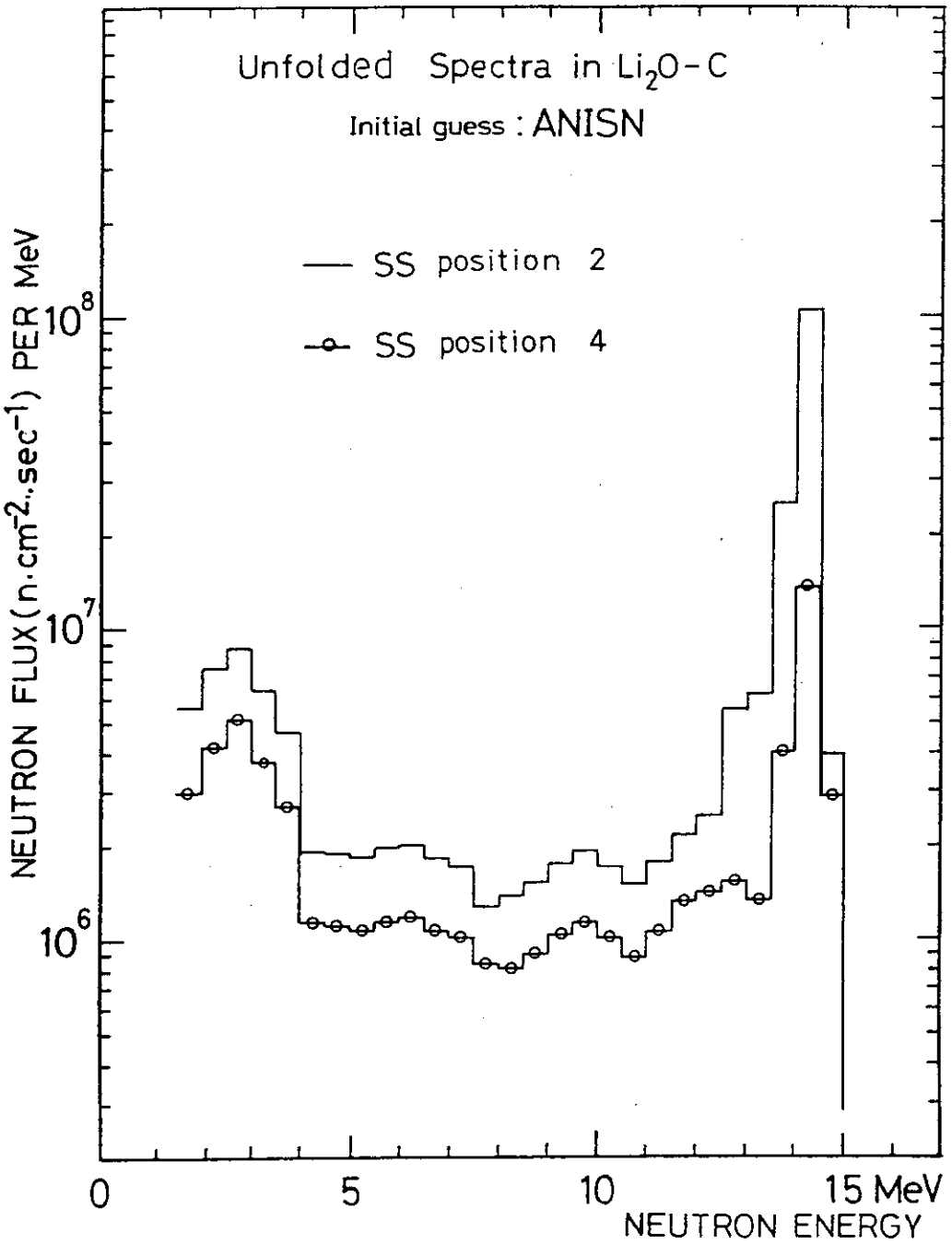

Fig. 7.4.3 Unfolded spectra in Li_2O-C assembly

7.5 Efficiency Calibration of an NE213 Liquid Scintillation Detector for FNS Time-of-Flight Experiments

Y. Oyama and H. Maekawa

TOF (Time-of-Flight) experiment to measure the surface leakage neutron spectra from a Lithium-Oxide plane assembly was started at FNS (Fusion Neutronics Source). The aim of this experiment was the evaluation of the nuclear data and method for the fusion reactor design. For this purpose it was desirable to measure the absolute neutron spectrum. A 50.8 mmϕ × 50.8 mmt NE213 liquid scintillator was used in this experiment, and the absolute effeciency of this detector was determined at the range of 0.5 - 16 MeV.

In case of measuring low energy neutron using an NE213 liquid scintillation detector with a low bias, the structure caused by inelastic scattering of Carbon exists in the high energy region of the effeciency curve.[1] And also in the TOF experiments for fusion neutronics, 14 MeV neutron induced gamma rays become an intense background source in the high energy region because of poor n-γ discrimination characteristics for the low light output (Fig. 7.5.1). As the good n-γ discrimination characteristics can be realized in case of a high bias for high energy neutrons, the two bias method to measure with two discrimination levels at the same time is very effective (Fig. 7.5.2).

The two biases were refered to the peak of 57 keV gamma ray of ^{241}Am and the half-height of 661 keV gamma ray slope of ^{137}Cs. The effeciency for each bias was determined by the following steps:

(1) Effeciency calculation by Monte Carlo method over the full energy range

In this calculation, the data in ENDF/B-IV and Verbinski's data[2] were used for the cross section of Hydrogen and Carbon and for the light output effeciency of NE213, respectively.

(2) Correction from the TOF measurement of ^{252}Cf neutron source

A relative effeciency of NE213 was obtained and the effeciency curve near the discrimination energy corrected by this measurement. The fission spectrum of ^{252}Cf was calculated by using the nuclear temperature of 1.42 MeV.

(3) Absolute check by the alpha counting method

Alpha particles from ^{3}T(d,n)^{4}He reaction were detected by a SSD,

and the count rate of NE213 was compared with the neutron flux at the detector estimated from the alpha count rate. However this absolute calibration was carried out only at 14.9 MeV and the reliability of effeciancy at the other energy points is dependent on the relative precision of (1) and (2) processes.

The results of the Monte Carlo calculation and the TOF measurement of ^{252}Cf spectrum are shown in Fig. 7.5.3. The effeciency curve from ^{252}Cf experiment were adjusted to the calculated one in 4 - 6 MeV. Those results show good agreement with each other for the ^{137}Cs bias, but the pulse height of energy was discriminated obscurely by the n-γ discriminator and its effect appeared on the effeciency curve for the ^{241}Am bias. The calculational effeciency at 14.9 MeV agreed well with the one measured by the alpha counting method within 6%.

References

1) Drosg M. et al. : Nucl. Inst. Meth., 176, 477 (1980).
2) Verbinski V.V. et al. : ibid., 65, 8 (1968).

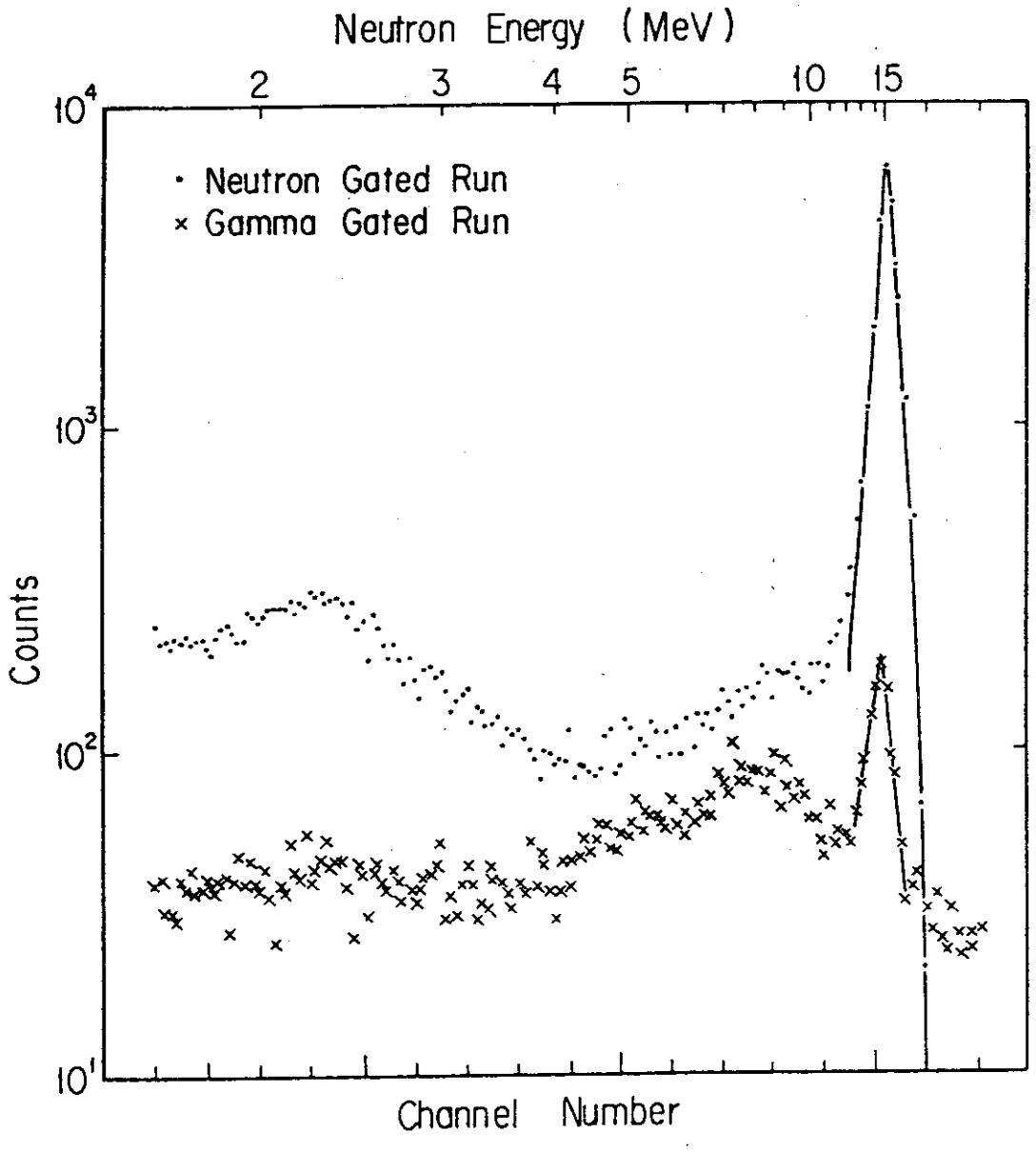

Fig. 7.5.1 Typical neutron and gamma time spectra measured by TOF method The gamma rays were observed above 5 MeV.

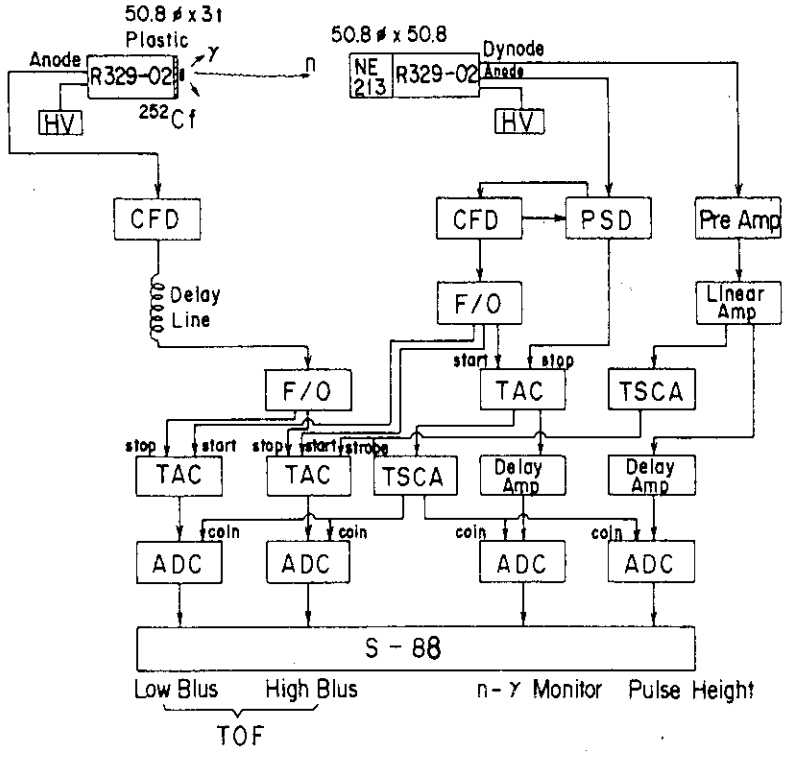

Fig. 7.5.2 Schematic diagram of electonic circuits
(CFD is aconstant fraction discriminator, F/O a fan-out, TAC a time-to-amplitude converter and TSCA a timing single channel analyzer.)

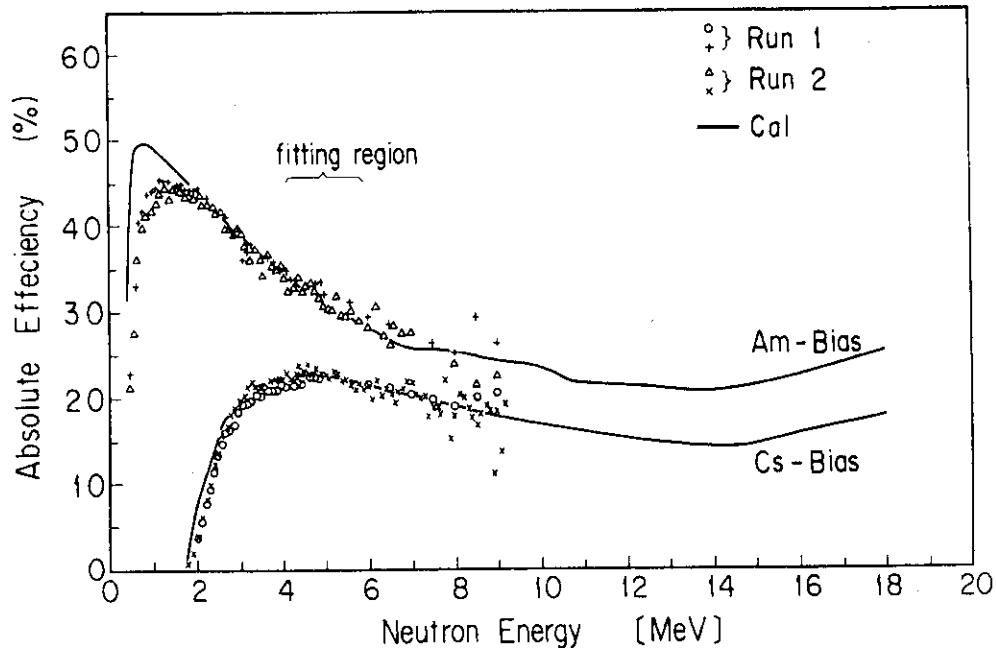

Fig. 7.5.3 Absolute effeciency curves determined in this worle

7.6 Characteristics of 14 MeV Neutron Collimater for Surface Leakage Neutron Spectrum Measurements

Y. Oyama and H. Maekawa

In the TOF (Time-of-Flight) experiment to measure the angular-dependent leakage spectra from a fusion benchmark assembly, it is very important to define the measuring area on the surface of assembly by a neutron collimator, as well as to shield a detector from background neutrons. The collimator-detector response function[1] is necessary for the absolute measurement. Therefore, the response function and the performance of the detector shielding were investigated by a ^{252}Cf neutron source and a 14 MeV pulsed neutron source.

The collimator-detector response function is defined as

$$f(r) = N \cdot \frac{C(r)}{S(r)} \quad ,$$

where S(r) is the source intensity at a distance r from the central axis of a collimator on the measured surface, C(r) the neutron counts for S(r) by the detector, and N a normalization factor.

The effective measured area on the surface of assembly, A_S, can be obtained from f(r),

$$A_S = \int_0^\infty 2\pi r f(r)\, dr \quad .$$

The collimator-detector system at FNS is shown in Fig. 7.6.1. This system has a pair of cylindrical collimators, and the radius of the detector is the same as that of the collimator opening, so that a clear-cut shape of the response function was obtained. The neutron detector is an NE213 liquid scintillator. The collimator has multiple layers to improve the shielding performance.

The ^{252}Cf neutron source was scanned across the collimator-detector axis to obtain the response function. The measurement of the response function for the 14 MeV D-T neutron source was also carried out with the TOF method to check the energy dependency.

The response functions measured by the two sources were very similar to each other. The finite source volume and the throat scattering in the collimator seemed to give a little difference of the slope shape.

These results were compared with the calculation which treated optically a pair of cyrindrical collimators. The calculational response was estimated from the overlap area which was made by a uniform circular neutron cone intercepting the detector area. These results are shown in Fig. 7.6.2 and Fig. 7.6.3.

The difference between the calculational and the experimental effective areas defined by the collimator was 8 - 10%. The effect of the finite source volume was estimated to be about 4% per 1 cm in diameter. The effective area can be determined to be about 5%. The overall signal-to-background ratio of this system was about 10^3 for 14 MeV neutrons.

Reference

1) Straker E.A. et al. : Nucl. Appl., 6, 168 (1969).

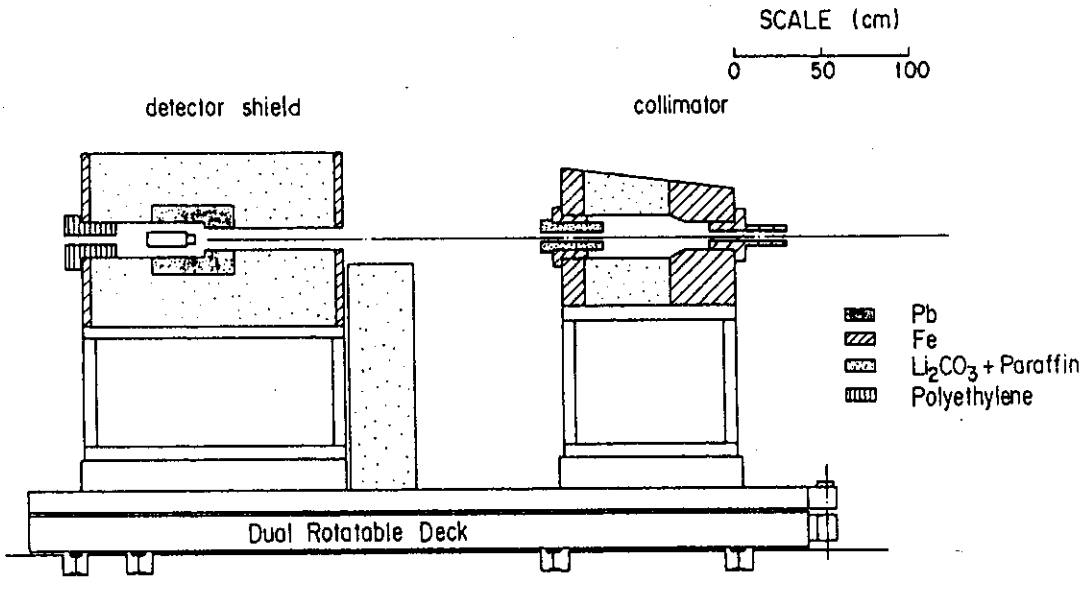

Fig. 7.6.1 Detector-collimator system at FNS
The additional shield is set in front of the detector shield to eliminate the neutron reflection on the deck.

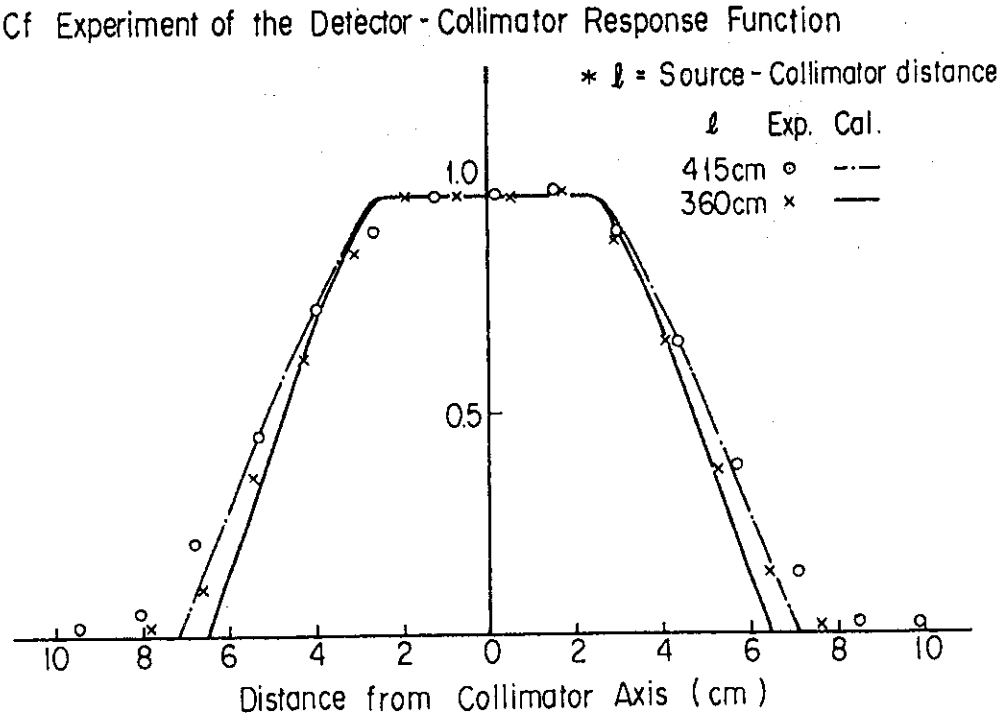

Fig. 7.6.2 Detector-collimator response function measured by ^{252}Cf source. The results are dependent on the distance between the source surface and collimator.

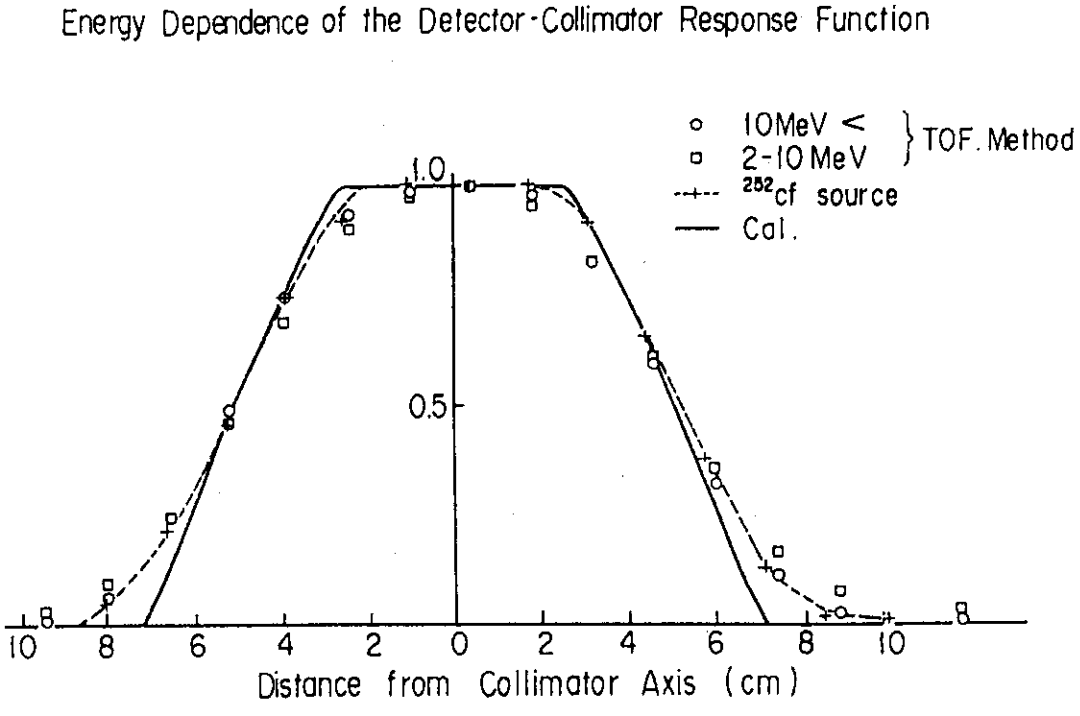

Fig. 7.6.3 Neutron energy dependence of detector-collimator response function
The result of TOF method was obtained with the air-cooled target assembly.

7.7 Preliminary Experiment on Beam Profiles of Fast Neutron Streaming through Straight Ducts by a Small-sized Spherical NE213 Scintillation Counter

T. Nakamura and Y. Oyama

In D-T fusion reactor design, it is anticipated that there would be a number of ducts, large or small, penetrating blanket and shield, NBI ports, vacuum exhaust pipes, fuel feed line and diagnosis ports, for example.[1] Preliminary experiments on the streaming characteristics of fast neutrons were performed by utilizing experimental holes prepared in the shield wall of the FNS target room.

A 14 mmϕ spherical NE-213 scintillation counter which was originally developed to measure neutron spectrum inside the blanket was mounted on a three-directional counter drive mechanism set in front of the duct to survey transverse and axial beam profiles. The section of this counter head is shown in Fig. 7.7.1. The counter was driven at the speed of 0.24 mm/sec and gamma-ray discriminated output signals above pulse height bias level corresponding 1 MeV or 2 MeV were recorded by multi-channel scaler set at one channel/sec.

An experiment on large-sized duct was carried out at the experimental hole connecting target room #1 and #2. D-D neutrons produced in a preparatory run prior to D-T operation was used in this case. Fig. 7.7.2 shows the plan view of the hole and the neutron source was located at the distance of 2.5 m from the entrance of the port. The neutron beam profile is described in Fig. 7.7.3.

By using the rotatable shield plug with a number of 36 mmϕ experimental holes, an experiment on small-sized duct streaming was undertaken for a group of holes offset by a unit of 50.6 mm from the center hole that was on the target axis. The beam profile change with the hole location is shown in Fig. 7.7.4. D-T neutrons were used in this experiment.

Reference

1) Sako, K., et al. : "First Preliminary Design of an Experimental Fusion Reactor," JAERI-M 7300, (1977).

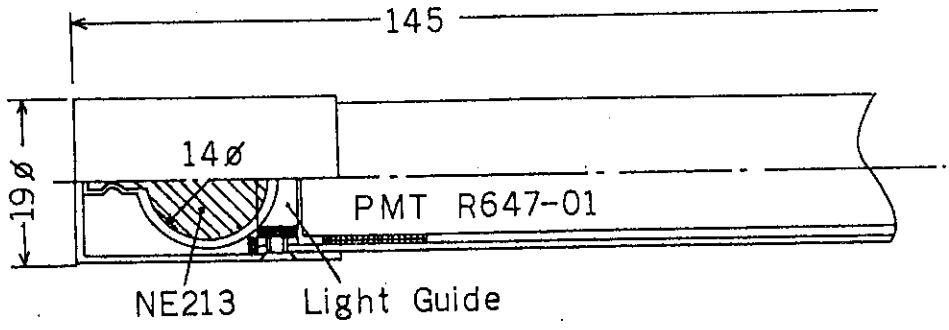

Fig. 7.7.1 Micro NE213 spherical detector

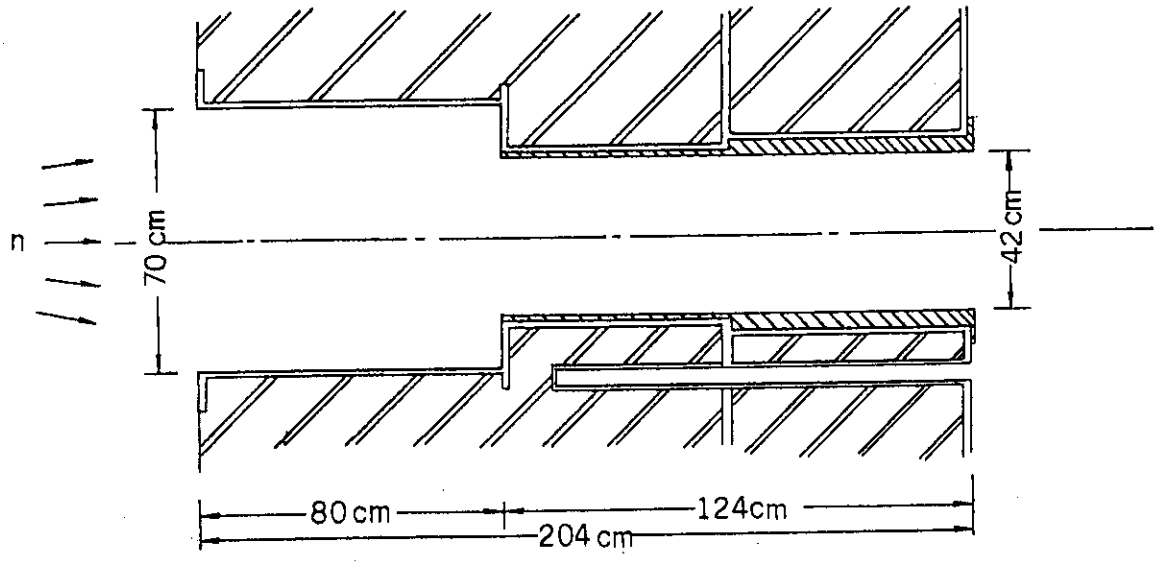

Fig. 7.7.2 Sectional view of experimental hole

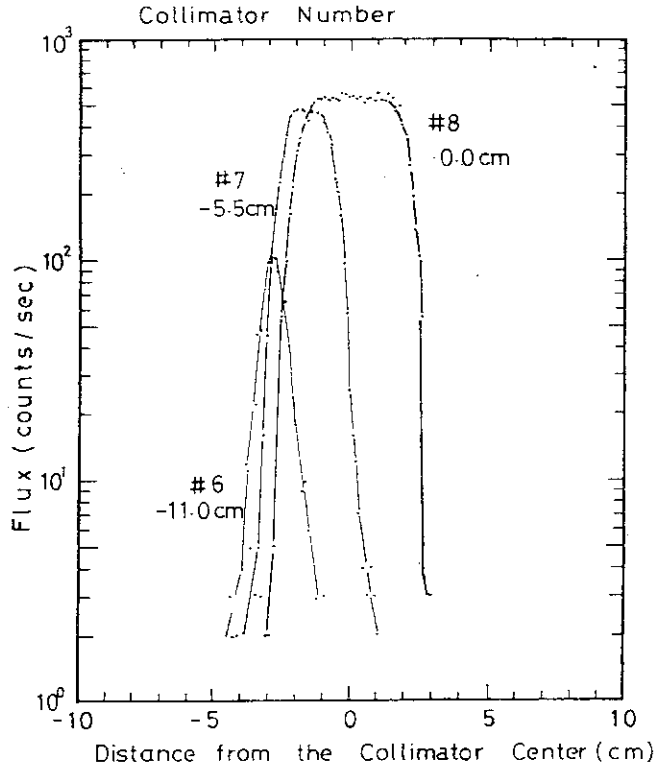

Fig. 7.7.3 Fast neutron flux distributions outside of narrow collimators

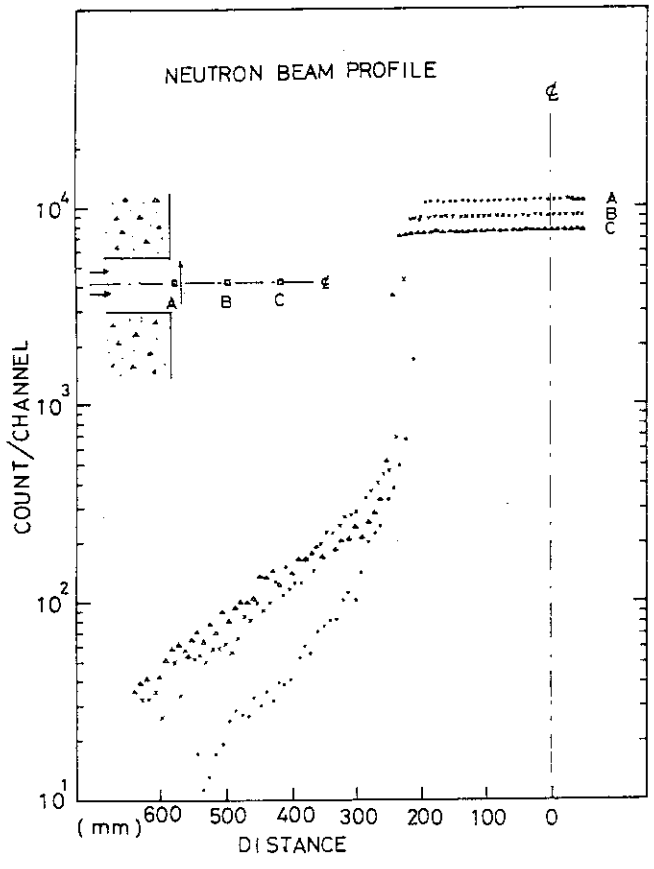

Fig. 7.7.4 Fast neutron flux distributions outside of duct

7.8 Application of Mercuric Iodide Detector for Plasma X-ray Measurement

M. Katagiri, N. Suzuki and M. Maeno

The electron density and the electron temperature of plasma can be diagnosed by measuring X-rays emitted from plasma. In this measurement, Si surface barrier detector is used commonly. The Si surface barrier detector, however, can not respond to high energy X-rays. Further, its S/N ratio is not good since its leakage durrent is large. This causes a problem in diagnosis of high-temperature plasma. We, therefore, tried to use a mercuric iodide (HgI_2) detector which has a large absorption coefficient and a small leakage current characteristic.

The HgI_2 crystal was fabricated by the temperature oscillation method. The size was 1 mm × 1.5 mm × 0.4 mmt. After carbon electrodes were prepared on the both sides of the crystal, it was covered with the humiseal. As it is necessary to isolate the detector from the microphonic noises and various electric-wave noises coming from plasma-experiment equipments, a special detector mount was constructed where the HgI_2 detector and the preamplifier were directly connected. The detector window is an aluminum foil with the thickness of 1.5 μm. Figure 7.8.1 shows the structure of the detector mount.

Using this detector, the plasma X-ray measurements were carried out in the JFT-2 Tokamak. Plasma X-rays could be measured without disturbances due to the microphonic noises and the electric wave noises; and S/N ratio was several times better than that of the Si surface barrier detector. Figure 7.8.2 shows the output signal of the preamplifier, induced by plasma X-rays. The large signal of the start part and the end part were due to the background hard X-rays. This effect can be reduced by making the thickness of the detector proper and by shielding the detector. The results of actual application showed that the HgI_2 detector was very useful for measuring high-energy plasma X-rays with a good S/N ratio.

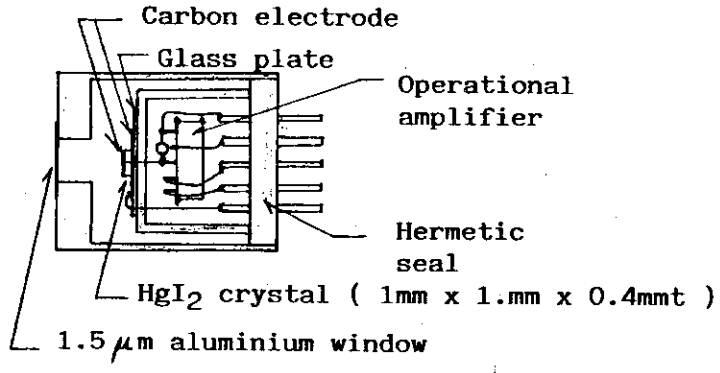

Fig. 7.8.1 The schematic structure of the detector mount for plasma X-ray measurements

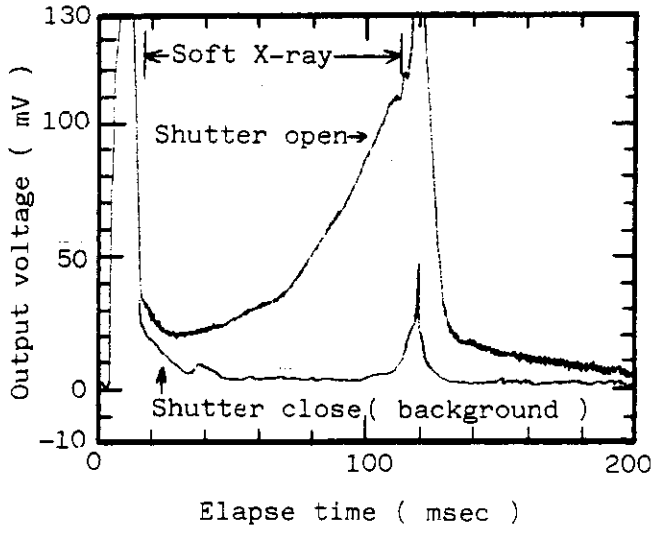

Fig. 7.8.2 The output signal of the preamplifier induced by one shot of plasma X-rays from JFT-2 Tokamak using a 1mm x 1.5mm x 0.4mmt HgI_2 detector

7.9 Measurements of Neutron Emission Distribution from High Speed Water-Cooled Target Assembly at FNS

Y. Ikeda, Y. Oyama, T. Fukabori*, Y. Seki, H. Maekawa and T. Nakamura

A target assembly is generally necessary to produce fast neutrons by means of any accelerator. Its structure changes according to the cooling method and the specification of heat production. As neutrons produced at the target interact with the structural materials of target assembly, it is expected that the angular distribution and the energy spectrum of emitted neutron become different from calculated ones on the basis of the reaction mechanism.[1] This situation makes the discrepancies between the experiments and the calculations using an actual neutron field.

A high speed water cooled target assembly has been used to perform integral experiments under various conditions at FNS. In Fig. 7.9.1, the horizontal and vertical cross sections of the target assembly are shown. It was designed to be able to cool the heat deposit at the target generated by D^+ beam of DC 3 mA and 400 keV, and to restrict the surface temperature not to exeed 100°C.[2] To achieve these conditions, it had to be made of large amounts of materials and was consequently complex. Therefore, the angular distribution and energy spectra emitted from the target were measured and compaired with Monte-Carlo calculations.

Reactions of $^{27}Al(n,\alpha)^{24}Na$ and $^{56}Fe(n,p)^{56}Mn$ were used to measure the flux distribution of D-T neutron emitted from the target assembly. Sixty five pairs of Al and Fe foils were set at 15 cm from the target in horizontal, vertical and axial planes. After irradiation for five hours, the reaction rates of each foils were measured using a 60 cm^3 Ge(Li) detector to deduce the fluxes. The angular distribution of the D-T neutron were measured by a 5.08 cmϕ × 5.08 cm NE213 scintilation counter placed on a goniometer. The distance between the target and the detector was 7.6 m and a pre-collimater was set in front of the detector. The measurement were performed at the angles of 5° interval and the distribution were deduced from the relative counting of neutron whose energy

---

* University of Kyushu

was higher than 4.8 MeV. At the same time, the neutron spectra at each positions were obtained by unfolding the measured pulse hight spectra, using the FORIST code.[3] In order to obtain the precise neutron spectra in each angle, TOF measurements were accomplished using the FNS pulsed beam and the NE213 counter. The setting of the detector was the same as above. The TOF spectra were taken at six angles of 0°, 30°, 45°, 60°, 90° and 105°.

In Fig. 7.9.2, the reaction-rate dibtribution on the horizontal plane, taken from the results of activation foils, are shown in comparison with the calculated ones by the Monte Carlo method, in which the target assembly was precisely simulated. The neutron energy corresponding to the emitted angle was calculated in due consideration of injected deuteron energy loss in the titanium layer. The absolute neutron yield was estimated by monitoring the associated alpha particles. In Fig. 7.9.2, a significant one to one correspondence between the measured and calculated values are observed in each case. The relative distribution of neutron flux at several angles taken from the NE213 scintilation counting and the TOF measurement are shown in Fig. 7.9.3 in comarison with the Monte Carlo calculation. The tendency of distribution is similar in each case.

Through those experimental results, it is concluded that the Monte Carlo calculation of the source neutron represents excellently the neutron emission process around the target assembly and it can be adopted to the analysis of integral experiments at FNS.

References

1) Liskien H. and Paulsen A. : Nuclear Data Table 11, 569 (1973).
2) Seki M., et al. : J. Nucl. Sci. Technol., 16, 838 (1979).
3) Radiation Shielding Information Center, Oak Ridge National Laboratory, PSR-92.

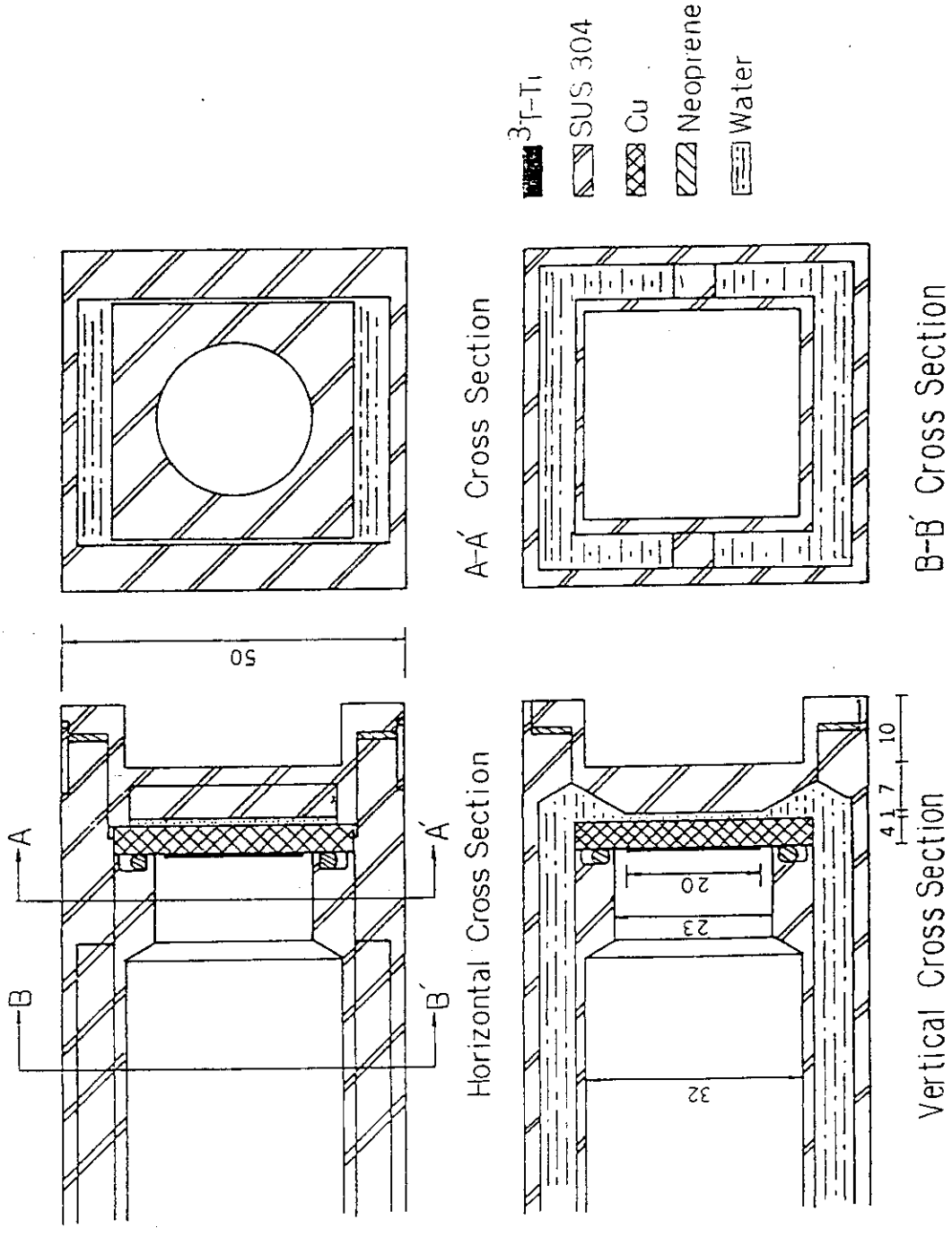

Fig. 7.9.1 Sectional view of high speed water-cooled target assembly

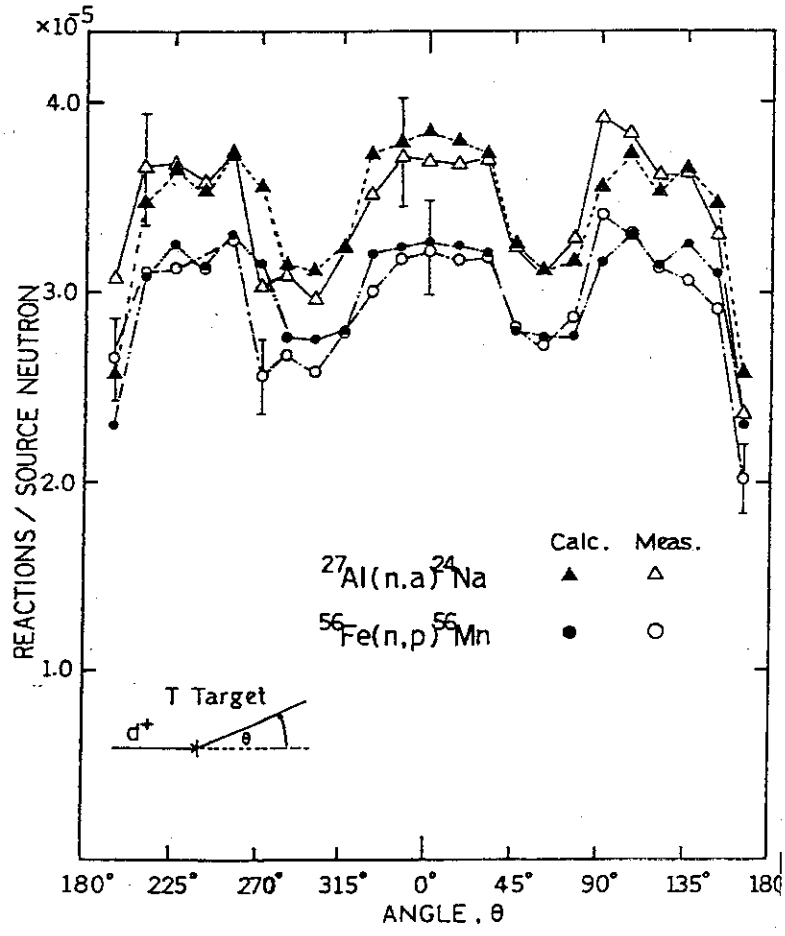

Fig. 7.9.2 Measured and calculated reaction-rate distributions of horizontal plane

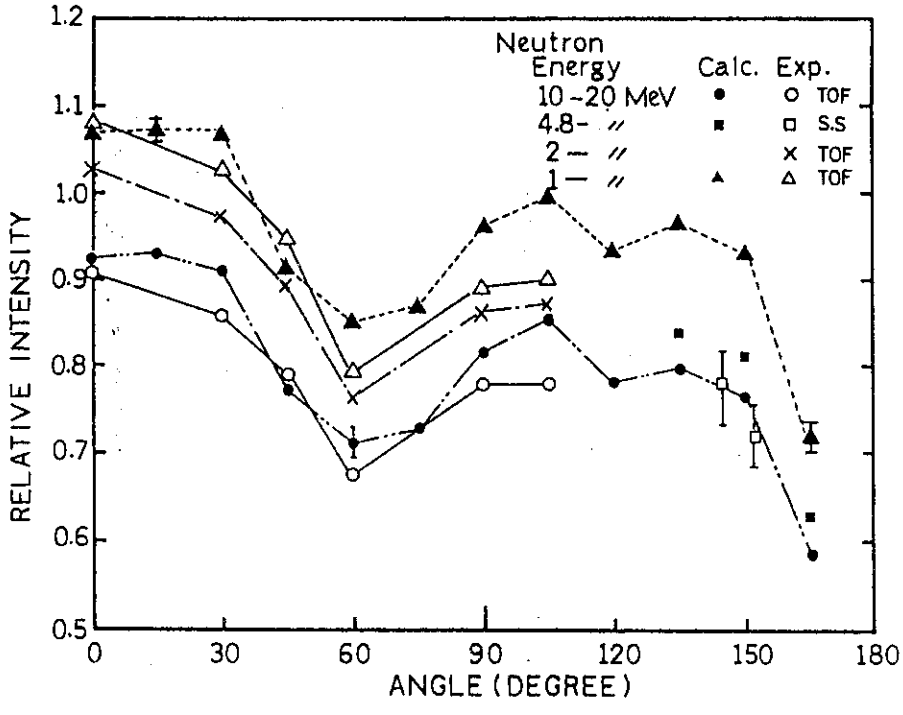

Fig. 7.9.3 Measured and calculated neutron flux distributions of horizontal plane

7.10 Source Characteristics of Air-Cooled Target Assembly at FNS

Y. Oyama and H. Maekawa

The measurement of surface leakage spectra from a Li_2O assembly was started at FNS to check the data and method for the fusion reactor design. The condition of source neutron is need for the analysis of the experiment. Therefore, the angular dependency of emitted neutrons and energy spectrum were measured by the TOF method with an NE213 liquid scintillation detector.

In case of using a thick Ti-^{3}T target, the angular distributions of the neutron emission and the energy spectra from tritium layer correspond to the reaction energy in $^3T(d,n)^4He$.[1] These distributions can be well approximated by the kinematic calculation using the mean reaction energy for the deuteron beam of 350 keV. The observed neutrons, however, is different from the calculation because some source neutrons are scattered by the materials of the target assembly, and it is necessary to measure them directly.

In the experiment, deuteron was accelerated by the FNS accelerator to 350 keV, and reacted with a tritium to produce 14 MeV neutrons. The TOF experiment was carried out by the pulsed neutron source, and its pulse width and peak current were $\sim$3 ns and $\sim$10 mA, respectively. The air-cooled target assembly used in the experiment is shown in Fig. 7.10.1. A 10 Ci Ti-^{3}T metal target was used. As the neutron yield monitor, a small surface barrier silicon detector was set to detect alpha particles in $^3T(d,n)^4He$ reaction.

The typical results of experiment are shown in Fig. 7.10.2 and Fig. 7.10.3. The angular distribution of emitted neutrons was strongly distorted between 60° and 90° by the frame of the target assembly. This distortion is smaller than that in the water-cooled target assembly.[2] The flux exclusive of the peak is 10% of the whole flux. It is not clear, however, whether this scattered flux was caused by the copper backing or by the stainless-steel flame of target assembly. The anisotropy factor of emitted neutron for the forward direction agreed well with each other within 2%. The effect of $D(d,n)^3He$ reaction was measured to be less than 2.5%.

References

1) Benveniste J. et al. : UCRL-4266 (1954).

2) Ikeda Y. et al. : "Measurements of Neutron Emission Distribution from High Speed Water-Cooled Target Assembly at FNS", 7.9, this report.

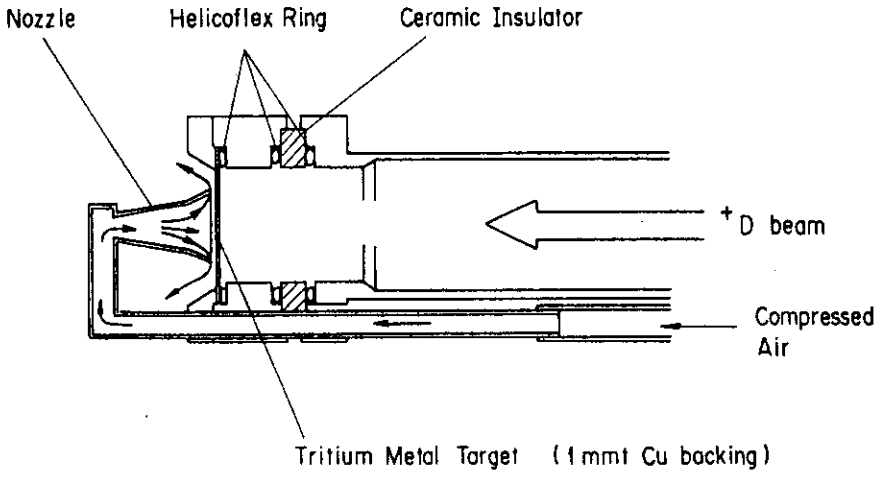

Fig. 7.10.1 Sectional view of air-cooled target assembly

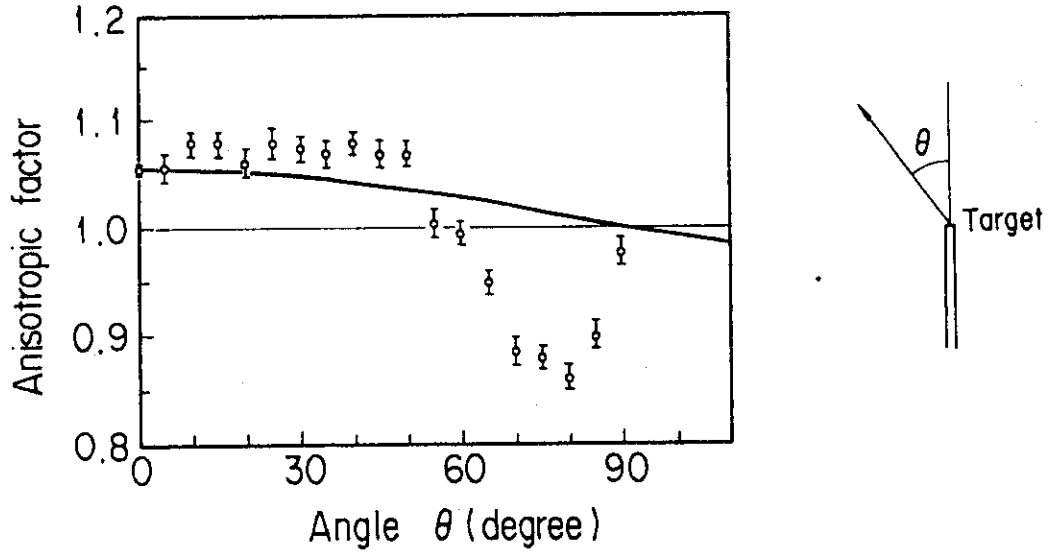

Fig. 7.10.2 Anisotropic factor of emitted neutrons from air-cooled target assembly

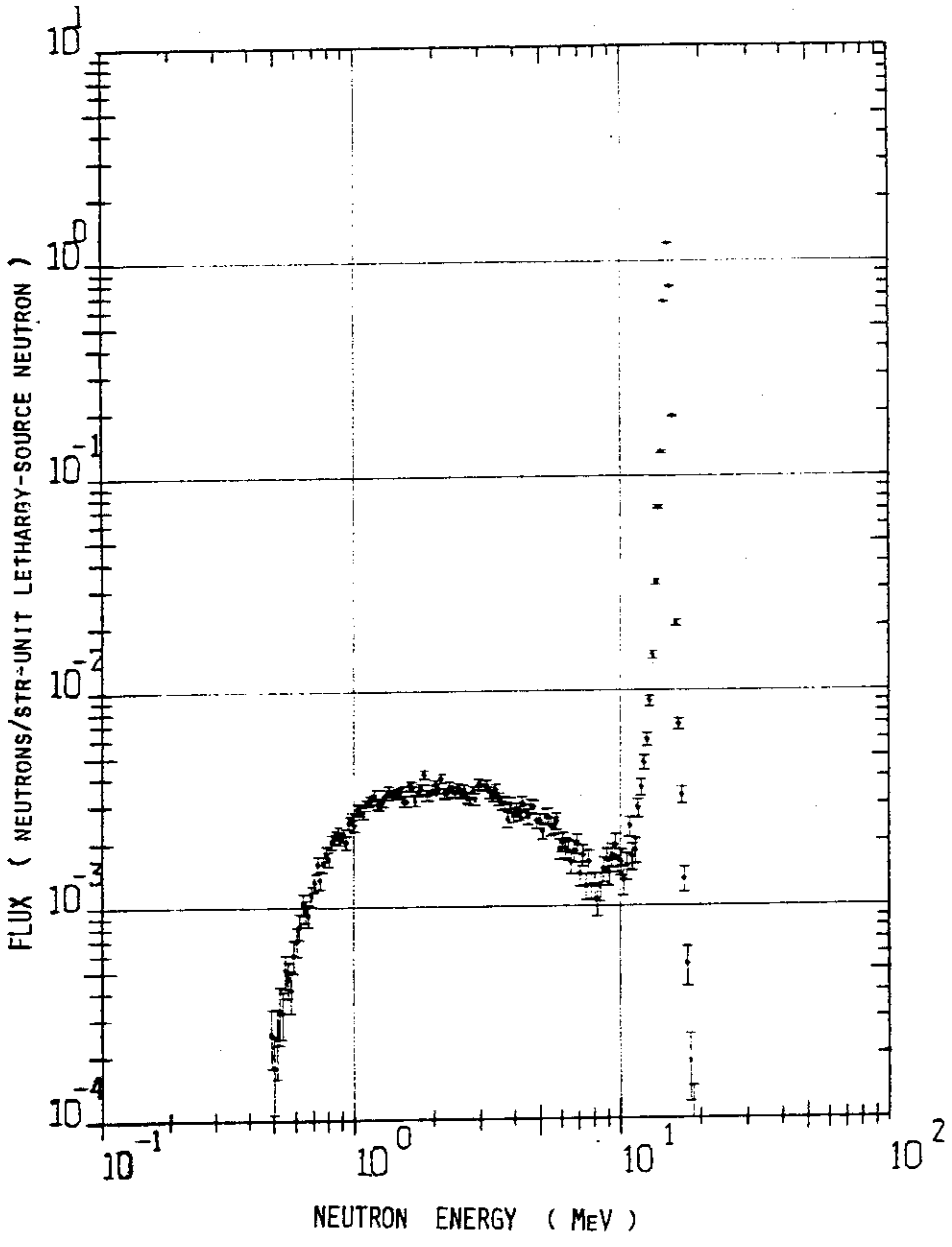

Fig. 7.10.3 Measured neutron spectrum from air-cooled target assembly at 0 degree

7.11 Operation Report of the Fusion Neutronics Source (I)

J. Kusano, C. Kutsukake and S. Tanaka

Following the installation and the inspection of the FNS completed at the end of March 1981, the training operation and the charactoristics test of D-D neutron were initiated prior to the D-T 14 MeV neutron generation. Before the usage of a tritium target, a few modifications were made for the beam-line of the accelerator system. They were reassembling some beam components and the installation of a Target Surface Temperature and Beam Profile Monitor (TSTPM) for 80° beam line, and the installation of additional vacuum pump, i.e. a 700 1/s cryo pump, at near the target of 0° beam line. The neccesities of cryo pump are: (1) the improvement of vacuum condition in the rotating target region. (2) temporary storage for the tritium gas releasing from the rotating target.

80° line operation

The 14 MeV neutron generation was initiated at the begining of August using the 80° beam line with a water cooled 25 Ci tritium target. In this operation, the source charactoristics were examined experimentally and then the neutronics experiments on a Li_2O-C sphere assembly were made.

The operating condition of the accelerator through these experiments were as follows; the beam energy was 330 keV and the beam current was 100 μA ∿ 2 mA D.C.

Next experiments, i.e., neutron spectrum measurement by means of the Time-of-Flight method, were carried out using the pulsed beam operation. The pulsed beam of about 26 mA peak current and 2.7 ns FWHM was obtained through the experiment by a beam bunching system.

0° line operation

Some test operation at a 0° beam line was performed prior to mounting a rotating target with 1000 Ci tritium. The carefuly and steady preparation was required for the high current beam operation using the rotating target with a large amount of tritium. In the middle of Oct., a 33 hours operation of 20 mA (full power of the ion beam) was achieved using a dummy target to examine the performance of the accelerator and many valuable informations were obtained as follows;

(1) The beam emittance of the 740A type high current ion source was

broadened slowly during the operation, and the beam transmission ratio was decreasing.

(2) The ion beam broading was observed at the entrance beam duct of the first stage quadrapole magnetic lens and at the entrance of 80° switching magnet chamber. It was observed that the temperature of these positions rised largely compared with the other position by beam hitting. And fair amount of D-D neutrons were generated at these positions.

(3) The trip of the vacuum station controller happened frequently due to sparking noise at the acceleration tube through the beam duct.

(4) The water level fluctuation of a reservoir tank in the 2nd target room for the cooling system of rotating target was observed and revealed to be caused by air mixing of the open-air type cooling system.

Some improvements of the accelerator system, i.e., the modifications of the vacuum station controller and the air release method in the reservoir tank have been made, but a operation using the tritiated rotating target has not been tried on 0° beam line.

TAP operation

The Tritium Adsorption Plant (TAP) operation has been started under on-beam condition since the first neutron generation in August. The charactoristics of the tritium removing in the vacuum exhaust are descrived in 7.12.

The proper piping system for the exhaust gas with high level tritium contamination were newly equipped for the tritium gas to be transfered effectively from the storage type vacuum pump system to the storage tank of TAP.

Remarks

Some problems remain, i.e., the handling technique for the target with a large amount of tritium and the improvement of the cooling water system for the rotating target. They would be solved and we will soon try the D-T neutron generation using rotating target.

7.12 Tritium Handling System of Fusion Neutronics Facility
—— Operation Characteristics ——

C. Kutsukake, J. Kusano, Y. Ikeda, Y. Oyama, H. Maekawa and T. Nakamura

As a tritium target of 1000 Ci is to be used at FNS, large amount of tritium gas would be released from the target. The construction of a tritium adsorption system (TAP) was completed in 1980 and we have been carrying out its cold tests since 1980. In the neutronics experiments that started in August 1981 using 80° beam line, it was able to obtain practical experiences about the transportation of a very small amount of vacuum exhaust gas, the removal of tritium from the exhaust gas and amount of tritium released from the walls of pipe-lines and tanks.

Operation of TAP

As a typical example of operation cycles, variation of gas pressure and tritium concentration in the storage tank are shown in Fig. 7.12.1. The tritium gas released from the target during the bombardment of accelerated deuteron beam was exhausted through the vacuum pumps and transfered into the storage tank via a monitor tank. Then, the exhaust gas stored in the storage tank were circulated through a tritium removal system (TRS) to collect tritium. After the tritium concentration was reduced low enough to release, the gas was exhausted from the stack being diluted with the building ventilation air.

Tritium Trap during Gas Transfer

The tritium concentration of each vacuum pump oil measured by a liquid scintillation method are shown in Table 7.12.1. It is clear from the table that the tritium concentration of vacuum pump oil near the target section is highest and so called differential pumping was working effectively. The measurement of tritium concentration in the exhaust gas from each pumping section showed the same result.

Process of Tritium Removal

The change of tritium concentration during the operation of TRS can be approximated by the sum of a exponential function, $e^{-1.50}$, and a nearly constant background. This background was due to the desorption of tritium in the walls of tanks and tritium monitor chamber and was

correlated strongly to the initial tritium concentration. The concentrations at the beginning and the end of TRS operation cycles are shown in Fig. 7.12.2. It is clear that the increased background can be reduced by a flashing.

Summary

1. The transfer of exhaust gas with tritium was performed well.
2. About 1% of tritium was trapped in the vacuum pump oil during the transfer to the TAP.
3. Tritium concentration can be reduced below the regulated concentration. The tritium handling system at FNS satisfied the designed specifications.
4. In the case that tritium concentration of the exhaust gas might be high, it should be important to examine how much the background level would increase.
5. In either case of the gas transfer and the tritium removal, the process of the tritium adsorption and desorption on the wall have a influence on measuring the tritium concentration. Then, it is necessary to invesigate the method to reduce the influence.

Table 7.12.1 Effect of differential pumping

Vacuum Station	Tritium Concentration	Ratio
# 0	2.3×10^{-2}	0.1
# 1	9.7×10^{-2}	0.4
# 2	1.5×10^{0}	5.9
# 3	2.4×10^{1}	93.6
Total	——	100.0

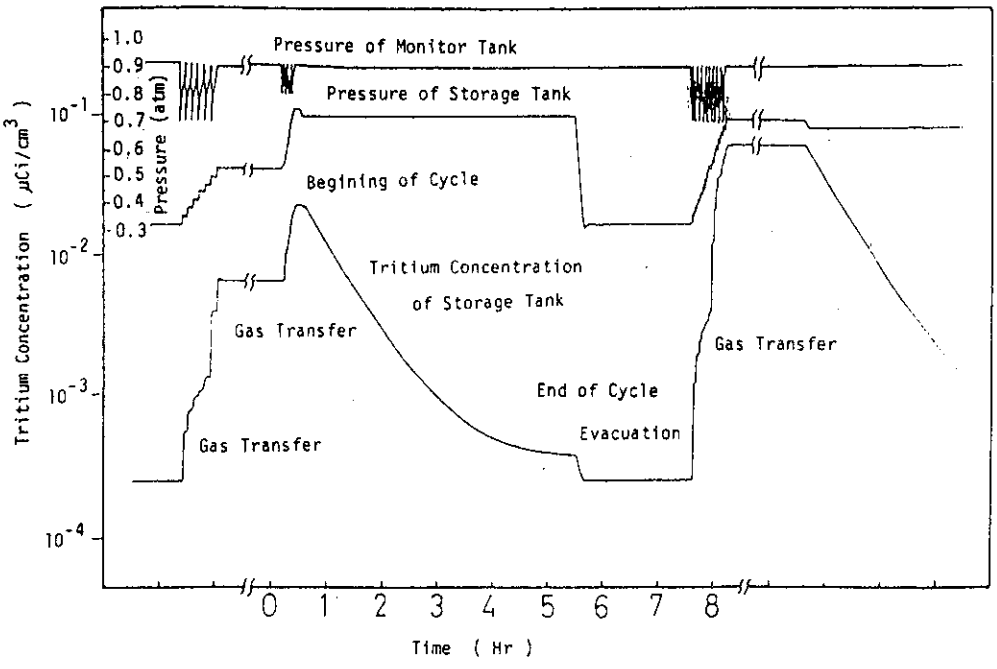

Fig. 7.12.1 Operating pattern of TAP

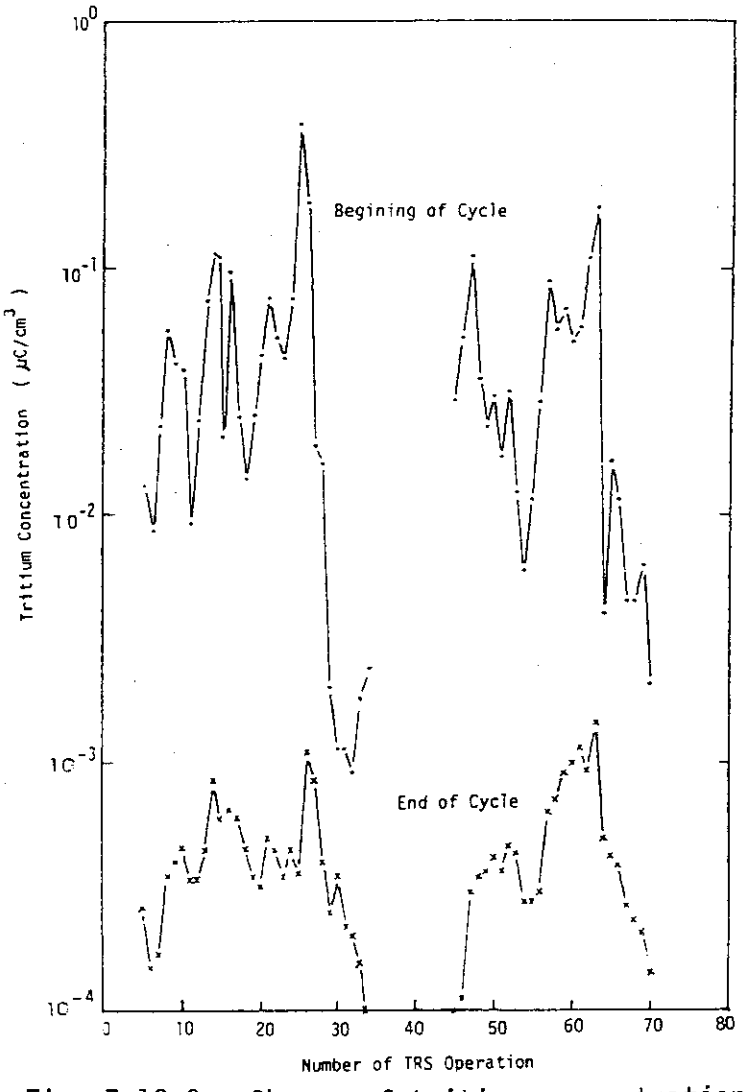

Fig. 7.12.2 Change of tritium concentration

7.13 Relation Between Temperature of Metal Target and Gas Release Rate

J. Kusano, Y. Oyama, Y. Ikeda, C. Kutsukake, S. Tanaka H. Maekawa and T. Nakamura

Recentry high intense 14 MeV neutron sources, i.e., FNS(JAERI) and OKTAVIAN(Osaka University) have been constructed in Japan and experiments on the fusion neutronics started. These devices are characterized by their high current ion acceleration (20 mA for d^+ beam) and by the usage of metal target having large amount of tritium (800 $\sim$ 1800 Ci).
Great interest is focused on the gas release from the point of view of the life-time extension of target and minimization of the tritium contamination. In case of Ti-T(Ti-D) metal target it has been considered that there is little gas released from the target when the surface temperature is less than 200°C. It is desireble to get accurate knowlege about the relation between the gas release and the surface temperature of target.

However, this had never been confirmed by in-situ measurement since there was no proper method to measure the target temperature when the accelerated beam hit on the target. We have developed successfully the measuring system of the temperature distribution on the target surface using a thermal image camera to detect infra-red. (TSTPM)[1]
The infra-red radiation from the target surface was reflected with a stainless-steel mirror and was led to the thermal image camera which was mounted on the beam duct at the distance of 1.7 m from the target. The temperature indication was calibrated by a calibrator for the thermocouples. This system was set on the beam line of FNS.
The schematic outline of experimental system is shown in Fig. 7.13.1. Two types of target, D-Ti-Cu and D-Sc-Cu, were set at the end of a 80 degree beam-line and were bombarded by 200 μA proton beam having the energy of 352 keV. The data of targets are given in Table 7.13.1.

Deuterization of targets and measurement of the ratio of D to Ti(Sc) were carried out by the Analytical Chemistry Laboratory of JAERI.

A half of its surface, made of aluminum, was painted as a black-body. A dummy target, i.e., without the deuterization, was painted in the same manner to determine the emissivity of the actual target surface. The emissivity was estimated to be 0.75 as the ratio of temperatures between titanium (scandium) to the black-body. The released

gas, i.e., deuteron was detected by a residual gas analyzer (RGA) that was set near the 80 degree magnet.

The temperature was adjusted by changing the flow-rate of cooling air under almost constant conditions of beam current, energy and focusing. And the same experiment was carried out in case of off-beam to heat up the target by a heat gun. A typical result of Ti-D target is shown in Fig. 7.13.2.

Summary:

1. In case of the Ti-D target, the quantity of gas release from the target increase remarkably when its temperature is over 120°c. If the surface temperature continue over 200°C for more than 5 minutes, most part of the adsorbed gas is discharged from the target.
2. On the contrary, in case of the Sc-D target, the gas release is almost negligibly small when the temperature is up to 380°C.

The authors would like to express their thanks to Mr. A. Hoshino of the Analytical Chemistry Laboratry of JAERI for his preparation and chemical analysis of deuterium targets.

Reference

1) Nakamura, T. and Maekawa, H.: "Surface Temperature and Beam Profile Monitor for Metal Target of FNS," JAERI-M 9672, pp.147-148 (1981).

Table 7.13.1 Data of D targets

Item	Thickness of D adsober	Atomic ratio (D : adsorber)	Deuterized temperature
Cu-Ti-D	6.5 μm (Ti)	1 : 1.65	400°C
Cu-Sc-D	12.2 μm (Sc)	1 : 1.38	600°c

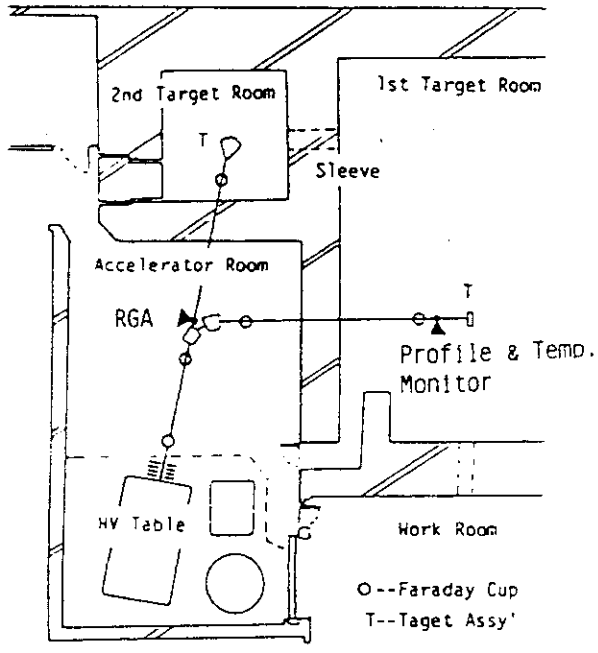

Fig. 7.13.1 Experimental arrangement

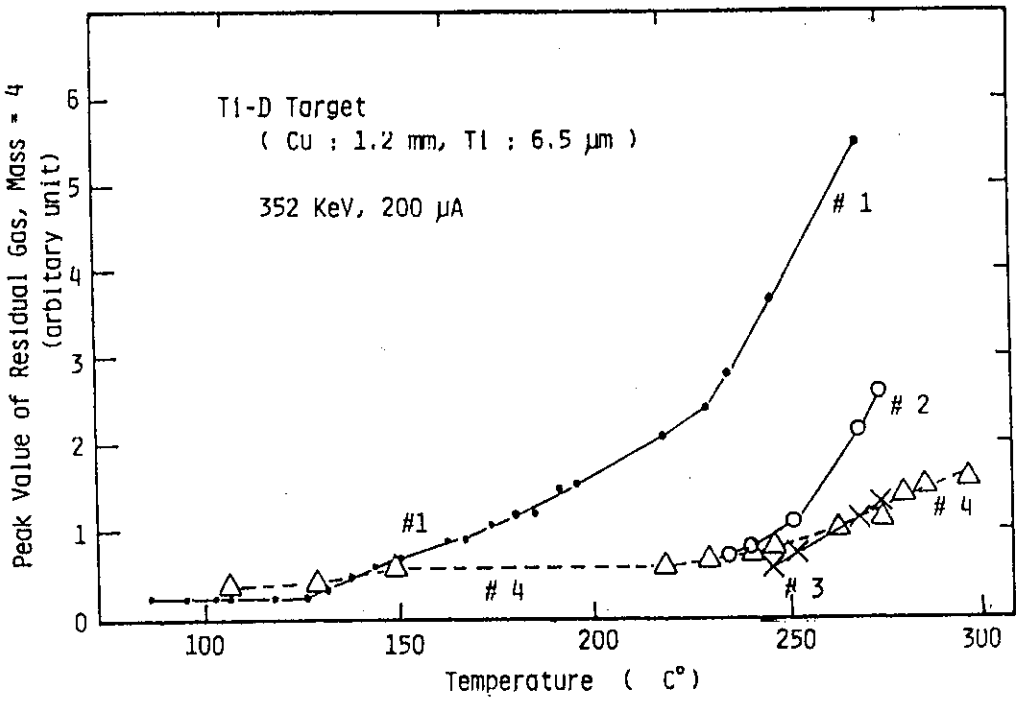

Fig. 7.13.2 Typical result of Ti-D target
Symbols of #1 - #4 mean first to fourth runs using the same target.

7.14 Pre-analysis for the Leakage Spectrum Measurements on Li_2O Plane Assembly

T. Fukumoto, Y. Seki, Y. Oyama and H. Maekawa

As the D-T fusion blanket will have many light nuclei and 14 MeV neutrons enter it from the core plasma, it is very important to study the anisotropic scattering in the fusion neutronics. It was planned to measure the angular-dependent neutron leakage spectra from a Li_2O plane assembly by the TOF method using the pulsed neutron source at FNS. Prior to this experiment, the pre-analysis was carried out to improve the experimental efficiency. Two items were examined in this analysis. They were to determine the characteristics of leakage spectra depending on the thickness of assembly and on the measuring angles. In addition the effect of finite size of the assembly on the leakage spectra was examined.

The thickness of Li_2O assembly was examined by a one-dimensional transport code ANISN,[1] and the angular dependence and the effect of finite size were examined by a two-dimensional transport code DOT3.5.[2] The calculational models are shown in Figs. 7.14.1 and 2 for ANISN and DOT3.5 calculations, respectively. The nuclide densities are summarized in Table 7.14.1. A 100-group cross-section set used in the ANISN calculations was made by the NJOY[3] code from ENDF/B-IV[4], and the P_5-S_{64} approximation was used and source neutrons of 14.2 MeV were assumed to be paralled beams. In the DOT3.5 calculations, the cross-section set GICX40[5] with neutron 42-group and the P_5-S_{16} approximation were used, and source neutrons of 14.4 MeV was assumed to be isotropical and first collision source method was employed.

The typical results are shown in Figs. 7.14.3 and 4. Considering the expected experimental error of about 10%, the following conclusions have been derived from this pre-analysis:

(1) The appropriate thicknesses of Li_2O assemblies are 5cm, 20cm and 40cm.

(2) The interval of measuring angles should be about 30°.

(3) The effect of finite radius exists in the leakage spectra. Two dimensional calculation should be needed in the main analysis.

References

(1) Engle, Jr., W.W.: "A User's Manual for ANISN, A One Dimensional Discrete Ordinate Transport Code With Anisotropic Scattering," K-1693, Oak Ridge National Laboratory (1967)

(2) Rhoades, W.A. and Mynatt, F.R.: "The DOT-III Two Dimensional Discrete Ordinates Transport Code," ORNL/TM-4280 (1973)

(3) Macfarlane, R.E. et al.: "The NJOY Nuclear Data Processing System; User's Manual," LA-7584-M (ENDF-272) (1978)

(4) Drake, M.K. (edited): "Data Formats and Procedures for the ENDF Neutron Cross Section Library," BNL-50274 (T-601, TID-4500), ENDF 102, Vol.1(1970) Rev.1974

(5) Seki, Y. and Iida, H.: "Coupled 42-group Neutron and 21-Group Gamma Ray Cross Section Set for Fusion Reacter Calculations," JAERI-M8818 (1980)

Table 7.14.1 Nuclide densities used in the calculations

Nuclide	Nuclide densities in the Li_2O assembly ($\times 10^{24}$ atom/cm^3)[2]
^{6}Li	3.9610×10^{-3}
^{7}Li	4.9422×10^{-2}
O	2.6691×10^{-2}
Cr	2.1753×10^{-4}
Fe	8.1933×10^{-4}
Ni	9.6490×10^{-5}

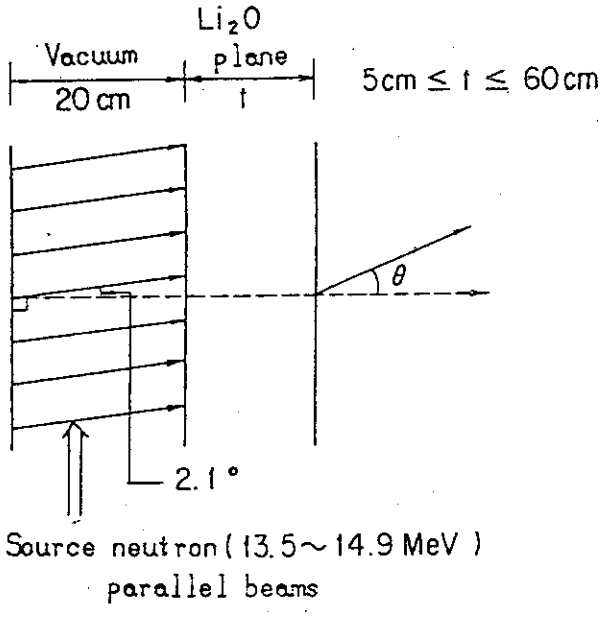

Fig. 7.14.1 Calculational model for ANISN

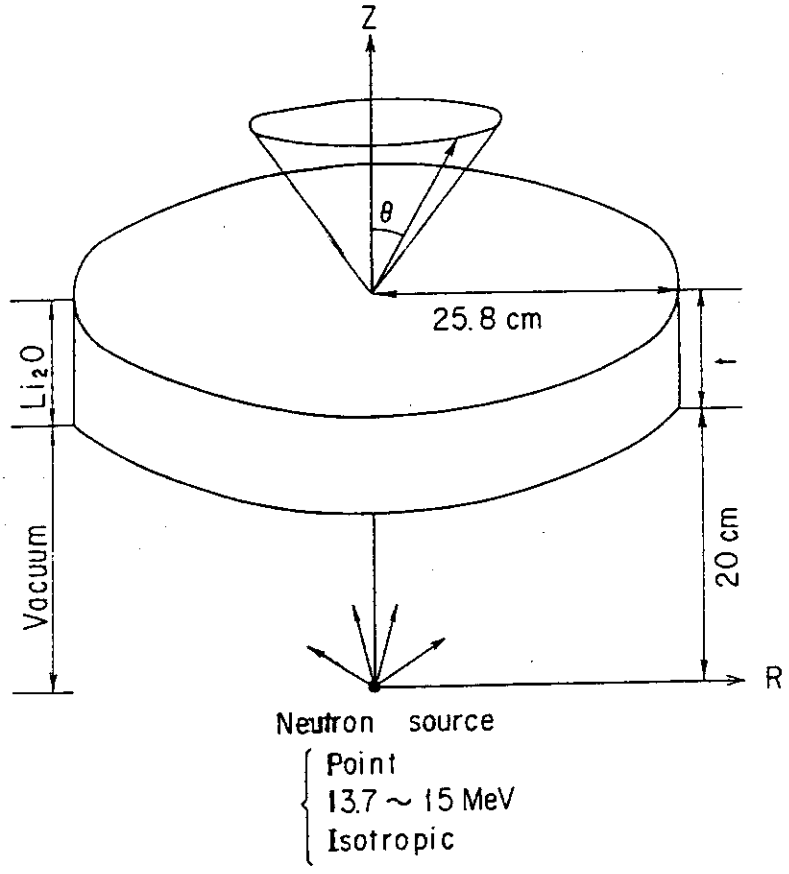

Fig. 7.14.2 Calculational model for DOT3.5

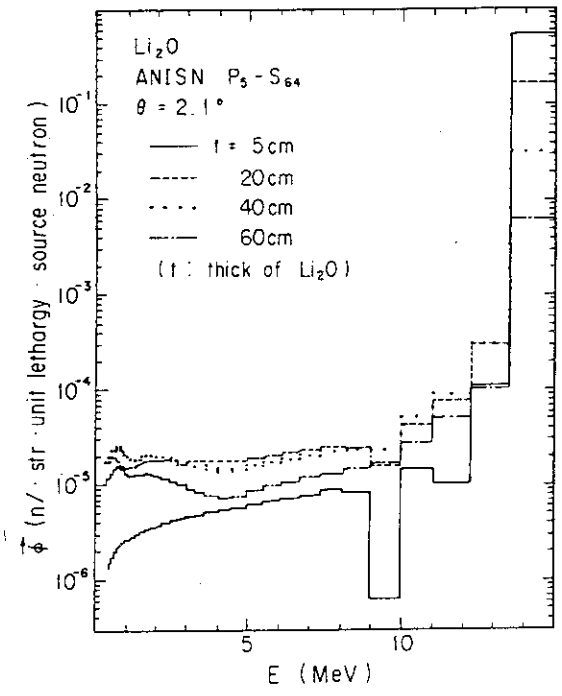

Fig. 7.14.3 Characteristics of leakage spectra depending on thickness of assembly

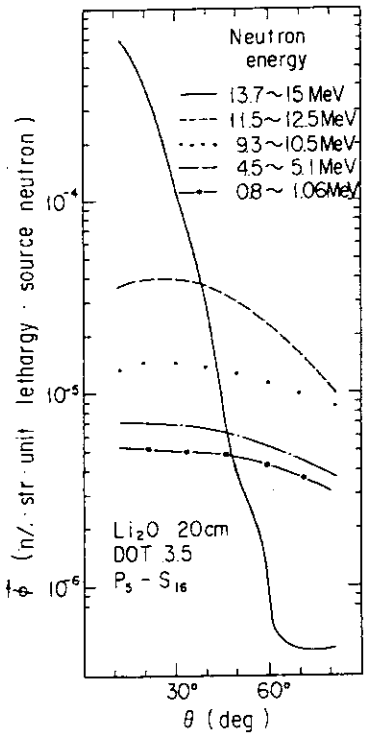

Fig. 7.14.4 Characteristics of leakage spectra depending on measuring angles

7.15 Analysis of Absolute Fission-Rate Distribution in Graphite-Reflected Lithium-Oxide Assembly

Y. Seki, H. Kawasaki*, H. Maekawa and T. Nakamura

The fission-rate distributions of ^{235}U, ^{237}Np, ^{238}U and ^{232}Th have been measured in a pseudo-spherical graphite-reflected lithium oxide (Li_2O-C) assembly in 1978.[1] The 14 MeV neutrons were generated at the center of the assembly by the D-T reaction with a 300 kV Cockcroft-Walton type accelerator. Details of the measurements can be found in Ref.(1). The One-dimensional calculational Model of the Li_2O-C Assembly is shown in Fig. 7.15.1. The fission-rate distributions are calculated using various nuclear data and methods listed in Table 7.15.1.
The fission cross sections of 4 nuclides are obtained using the same processing method as the transport cross sections except for the thermal fission cross section of ^{235}U, which is derived for the mixture of the graphite region using the SRAC[7] code system.

The calculated and measured fission rates of ^{237}Np and ^{238}U mostly agreed within experimental errors. Figures 7.15.2 and 3 show the distributions of the ratio of the calculated and measured fission-rates (C/E) of ^{235}U and ^{232}Th, respectively. For both nuclides, disagreement in the graphite region is apparent. Further investigations using recently evaluated nuclear data and refined energy group structure are being conducted.

References

1) Maekawa, H., et al.: J. Nucl. Sci. Technol., 16 [5], 377 (1979).
2) Suzuki, T., Ishiguro, Y. and Matsui, Y.: JAERI-M 9492 (1981) (in Japanese).
3) Seki, Y. and Iida, H.: JAERI-M 8818 (1980).
4) Macfarlane, R.E., et al., LA-7584-MS (1978).
5) Hasegawa, A.; to be published.
6) Engle, W.W., Jr.; K-1693 (1967).
7) Tsuchihashi, K., et al.: JAERI-M 9781 (1981) (in Japanese).
8) Maekawa, H. and Seki, Y.: J. Nucl. Sci. Technol., 14 [2], 97 (1977).

* Century Research Center Corp. Ltd.

Table 7.15.1 Description of 5 calculational procedures

Items	Calculational procedures 1	2	3	4	5
Nuclear data file	ENDF/B-4	ENDF/B-4*	ENDF/B-4	ENDF/B-3,4**	ENDF/B-4
Name of Xsec set	GICXLI20	GICXLI20	2)	GICX40[3]	GICX40V4[3]
Process code	NJOY[4]	NJOY	PROF-GROUCH-GII[5]	SPTG4Z[5]	NJOY
Energy group No.	100	100	119	42	42
Weighting function	1/E	1/E	Constant	1/E	Li-spectrum***
Transport code	ANISN[6]	ANISN	PALLAS-TS[2]	ANISN	ANISN
Approximation	P_5-S_{64}	P_5-S_{64}	P_∞-S_{20}	P_5-S_{64}	P_5-S_{64}
Symbol used in Figs.					

* ENDF/B-5 data used for ^{12}C

** ENDF/B-3 data used for ^{6}Li, ^{7}Li and ^{12}C

*** Calculated neutron spectrum in Li-region of Li-C Assembly[8]

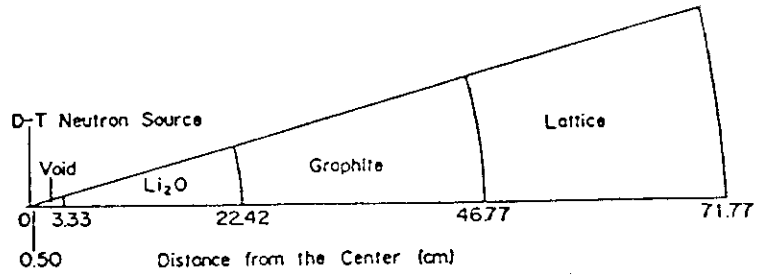

Fig. 7.15.1 Calculational model of Li_2O-C assembly

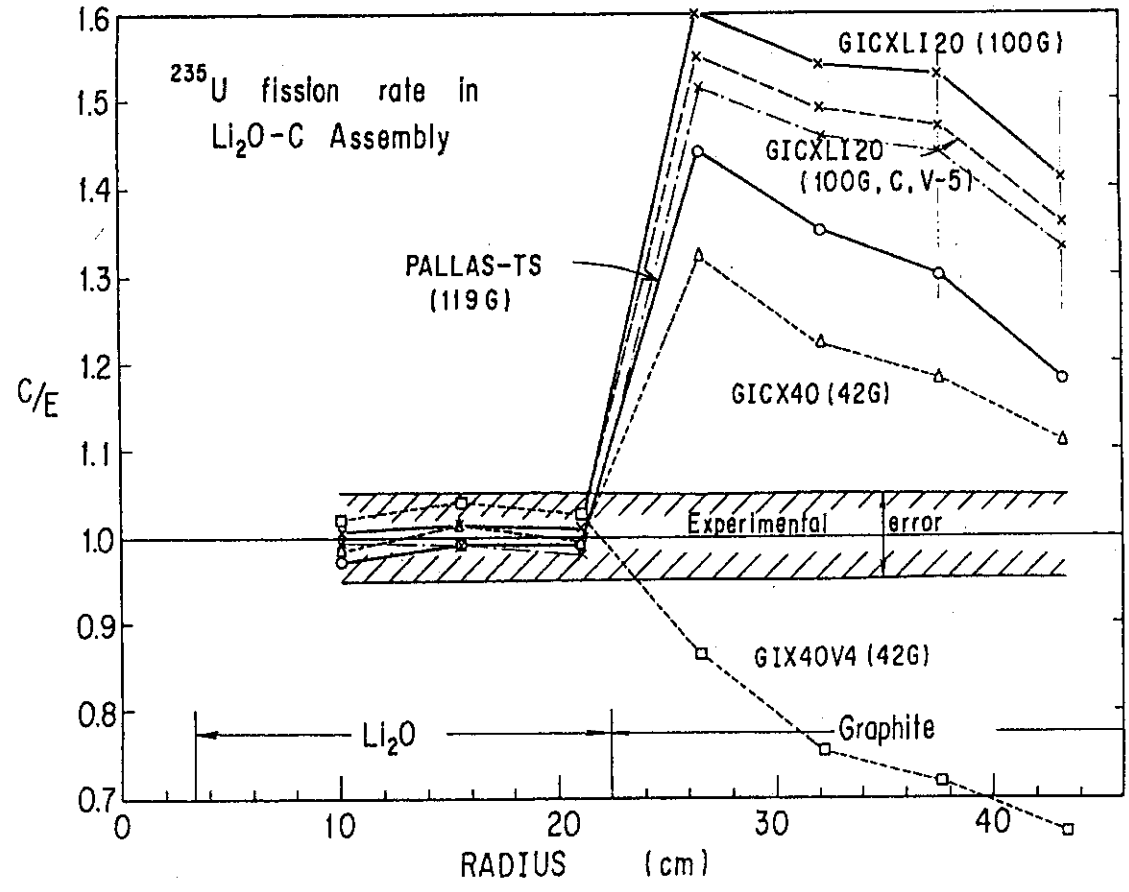

Fig. 7.15.2 C/E of ^{235}U fission-rate in Li_2O-C assembly

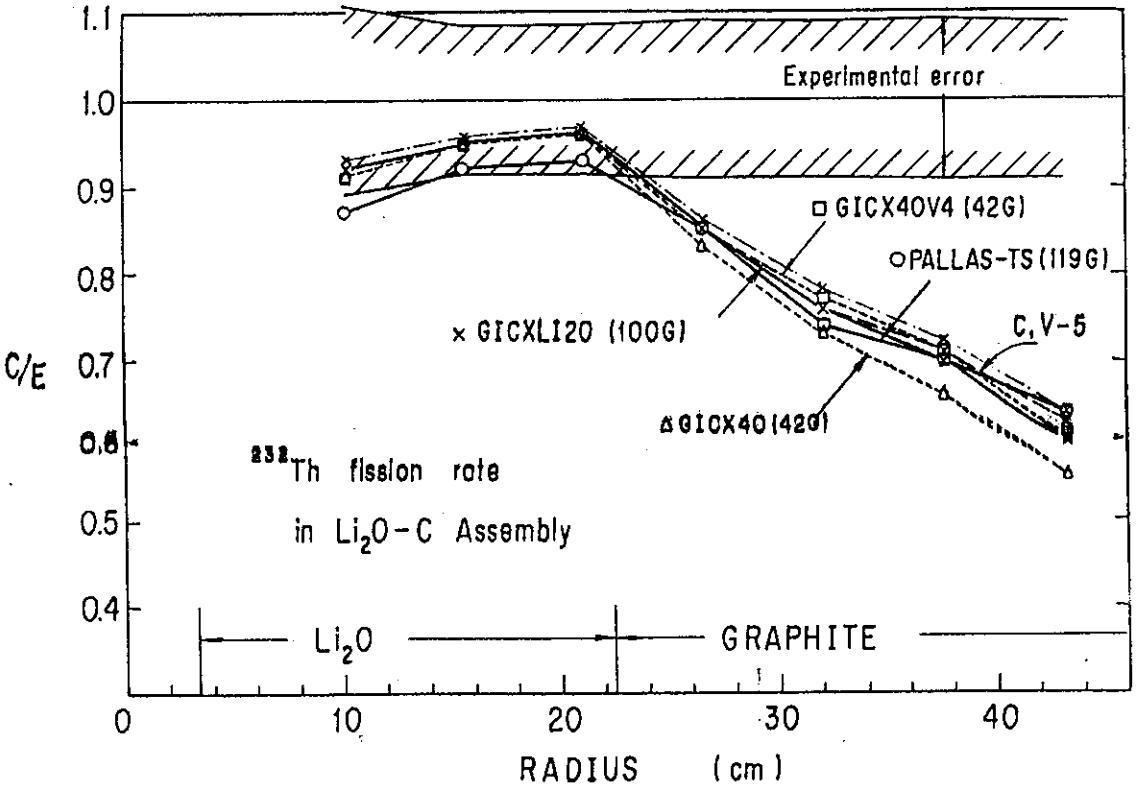

Fig. 7.15.3 C/E of ^{232}Th fission-rate in Li_2O-C assembly

7.16 Numerical Simulation of Two-Fluid, Two-Dimentional MHD Equations of a Toroidal Plasma

T. Fujisawa

A numerical simulation of two-fluid, two-dimensional, nonlinear MHD equations of a toroidal plasma has been performed in an attempt to incorporate the effect of the electric field due to the space charge of plasma constituents and the effect of the electromagnetic self- and mutual-induction due to a plasma current. It is well known that the electric field makes it difficult to realize the simulation because of rapid numerical instability. To avoid it, a stabilization coefficient smaller than unity is introduced for the calculation of a scalar potential which is used to obtain the electric field. The mutual-induction is, on the other hand, useful to improve numerical stability of the simulation and to realize rather smooth profiles of a plasma, but it costs a longer computing time. The magnetic field due to a plasma current is calculated from a vector potential. A radial transport velocity is determined from the parallel and perpendicular components of the plasma flow, and the ambipolar potential acts so as to keep equal the radial velocities of the plasma constituents. The velocities are assumed zero for r=a. As one of the simple means to stabilize the simulation, the upstream-downstream difference scheme is adopted for the calculation of spatial derivatives such as in transport terms. Another means to depress spatial numerical instability is an artificial diffusion term with a small coefficient, which is used when the hydrodynamics equations are time integrated.

Two-dimensional time evolutions of the density, velocity, temperature, and others are calculated, starting from a set of initial profiles. An example of the calculations shows that the average radial transport velocities (or confinement times) of electrons and ions become approximately equal, and agree well with the tokamak experiments. But in the calculation, the clear herical structures of higher modes in velocity as has been reported are not seen; nor are the magnetic islands. A very large electric field due to the ambipolar potential is

seen, especially for E_r, in contrast with the experimental results of tokamaks. But it seems that the large electric field does not make markedly worse the performace of the simulation. Increase in the stabilization coefficient shows a tendency toward decrease in the electric field, but the increase is limited by numerical instability. In calculating plasma dynamics at higher densities and temperatures it is necessary further to improve the numerical stability and performance of the simulation, and to reduce computing time.

Reference

1) Fujisawa T.: "Numerical Simulation of Two-Fluid, Two-Dimensional, MHD Equations of a Toroidal Plasma," JAERI-M 9944 (1982).

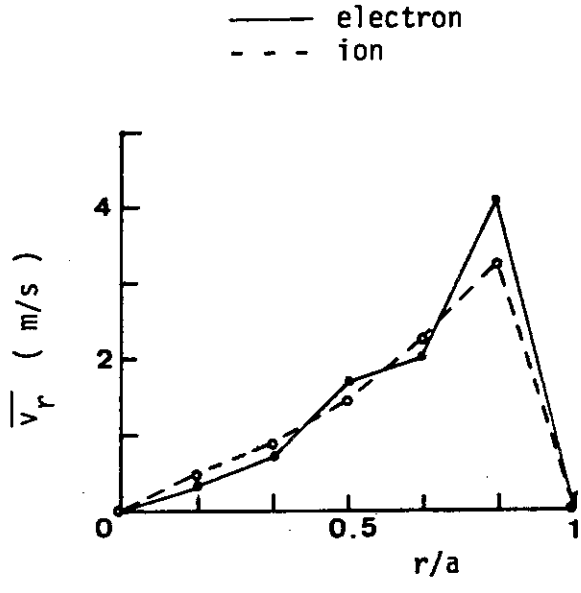

Fig. 7.16.1 Average radial transport velocities of plasma constituents

8. Activities of the Committees

8.1 Activities Related to the NEA Committee on Reactor Physics

J. Hirota

During this one year period, the Committee on Reactor Physics held the meeting three times, keeping the close relation with the NEA Committee on Reactor Physics (NEACRP). For the 6th International Conference on Radiation Shielding (ICRS) to be held in Tokyo in 1983, a Preparatory Committee was set up under the Committee in April and prepared a preliminary information sheet of the 6th ICRS to present at the 24th meeting of the NEACRP in September.

The Committee on Reactor Physics held the 39th meeting in June : Summaries of the 2nd NEACRP ad-hoc Working Group Meeting on Evaluation Coordination held in April and the 5th meeting of the NEA Data Bank Committee held in May were reported and the Japanese situation in the future framework for evaluation coordination was discussed. As to the 3rd Specialists' Meeting on Reactor Noise (SMORN-III) to be held in Tokyo in October, the draft technical agenda and Information Sheet II were distributed. Following preliminary discussions on the contributions from Japan to the topics of the 24th meeting of the NEACRP, activity plans of the Subcommittees on Reactor System, Fusion Reactor and Shielding, and the Preparatory Committee for the 6th ICRS in this fiscal year were discussed.

The Committee held the 40th meeting in August, mainly to make preparations for the 24th meeting of the NEACRP. The research activities in Japan for the period from September 1980 to August 1981 were discussed to prepare the review-paper[1]. For contributions from Japan to the topics of the meeting, eleven papers were presented, which were as follows; "Sodium Void Reactivity Worths in Plate and Pin Cell Assemblies", "On the Geometric Modelling for Pin/Plate Heterogeneity Calculation", "Application of a Three-Dimensional Discrete Ordinates Transport Code to Shielding Design and Analysis", "Space-and-Angle Finite Element Method for Solving Three-Dimensional Multi-Group Neutron Transport Problems", "Three-Dimensional Neutron Streaming Calculations Using the Monte Carlo Coupling Technique", "Measurements of Fission Products Decay Heat for Fast Neutron Fissions", "Decay Heat Calculations Based on Theoretical Estimation of Average Beta- and Gamma-Energies Released from Short-Lived Fission Products", "High Subcriticality Measurements by Exponential and Pulsed Neutron Source

Experiments with Low-Enriched Uo_2 Lattices in Water", "An Analytical Study on Uncertainties of Reactivity Scale (β_{eff}) of Large LMFBR Cores", "Transient Effect on Reactivity in Reactor Point Kinetics Calculation" and "Refuelling Analysis of Pu-Fuelled HWR-FUGEN". After the discussions, it was decided to present these papers except two papers at the 24th meeting.

The Committee held the 41st meeting in March 1982 : The activities of the Committee and the Subcommittees in this fiscal year were summarized. The summary record of the 3rd NEACRP ad-hoc Working Group Meeting on Evaluation Coordination held in association with the 24th meeting of the NEACRP was distributed and the progress of the work was discussed in connection with the next meeting to be held at the end of March. Then, results calculated for the NEACRP Benchmark Tests were reported and discussed, which included the followings; Burn-up Calculations Applied to the NEACRP Fast Breeder Benchmark, Shielding Benchmark Exercises and a LWR Benchmark Problem with Adjacent Poisoned Fuel Rods. In addition, "Description of the Pin and Plate Geometry CADENZA Assemblies for the International Comparison of Calculations" (NEACRP-A-445) was distributed and it was requested to participate in this benchmark test. As to studies of fusion reactor neutronics, the present status of experiments and analyses at FNS in JAERI and OKTAVIAN in Osaka Univeasity was reviewed. Finally, activity plans of the Committee and the Subcommittees in the next fiscal year were discussed.

Reference

1) Hirota J. : "Reactor Physics Activities in Japan - September 1980 to August 1981", NEACRP-L-255 (Japan).

8.2 Activities of the Subcommittees on Reactor Physics

J. Hirota

The Subcommittees on Reactor System, Fusion Reactor and Shielding held the meeting three, two and two times respectively during this one year period, discussing topics of relevance to each field and working for each aim.

The Subcommittee on Reactor System held the 5th meeting in June : According to the plan of the Subcommittee in this fiscal year, the present status of code systems for reactor analysis was reported, which included a criticality safety code system using the Monte Carlo method, a code system for evaluation of nuclear performance of fast reactors and SRAC ; a standard computer code system for lattice cell and core calculations on reactor design and analysis. The Subcommittee held the 6th meeting in September to continue discussions on code systems : Code systems for power distribution prediction and burn-up calculation in BWR and for core and fuel management in PWR were reported. A brief summary of the 24th meeting of the NEACRP was also reported. The Subcommittee held the 7th meeting in February 1982 : Results of burn-up calculations applied to the NEACRP Fast Breeder Benchmark and preliminary results obtained for a LWR Benchmark Problem with adjacent poisoned fuel rods were reported and discussed. As to the present status of code systems, HELIOS ; a code system for group constant calculations of BWR fuel assembly was presented. Then, a summary of the 3rd Specialists' Meeting on Reactor Noise (SMORN-III) was reported. In addition, experiments and analyses carried out at FCA to evaluate actinide cross sections were presented.

The Subcommittee on Fusion Reactor held the 6th meeting in June : Results of the performance tests and the preliminary experiments at FNS were reported. It was also reported that measurements of double differential cross sections were in progress at OKTAVIAN. Then, the plans of experiments to be carried out in near future using FNS and OKTAVIAN were discussed. The Subcommittee held the 7th meeting in September : A nuclear Design of the next fusion machine was reported and problems such as tritium breeding, induced activity, local heating and radiation damage were discussed. A system design of a commercial fusion reactor was also reviewed.

The Subcommittee on Shielding held the 12th meeting in July : Progress in the preparations for the 6th International Conference on Radiation Shielding (ICRS) and the calculations for the NEACRP Shielding Benchmark Exercises of FBR and PWR radial shielding was reported. It was also reported that the calculation for the ANS Gamma Ray Shielding Benchmark applicable to nuclear

radwaste facility was in progress. The Subcommittee held the 13th meeting in February 1982 : Results calculated for the NEACRP Shielding Benchmark Exercises were presented and discussed, including those for the Winfrith ASPIS Experiment. Then, the activities of the two Working Groups on Sensitivity and Uncertainty Analysis and on Shielding Analysis Method in this fiscal year were summarized.

The Preparatory Committee for the 6th ICRS held the meeting in June, September and March 1982. A preliminary information sheet of the 6th ICRS prepared by the Committee (NEACRP-A-491) was presented at the 24th meeting of the NEACRP. The NEACRP agreed to assist in the organization of the Conference and Dr. Rief (EURATOM Joint Research Centre) was nominated to represent the NEACRP on an International Organizing Committee to be set up for the 6th ICRS. The Preparatory Committee finished by the end of this fiscal year and a Japanese Organizing Committee for the 6th ICRS is set up in the next fiscal year.

8.3 Activities of the Japanese Organizing Committee for SMORN-III

J. Hirota and Y. Shinohara

The Japanese Organizing Committee and the Technical Program Committee held the meeting one and four times respectively to make preparations for the 3rd Specialist's Meeting on Reactor Noise (SMORN-III). After SMORN-III, both Committees held the last meeting jointly to evaluate the achievements in SMORN-III.

The Technical Program Committee held the 4th meeting in April : The technical agenda prepared by the International Organizing Committee were reported and the comments on the Reactor Noise Analysis Benchmark Test made by members of the International Organizing Committee were discussed. The Japanese Organizing Committee held the 2nd meeting in July to nominate Japanese participants in SMORN-III and to discuss the final program. The Committee held the 5th meeting in August to discuss the details of the technical program and to prepare the status report of the Benchmark Test (NEACRP-A-455) to be presented at the 24th meeting of the NEACRP. The Committee held the 6th meeting in September and the 7th meeting in October to discuss preliminary results of the Benchmark Test and SMORN-III papers.

During SMORN-III, members of the Technical Program Committee made efforts to help the Session Chairmen for smooth conduct of sessions. Prior to the presentation of "Summary Report on Reactor Noise Analysis Benchmark Test"[1] by Prof. Suda, an informal meeting was held to discuss with the applicants for the Benchmark Test. After SMORN-III, the Japanese Organizing Committee and the Technical Program Committee held the 3rd meeting and the 8th meeting jointly to discuss the highlights of SMORN-III. According to a proposal made at this meeting, members of the Technical Program Committee completed a review-paper[2], referring to various papers presented at SMORN-III and summarizing recent progress in safety-related applications of reactor noise analysis.

References

1) Suda N. : "Summary Repost on Reactor Noise Analysis Benchmark Test", Prog. Nucl. Energy, Vol.9, Reactor Noise-SMORN III, 693.

2) Hirota J. et al. : "Recent Progress in Safety-Related Applications of Reactor Noise Analysis", Nihon-Genshiryoku-Gakkai Shi (J. At. Energy Soc. Japan), 24 (3), 188 (1982) (in Japanese).

Publication Lists

1. Nuclear Data and Group Constants

(1) Takano H., Inoue H*.: "Doppler Effect of Structural Materials in Fast Reactors," J. Nucl. Sci. Technol., 18, 315 (1981).

(2) Kikuchi Y., Hasegawa A., Takano H.: "Benchmark Tests of JENDL-1," JAERI-1275 (1982).

2. Theoretical Methods and Code Development

(1) Nakagawa M., Yoshida H.: "Burn Up Calculation Applied to the NEACRP Fast Breeder Benchmark," JAERI-M 9743 (1981).

(2) Ishiguro M., Harada H., Nanba K*., Fujii M., Fujimura T., Nakamura Y.: "Parallel Computation for Solving the Tridiagonal Linear System of Equations," JAERI-M 9703 (1981) (in Japanese).

(3) Hasegawa A.: "EXPANDA-General User's Guide," JAERI-M 9791 (1981).

(4) Tsuchihashi K.: "Research Reactor Core Conversion from the Use of Highly Enriched Uranium to the Use of Low Enriched Uranium Fuels," Guidebook Addendum Heavy Water Moderated Reactors Appendix D IAEA (to be published) (1982).

(5) Gotoh Y.: "Study of Stochastic Reactor Kinetic Equation," Progr. Nucl. Energy., Vol.9, p303∿311 (1982).

3. Integral Experiment and Analysis

(1) Ōbu M.: "Preparation and Characteristics of Fission Chambers with Actinide Nuclides," JAERI-M 9757 (1981) (in Japanese).

(2) Shirakata K., et al.: "Experiment and Analysis of Sodium Void Reactivity Worth on FCA Assembly VII-1," JAERI-M 9931 (1982) (in Japanese).

(3) Tsuchihashi K., Akino F., Nagaoka Y. and Ishiguro Y.: "Benchmark Calculations by the Thermal Reactor Standard Nuclear Design Code System SRAC," JAERI-M 9781 (1981) (in Japanese).

(4) Kaneko Y., Akino F., Tsuchihashi K., Kitadate K., Takeuchi M. and Gotoh Y.: "The Meaning of Development of Multipurpose Very High Temperature Gas Cooled Reactor," Research on Reactor Physics, FAPIG 99 p38∿41 (1981). (in Japanese)

4. Shielding

(1) Suzuki T., Ishiguro Y. and Matsui Y.: "PALLAS-TS: A One-Dimensional Neutron Transport Code for Analyzing Fusion Blanket Neutronics," JAERI-M 9492 (1981) (in Japanese).

(2) Sasamoto N. and Takeuchi K.: "Revision of Multi-Group Neutron Cross Section Libraries for PALLAS," JAERI-M 9527 (1981) (in Japanese).

(3) Takeuchi K. and Sasamoto N.: "Three-Dimensional PALLAS Calculation of PCA Blind Test," NUREG/CR-1861, 6.8.1-6.8.13 (1981).

(4) Takeuchi K., Tanaka S. and Kinno M.: "Transport Calculation of Gamma Rays Including Bremsstrahlung by the Discrete Ordinates Code PALLAS," Nucl. Sci. Eng., 78(3), 273 (1981).

(5) Takeuchi K. and Tanaka S.: "A Code for Direct Integration of Transport Equation in One-Dimensional Plane and Spherical Geometries," JAERI-M 9695 (1981).

(6) Takeuchi K. and Sasamoto N.: "Fundamental Theory of Direct Integration Method for Solving the Steady-State Integral Transport Equation for Radiation Shielding Calculation," Nucl. Sci. Eng., 80(4), 536 (1982).

(7) Sasamoto N. and Takeuchi K.: "Direct Integration Method for Solving the Neutron Transport Equation in Three-Dimensional Geometry," Nucl. Sci. Eng., 80(4), 554 (1982).

5. Reactor and Nuclear Instrumentation

(1) Wakayama N.: "Some Consideration and Techniques to Enhance Reliability of Nuclear Power Plant Control and Instrumentation," J. SI-CE, Vol.20 (11), pp.1016∿1022 (1981) (in Japanese).

(2) Yamada M. and Fukuda M.: "The Development of Coastal Diffusion Observation Method with a Model Airplane," JAERI-M 9908 (1982) (in Japanese).

(3) Terada H., Malinovski J. and Blick H.: "Performance Test of SPECTRAN-F and SPECTRAN-III Computer Programs for Resolving the Cs-137-Ag-110m Double Peak in Gamma-ry Spectrometric Analysis," KFA Jul-1740 (1981).

(4) Terada H., Katagiri M. and Wakayama N.: "Verification Experiment for Nondestructive Measuring Method of Fission Product Plateout," J. At. Energy Soc. Japan, Vol.23 (10) pp.762∿771 (1981) (in Japanese).

(5) Kakuta T., et al.: "Heat and Radiation Resistant Cable for the Use on LMFBR," IEEE Trans. N. S., NS-29(1), pp.695∿699 (1982).

(6) Kakuta T., et al.: "Development of Inorganic Materials Insulated Flexible Tri-axial Cable for FBR," Proc. of the 30th Int. Wire and Cable Symposium, pp.286∿293 (1981).

(7) Sakai E., Miyazawa T. and Sekiguchi N.: "Summary of In-pile Loop Experiments Related to the Development of the Fuel Failure Detection Systems for LMFBRs in Japan," IAEA/IWGFBR Specialists' Meeting on Fuel Failure Detection and Localization, Karlsruhe, 11-14 May 1981.

(8) Sakai E., Murakami Y. and Nakatani H.: "Performance of a High-purity Germanium Gamma-ray Spectrometer System Using a Closed-cycle Cryogenic Refrigerator," IEEE Trans. on Nucl. Sci., Vol.NS-29(1) pp.760∿763 (1982).

(9) Sakai E.: "Present Status of Room Temperature Semiconductor Detectors," Proc. of 1981 INS Symposium on Nuclear Radiation Detectors, ed. by Fushimi K. et al. (1981). Also in Nuclear Instruments and Methods in Physical Research, Vol.196 pp.121∿130 (1982).

(10) Sakai E.: "Recent Progress in Nuclear Radiation Detectors," Proc. of the 15th Japan Conference on Radioisotopes, Nov.26 1981, Tokyo, pp.105∿120 (1982) (in Japanese: English version of the test can be available on request).

(11) Sakai E.: Japanese translation of IEC publication 697-1981, "Germanium Semiconductor Detector Gamma-ray Efficiency Determination Using a Standard Re-entrant Beaker Geometry," JAERI-M 9829 (1981).

(12) Yamamoto S., Katagiri M., et al.: "Magnetrohydrodynamic Activity in the JFT-2 TOKAMAK with High Power Neutral Beam-injection Heating," J. of Nuclear Fusion, 21 (B) (1981).

(13) Wakayama N. and Katagiri M.: "Measurement Method of Radioactivities Deposited in the Primary Cooling System," Decommissioning Handbook on Nuclear Reactor, pp.62∿90, Science Forum (1981) (in Japanese).

(14) Mukaiyama T., Kuroi H.: "The Expected Performance and Benefits of an Advanced Containment and Surveillance System of the Fast Critical Facility FCA of JAERI," Proceedings of 22nd Annual Meeting of Institute of Nuclear Material Management (San Francisco, July 1981).

6. Reactor Control and Diagnosis

(1) Shimazaki J., Fujii Y., Shinohara Y. and Araki H.: "Simulation Study of Neutronic and Acoustic Methods of Boiling Detection," PNC N941 81-116 (1981).

(2) Oguma R., Hayashi K. and Kitajima T.: "An On-Line Leak Detection Method for OWL-1 Loop by ARX Modeling Using Dewpoint Signals," J. Nucl. Sci. Technol., Vol.18, No.10, pp.756∿765 (1981).

(3) Oguma R.: "Method to Estimate Signal Transmission Paths in Dynamic Systems and its Application to Reactor Noise Analysis," J. Nucl. Sci. Technol., Vol.18, No.11, pp.835∿844 (1981).

(4) Oguma R.: "Coherence Analysis of Systems with Feedback and its Application to a BWR Noise Investigation," Prog. Nucl. Energy, Vol. 9, pp.137∿148 (1981).

(5) Oguma R.: "A New Method for Coherence Analysis of Systems with Feedback Effect Based on Autoregressive Modeling," JAERI-M 9576 (1981) (in Japanese).

(6) Hayashi K., Oguma R. and Watanabe K.: "Computer Code -STAR: Statistical Analysis of Random Data- for Dynamic Analysis and Diagnosis of Nuclear Reactor Systems," JAERI-M 9761 (1981) (in Japanese).

(7) Hayashi K. and Oguma R.: "Identification of Autoregressive Model Based on Burg Algorithm and Its Application to Diagnosis of Nuclear Reactor," JAERI-M 82-009 (1982) (in Japanese).

7. Fusion Reactor Technology

(1) Oyama, Y. and Tanaka, S.: "Neutron Dosimetry by the Spectrum Weighting Function Method with a NE213 Liquid Scintillator," JAERI-M 9982 (1981).

(2) Nakamura, T., et al.: "Integral Experiments on Lithium Oxide Spherical Assembly with Graphite Reflector and on Duct Streaming," Third IAEA Technical Committee Meeting and Workshop on Fusion Reactor Design and Technology, Tokyo, Oct. 5-16, (1981).

(3) Fujisawa T.: "Numerical Simulation of Two-Fluid, Two-Dimensional, MHD Equations of a Toroidal Plasma," JAERI-M 9944 (1982).

8. Activities of the Committees

(1) Hirota J.: "Reactor Physics Activities in Japan - September 1980 to August 1981," NEACRP-L-255 (Japan).

(2) Hirota J., Shinohara Y., Saito K*., Kuroda Y*., Fukunishi K*., Nishihara H*., Fujita Y*., Tsunoda T*., Tamura S*. and Suda N*.: "Recent Progress in Safety-Related Applications of Reactor Noise Analysis," Nihon-Genshiryoku-Gakkai Shi (J. At. Energy Soc. Japan), 24 (3), 188 (1982) (in Japanese).